2013

Molecular Dynamics of Interfacial Phenomena at Air/ice, Air/ water, and Air/salt Water Interfaces

Thilanga Prabhash Liyana Arachchi
Louisiana State University and Agricultural and Mechanical College

MOLECULAR DYNAMICS OF INTERFACIAL PHENOMENA AT AIR/ICE, AIR/WATER, AND AIR/SALT WATER INTERFACES

A Dissertation

Submitted to the Graduate Faculty of the
Louisiana State University and
Agriculture and Mechanical College
In partial fulfillment of the
Requirements for the degree of
Doctor in Philosophy

In
The Gordon A. and Mary Cain Department of Chemical Engineering

By
Thilanga Prabhash Liyana Arachchi
B.S., Louisiana State University, 2008
May 2013

ACKNOWLEDGEMENTS

First and foremost I would like to express my deepest gratitude to my advisor Dr. Francisco R. Hung, for his invaluable guidance and support. He has always provided me the appropriate guidance, giving the freedom to implement my own ideas and provided me positive feedback in order for me to implement them. I have been fortunate to benefit from his expertise in molecular simulation, and I am grateful to him for his career advice on how to pursue my goals in future.

I want to especially thank my experimental collaborator, Dr. Kalliat T. Valsaraj, for all the helpful discussions and for his advice. Also I would like to thank Dr. Franz Stefan Ehrenhauser for very helpful discussions. I sincerely thank the Dean's representative, Dr. Daniel E Sheehy, and my committee members, Drs. Bin Chen Krishnaswamy Nandakumar, for their invaluable suggestions on my research work. I would also like to thank all those in the Cain Department of Chemical Engineering at Louisiana State University.

I gratefully acknowledge funding from the National Science Foundation, Gulf of Mexico Research Initiative (GoMRI), Louisiana Board of Regents and the Cain Department of Chemical Engineering at LSU. We also used high performance computational resources from High Performance Computing at Louisiana State University (http://www.hpc.lsu.edu), and the Louisiana Optical Network Initiative (http://www.loni.org).

I am also very grateful to my parents and especially my wife Sulakshi, for giving me all the support, patience and love.

TABLE OF CONTENTS

ABSTRACT

The purpose of this research is to investigate the adsorption of organic contaminants, namely polycyclic aromatic hydrocarbons (PAHs) and green leaf volatiles (GLVs), as well as their interactions with reactive oxygen species (ROSs) on atmospheric air/water and air/ice interfaces. In another series of projects, we studied several intermediate and semi-volatile organic compounds from oil (IVOCs and SVOCs, e.g., alkanes with 17-31 carbon atoms), surfactants and dispersants at air/salt water interfaces. These simulations are relevant to understand the fate of these compounds during the recent 2010 Deepwater Horizon (DWH) oil spill.

The adsorption of gas-phase aromatics (benzene, naphthalene and phenanthrene), ROSs (O_3, OH, H_2O_2 and HO_2) and GLVs (2-methyl-3-buten-2-ol (MBO) and methyl salicylate (MeSA)) on atmospheric air/water or air/ice interfaces was investigated using classical molecular dynamics (MD) simulations and potential of mean force (PMF) calculations. All aromatics, ROSs and GLVs exhibit a strong preference to be adsorbed at air/water or air/ice interfaces. The adsorption of both naphthalene and ozone onto 1-octanol, 1-hexadecanol or 1-octanal coated air/ice interfaces is enhanced when compared to bare air/ice interfaces. Classical MD simulations were performed to investigate the growth of ice from supercooled aqueous solutions of benzene, naphthalene, phenanthrene, •OH, H_2O_2, or •HO_2. All solutes in the supercooled aqueous solutions are displaced to the air/ice interface during the freezing process at both 270 K. In contrast, only a fraction of benzene, H_2O_2 and •HO_2 molecules become trapped inside the ice lattice during the freezing process at 260 K. Our simulations of

oil hydrocarbons (IVOCs and SVOCs) and dispersants at air/sat water interfaces were performed in collaboration with experiments from K. T. Valsaraj's group. We found that n-alkanes (C15 to C20) exhibit a strong preference to stay at both bare and SDS coated-air/salt water interfaces, as opposed to either staying in the gas phase or being dissolved in bulk of salt water solution. Our results suggest that, from the thermodynamic point of view, n-alkanes have a stronger tendency to remain at the air/salt water interface, and thus are more likely to be ejected to the atmosphere, as their chain length increases, and as the SDS concentration increases.

CHAPTER 1 INTRODUCTION

1.1. Adsorption of Organics and Reactive Oxygen Species on Air/water and Air/ice Interfaces: Background and Motivation

Aerosols represent an important portion of particulate matter and play an important role in climate, air quality and fate of pollutants in the atmosphere, although significant uncertainties remain due to limited knowledge on their sources, composition and path of formation.[1-10] Organics represent a major fraction of particulate matter, and a significant part of these are secondary (formed in the atmosphere). These secondary organic aerosols (SOAs) remain poorly understood at present, and are an important factor in the well-known smog-fog-smog cycle.[11] Here, fog forms by condensation of water on sub-micron particles, which then takes up organics from different sources (automobile emissions, plants, etc.). These organics then react with atmospheric oxidants [e.g., ozone and radicals such as hydroxyl (•OH) and nitrate ($•NO_3$)] to yield more organics and SOAs in the near-surface atmosphere, providing particles where water can condense in the next fog episode.[1, 11] Possible pathways for oxidation/nitration reactions during a smog-fog-smog cycle include reactions in the gas phase, at the air/water interface or within the bulk of the water drops. Oxidation and nitration reactions at air/water interfaces can exhibit kinetics that are much faster than those of their homogeneous counterparts in the gas and bulk water phases.[1, 12, 13] Therefore, chemical processing within atmospheric fog droplets have a profound impact on the climate, air quality and fate of pollutants in the atmosphere.

In this dissertation we focused on molecular modeling of two types of organic compounds at atmospheric air/water and air/ice interfaces, namely polycyclic aromatic hydrocarbons (PAHs) and green leaf volatiles (GLVs). PAHs consist of two or more carbon-hydrogen rings

in which at least one ring has an aromatic structure. PAHs are ubiquitous pollutants in the environment. They typically arise from the incomplete combustion of fossil fuels, automobile emissions, oil cracking, forest fires and volcanoes. PAHs are known to have important carcinogenic and mutagenic effects.[14] The current list of 126 priority pollutants from the U. S. Environmental Protection Agency (EPA) contains 16 PAHs.[15] Furthermore, these compounds can undergo photochemically-induced oxidation and nitration reactions with reactive oxygen species (ROSs) [e.g., ozone (O_3) and radicals such as singlet oxygen, hydroperoxy (HO_2), hydroxyl (OH) and nitrate (NO_3)].[1] Reactions of PAHs with ROS produce oxy- and nitro-PAHs that are even more toxic than PAHs (up to 105 times larger carcinogenic and mutagenic activities [14, 16]), and contribute to the formation of secondary organic aerosols. In the gas-phase, PAHs mainly reacts photo-chemically with OH radicals.[14] Under normal atmospheric conditions PAHs are typically nonreactive, but they react in the presence of high concentrations of gases such as ozone and OH radicals.[1, 17, 18] Among PAHs, naphthalene has the highest vapor pressure and exists predominantly in the gas phase.[14]

PAHs can be adsorbed at the surfaces of water droplets, atmospheric aerosols, fog, mist, ice and snow. This process consists of adsorption to the air/ice or air/water interface and dissolution in the bulk QLL or in bulk water.[19] Heterogeneous reactions of PAHs at air/water and air/ice interfaces can have faster kinetics than their homogeneous counterparts in the gas phase.[1, 12, 13] Although PAHs are hydrophobic, the air-water interface can uptake significant amounts of these compounds; recent molecular dynamics (MD) simulations indicate the presence of deep free energy minima for adsorption of PAHs at the

air-water interface.[20] It is also observed that the free energy minima tend to get deeper when the size of the PAH increases.[20] Energy minima at the interface suggest that heterogeneous reactions are possible due to the preference of benzene, naphthalene, phenanthrene and anthracene to stay on the water interface, as compared to dissolution in bulk water.[20] The uptake of PAHs at air-water and air/ice interfaces can be further enhanced by the presence of water-soluble organic compounds at the interfaces. These compounds (collectively called humic-like substances) have been identified in fog[21-26] and can also affect the reactivity of PAHs with ROS. The processes taking place at atmospheric air/water and air/ice interfaces (water droplets, atmospheric aerosols, fog, mist, ice and snow) therefore have a profound impact on the fate and transport of PAHs and other trace gases in the atmosphere. However, and despite their relevance, a fundamental understanding of the adsorption and heterogeneous reactions of PAHs and ROSs at air/ice interface is still lacking.[1] The adsorption and photochemical transformations of PAHs and ROSs at the air/water interface has been the subject of several recent experimental and simulation studies.[12, 13, 20, 25, 27-32] Very recently, the effect of surfactants on the behavior of PAHs at the air/water interface has been studied via molecular simulations.[33] Similarly, several studies have focused on the adsorption and reactions of these compounds at air/ice interfaces.[34-43] Despite recent progress in the area, a fundamental understanding of the processes taking place between PAHs and ROSs at the air/ice interface is still lacking. The physical properties of the QLL are not completely understood,[44, 45] and even less is known about how pollutants interact and undergo chemical reactions at the QLL.[45] Molecular simulation studies in this area can provide information of the processes occurring at the

molecular level, which in turn can complement experiments and assist in the interpretation of experimental results. Molecular simulation studies can also provide insights to understand if the QLL acts as sub-cooled water or represents a rather different environment. In this dissertation we have focused on the properties of PAHs at atmospheric air/ice interfaces, as well as their interactions with ROSs at these interfaces.

As mentioned above, many studies have focused on PAHs on atmospheric air/water interfaces; however, other organic compounds at these interfaces have not been studied in detail. A number of characterization efforts have focused on the organic fraction of atmospheric fog, which can vary depending on the source, altitude and latitude of the measurements.[12, 22, 46-50] This organic fraction can be split into particulate and water-soluble organic carbon (WSOC). The latter accounts for 70-80% of the total mass of carbon in fog waters,[51] but about 40% of WSOC is unidentified due to difficulties in analytical sampling and analysis.[46, 48, 52] Much of the organics in fog waters arise from the chemical processing of anthropogenic, soil-derived and biogenic organic precursors; the latter represent a major source of WSOC in fog.[53, 54] Among the biogenic volatile organic compounds (BVOCs) emitted from vegetation, isoprene and monoterpenes have been widely studied and are known to produce SOAs via oxidation and nitration reactions.[55-60] However, a large fraction of BVOC emissions also come from compounds other than isoprene and monoterpenes.[61, 62] Of these, green leaf volatiles (GLVs) are a group of BVOCs and consist of oxygenated hydrocarbons emitted in large quantities by plants, especially when they are subject to mechanical stress (grass cutting, animal grazing) or local weather changes.[6, 63-65] Organic compounds in GLVs include 2-methyl-3-buten-2-ol

(MBO), cis-3-hexen-1-ol, cis-3-hexenylacetate, methyl salicylate (MeSa) and methyl jasmonate. However, and despite their relevance, a fundamental understanding of the adsorption and heterogeneous reactions of GLVs at air/water interface is still lacking.

In chapter 2 of this dissertation we report a molecular dynamics simulation study where we elucidate molecular-level details of the adsorption and the interactions between naphthalene and ozone molecules at the air/ice interface. In chapter 3 we studied how the adsorption of naphthalene and ozone on air/ice interfaces is affected by the presence of varying concentrations of surfactant species at these interfaces. We also investigated how the structural properties of these surfactant species change with variations in their concentrations. We also investigated how surfactants affect the structural and dynamical properties of naphthalene at the surfactant-coated air/ice interfaces. Afterwards, we report MD simulations of ice growth from supercooled water containing dissolved aromatic molecules (chapter 4) and ROSs (chapter 5). These compounds are known to be solvated to a considerable degree in bulk water at environmental conditions. Because of this fact, ice growth from supercooled aqueous solutions of these compounds is a process that can occur in natural environmental conditions, for example during freezing of lakes, formation of ice at the sea and formation of snow pellets. As a result, PAHs and ROSs could become trapped into the ice lattice and then undergo photochemical reactions in such an environment. In chapters 6 and 7 we investigated the adsorption of two GLVs, MBO (chapter 6) and MeSa (chapter 7), as well as their interactions with ROSs at the air/water interface using molecular simulations.

1.2. Adsorption of Oil Organics and Dispersants on Atmospheric Air/salt Water Interfaces: Background and Motivation

The Deepwater Horizon (DWH) was an oil drilling rig located in the in the Gulf of Mexico approximately 75 km from the coast of Louisiana. On the 20th of April 2010, the DWH oil rig exploded and consequently sank due to a rupture of the riser pipe on the seafloor at approximately at 1500 m depth.[66] Due to the DWH accident, millions of barrels of oil released into the waters of the Gulf of Mexico during April to July, 2010 resulting in the largest oil spill ever in Gulf of Mexico region and caused significant environmental damage.[67] Although a considerable fraction of the oil-gas mixture remained dissolved in the bulk water a large fraction of the oil leaked from the 2010 Deepwater Horizon (DWH) accident accumulated on the surface of the sea. A significant part of this oil evaporated into the atmosphere and contributed to the formation of organic aerosols.[68-70] The evaporation process from the oil spill consists first of evaporation of small hydrocarbons containing less than 6 carbon atoms, which are soluble in the water to a considerable degree. Hydrocarbons containing less than 10 carbon atoms evaporated within a few hours within reaching the sea surface; the hydrocarbons containing 10 to 16 carbon atoms evaporated within few hours to few days after they reached the sea surface. Finally, hydrocarbons containing more than 16 carbon atoms which evaporated very slowly, if at all.[68, 69] These volatile organic carbon (VOC), intermediate volatile organic carbon (IVOC) and semi volatile organic carbon (SVOC) species are oxidized in the atmosphere, which leads to formation of lower volatile compounds causing them to nucleate in to new particles forming SOAs. SOAs are important to understanding the faith of pollutants in the atmosphere and important contributor to air quality and climate change.[71] In the atmosphere, aerosol particles scatter the solar radiation

and act as environment for condensation of water during process such as cloud formation which in return effect the climate and air quality.[72] The inability to quantify the molecular composition and mass of the atmospheric aerosols prevents progress in understanding aerosol chemistry due to difficulties in experimental methods.[73, 74] Furthermore, theoretical studies point to the importance of SVOCs and IVOCs as important precursors in aerosol formation.[7, 75] De Gouw et al. [68] shows that hydrocarbons in the range between C14-C16 which evaporated over a time period less than 100 hours resulted in SOAs detected downwind of the oil spill region. However, the fate of other organic compounds from oil, such as the heavier IVOCs (C17-C18) and the semi-volatile organic compounds (SVOCs, C19-C31) has not been addressed so far. The hypothesis behind our work is that the fraction of these compounds that reach the sea surface didn't evaporate but remained there, and phenomena such as bubble-bursting and white caps (breaking waves) on the sea surface will carry these compounds, as well as the dispersants released to combat the spill, into the atmosphere. Even though breaking waves and bursting bubbles are an important source of generation of aerosols at the sea surface,[76] negligible data has been gathered so far on wave- and bubble-generated aerosolization of oil near the DWH accident site. These processes generate water droplets that are expected to contain oil and gas components, marine salts, and dispersants; the water in these droplets eventually evaporates and aerosols are formed. However, much remains to be done to accurately determine how much and which organics are transported into the atmosphere through wave-breaking and bubble-bursting aerosolization. In particular, molecular simulations can provide answers to many of the "how?" and "why?" questions that will surface as the experimental results are interpreted.

Furthermore, the interfacial properties such as structural properties of water at the interface and the interfacial width can be significantly influenced by the presence of hydrocarbons and surfactants at air/water interfaces.[77-80] In chapter 8 of this dissertation, we studied the properties of the alkanes pentadecane (C15) and icosane (C20) on air/salt water interfaces that are either bare or coated with a standard anionic surfactant, sodium dodecyl sulfate (SDS) using classical MD simulations. We also investigated how the structural properties of these alkane species and SDS molecules change with variations in their concentrations. Our results suggest that, from the thermodynamic point of view, alkanes have a stronger tendency to remain at the air/salt water interface (and thus are more likely to be ejected to the atmosphere) as their chain length increases, and as the SDS concentration increases. These results are in agreement with what the group of K. T. Valsaraj observed in their experiments, namely that more alkanes are ejected when dispersant is present in the system.

CHAPTER 2 A MOLECULAR SIMULATION STUDY OF THE ADSORPTION OF NAPHTHALENE, PHENANTHRENE AND OZONE ON ATMOSPHERIC AIR/ICE INTERFACES[†]

Contents of this chapter have already been published (T. P. Liyana-Arachchi, K. T. Valsaraj and F. R. Hung, A molecular simulation study of the adsorption of phenanthrene, naphthalene and ozone on atmospheric air/ice interfaces. J. Phys. Chem. A 2011, 115, 9226-9236). In this chapter, we report molecular dynamics (MD) results of the adsorption of gas-phase phenanthrene, naphthalene and ozone on atmospheric air/ice interfaces. The main objective of this study was to investigate the adsorption of gas-phase phenanthrene. naphthalene and ozone on atmospheric air/ice interfaces and air/ice interfacial properties under the influence of naphthalene and ozone. The rest of this chapter is structured as follows. Section 2.1 is the introduction. Section 2.2 contains a description of our computational models and methods. In Section 2.3 we present results and discussion and in Section 2.4 we summarize our main findings.

2.1. Introduction

The adsorption and photochemical transformations of PAHs and ROSs at the air/water interface has been the subject of several recent experimental and simulation studies.[12, 13, 20, 25, 27-32] Very recently, the effect of surfactants on the behavior of PAHs at the air/water interface has been studied via molecular simulations.[33] Similarly, several studies have focused on the adsorption and reactions of these compounds at air/ice interfaces.[34-43] Sorption to ice is important for the fate of organic contaminants in colder climate and in cold ecosystems at high latitudes and altitudes. PAHs have been observed in snow in both urban

[†] Reprinted with permission of J. Phys. Chem. A 2011, 115, 9226-9236

and remote areas.[81-94] PAHs are present in snow in relatively low concentrations at remote high-latitude areas, but exhibit much larger concentrations near urban centers.[14] The sorption mechanism consists of the adsorption of organic molecules to the air-ice interface, dissolution in the quasi-liquid layer (QLL) at the ice surface, and incorporation in the solid ice crystal.[95] The QLL at the ice surface is a transitional liquid-like layer observed at temperatures close to the melting point. Experiments indicate that the QLL exists on the crystalline ice surface.[96-101] It is hard to estimate the thickness of the QLL, because the values obtained for thickness of the QLL are highly dependent on the experimental techniques used to measure it.[96, 101-108] Justified by the existence of a QLL, the ice surface has been assumed to behave similarly to a subcooled water surface at temperatures between 0 ºC and -30 ºC. Based on this assumption, calculations of equilibrium partitioning in the atmosphere have estimated the air-ice interfacial partitioning by extrapolating adsorption constants for the air-water interface.[109-111] However, controversy exists regarding the validity and accuracy of this extrapolation. Roth *et al*.[95] compared snow surface sorption of organic vapors to extrapolated water adsorption and found an extrapolation error up to an order of magnitude. According to the surface Raman spectra obtained by Kahan *et al*.,[39] the surfaces of ice and water exhibit different degrees of hydrogen bonding between the water molecules, indicating a different environment presented by the QLL from that of liquid water. In recent studies, Donaldson and coworkers have found significant differences in the photolysis rates of PAHs and the reactivity of hydroxyl radicals at air-ice and air-water interfaces.[36, 37, 40, 41] In contrast, results from Ram and Anastasio[34] suggest that the photolysis rates of phenanthrene, fluoranthene and pyrene in

bulk ice and in aqueous solution are similar. Recent results from the Donaldson group also suggest that self-association of naphthalene molecules is enhanced at air-ice interfaces as compared to air-water interfaces.[38] In addition, results from our recent combined experimental-simulation study suggest that surface adsorption is the predominant mechanism for the uptake of phenanthrene in thin water and ice films; incorporation of phenanthrene in the solid ice structure was negligible.[43] Furthermore, the interfacial air-water and air-ice partition constants of phenanthrene increased greatly in the presence of surface-active substances, suggesting that these compounds can lead to important increases in the uptake of organic compounds by atmospheric water and ice films.

Despite recent progress in the area, a fundamental understanding of the processes taking place between PAHs and ROSs at the air/ice interface is still lacking. The physical properties of the QLL are not completely understood,[44, 45] and even less is known about how pollutants interact and undergo chemical reactions at the QLL.[45] Molecular simulation studies in this area can provide information of the processes occurring at the molecular level, which in turn can complement experiments and assist in the interpretation of experimental results. Molecular simulation studies can also provide insights to understand if the QLL acts as sub-cooled water or represents a rather different environment. Here we report a molecular dynamics simulation study where we elucidate molecular-level details of the adsorption and the interactions between phenanthrene, naphthalene and ozone molecules at the air/ice interface. Among the previous simulation studies of PAHs at the air/ice interface,[34-43] only the work of Ardura *et al.* [38] considered naphthalene, and this study was focused on the self-association of this compound at the air/ice interface. We first report results for the

potential of mean force (PMF) of naphthalene and ozone at the air/ice interface, and compare those against simulated results obtained for the air/water interface. Afterwards, we report results for the density profiles of the different species for varying concentrations of naphthalene and ozone at the air/ice interfaces. Finally, and following the molecular simulation work of Vácha *et al.*[29] for air/water interfaces, we have monitored the number of contacts between naphthalene and ozone at the air/ice interface for varying concentrations of these two species. These contacts could probably lead to chemical reactions between naphthalene and ozone, and following Vácha *et al.*,[29] we assumed that the reaction rate is proportional to the number of these contacts, in an attempt to obtain insights into the possible reaction mechanism between naphthalene and ozone at air/ice interfaces.

2.2. Models and Methods

The TIP5P water model[112] was used in our simulations with the air/ice and air/water interfaces. This water model has been used in previous simulation studies of PAHs at air/ice interfaces,[35, 38, 113] and is capable of reproducing the experimental melting point of hexagonal ice I_h at 1 bar.[114] Phenanthrene, naphthalene and ozone were modeled using the force fields and parameters from the previous work of Vácha *et al.,*[20, 28, 29] which can reproduce experimental values of the free energies of hydration. Since these force fields were parameterized by Vácha *et al.,*[20, 28, 29] in combination with the SPC/E water model,[115] we first verified that the experimental free energies of hydration were also correctly reproduced when these naphthalene and ozone force fields are used in combination with the TIP5P water model (see §2.1.1 and §2.2.1 below).

Classical molecular dynamics (MD) simulations were conducted using the GROMACS software[116] in the NVT ensemble (constant number of molecules, volume and temperature). For simulations on air/ice and air/water, we considered orthorhombic simulation boxes of dimensions 27 Å×31.4 Å×240 Å, and 27 Å×31.4 Å×260 Å (*x*, *y* and *z* respectively). Periodic boundary conditions were applied in all three directions. A wide range of concentrations for naphthalene and ozone were considered in our simulations: 1 to 90 molecules of naphthalene, and 1 to 400 molecules of ozone. Regarding phenanthrene adsorption we used up to 4 phenanthrene molecules. The concentration of ozone in air in Baton Rouge, Louisiana averages about 80-100 $\mu g/m^3$, with occasional maximum values of 240 $\mu g/m^3$ (which exceeds the National Ambient Air Quality Standard, NAAQS).[12] Similarly, the concentration of PAHs in air in Houston and Baton Rouge (in the Texas-Louisiana Gulf Coast corridor) ranges between 0.00053 and 0.03224 mg/cL.[48] These atmospheric concentrations are much lower than the 'overall' concentrations of naphthalene and ozone considered in our paper (obtained by dividing the number of molecules of the species of interest by the volume of the vacuum regions in our systems). However, the concentrations of these species used in our study should be considered more as 'surface' concentrations rather than 'overall' concentrations, due to the small system sizes considered in our study. In that sense, the experimental surface concentrations of these species are different from the atmospheric concentrations and are more difficult to define precisely, as the surface concentrations depend on the partition between gas phase and the air/ice interface. In order to analyze atmospherically-relevant concentrations and obtain statistically-relevant

results from MD simulations, one would need to consider prohibitively large system sizes that are beyond the capacities of current computational resources.

For the simulations of phenanthrene, naphthalene and ozone on water films, we placed a slab of 1344 TIP5P water molecules in the center of the simulation box, forming two interfaces with vacuum regions mimicking air. In the simulations of phenanthrene, naphthalene and ozone on air/ice interfaces, we placed 576 TIP5P water molecules arranged into 5 bi-layers of hexagonal ice I_h in the middle of the simulation box, creating the ice slab. These molecules were fixed in space. Afterward, and following previous studies,[38, 113, 117] we placed two thin layers, both formed by 768 'mobile' water molecules on both sides of the immobile ice slab (these 'mobile' water molecules were not fixed in space). Part of these 'mobile' water molecules that are near the immobile ice slab gradually freeze during the equilibration part of our simulations. The 'mobile' water molecules that remain unfrozen intend to mimic the QLL of water that forms at the air/ice interface, and this simulated QLL eventually exhibit a stable thickness during the equilibration part of our simulations.

In this study we have considered an ice slab where the basal plane (0001 face) of hexagonal ice I_h is in contact with the QLL. A recent molecular simulation study[117] suggests that the thickness of the QLL is similar for different water models, provided that the same undercooling temperature with respect to the melting point of the specific water model is considered. The thickness of the QLL also depends on the plane of ice I_h [basal (0001), prism (1010) or secondary (1120) faces] that is initially exposed to the air interface when surface premelting occurs.[117, 118] For each simulated system we first relaxed our initial configurations using the steepest descent energy minimization method. A time step of 1 fs

was used in all our simulations and data were collected every 10 ps. Bond lengths were constrained using the LINCS algorithm.[119] Temperature coupling was done using the velocity-rescaling algorithm of Parrinello *et al.* [120, 121] with a coupling constant of 0.1 ps. A cut-off distance of 0.9 nm was used for the Lennard-Jones interactions. The particle-mesh Ewald (PME) method[122] was used with a cutoff of 0.9 nm and a grid spacing of 0.12 nm in order to account for long-range Coulombic interactions.

2.2.1. Potential of Mean Force (PMF) Calculations

In our first series of simulations, we determined the free energy profile associated with moving one molecule of naphthalene or ozone from the gas phase into the water slab (air/water system) or into the QLL (air/ice system). The constraint force method [123-125] was used in these simulations. In this method, the z-distance between the center of mass of naphthalene or ozone molecule and the center of mass of the water or ice slabs is constrained. The force that needs to be applied to the naphthalene or ozone molecule in order to keep this distance fixed is then calculated in the simulation. This was done using increments of 1 Å using multiple simulations along the z-axis. The potential of mean force (PMF) can then be obtained from integration of this force.[123-125] We assumed the free energy in gas phase to be zero. Calculations of the PMF of naphthalene and ozone on air/water systems were carried out in order to verify that our adopted force fields were able to reproduce experimental values of the free energies of hydration. Each of these simulations were run for ~ 2 ns; after an equilibration period of ~ 1 ns, the forces were averaged over ~ 1 ns. To determine the PMF of naphthalene and ozone on air/ice systems, each of the simulations were run for ~ 6 ns, of which ~2 ns were used for equilibration and ~ 4 ns were used to average the forces at each

value of *z*-distance considered (during the 2 ns equilibration period the QLL was able to reach its equilibrium thickness). PMF simulations were run at 270 K on ice and at 298 K on water.

2.2.2. Conventional MD Simulations

Each 'conventional' MD simulation for the air/ice systems was equilibrated over at least 4 ns (regarding adsorption of phenanthrene this was 2.5 ns). Afterward, a production run of 8 ns was conducted (regarding adsorption of phenanthrene this was 10 ns). phenanthrene adsorption on to air/water was also done for the purpose of investigating the differences between air/ice and air/water interfaces (For this 2.5 ns equilibration time period and a 10 ns production run was used). In these MD simulations we investigated the adsorption of phenanthrene, naphthalene and ozone on air/ice interfaces. Also phenanthrene adsorption on air/water interfaces was investigated. We also investigated the interactions between naphthalene and ozone at the air/ice interface. For the air/ice interface, we evaluated the distribution of the angle between the aromatic plane of phenanthrene or naphthalene and the ice/QLL surface (*xy*-plane). Angular distribution of phenanthrene on air/water was also investigated. This property was evaluated for varying numbers of naphthalene and ozone molecules at the air/ice interface and for 2 molecules per surface of phenanthrene on both water and ice surfaces. The residence time of phenanthrene and naphthalene molecules at the air/ice interface and in the bulk QLL was also calculated in our simulations, using two naphthalene and phenanthrene molecules per interface. For the analysis of the ozonolysis reaction rate at varying number of ozone and naphthalene molecules at the air/ice interface, we assumed that the rate of reaction is proportional to the number of contacts between naphthalene and ozone. Following Vácha *et al.*,[29] we defined a contact as when hydrogen

atoms of a naphthalene molecule are within 3.5 Å from two side oxygen atoms of an ozone molecule (this distance corresponds to the first minimum observed after the first maximum in the radial distribution function between hydrogen atoms of naphthalene and the two side oxygen atoms on ozone). Vácha *et al.*[29] indicate that the results do not vary appreciably if a different value of distance is used. We used the software VMD[126] for all our visualizations.

2.3. Results and Discussion

2.3.1. PMF of Naphthalene and Ozone in Air/water Systems

In Figure 2.1 we present the PMF when one molecule of naphthalene or one molecule of ozone moves from the gas phase to the air/water interface, and then across the water slab. These systems have been studied in previous simulation studies.[20, 28, 29] As mentioned above, the force fields that we used for naphthalene and ozone were initially parameterized[20, 28, 29] in combination with the SPC/E water model to reproduce the experimental free energies of hydration of naphthalene and ozone. Therefore, the purpose of our PMF calculations is to test the performance of our adopted force fields for naphthalene and ozone, when used in combination with the TIP5P water model.

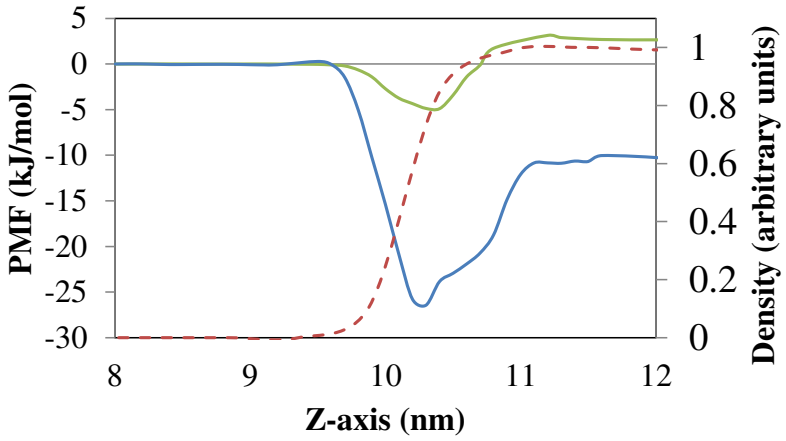

Figure 2.1. PMF of one molecule of naphthalene (blue line) and one molecule of ozone (green line) at 298 K. The density profile of water is represented as the red dashed line.

From Figure 2.1, the simulated hydration free energy obtained for naphthalene is about -10 kJ/mol, and for ozone is about +2.8 kJ/mol. These results are very similar to those obtained by Vácha *et al.* in their simulation studies,[20, 28] and are comparable with the experimental values of the free energies of hydration for these two molecules (between -7.5 kJ/mol and -10.3 kJ/mol for naphthalene, and between +2.9 and +3.7 kJ/mol for ozone, as determined from Henry's law constants[20, 28]) In addition, the free energy minima determined in our PMF calculations (-26.4 kJ/mol for naphthalene and -4.9 kJ/mol for ozone) are very similar to those reported in simulations by Vácha *et al.*[20, 28] These results show that the combination of force fields used in our study can reproduce experimental values of the free energy of hydration of naphthalene and ozone, as well as previous simulation results of the PMF for naphthalene and ozone in air/water systems.

2.3.2. Air/ice Systems: Density Profiles of the Mobile Water Molecules

For air/ice systems, as described before in the section on Simulation details, part of the thin layers of mobile water that we placed near the fixed ice slab gradually freeze during the equilibration part of our simulations. In Figure 2.2a we present the time evolution of the density profiles of the mobile water molecules in air/ice systems at 270 K, when 3 ozone and 15 naphthalene molecules are present at each air/ice interface. Some variations in the density profile of the mobile water molecules are observed during the initial equilibration period (the first 4 ns of our runs), but no significant variations in the density profiles are observed during the production period (last 8 ns). These results suggest that part of the mobile water molecules freeze or melt during the first 4 ns of our simulations, as suggested by the large peaks and the deep local minima found in the density of the mobile water molecules that are

close to the immobile ice slab. These results also suggest that the mobile water molecules that remain unfrozen (the QLL in our systems) eventually reach a stable thickness during the equilibration part of our simulations. Similar trends were observed for all the concentrations of ozone and naphthalene considered in our study, as well as for all our air/ice systems at 250 K. In Figure 2.2b we depict the density profiles of the mobile water molecules at 270 K and 250 K, when 15 naphthalene and 3 ozone molecules are present at each air/ice interface. More fluctuations in the density profile are observed at 250 K as compared to that at 270 K, suggesting that the thickness of the QLL decreases with a reduction in temperature, as expected. Similar temperature trends were observed for different concentrations of naphthalene and ozone at the air/ice interfaces.

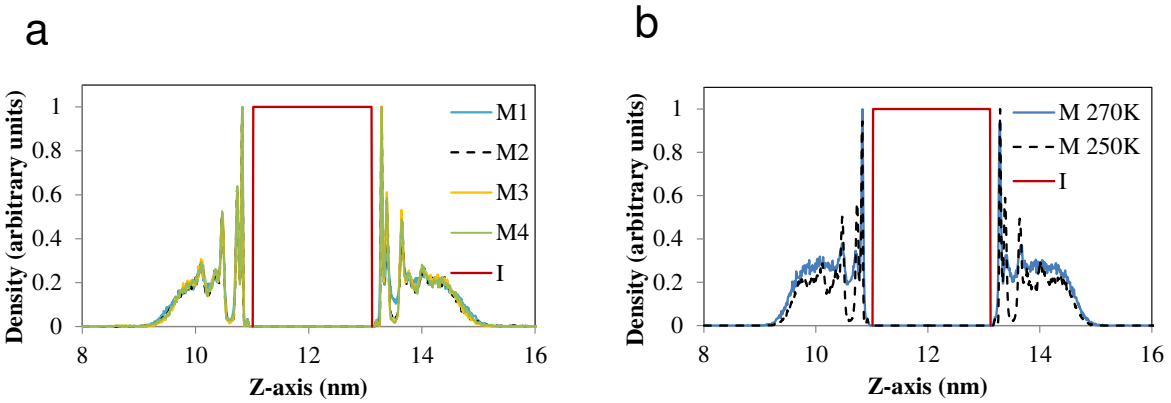

Figure 2.2. Average density profiles of 'mobile' (M) and 'immobile' (I) water molecules in air/ice systems. (a) Density profiles of 'mobile' water molecules at 270 K, averaged over the following time periods: M1 = 2 to 3 ns; M2 = 4 to 5 ns; M3 = 8 to 9 ns; M4 = 11 to 12 ns (3 ozone and 15 naphthalene molecules at each air/ice interface). (b) Density profiles of 'mobile' water molecules at 270 K and 250 K (3 ozone and 2 naphthalene molecules at each air/ice interface)

In Figure 2.3 we present the density profile of the mobile water molecules for fixed number of ozone molecules and varying number of naphthalene molecules at the air/ice interface (Fig. 2.3a), and for varying number of ozone molecules while keeping constant the number of naphthalene molecules (Fig. 2.3b). Important changes in the density profile of the

mobile water molecules are observed when the number of naphthalene molecules at the air/ice interface increases while keeping the number of ozone molecules constant. In contrast, variations in the number of ozone molecules while keeping constant the number of naphthalene molecules produce negligible variations in the density profiles of the mobile water molecules. These observations suggest that the thickness of the QLL experience a significant reduction with increasing concentrations of naphthalene at the air/ice interface, whereas changes in the ozone concentration at this interface do not affect significantly the thickness of the QLL. However, this effect seems to occur only for sub-monolayer coverage of naphthalene; in Figure 2.5, the density profiles of the mobile water molecules seem to be unaffected when the concentration of naphthalene changes from 15 to 45 molecules per interface (the former is close to monolayer surface coverage).

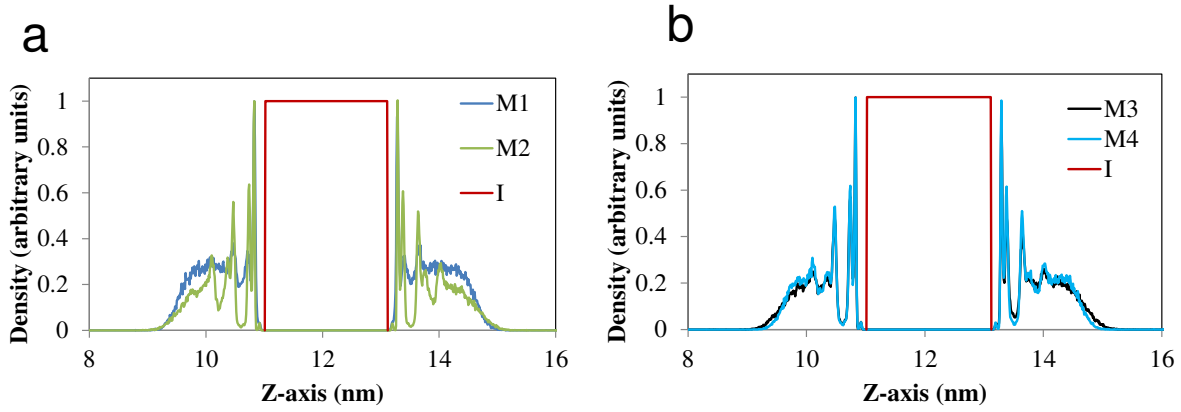

Figure 2.3. Density profiles of mobile (M) and immobile (I) water molecules in air/ice systems at 270 K, for: (a) constant concentration of ozone (3 molecules per interface) and varying concentrations of naphthalene (M1 = 2 molecules of naphthalene, M2 = 45 naphthalene molecules per interface); and (b) constant concentration of naphthalene (15 molecules per interface) and varying concentrations of ozone (M3 = 3 ozone molecules, M4 = 200 ozone molecules per interface).

The reasons behind why increases in naphthalene surface concentration at sub-monolayer coverage promotes freezing of the mobile water molecules are not clear to us (it might be an effect of naphthalene-water interactions), and should be investigated in

follow-up studies. In contrast, the results shown in Figure 2.3 suggest that changes in the ozone concentration at this interface do not affect significantly the thickness of the QLL.

2.3.3. PMF of Naphthalene and Ozone in Air/ice Systems

In Figure 2.4 we present the PMF obtained by moving one naphthalene or one ozone molecule from the gas phase into the layer of mobile water molecules in air/ice systems at 270 K. The PMF profiles exhibit deep minima at the air/ice interface, suggesting that both naphthalene and ozone prefer to be adsorbed at the air/ice interface, rather than staying in the gas phase or being dissolved in the QLL.

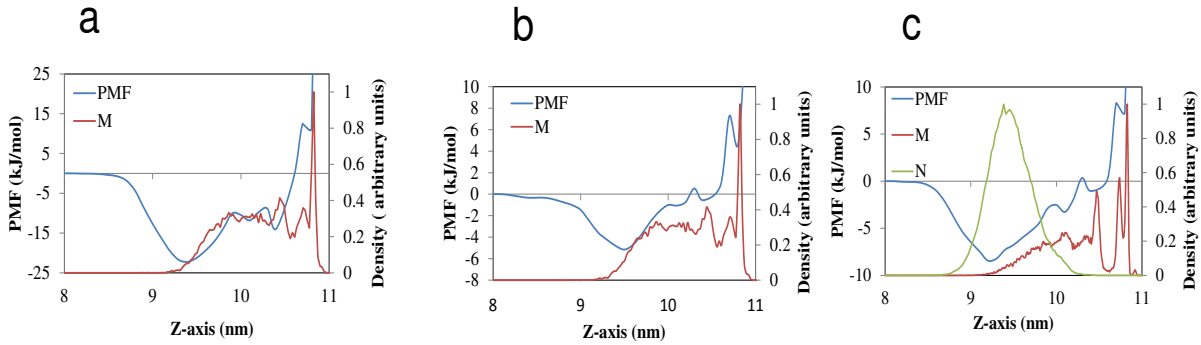

Figure 2.4. PMF on air/ice systems at 270 K. (a) One naphthalene molecule moving into a bare air/ice interface. (b) One ozone molecule moving into a bare air/ice interface. (c) One molecule of ozone moving into an air/ice interface coated with 15 naphthalene molecules. The density profiles of mobile water (M) and naphthalene (N) molecules are also depicted.

In addition, all PMF profiles show a very sharp increase as the molecule of naphthalene or ozone is dragged near the 'mobile' water molecules that froze during the equilibration period of the simulations (as signaled by the sharp peaks observed in the density profiles in Fig. 2.3). This result suggests that incorporation of ozone or naphthalene into the crystalline structure of ice is thermodynamically unfavorable. The minima in the PMF for naphthalene and ozone at the bare air/ice interface are -22.2 kJ/mol and -5.1 kJ/mol. In Figure 4c we show the PMF of one ozone molecule moving into an air/ice interface coated with 15 naphthalene

molecules. The minimum in the PMF in this case is -8.4 kJ/mol, which is 65% deeper than the minimum observed for a bare air/ice interface. This result suggests that the surface adsorption of ozone on air/ice interfaces is enhanced by the presence of naphthalene molecules at the interface. From the results shown in Figure 2.4, it is not possible to obtain an accurate estimation of the free energy of hydration of naphthalene and ozone in the QLL, mainly because the thickness of the QLL in our simulated systems does not allow the PMF to converge to a stable value (in contrast to what was observed for air/water systems, see Figure 1).

2.3.4. Residence Time of Phenanthrene and Naphthalene Molecules in Bulk QLL

We carried our conventional (i.e., unbiased) MD simulations of air/ice and air/water systems considering a total of 2 phenanthrene and naphthalene molecules per interface (no ozone molecules), in order to estimate the fraction of the simulation time that the phenanthrene and naphthalene molecules spend at the interface, as well as the fraction of time they spend inside the QLL. We arbitrarily defined the interface as the point where the density of the mobile water molecules reaches a value of 900 kg/m^3. At 270 K, the naphthalene molecules spend 9.9% of the total simulation time within the bulk of the QLL, as compared to 4.5% at 250 K. For phenanthrene resident time was 7.2% at 267 K and 4.8% at 260 K. Visual inspection of video clips of the time evolution of our systems suggest that, within the total simulated time, phenanthrene and naphthalene was not incorporated into the lattice structure of ice. Rather, phenanthrene and naphthalene was only adsorbed onto the surface and bulk of the QLL in air/ice systems. These results suggest that surface adsorption is the dominant mechanism for uptake of naphthalene from vapor phase on thin ice films as

opposed to dissolution in the bulk of the QLL. With decreasing temperature, phenantherene and naphthalene exhibits an increasing tendency to remain at the surface, suggesting that as the temperature drops, surface adsorption becomes more dominant than dissolution in the bulk QLL. This tendency of phenanthrene and naphthalene to predominantly remain at the surfaces has an impact on surface processes, such as heterogeneous reactions between naphthalene and incoming ROSs. For example, Kahan *et al.*[41] indicate that the rate of anthracene photolysis at air/ice interfaces is five times larger than those observed when anthracene is within an ice matrix or in room-temperature aqueous solution. Furthermore, the observation that phenanthrene and naphthalene was only adsorbed at the air/ice interface also agrees with a recent study[127] that concluded that terpenoids have a strong tendency to be adsorbed on ice surfaces, as opposed to be absorbed onto the crystalline structure of ice. In particular, steric effects were argued to hinder the absorption of relatively large terpenoids onto the crystalline structure of ice.

2.3.5. Effects of Varying Concentrations of Naphthalene and Ozone Molecules at the Air/ice Interface

Looking again at Figures 2.4b and 2.4c, it can be observed that the PMF minimum for ozone is slightly displaced towards the gas phase and away from the bulk of the mobile water molecules when naphthalene molecules coat the air/ice interface. Furthermore, in a naphthalene-coated air/ice interface (Figure 2.4c), the *z*-coordinate at which the PMF minimum for ozone is observed is slightly smaller than the *z*-coordinate at which the density profile of naphthalene reaches its maximum. These observations suggest that when a significant number of naphthalene molecules are present at the air/ice interface, ozone molecules have a tendency to adsorb on top of the already adsorbed naphthalene molecules,

rather than adsorbing directly on the air/ice interface. This observation suggests that when the surface concentration of naphthalene is significant, it can hinder the surface adsorption of ozone and its further dissolution in the bulk of the QLL. Therefore, in what follows we study in detail how varying concentrations of ozone and naphthalene affect properties such as local density profiles, orientation of the molecules and interactions between ozone and naphthalene in the air/ice interface. These properties are relevant because they affect the chemical reactions between PAHs and ROSs that can take place at atmospheric air/ice interface.

(a) Varying Number of Naphthalene Molecules, Constant Ozone Molecules per Air/ice Interface

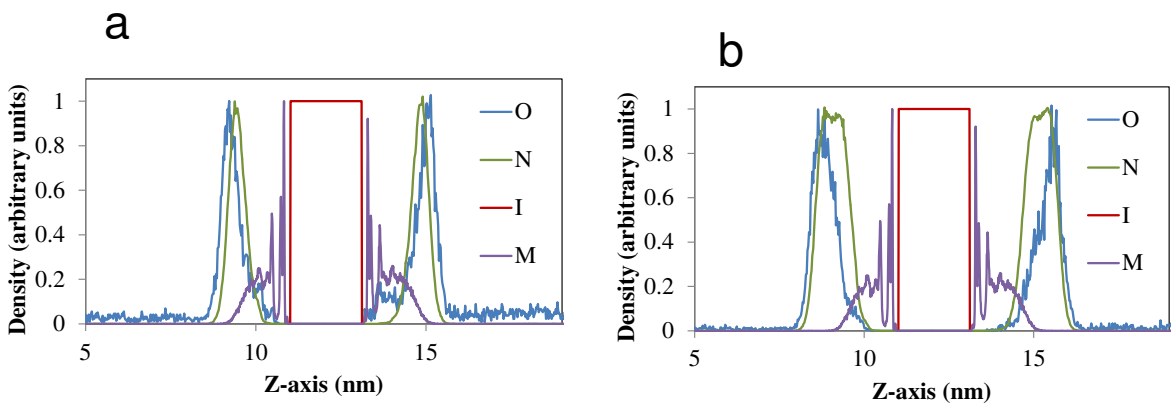

Figure 2.5. Density profiles at 270 K on air/ice systems, for: (a) 15 naphthalene and 3 ozone molecules per air/ice interface, (b) 45 naphthalene and 3 ozone molecules per air/ice interface. Letters O, N, I and M represent ozone, naphthalene, immobile water molecules (ice slab) and mobile water molecules.

In Figure 2.5 we present density profiles of naphthalene, ozone, mobile and immobile water molecules in air/ice systems at 270 K, for two concentrations of naphthalene, 15 and 45 molecules per air/ice interface (the former is close to monolayer surface coverage, while the latter is beyond monolayer coverage for the area size of our simulation box. Side views of representative simulation snapshots of these systems are depicted in Figure 2.6. The density profiles presented in Figure 2.5 indicate that both naphthalene and ozone prefer to stay at the air/ice interface, as opposed to remaining in the gas phase or entering the bulk of the ice

phase. Comparing the positions of the peaks in the densities of naphthalene and ozone, it is observed that naphthalene is closer to the mobile water molecules forming the QLL. This observation is consistent to the PMF results shown in Figure 2.4, and indicates that when naphthalene molecules are present at the air/ice interface, the molecules of ozone tend to remain on top of the naphthalene film (although there is significant overlap between the density profiles of naphthalene and ozone, see Fig. 2.5). These trends were consistently observed when the number of naphthalene molecules per interface was varied between 2 and 45.

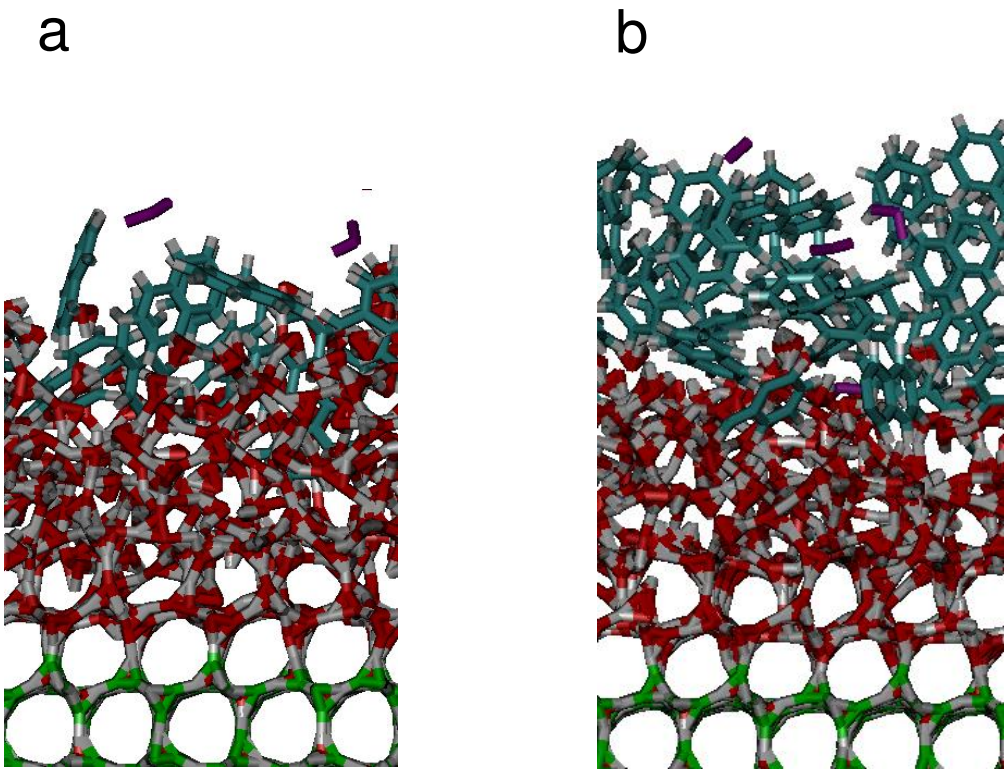

Figure 2.6. Side view of representative simulation snapshots of naphthalene and ozone on air/ice interfaces at 270 K. (a) System with 15 naphthalene and 3 ozone molecules per air/ice interface. (b) System with 45 naphthalene and 3 ozone molecules per air/ice interface. Naphthalene = dark cyan and gray; ozone = purple; mobile water molecules = red and gray; immobile water molecules = green and gray

Visual inspections of simulation snapshots (Fig. 2.6) and video clips of the time evolution of our systems suggest that ozone molecules tend to penetrate into the naphthalene

films at the air/ice interface; however, the ozone molecules do not remain inside the naphthalene films for long periods of time. These observations agree with the trends shown in the density profiles of Figure 2.5. Since ozone molecules mostly prefer to stay on top of the naphthalene film, most of the contacts between naphthalene and ozone (which could lead to chemical reactions between them) should take place in this region. Nevertheless, overall contacts between nearby naphthalene and ozone molecules could occur in several ways: 1. Between naphthalene and ozone molecules that are both in direct contact with the mobile water molecules in the QLL, 2. Between naphthalene molecules that are in direct contact with the mobile water molecules, and ozone molecules that are close to these naphthalene molecules, but are not in direct contact with the mobile water molecules,3. Between naphthalene molecules that are not in direct contact with the mobile water molecules, and ozone molecules which are in direct contact with these mobile water molecules and 4. Between naphthalene and ozone molecules that are not in direct contact with the mobile water molecules. The density profiles shown in Fig. 2.5 suggest that at low concentrations of naphthalene, case (2) would be the most dominating, although in principle all cases could be observed. For high concentrations of naphthalene, again all four possible scenarios could take place but case (4) would be the most dominating as the layer of naphthalene would become thicker and ozone tends to lie on top of the naphthalene film. For higher concentrations of naphthalene molecules at the air/ice interface, we did not observe fluctuations in the density profiles (Fig. 2.5), which suggests that naphthalene remains as a liquid-like phase and does not crystallize on the air/ice interface.

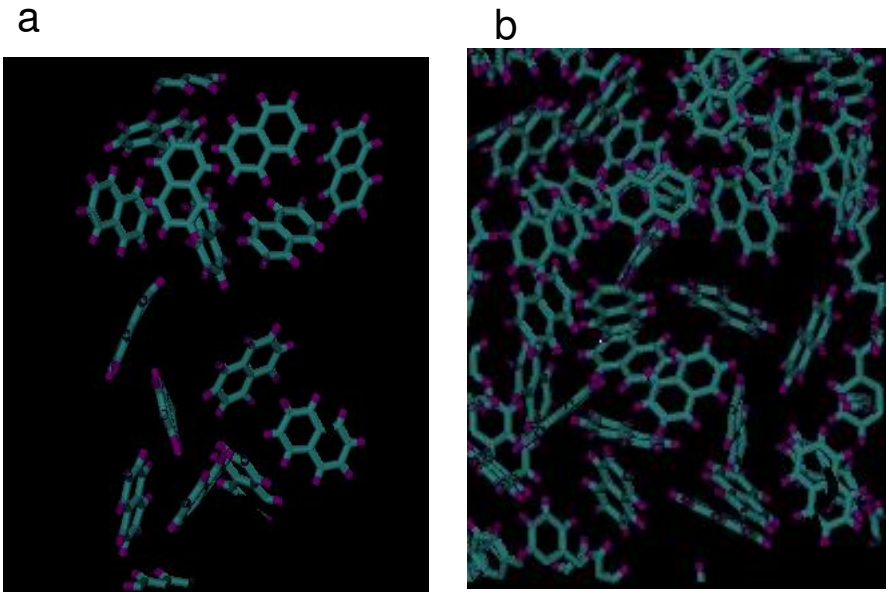

Figure 2.7. Top views of representative simulation snapshots of systems of naphthalene and ozone on air/ice interfaces at 270 K. (a) System with 15 naphthalene molecules per interface. (b) System with 45 naphthalene molecules per interface. black background represents ice surface

Figure 2.7 depicts top views of simulation snapshots of air/ice systems. These snapshots suggest that naphthalene molecules tend to make larger aggregates as the number of naphthalene molecules at the air/ice interface increases, due to the strong interactions between naphthalene molecules. Previous studies[36, 38] suggest that naphthalene molecules have a larger tendency to interact with each other and form clusters at the air/ice interface as compared to the air/water interface, which in turn affect the reactivity of PAHs with ROSs at these interfaces.

The orientation of naphthalene molecules at the air/ice interface was also monitored in our MD simulations. This orientation is relevant to the reactions between naphthalene and oxidizing species (e.g., ozone and hydroxyl radicals), because the reactivity of ozone with naphthalene depends on a detailed interaction between these two molecules. In Figure 2.8a we present the angle distribution between the aromatic rings of naphthalene and the air/ice interface at different concentrations of naphthalene. An angle of 0° indicates that the rings of

the naphthalene molecule remain flat with respect to the interface, and ±90° represents the naphthalene molecule lying perpendicular to the interfaces.

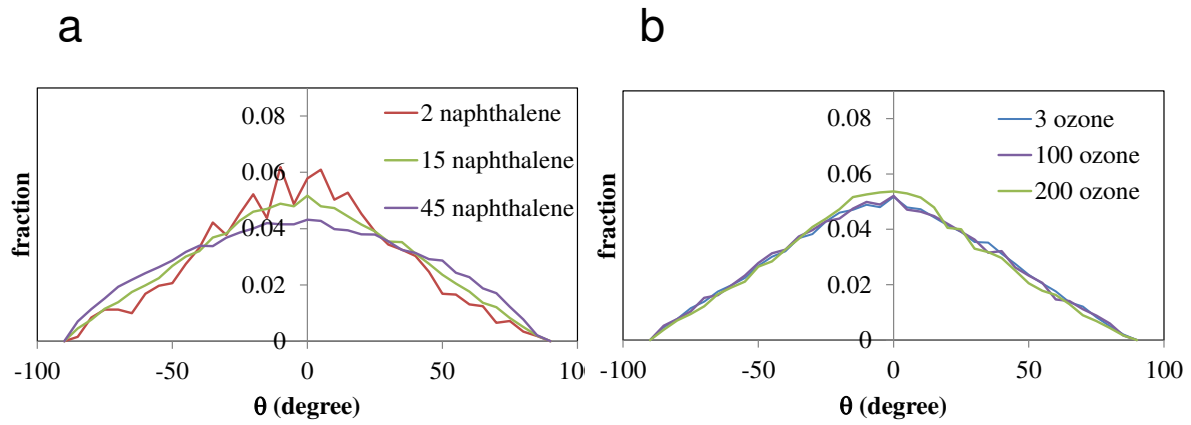

Figure 2.8. Average angle distributions of naphthalene molecules at air/ice interface at 270 K. (a) For constant 3 ozone molecules and varying number of naphthalene molecules per air/ice interface. (b) For constant 15 naphthalene molecules and varying number of ozone molecules per air/ice interface.

From Figure 2.8, it can be observed that in all cases (2 to 45 naphthalene molecules per air/ice interface) the naphthalene molecules prefer to lie flat at the interfaces with air. However, naphthalene retains a considerable ability to rotate around its molecular axis, as signaled by the wide distribution of angles observed. From Figure 2.8, the angle distribution of naphthalene gets narrower as the number of naphthalene molecules decreases while keeping a constant number of ozone molecules, indicating that naphthalene has a lesser preference to be flat at larger concentrations at the air/ice interface (see also Fig. 2.6b). At low concentrations of naphthalene at the air/ice interface, interactions between naphthalene molecules will be minimal and naphthalene will interact primarily with water molecules at the QLL, and therefore naphthalene molecules prefer to lie flat at the air/ice interface to maximize favorable interactions with water molecules. When the naphthalene concentration is high at the air/ice interface, naphthalene molecules tend to make larger aggregates by readily interacting with each other.

We also examined the effect of temperature on the orientation of naphthalene at varying concentrations of this species. Our results (not shown for brevity) indicate that when the concentration of naphthalene is low, these molecules show a larger preference to lie flat at a temperature of 250 K, as compared to what was observed at 270 K. In contrast, for high concentrations of naphthalene, the angular distributions were similar at 270 K and 250 K. These observations indicate that at low concentrations of naphthalene, the effect of temperature on the orientation of naphthalene is more significant as compared to what is observed at high concentrations of naphthalene at the air/ice interface. We also calculated the average mean square displacement (MSD) value of naphthalene molecules at the air/ice interface on xy plane (also not shown for brevity). We did not observe any significant changes in the values of the MSD as the concentration of naphthalene at the air/ice interface was varied at constant temperature. The trends observed in Figs. 2.5-8 for a temperature of 270 K are consistent with those observed at a temperature of 250 K.

(b) Varying Number of Ozone Molecules, Constant Naphthalene Molecules per Air/ice Interface

Figures 2.8b, 2.9 and 2.10 represent properties of the naphthalene film (15 naphthalene molecules per air/ice interface) as the number of ozone molecules is varied from 3 to 200 molecules per interface. The results shown in Figure 8b suggest that the orientation of naphthalene at the interface seems to be unaffected by the concentration of ozone molecules. At low ozone concentrations, the ozone molecules prefer to stay on top of the naphthalene molecules, as seen in the density profiles (Figure 2.9a) and simulation snapshots (Figure 2.10a).

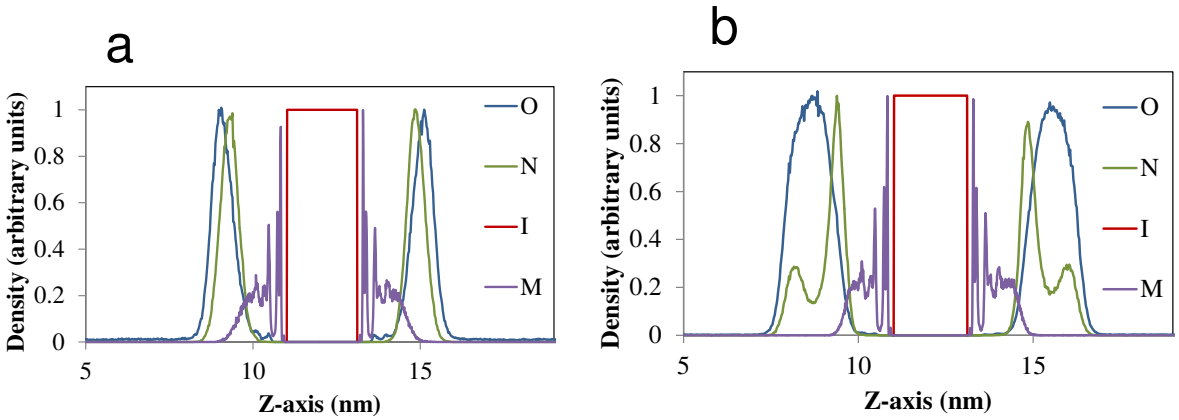

Figure 2.9. Density profiles of naphthalene and ozone molecules at 270 K on air/ice systems: (a) 15 naphthalene and 50 ozone molecules per air/ice interface, (b) 15 naphthalene and 200 ozone molecules per air/ice interface. Letters O, N, I and M represents ozone, naphthalene, immobile and mobile water molecules.

As the ozone concentration at the interface increases to larger values, most of the naphthalene molecules still prefer to stay close to the mobile water molecules in the QLL, but a significant fraction of the naphthalene molecules spend a considerable amount of time away from direct contact with these mobile water molecules, as indicated by the secondary small peaks in the density profiles of naphthalene (Figure 2.9b), and by simulation snapshots (Figure 2.10b). Visual inspection of video clips of the simulation trajectories indicates that naphthalene molecules spend a significant time inside the thicker layer of ozone observed at larger concentrations of this species. We did not observe any significant changes in the MSD of the molecules of naphthalene in the *xy* plane as the concentration of ozone was varied (results not shown for brevity). Among the four possibilities discussed previously in §2.3.5.(a). for the overall contacts between naphthalene and ozone molecules, all four possibilities could take place at low or high concentrations of ozone; case (2) would be the most dominant in the former scenario, whereas in the latter scenario it is not clear which case would be the most dominant

(c) Number of Contacts between Naphthalene and Ozone Molecules

The reactions between PAHs and ROSs at the air/water and air/ice interface have been proposed to occur via the Langmuir-Hinshelwood mechanism,[17, 18, 27, 37, 128-131] in which the ozone and naphthalene molecules adsorb simultaneously onto the air/ice or air/water interface and then interact and react at the surface. Another possibility is the Eley-Rideal mechanism,[128] in which ozone adsorbs directly on top of naphthalene already adsorbed at the interface and then reacts. Most experimental studies of PAHs and ROSs on air/water and air/ice interfaces have fitted their data to the equations of the Langmuir-Hinshelwood mechanism.[17, 18, 27, 37, 128-131] In this work, we have followed the study of Vácha *et al.*[29] and monitored the number of contacts between molecules of naphthalene and ozone at the air/ice interface, but now considering a wider range of concentrations for these two species. These contacts could probably lead to chemical reactions between naphthalene and ozone, and we can assume that the reaction rate is proportional to the number of these contacts.

In the first system we considered, we kept constant the number of molecules of naphthalene (15 molecules per air/ice interface) and monitored the number of contacts while varying the number of ozone molecules. Afterwards, we kept constant the number of molecules of ozone (3 molecules per air/ice interface) and monitored the contacts while varying the number of naphthalene molecules. These results are shown in Figure 2.11. When the number of ozone molecules was held constant, the number of contacts showed a linear relationship to the number of naphthalene molecules at the air/ice interface (Figure 2.11a). However, when the naphthalene concentration was held constant, for all systems we observed

a linear relationship at low ozone concentrations and a saturation effect when the ozone concentration was further increased at the air/ice interface (Figure 2.11b).

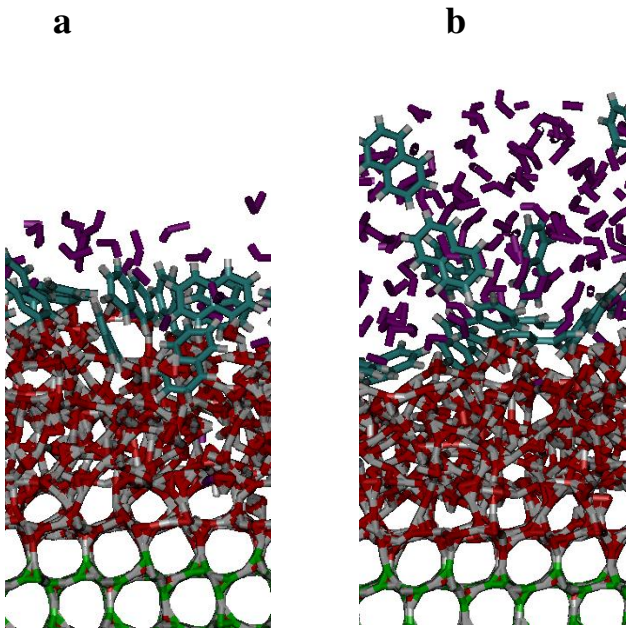

Figure 2.10. Side views of representative simulation snapshots of naphthalene and ozone adsorption on the air/ice interface at 270 K, for systems containing (a) 15 naphthalene and 50 ozone molecules per air/ice interface; and (b) 15 naphthalene and 200 ozone molecules per air/ice interface. Naphthalene = dark cyan and gray; ozone = purple; mobile water molecules = red and gray; immobile water molecules = green and gray.

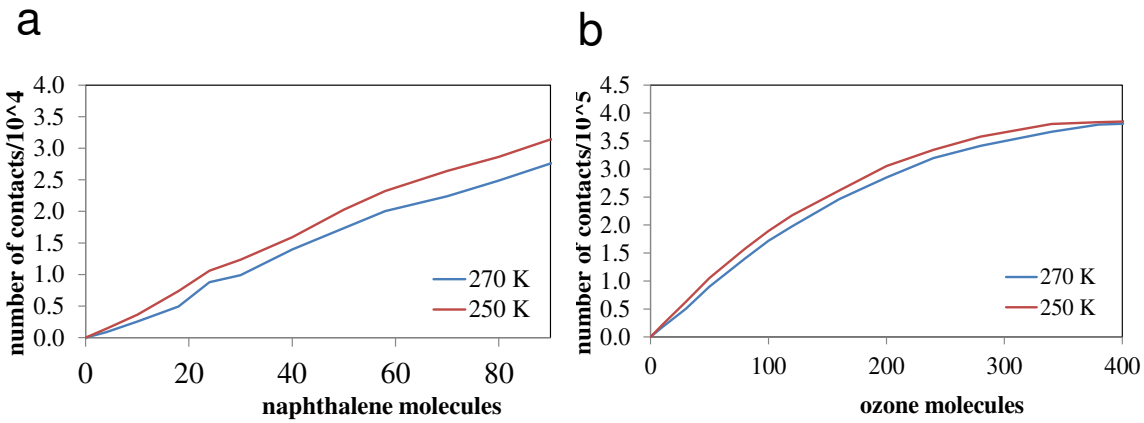

Figure 2.11. (a) Number of contacts with respect to number of naphthalene molecules when number of ozone molecules is constant (3 molecules per interface) on air/ice at 270 K and 250 K (b) Number of contacts with respect to number of ozone molecules when number of naphthalene molecules is constant (15 molecules per interface) on air/ice at 270 K and 250 K.

There was no significant difference in number of contacts between naphthalene and ozone molecules as the temperature decreases. Our results for air/ice systems are in

agreement with those of Vácha *et al.*[29] at low concentrations of ozone (up to 24 ozone molecules). However, the plateau in the number of contacts (Fig. 2.11b) was not observed in the work of Vácha *et al.*,[29] possibly because they only considered systems of 32 molecules of naphthalene and up to 24 ozone molecules. Based on the nonlinear relationship between the number of contacts and ozone concentration for fixed naphthalene concentration at the air/ice interface (Figure 2.11b), we can assume that the rate of reaction has a nonlinear relationship to surface ozone concentration. As discussed before, in our study both naphthalene and ozone are adsorbed at the air/ice interface forming films that are a few nm thick during the simulations (Figs. 2.5 and 2.9). Furthermore, the contacts taking place between naphthalene and ozone molecules could occur at the air/ice interface in several ways (cases 1-4 in §2.3.5.(a) and §2.3.5.(b)). Therefore, our simulation results do not provide any firm evidence supporting or ruling out either of the two possible reaction mechanisms. Further studies are needed in order to come to firm conclusions about the reaction mechanism between naphthalene and ozone at atmospheric air/ice interfaces

2.3.6. Phenanthrene Orientation at the Air/ice and Air/water Interfaces

From Figure 2.12, we observe that phenanthrene molecules prefer to adopt a flat orientation at the interface with considerable angular flexibility (ability to rotate around the molecular axis). For the case of phenanthrene at the air/water interface, the average angular distribution was found to be very similar for the two temperatures considered (296 K and 280 K), with a somewhat narrower distribution found for the lower temperature. This result suggests that varying temperatures have no significant effects on the orientation of phenanthrene at the air/water interface.

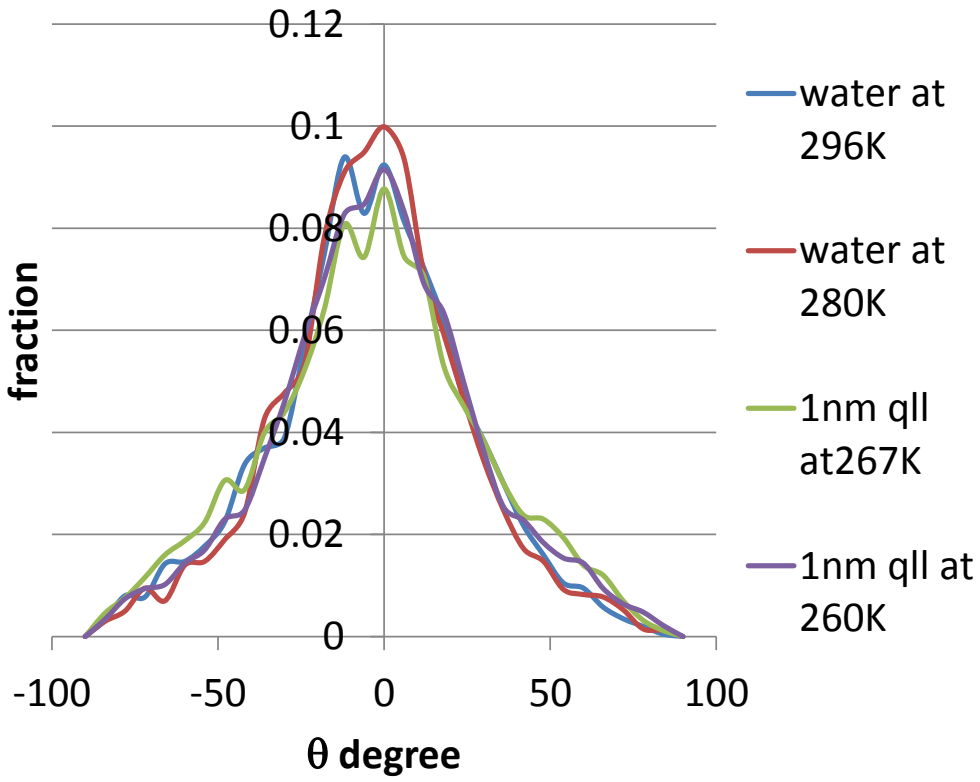

Figure 2.12. Average distribution of the angle between the aromatic rings of the phenanthrene molecules and the air/water or air/ice interface at different temperatures

For systems of phenanthrene at the air/ice interface, we observe that with changing temperature (267 K and 260 K), the angle distributions of phenanthrene did not change significantly with temperature, with a somewhat narrower distribution found for the lower temperature. The angle distributions were similar to those observed for the air/water interface.

2.4. Concluding Remarks

MD simulations were carried out to investigate the adsorption of phenanthrene, naphthalene and ozone on air/ice interfaces. We first verified that our combination of force fields (TIP5P[112] for water and the force fields used by Vácha *et al.*[20, 28, 29] for naphthalene and ozone) were able to reproduce experimental free energies of hydration and previous simulation results. The thickness of the QLL formed by 'mobile' water molecules in

our simulations reach a stable value after equilibration time period. As expected, the simulated thickness of the QLL decreases with temperature, but also decreases with increasing concentrations of naphthalene at the air/ice interface. However, this effect seems to occur only for sub-monolayer coverages of naphthalene; increasing the surface concentration of naphthalene beyond monolayer coverage seems to have negligible effect in the thickness of the QLL. Similarly, changes in the ozone concentration do not affect the thickness of the QLL. Surface adsorption was found to be the predominant mechanism for the uptake of phenanthrene, naphthalene and ozone on ice films. Our results for naphthalene and ozone in air/ice systems show deep free energy minima for these two species at the air/ice interface (-22.2 and -5.1 kJ/mol); these values are comparable to those determined for air/water interfaces (-26.4 and -4.9 kJ/mol). Our results also suggest that incorporation of ozone or naphthalene into the crystalline structure of ice is thermodynamically unfavorable. When the air/ice interface is coated with naphthalene, the free energy minimum observed for ozone is deeper than that observed for ozone in a bare air/ice interface, indicating that surface adsorption of ozone is enhanced by the presence of naphthalene molecules at the air/ice interface. Furthermore, ozone tends to adsorb on top of the naphthalene film; although significant penetration of ozone into this film is also observed, the ozone molecules do not remain inside the naphthalene film for long periods of time. Larger aggregates of naphthalene molecules were observed as the concentration of naphthalene increases at the air/ice interface. Naphthalene and phenanthrene molecules tend to adopt a flat orientation on the air/ice interface; less variation in the orientation was observed for lower concentrations of naphthalene at a fixed concentration of ozone. In contrast, variations in the ozone

concentration do not affect significantly the orientation of naphthalene at the air/ice interface. However, as the concentration of ozone increases, most of the naphthalene molecules still prefer to stay close to the mobile water molecules in the QLL, but a significant fraction of the naphthalene molecules spends a considerable amount of time inside the thicker layer of ozone. We also analyzed the number of contacts between naphthalene and ozone at the air/ice interface upon variations in the concentrations of these two species. These contacts were assumed to be proportional to the reaction rate between these two species. When the number of ozone molecules was held constant, the number of contacts showed a linear relationship to the number of naphthalene molecules. However, when the naphthalene concentration was held constant, for all systems we observed a linear relationship at low ozone concentrations and a plateau in the number of contacts is reached at high ozone concentrations. Our simulation results do not provide any firm evidence supporting or ruling out either the Langmuir-Hinshelwood or the Eley-Rideal mechanism of reaction between naphthalene and ozone.

CHAPTER 3 ADSORPTION OF NAPHTHALENE AND OZONE ON ATMOSPHERIC AIR/ICE INTERFACES COATED WITH SURFACTANTS: A MOLECULAR SIMULATION STUDY[‡]

Contents of this chapter have already been published (T. P. Liyana-Arachchi, K. T. Valsaraj and F. R. Hung, Adsorption of naphthalene and ozone on atmospheric air/ice interfaces coated with surfactants: A molecular simulation study. J. Phys. Chem. A 2012, 116, 2519-2528). In this chapter, we report molecular dynamics (MD) results of the adsorption of gas-phase naphthalene and ozone on to air/ice interfaces coated with different surfactant species (1-octanol, 1-hexadecanol or 1-octanal). The main objective of this study was to investigate the adsorption of gas-phase naphthalene and ozone on atmospheric surfactant coated air/ice interfaces and investigate the air/ice interfacial properties under the influence of surfactants. The rest of this chapter is structured as follows. Section 3.1 is the introduction. Section 3.2 contains a description of our computational models and methods. In Section 3.3 we present results and discussion and in Section 3.4 we summarize our main findings.

3.1. Introduction

Snow or ice represents an important environment in the atmosphere and on the earth's surface due to the fact that they play an important role in the storage and reactions of environmentally relevant trace gases.[2, 132] Surface processes, such as adsorption and chemical reactions, are enhanced at snow and ice surfaces due to their large surface area.[2] Polycyclic aromatic hydrocarbons (PAHs) have been detected in snow and ice in both urban and remote areas.[81-94] PAHs are known to have carcinogenic and mutagenic effects,[14] and can also undergo oxidation and nitration reactions with reactive oxygen species

[‡] Reprinted with permission of J. Phys. Chem. A 2012, 116, 2519-2528

(ROSs)[133, 134] to yield compounds such as oxy- and nitro-PAHs which are even more toxic.[14, 16, 133, 134] Heterogeneous reactions of PAHs on snow and ice have faster kinetics compared to those observed in homogenous gas phases.[12, 13, 133] As a result, it is important to fundamentally understand the adsorption process as well as the structural and dynamical properties of PAHs and ROSs at the air/ice interface, because these properties affect the reaction rate between these compounds at these interfaces. Although PAHs are hydrophobic, the air/ice interface can uptake significant amounts of these compounds. In our previous molecular dynamics (MD) studies,[135] we observed a deep free energy minimum for adsorption of naphthalene and ozone at air/ice interfaces, and the presence of naphthalene at the air/ice interfaces enhanced the adsorption of ozone to the air/ice interface. A large fraction of phenanthrene and naphthalene molecules tend to remain adsorbed at the air/ice interface, rather than dissolved into the quasi-liquid layer (QLL) or incorporated into the ice crystals.[135, 136] These observations have implications in the heterogeneous reactions between PAHs and ROSs at the air/ice interface.

Surfactant-like molecules can significantly affect the interfacial properties of PAHs and ROSs when adsorbed at air/ice interfaces. Atmospheric water and ice films typically contain surfactants such as humic and fulvic acids like species.[21, 23-26, 48, 137] Organic species can be found in samples of water droplets and snowflakes from both urban and rural areas, although the concentration is found to be much higher near cities.[138-140] Surface-active organic molecules such as alcohols, acids, amines, carbonyls, etc., are important contributors to the total organics found on atmospheric air/water interfaces.[48] The molecular composition of the organic film on atmospheric water and ice surfaces varies drastically

depending on the source, altitude and latitude of the measurements, which leads to difficulties in analytical sampling and analysis.[141] For example, about 40%-50% of organic compounds in fog water could not be fully characterized in the experimental analysis of Raja *et al.*;[48] these compounds were assumed to be high molecular weight humic-like substances. The presence of such organic films could alter the interfacial properties of ice surfaces, and could cause changes in heterogeneous reactivities at these interfaces. Some studies show that the uptake of PAHs at air/water and air/ice interfaces is further enhanced by the presence of films composed of organic compounds at air/water and air/ice interfaces.[129, 142, 143]

In this work we studied how the adsorption of naphthalene and ozone on air/ice interfaces is affected by the presence of varying concentrations of surfactant species at these interfaces. We also investigated how the structural properties of these surfactant species change with variations in their concentrations. We also investigated how surfactants affect the structural and dynamical properties of naphthalene at the surfactant-coated air/ice interfaces. All of the above investigations were done using three different surfactant models (1-octanol, 1-hexadecanol and 1-octanal). We selected model organic surfactant compounds with different organic functional groups that have either been found, or could be expected to exist on environmental ice surfaces.[33, 144] This was done in order to understand if functional groups in the surfactants have any effect on the interfacial properties, as well as to probe how different functional groups affect the adsorption of PAHs and ROSs at the air/ice interface.

3.2. Simulation Details

In this study we have used the same models for water, naphthalene and ozone that we used in our previous studies of adsorption of phenanthrene, naphthalene and ozone on bare

air/ice interfaces.[135, 136] Water was modeled using the TIP5P water model,[112] and naphthalene and ozone were modeled using the force fields and parameters from the previous work of Vácha *et al.*[20, 145, 146] The force fields for naphthalene and ozone were parameterized by Vácha *et al.*[20, 145, 146] to reproduce the free energy of solvation of these species in combination with the SPC/E water model.[115] However, in our previous study[135] we determined from calculations of the potential of mean force that these force fields for naphthalene and ozone, when used in combination with the TIP5P water model, can also reproduce the experimental values of the free energies of hydration of these species. We used the OPLS-all atom force field[147] to model the surfactant species considered in this study (1-octanol, 1-hexadecanol and 1-octanal).

Classical molecular dynamics (MD) simulations were conducted using the GROMACS software[116] in the NVT ensemble (constant number of molecules, volume and temperature). For simulations on the surfactant-coated air/ice interfaces, we considered orthorhombic simulation boxes of dimensions 27 Å × 31.4 Å × 240 Å (x, y and z respectively). Periodic boundary conditions were applied in all three directions. For the simulations of naphthalene and ozone on surfactant-coated air/ice interfaces, we placed 576 TIP5P water molecules arranged into 5 bi-layers of hexagonal ice I_h in the middle of the simulation box, creating an ice slab. These water molecules were fixed in space. Following previous studies,[117, 135, 136, 148] we placed two thin layers, both formed by 768 TIP5P 'mobile' (i.e., not subject to any motion constraints) water molecules on both sides of the immobile ice slab. Part of these 'mobile' water molecules that are near the immobile ice slab gradually freeze during the equilibration part of our simulations.[135] The 'mobile' water molecules that remain

unfrozen intend to mimic the QLL of water that forms at the air/ice interface. Following our previous work, [135, 136] we have considered an ice slab in which the basal plane (0001 face) of hexagonal ice I_h is in contact with the QLL. The ice slab and the two QLLs of water form two interfaces with vacuum, which intend to mimic two atmospheric air/ice interfaces. Up to 18 molecules of 1-octanol, 1-hexadecanol and 1-octanal, and up to 2 naphthalene molecules and 1 ozone molecule per air/ice interface were considered in our simulations. The simulated 'overall' concentrations of these species (equal to the number of molecules of the species of interest divided by the total volume of the vacuum regions) are much larger than the reported 'overall' concentration of carbonyls, alcohols, PAHs and ozone in air, which can range between 0.3922 – 1.0800 mg/cL (carbonyls), 0.3339 – 0.1040 mg/cL (alcohols), 0.00053 – 0.03224 mg/cL (PAHs) and 80 – 100 $\mu g/m^3$ (ozone) in Houston and Baton Rouge (in the Texas-Louisiana Gulf Coast corridor).[12, 48] However, and due to the small sizes of our simulated systems, the concentrations of the species used in our study should be viewed as 'surface' concentrations rather than 'overall' atmospheric concentrations (the reported values listed above). The experimental surface concentrations of these species are different from the atmospheric concentrations and are more difficult to define precisely, as the surface concentrations depend on the partition coefficients of each species between gas phase and the air/ice interface (and most of these partition coefficients are not readily available for our specific systems). In order to analyze concentrations as low as atmospheric concentrations and obtain statistically-relevant results from MD simulations, it would be necessary to consider much larger system sizes which are beyond the current computational resources.

Another way would be to determine the adsorption isotherm of each species, but this study is beyond the scope of the present work.

The initial configurations of each simulated system were first relaxed using the steepest descent energy minimization method. A time step of 1 fs was used in all our MD simulations and data were collected every 10 ps. Bond lengths were constrained using the LINCS algorithm.[119] Temperature coupling was done using the velocity-rescaling algorithm of Parrinello *et al.* [120, 121] with a coupling constant of 0.1 ps. A cut-off distance of 0.9 nm was used for the Lennard-Jones interactions. The particle-mesh Ewald (PME) method[122] was used with a cutoff of 0.9 nm and a grid spacing of 0.12 nm in order to account for long-range Coulombic interactions.

In this study we performed both potential of mean force (PMF) calculations and conventional MD simulations. In the former series of calculations, we determined the free energy profile associated with moving one molecule of naphthalene or ozone from the gas phase into the air/ice interface. As in our previous paper,[135] the constraint force method[123-125] was used in these simulations. In this method, the z-distance between the center of mass of naphthalene or ozone molecule and the center of mass of the ice slabs is constrained. The force that needs to be applied to the naphthalene or ozone molecule in order to keep this distance fixed is then calculated in the simulation. This procedure was done using increments of 1 Å in multiple simulations along the z-axis. The potential of mean force (PMF) can then be obtained from integration of this force,[123-125] taking as reference point the free energy of the molecule of interest in the gas phase, which was assigned a zero value. To determine the PMF of naphthalene and ozone on surfactant-coated air/ice systems, each of

the simulations were run for ~ 6 ns, of which ~2 ns were used for equilibration and ~ 4 ns were used to average the forces at each value of *z*-distance considered. PMF simulations were run at 270 K on ice.

Afterwards, we performed 'conventional' MD simulations of surfactant-coated air/ice systems, which were equilibrated over at least 4 ns. After equilibration, production runs of at least 8 ns were conducted. In these MD simulations we investigated the adsorption of naphthalene and ozone on surfactant-coated air/ice interfaces. We evaluated the distribution of the angle between the aromatic plane of naphthalene and the air/ice surface (*xy*-plane) using two naphthalene molecules per air/ice interface. This was evaluated using the angle formed between the vector normal to the aromatic plane and the vector normal to the air/ice surface (z-direction). We also determined the angle formed between the normal to the air/ice surface (*z*-direction) and a vector joining the first and last carbon atoms in each surfactant molecule (i.e., C1-C8 for 1-octanol and 1-octanal, and C1-C16 for 1-hexadecanol). This property was evaluated for varying number of molecules (5 to 18) of the different surfactant species at each air/ice interface. Additionally, the density profiles of naphthalene with respect to density profiles of water and surfactants were also investigated. This was investigated with 2 naphthalene molecules at each air/ice interface and varying concentrations of surfactants at the air/ice interface. We also investigated the average distance between the naphthalene molecules at the surfactant-coated air/ice interfaces. Regarding the dynamical properties of the naphthalene molecules at the surfactant-coated air/ice interfaces, we calculated the average mean square displacement and diffusion coefficient of naphthalene molecules (2 molecules per interface) at the surfactant-coated air/ice interfaces. We also compared these

properties determined at surfactant-coated air/ice interface with those obtained at bare air/ice interfacial properties. We used the software VMD[126] for all our visualizations. Simulations considering surfactant-coated and bare air/ice interfaces were carried out at 270 K.

3.3. Results and Discussion

3.3.1. Air/ice Systems: Density Profiles of the Mobile Water Molecules

In our previous work[135] with simulated air/ice systems, it was observed that part of the thin layers of mobile water that we placed near the fixed ice slab gradually froze during the equilibration part of the simulations. This simulated QLL eventually exhibits a stable thickness during the equilibration part of our simulations.[135]

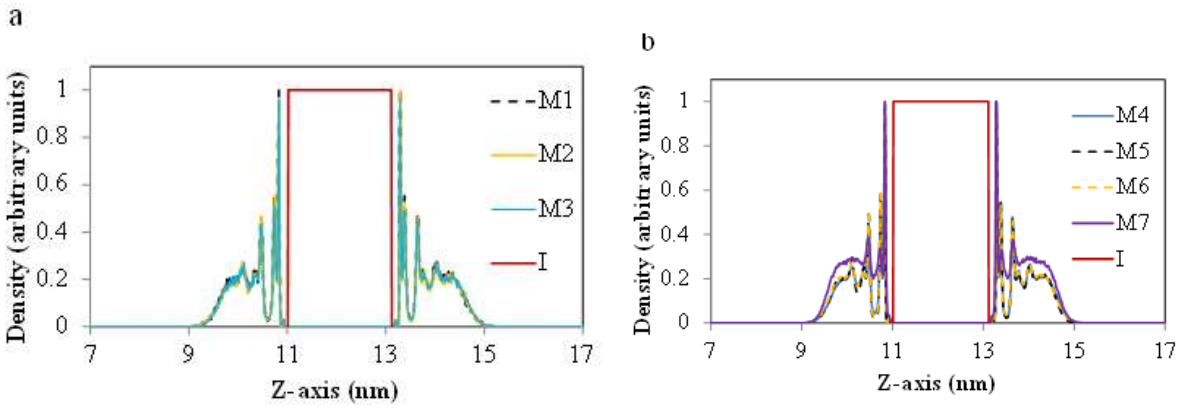

Figure 3.1. Average density profiles of 'mobile' (M) and 'immobile' (I) water molecules in air/ice systems. All values are normalized by dividing by the largest value of the local density of 'mobile' and 'immobile' water. **(a)** Density profiles of 'mobile' water molecules at 270 K, averaged over the following time periods: M1 = 4 to 5 ns; M2 = 7 to 8 ns; M3 = 11 to 12 ns. 18 molecules of 1-octanol and 2 molecules of naphthalene are present at each air/ice interface. **(b)** Density profiles of mobile (M) and immobile (I) water molecules in air/ice systems at 270 K with 2 naphthalene molecules and 18 surfactant molecules per interface. M4 = 1-octanol, M5 = 1-hexadecanol, M6 = 1-octanal, M7 = no surfactants present.

In Figure 3.1a we show the time evolution of the density profiles of mobile water molecules during the 8 ns production run period (i.e., after the 4 ns equilibration part), when 18 1-octanol molecules and 2 naphthalene molecules were present at each air/ice interface. Significant variations were not observed in the density profiles of mobile water molecules

during this period. These results suggest that part of the mobile water molecules freeze during the first 4 ns of the simulations (equilibration time period) and reach the equilibrium QLL thickness, which is consistent with what we observed in our previous work.[135] These results are consistent with the trends we observed when the air/ice interface was coated with 1-hexadecanol and 1-octanal. In Figure 1b we present the density profile of the mobile water molecules averaged over the production run period at the surfactant-coated air/ice interfaces (18 molecules of 1-octanol, 1-octanal or 1-hexadecanol, and 2 naphthalene molecules per air/ice interface). Changes in the density profile of the mobile water molecules were observed when the number of surfactant molecules at the air/ice interface was increased from 0 to 18 while keeping two naphthalene molecules at each air/ice interface (Figure 3.1b). It can be observed that there are more fluctuations in the density profiles of the mobile water molecules when surfactants are present. In contrast, variations in the structure of the surfactant molecule (1-octanol, 1-octanal or 1-hexadecanol) while keeping the same molar concentrations at the air/ice interface produce negligible variations in the density profiles of the mobile water molecules. These observations suggest that the thickness of the QLL is reduced when surfactants are present at the air/ice interface. This behavior might be an effect of the additional intermolecular interactions that arise when surfactants are added to bare air/ice interfaces; this point deserves further investigation in future studies.

3.3.2. PMF of Naphthalene and Ozone in Air/ice Systems

In Figure 3.2 and 3.3 we present the PMF obtained by moving one naphthalene or one ozone molecule from the gas phase into air/ice interfaces coated with 1-octanol, 1-hexadecanol or 1-octanal (18 molecules of surfactant per air/ice interface) at 270 K.

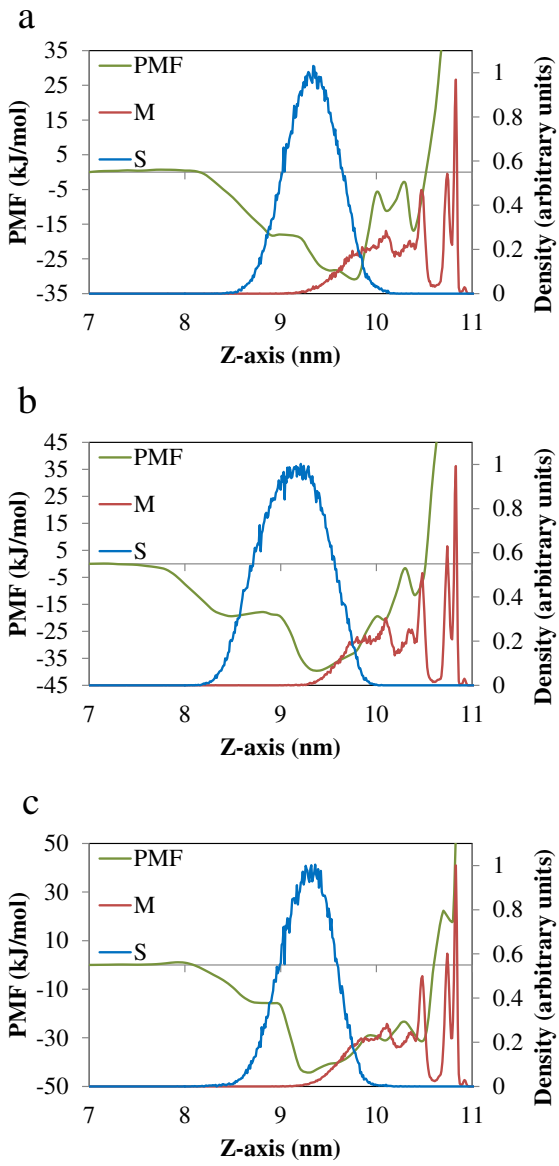

Figure 3.2. PMF (green lines) of moving one naphthalene molecule from the gas phase into the mobile water molecules in surfactant-coated air/ice systems at 270 K. In all cases, 18 molecules of surfactant are present in each air/ice interface. **(a)** Air/ice interface coated with 1-octanol. **(b)** Air/ice interface coated with 1-hexadecanol. **(c)** Air/ice interface coated with 1-octanal. The density profiles of mobile water (M, red lines) and surfactant (S, blue lines) molecules are also depicted. These density profiles are normalized with respect to the maximum value of the local density of the corresponding species found in the simulation box

For both ozone and naphthalene, PMF profiles exhibit deep minima at the surfactant-coated air/ice interface, and sharp increases in the PMF are observed as the naphthalene or ozone molecules are dragged into the 'mobile' water molecules that froze during the equilibration period of the simulations.

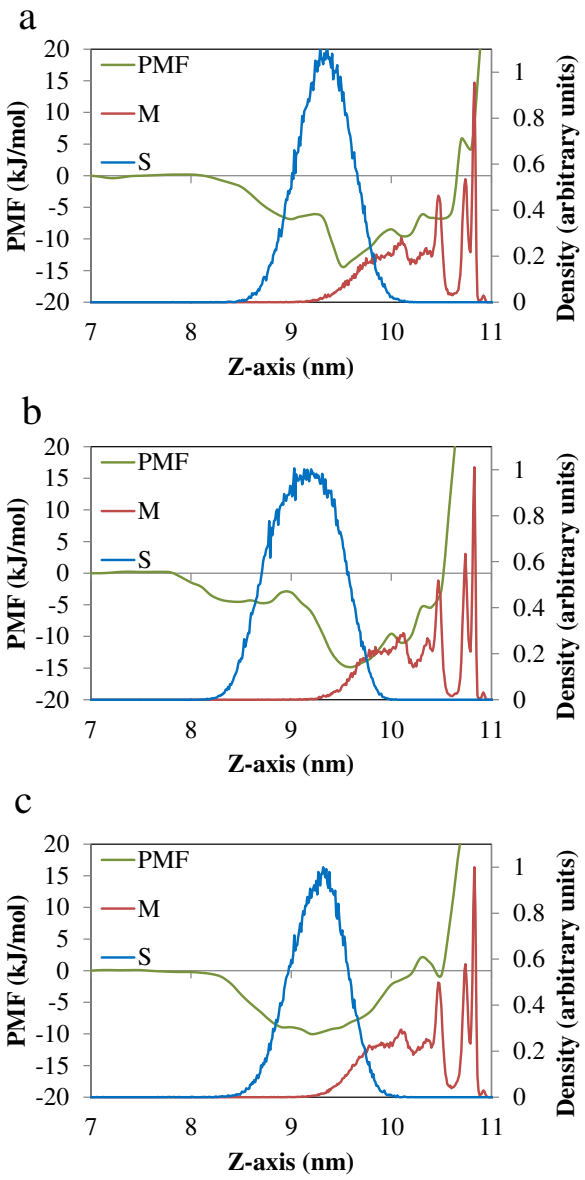

Figure 3.3. PMF (green lines) of moving one ozone molecule from the gas phase into the mobile water molecules in surfactant-coated air/ice systems at 270 K. In all cases, 18 molecules of surfactant are present in each air/ice interface. **(a)** Air/ice interface coated with 1-octanol. **(b)** Air/ice interface coated with 1-hexadecanol. **(c)** Air/ice interface coated with 1-octanal. The density profiles of mobile water (M, red lines) and surfactant (S, blue lines) molecules are also depicted. These density profiles are normalized with respect to the maximum value of the local density of the corresponding species found in the simulation box.

These observations suggest that both naphthalene and ozone prefer to be adsorbed at the surfactant-coated air/ice interface, as compared to staying in the gas phase, being dissolved in the QLL or embedded in the crystalline structure of ice. In our previous simulation study for naphthalene and ozone on bare air/ice interfaces,[135] we also determined that the

incorporation of naphthalene and ozone into the crystalline structure of ice is thermodynamically unfavorable. In these bare air/ice systems, the minima in the PMF for naphthalene and ozone was observed at the air/ice interfaces and are about -22.2 kJ/mol and -5.1 kJ/mol, respectively. In comparison, our results show that when 18 molecules of 1-octanol, 1-hexadecanol or 1-octanal are present at the air/ice interface, the naphthalene PMF minima values are -30.5 kJ/mol, -39.6 kJ/mol and -44.3 kJ/mol (Fig. 3.2), and the ozone PMF minima values were -14.3 kJ/mol, -14.9 kJ/mol and -10.02 kJ/mol (Fig. 3). These results indicate that for the surfactants considered, adsorption of both naphthalene and ozone on air/ice interfaces is enhanced by the presence of surfactants at the interfaces. The PMF minima for naphthalene and ozone depend on the specific surfactant present at the interfaces. 1-octanal seems to interact stronger with naphthalene at the air/ice interfaces than 1-hexadecanol, which in turn interacts stronger than 1-octanol. In contrast, ozone seems to interact stronger with 1-octanol and 1-hexadecanol than with 1-octanal. The PMF minimum for naphthalene becomes deeper with increasing length of the hydrophobic tail of the surfactant (naphthalene has a deeper minimum when 18 molecules of 1-hexadecanol are present at the air/ice interface, as compared to when the same number of molecules of 1-octanol are present). In contrast, increasing the length of the hydrophobic tail does not have a significant effect on the adsorption of ozone (the PMF minima were similar when the air/ice interfaces are coated with 1-octanol or 1-hexadecanol with the same molar concentration). For the case of adsorption of naphthalene on air/water interfaces, the PMF minimum also becomes deeper when these interfaces are coated with 1-octanol, changing from about -25 kJ/mol (bare air/water interfaces) to about -32 kJ/mol (air/water interfaces coated with

1-octanol).[33] This change represents a reduction of about 28% in the PMF minimum value with respect to the value on bare air/water interfaces. Similarly, the value of the PMF minimum of naphthalene on air/ice interfaces coated with 1-octanol decreases in about 37% with respect to the value observed on bare air/ice interfaces. This comparison suggests that surfactants have a somewhat larger effect on the adsorption of naphthalene on air/ice interfaces than on air/water interfaces.

The position of the z coordinate where the PMF minimum of naphthalene and ozone is observed, relative to the density profiles of the different species in the air/ice systems, gives insights on whether these molecules prefer to adsorb on top of already adsorbed surfactant molecules, stay dissolved in the surfactant layer, or adsorb inside the 'mobile' water molecules in the QLL. From Figures 3.2 and 3.3, in all cases the PMF minima of both naphthalene and ozone are located deep into the surfactant layer and close to the interface with the mobile water molecules in the QLL. Therefore, thermodynamics suggests that both naphthalene and ozone prefer to stay dissolved in the surfactant layer and close to the QLL, rather than to adsorb on top of the surfactants near the air region in our systems, or deep into the QLL. The results presented in Figs. 3.2 and 3.3 suggest that surface adsorption is the dominant mechanism for uptake of naphthalene from vapor phase on thin surfactant-coated ice films, as opposed to dissolution into the QLL or incorporation into the crystalline ice. The tendency of naphthalene and ozone to preferably remain at the air/ice interface, and the enhancement of surface adsorption with the presence of surfactants, are relevant to surface processes such as heterogeneous reactions between naphthalene and ozone at the air/ice interfaces. The trends observed for the PMF of both naphthalene and ozone are in agreement

with previous experimental and simulation results obtained for phenanthrene, naphthalene and ozone adsorption at bare and surfactant-coated air/water and air/ice interfaces.[135, 136]

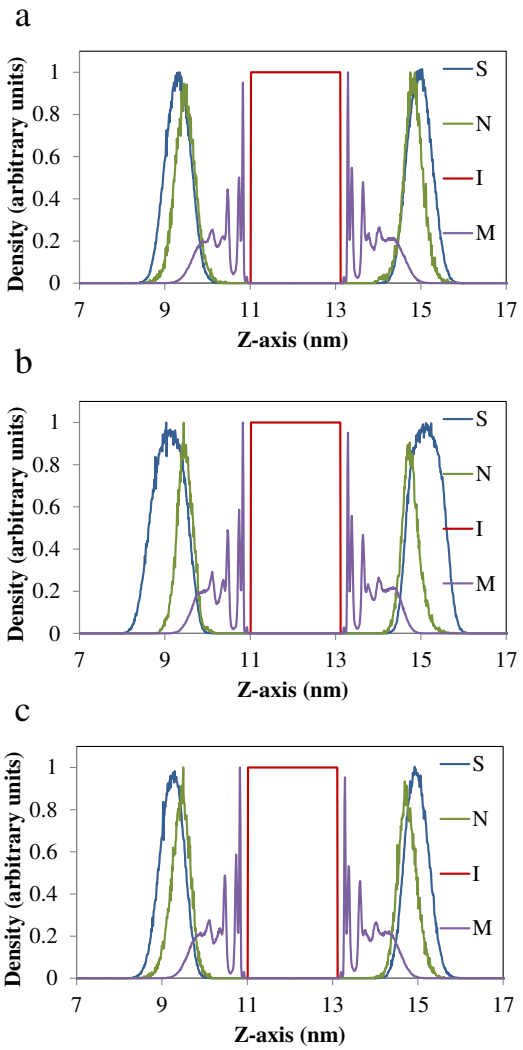

Figure 3.4. Density profiles of the species in different air/ice systems at 270 K. Letters S (blue line), N (green line), I (red line) and M (purple line) represent surfactant, naphthalene, immobile and mobile water molecules. **(a)** 18 molecules of 1-octanol and 2 molecules of naphthalene per air/ice interface. **(b)** 18 molecules of 1-hexadecanol and 2 molecules of naphthalene per air/ice interface. **(c)** 18 molecules of 1-octanal and 2 molecules of naphthalene per air/ice interface. The density profile of each species is normalized by dividing by the maximum value of the local density of each species in the simulation box.

3.3.3. Density Profiles

In Figure 3.4 we present density profiles of naphthalene, surfactants and mobile and immobile water molecules in air/ice systems at 270 K, as obtained from 'conventional' MD

simulations. In these systems 18 molecules of surfactant (1-octanol, 1-octanal or 1-hexadecanol) and 2 molecules of naphthalene are present at each air/ice interface.

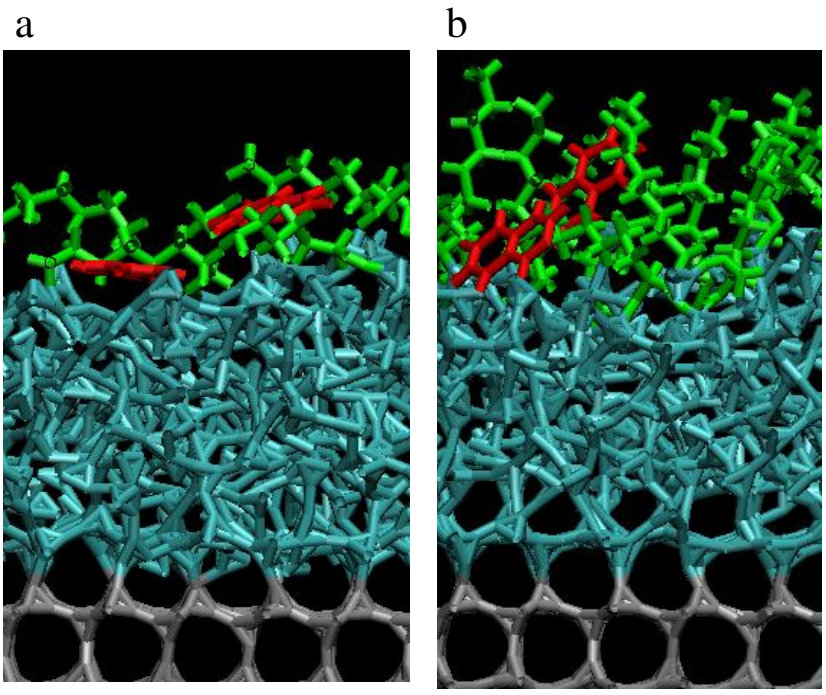

Figure 3.5. Side view of representative simulation snapshots of naphthalene and 1-octanol on air/ice interfaces at 270 K. **(a)** System with 2 molecules of naphthalene and 5 molecules of 1-octanol per air/ice interface. **(b)** System with 2 molecules of naphthalene and 18 molecules of 1-octanol per air/ice interface. Naphthalene = red; 1-octanol = green; mobile water molecules = cyan; immobile water molecules = gray.

Side views of representative simulation snapshots of these systems are depicted in Figures 3.5, 3.6 and 3.7. Density profiles of systems where 5 molecules of surfactants and 2 molecules of naphthalene are present at each air/ice interface are not shown for clarity. The density profiles and the snapshots indicate again that naphthalene prefers to stay at the surfactant-coated air/ice interfaces, as opposed to remaining in the gas phase or entering the bulk of the ice phase. When we compare the z coordinates of the peaks in the density profiles of naphthalene and surfactants (Fig. 3.4), we observe that the peaks for naphthalene are closer to the mobile water molecules in the QLL; the surfactant peaks are a little farther from these

water molecules. Density profiles of systems where 5 molecules of surfactants are present at the air/ice interface had similar trends.

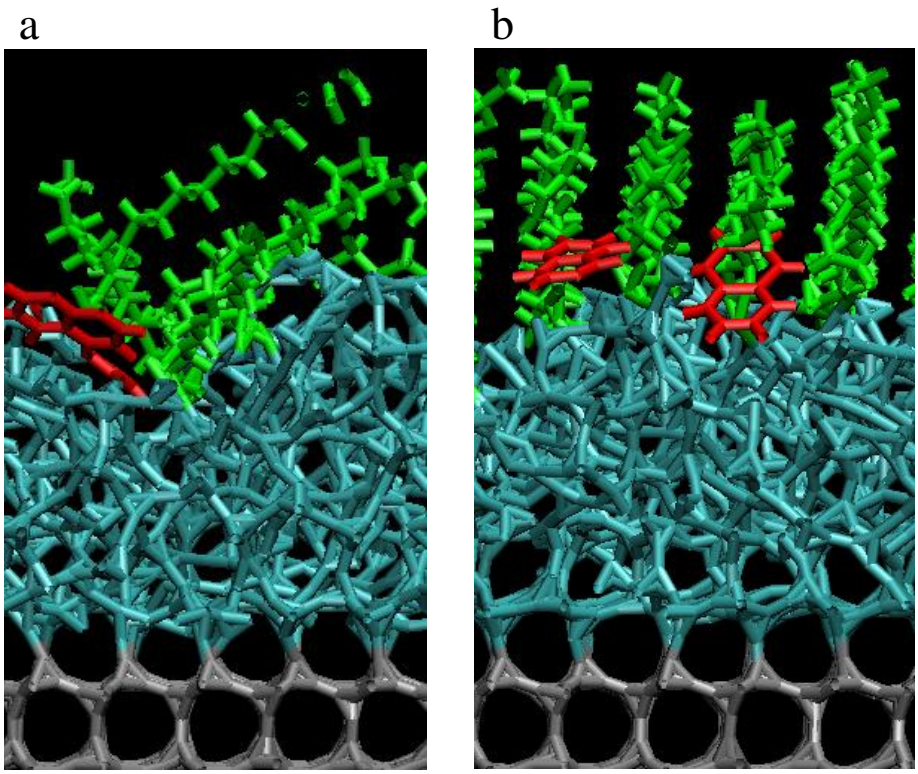

Figure 3.6. Side view of representative simulation snapshots of naphthalene and 1-hexadecanol on air/ice interfaces at 270 K. **(a)** System with 2 molecules of naphthalene and 5 molecules of 1-hexadecanol per air/ice interface. **(b)** System with 2 molecules of naphthalene and 18 molecules of 1-hexadecanol per air/ice interface. Naphthalene = red; 1-hexadecanol = green; mobile water molecules = cyan; immobile water molecules = gray.

Visual inspections of simulation snapshots (Figs. 3.5-7) and video clips of the time evolution of our systems also indicate that naphthalene molecules tend to penetrate into the surfactant films at the air/ice interface. Significant overlap in the density profiles of naphthalene and surfactants are observed in Fig. 3.4, in agreement with the PMF results shown in Figs. 3.2 and 3.3. These results indicate that even when considerable concentrations of surfactant molecules are present at the air/ice interface, naphthalene molecules have a tendency to stay dissolved in the surfactant layer and to adsorb directly onto the air/ice interface, rather than adsorbing on top of the surfactant molecules and close to the air region.

These results were consistent for both low and high concentrations of surfactants (1-octanol, 1-hexadecanol and 1-octanal) at air/ice interface.

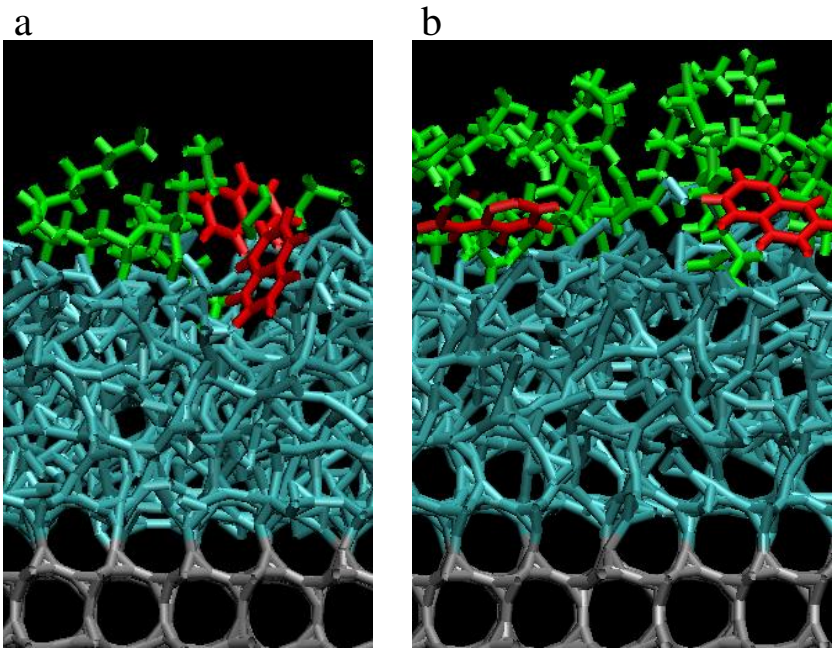

Figure 3.7. Side view of representative simulation snapshots of naphthalene and 1-octanal on air/ice interfaces at 270 K. **(a)** System with 2 molecules of naphthalene and 5 molecules of 1-octanal per air/ice interface. **(b)** System with 2 molecules of naphthalene and 18 molecules of 1-octanal per air/ice interface. Naphthalene = red; 1-octanal = green; mobile water molecules = cyan; immobile water molecules = gray.

3.3.4. Structural Properties of Surfactants at the Air/ice Interface

The orientation of surfactant (1-octanol, 1-octanal or 1-hexadecanol) molecules at the air/ice interface was monitored in our MD simulations when 2 naphthalene molecules were present at the air/ice interface. Figure 3.8 presents the angle distribution between the vector of the end carbon atoms of the alkyl groups of each surfactant molecule and the air/ice interface (xy-plane). A value of 1 for cos(θ) represents that the alkyl group of the surfactant molecules remains flat with respect to interface and a value of 0 for cos(θ) represents the alkyl group of the surfactant molecule lying perpendicular to the interface.

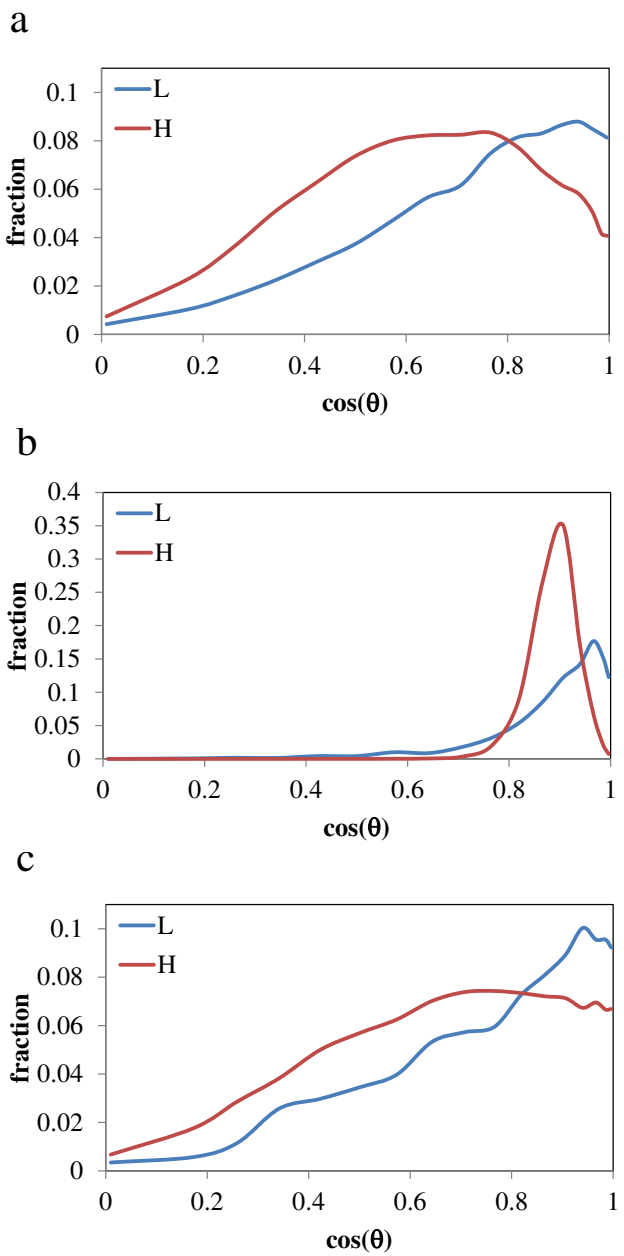

Figure 3.8. Average angle distributions of surfactant molecules at air/ice interface at 270 K. **(a)** Systems with 2 naphthalene molecules and varying number of 1-octanol molecules per air/ice interface. **(b)** Systems with 2 naphthalene molecules and varying number of 1-hexadecanol molecules per air/ice interface. **(c)** Systems with 2 naphthalene molecules and varying number of 1-octanal molecules per air/ice interface. L and H represent 5 and 18 surfactant molecules per air/ice interface.

From Figure 3.8, it can be observed that none of the surfactant species prefer to lie flat at the air/ice interface; rather, they tend to orient at a tilted angle at the air/ice interface (in a way that the hydrophilic end pointing towards the ice surface). Our results suggest that the angle distribution of the surfactants depends on the hydrophilic end group and the length of

the hydrophobic tail, as well as on the concentration of each surfactant at the air/ice interface. When larger concentrations of 1-hexadecanol are present at the air/ice interface, the angular distribution is narrower as compared to 1-octanol or 1-octanal at the same molar concentrations. These trends suggest that as the alkyl chain (hydrophobic tail) gets longer, the angular distribution becomes narrower (see Figs. 3.6 and 3.8). It was also observed that as the surfactant concentration increases, for all species the preferred tilt angle increases with respect to the ice surface as compared to lower concentrations of each species. This observation suggests that the concentration of each surfactant species has a significant effect on the orientation at the air/ice interface, which is in agreement with previous results obtained from simulations of surfactants at air/water interfaces.[149] At low concentrations of surfactants at the air/ice interface, surfactants interact primarily with the water molecules at the QLL rather than with other surfactant molecules. However, at larger concentrations, the interactions between surfactant molecules become more important, making the surfactant molecules to align closer to perpendicular with respect to the air/ice interface (*xy* plane).

3.3.5. Structural and Dynamical Properties of Naphthalene Molecules at the Surfactant–Coated Air/ice Interface

The orientation of naphthalene molecules at the surfactant-coated air/ice interfaces was investigated in the MD simulations. This orientation is relevant to the reactions between naphthalene and incoming oxidizing species due to the fact that the reactivity of ozone with naphthalene depends on a detailed interaction between these two molecules.

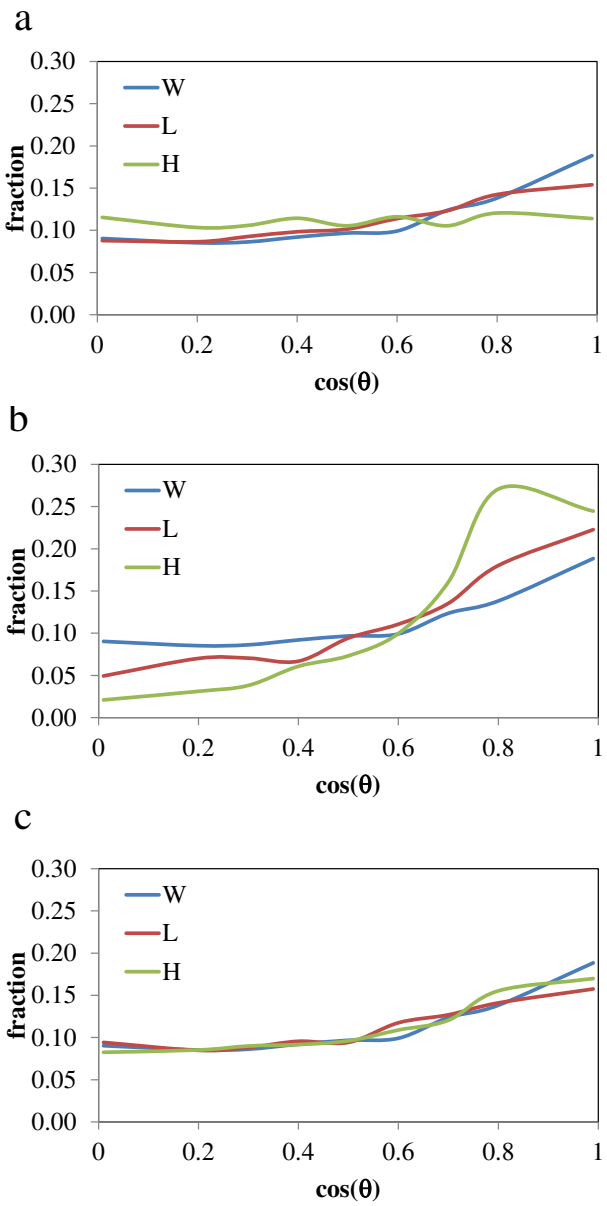

Figure 3.9. Average angle distributions of naphthalene molecules at 270 K at air/ice interfaces coated with varying concentrations of different surfactant molecules (W, L and H = 0, 5 and 18 surfactant molecules per air/ice interface). **(a)** Systems with 2 naphthalene molecules and varying number of 1-octanol molecules per air/ice interface. **(b)** Systems with 2 naphthalene molecules and varying number of 1-hexadecanol molecules per air/ice interface. **(c)** Systems with 2 naphthalene molecules and varying number of 1-octanal molecules per air/ice interface.

Figure 3.9 presents the angle distribution between the aromatic rings of naphthalene and the air/ice interface for the case where two naphthalene molecules are present at the surfactant-coated air/ice interface. A value of 1 for cos(θ) represents that the aromatic ring is parallel to the ice surface and a value of 0 for cos(θ) represents the aromatic ring is

perpendicular to the ice surface. We monitored the angular distribution of naphthalene molecules for systems of up to 18 molecules of surfactant per air/ice interface were present. Naphthalene prefers to lie flat at bare air/ice interfaces, but when the interface is coated with 1-octanol, naphthalene's preference to align flat at the ice surface decreases, in agreement to simulation results obtained for the air/water interface.[149] In contrast, when the air/ice interface is coated with 1-hexadecanol, naphthalene's preference to be at a flat orientation is enhanced as compared to that observed in bare air/ice interfaces. No significant variations in the angular distribution are observed when the air/ice interface is coated with increasing concentrations of 1-octanal. The angular distributions of naphthalene are similar when low concentrations of 1-octanol or 1-octanal are present at the air/ice interface. However, as the 1-hexadecanol concentration increases, naphthalene prefers to orient at a tilted angle. These results suggest that the specific surfactant molecule and its concentration at the air/ice interface play a major role in the orientation of naphthalene at these interfaces.

We also calculated the average distance between centers of mass of two naphthalene molecules at the surfactant-coated air/ice interfaces, for the case where two naphthalene molecules were adsorbed to each surfactant-coated air/ice interface, and up to 18 surfactant molecules were present at each interface. This distance is important since naphthalene exhibits a tendency to self-associate at the air/ice interface.[148] The average distances between two naphthalene molecules when 18 molecules of 1-octanol, 1-hexadecanol or 1-octanal are present at the air ice interface is 1.12±0.38 nm, 1.21±0.35 nm and 1.18±0.37 nm, respectively. On bare ice interfaces the average distance between naphthalene molecules were 1.10±0.39 nm. Although we observe slight increases in the average distances between

naphthalene molecules in surfactant-coated air/ice interfaces as compared to bare air/ice interfaces, such increases are not significant (especially considering the standard deviations reported above). Similar results were observed at low surfactant concentration at the air/ice interface.

The mean square displacement (MSD) of naphthalene molecules on surfactant-coated air/ice surfaces is shown in Figure 3.10 for bare air/ice interfaces, and when 18 molecules of 1-octanol, 1-hexadecanol and 1-octanal are present at the interfaces. All systems contain 2 molecules of naphthalene per air/ice interface.

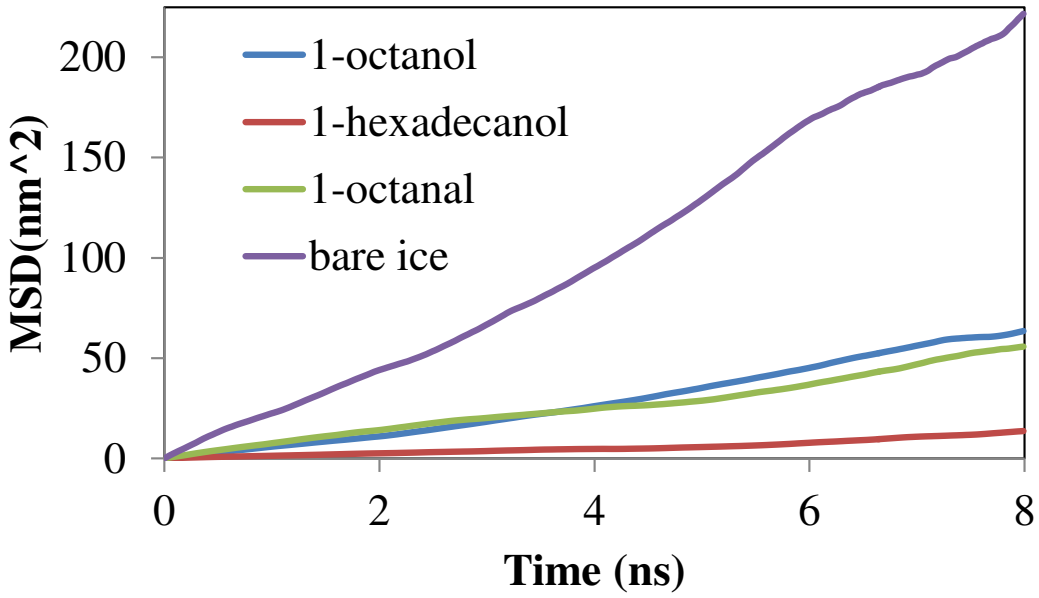

Figure 3.10. Average mean square displacement of naphthalene molecules on bare or surfactant-coated air/ice interfaces at 270 K.

These results indicate that the dynamics of naphthalene at the surfactant-coated air/ice interface are significantly slower when compared to those in bare air/ice interfaces. No significant changes are observed in the MSDs of naphthalene when 1-octanol or 1-octanal are present at the air/ice interface, however the dynamics of naphthalene becomes slower when the air/ice interfaces are coated with 1-hexadecanol. The average diffusion coefficients of

naphthalene molecules were found to be 5.76, 1.86, 1.07 and 0.25 ($\times 10^{-5}$ cm^2/s) on air/ice interfaces that are bare or coated with 1-octanol, 1-octanal and1-hexadecanol, respectively. These results indicate that the diffusion of naphthalene molecules at the air/ice interface is hindered by the presence of surfactants at the air/ice interface; the restriction in motion depends on the chemical details of the surfactants (head group, chain length). Furthermore, the density profiles (Figure 3.4) show that for the 1-hexadecanol system, naphthalene is adsorbed farther away from the gas phase as compared to the 1-octanol and 1-octanal systems. Those observations help in explaining the large reduction observed in the diffusion coefficient of naphthalene in the 1-hexadecanol system, because near the gas phase, the diffusion of naphthalene should be less hindered due to the lack of other molecules restricting its movement.

3.4. Concluding Remarks

MD simulations were performed to investigate the adsorption of naphthalene and ozone on surfactant-coated air/ice interfaces. The thickness of the QLL formed by 'mobile' water molecules in our simulations reaches a stable value after ~4 ns and maintained an equilibrium thickness during the production run period of 8 ns. The thickness of the QLL decreases with increases in the surfactant concentration at the air/ice interfaces; no significant differences in the QLL thickness are observed for identical concentrations of different surfactants (1-octanol, 1-hexadecanol, or 1-octanal). Surface adsorption is found to be the predominant mechanism for uptake of naphthalene and ozone on surfactant-coated ice films, as opposed to dissolution into the QLL or incorporation into the crystalline ice. PMF calculations show deep free energy minima for naphthalene and ozone adsorption at surfactant-coated air/ice interfaces.

These PMF minima are significantly deeper than those observed for naphthalene and ozone on bare air/ice interfaces, suggesting that the presence of surfactants enhances the adsorption of naphthalene and ozone on air/ice interfaces. For naphthalene, the PMF minimum becomes deeper when the air/ice interface is coated with 1-hexadecanol, as compared to when air/ice interface is coated with 1-octanol, which suggests that increasing the hydrophobic tail length of the surfactants enhances the adsorption of naphthalene on air/ice interfaces. In contrast, the PMF minima for ozone in 1-octanol or 1-hexadecanol-coated air/ice interfaces are similar. Both naphthalene and ozone prefer to stay dissolved in the surfactant layer and close to the mobile water molecules in the QLL, rather than to adsorb on top of the surfactants and near the air region in our systems. All the surfactants studied tend to adopt a tilted orientation at the air/ice interface, with the angle distribution and the most preferred angle varying between different surfactants. As the surfactant concentration increases, surfactant molecules prefer to have a more perpendicular orientation with respect to the air/ice interface. The specific surfactant and its concentration affect the orientation of naphthalene molecules at the ice surfaces; in most cases, naphthalene prefers to lie flat at the surfactant-coated air/ice interfaces, except at high 1-hexadecanol concentrations. Our results suggest that the presence of surfactants at the air/ice interfaces have no significant effects on the self-association of naphthalene molecules at these interfaces (at least for the surfactants considered and the range of concentrations studied in this paper). In contrast, the dynamics of naphthalene molecules at the air/ice interface are significantly slower when surfactants are present at the air/ice interface compared to bare air/ice interface; the slowest dynamics were observed for 1-hexadecanol-coated air/ice interfaces.

CHAPTER 4 ICE GROWTH FROM SUPERCOOLED AQUEOUS SOLUTIONS OF BENZENE, NAPHTHALENE AND PHENANTHRENE[§]

Contents of this chapter have already been published (T. P. Liyana-Arachchi, K. T. Valsaraj and F. R. Hung, Ice growth from supercooled aqueous solutions of benzene, naphthalene and phenanthrene. J. Phys. Chem. A 2012, 116, 8539-8546). In this chapter, we report molecular dynamics (MD) results of the ice growth from supercooled aqueous solutions of benzene, naphthalene or phenanthrene. The main objective of this study is to explore the fate of benzene, naphthalene or phenanthrene molecules after freezing of the supercooled aqueous solutions. The rest of this chapter is structured as follows. Section 4.1 is the introduction. Section 4.2 contains a description of our computational models and methods. In Section 4.3 we present results and discussion and in Section 4.4 we summarize our main findings.

4.1. Introduction

Polycyclic aromatic hydrocarbons (PAHs, e.g., naphthalene, phenanthrene) are molecules that exhibit at least two fused aromatic rings. These compounds are ubiquitous atmospheric pollutants and are known to have important carcinogenic, mutagenic and teratogenic effects.[14] PAHs can react with reactive oxygen species (ROSs) [e.g., ozone, hydroperoxy, hydroxyl and nitrate][1] and produce oxy- and nitro-PAHs which exhibit enhanced toxicity.[14, 16] PAHs can be adsorbed at atmospheric air/water interfaces (water droplets, aerosols, fog, mist), a process that typically involves adsorption at the interface and dissolution in the bulk water.[19] Similarly, PAHs can also adsorb at atmospheric air/ice interfaces (ice, snow). The sorption mechanism in this case consists of adsorption of the

[§] Reprinted with permission of J. Phys. Chem. A 2012, 116, 8539-8546

PAHs to the air/ice interface, dissolution in the quasi-liquid layer (QLL, a transitional liquid-like layer observed when ice is exposed to a free surface such as air at temperatures close to the melting point[96-101]), and incorporation into the solid ice crystal.[95]

Adsorption of PAHs and ROSs at the air/water and air/ice interfaces are of particular importance because heterogeneous reactions between these compounds at these interfaces can exhibit kinetics that are much faster than those of their homogeneous counterparts in the gas phase.[1, 12, 13]

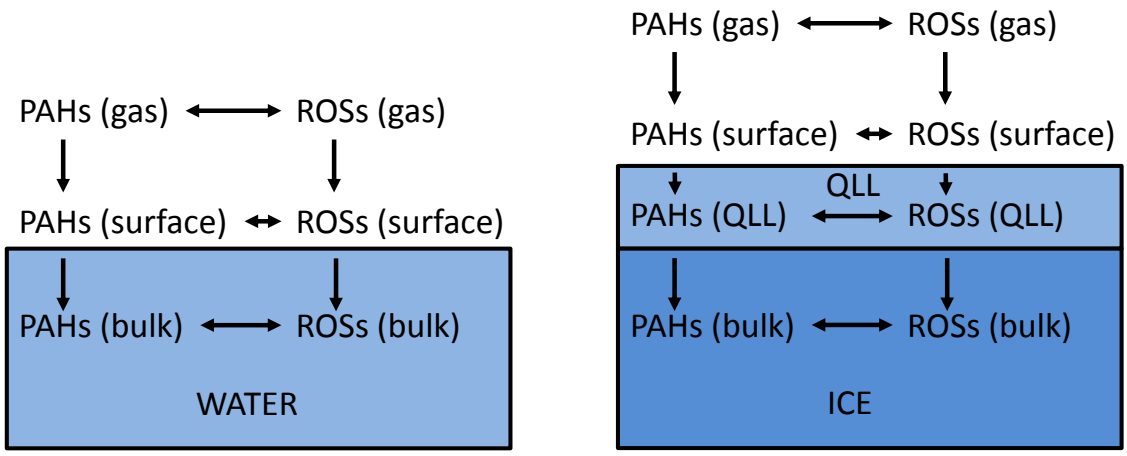

Figure 4.1. The multiple ways in which photochemical reactions between PAHs and ROSs can take place in atmospheric air/water (left) and air/ice (right) systems.

In principle, photochemical reactions between PAHs and ROSs can occur in multiple ways (Figure 41). PAHs and ROSs can adsorb and remain on the air/water or air/ice interface (i.e., without migrating to the bulk water or into the QLL), and undergo heterogeneous reactions at these interfaces. Another possibility would be that PAHs and ROSs become dissolved in the bulk water or inside the QLL, and then undergo photochemical reactions. For the particular case of PAHs and ROSs in ice/snow, these species could also become trapped into the lattice structure of ice and undergo reactions in that environment. A final possibility is for PAHs and ROSs to react in the gas phase (Figure 4.1). Therefore, a fundamental

understanding of the properties of PAHs and ROSs in air/water and air/ice systems can lead to an improved understanding of the multiple ways these species can undergo photochemical reactions in atmospherically relevant systems.

Previous molecular dynamics (MD) simulations from our group have indicated the presence of deep free energy minima for adsorption of gas-phase PAHs (naphthalene, phenanthrene) and ROSs (ozone) at air/ice interfaces,[135, 136, 150] suggesting that there is a thermodynamic incentive for these molecules to remain at such interfaces rather than being dissolved inside the QLL or incorporated in the lattice structure of ice. We have also observed that the thickness of the QLL affects the distribution of PAHs in the QLL and at the air/ice interface; as the QLL becomes less thick due to a decrease in temperature, PAHs tend to spend less time inside the QLL and remain for longer times at the air/ice interface.[136] These simulations studies[135, 136, 150] are relevant for the scenario described above where PAHs and ROSs undergo chemical reactions at the air/ice interface or within the QLL. However, some PAHs such as naphthalene and phenanthrene are known to be solvated to a considerable degree in bulk water at environmental conditions.[20, 135, 136, 149] Because of this fact, ice growth from supercooled aqueous solutions of PAHs is a process that can occur in natural environmental conditions, for example during freezing of lakes, formation of ice at the sea and formation of snow pellets. As a result, PAHs and ROSs could become trapped into the ice lattice and then undergo photochemical reactions in such an environment. Here we report MD simulations of ice growth from supercooled water containing dissolved aromatic molecules, namely benzene, naphthalene and phenanthrene. The first objective of our simulations is to explore the fate of those aromatic molecules after the freezing process,

namely how likely it is for these molecules to become trapped inside the crystalline structure of ice, or if they are displaced to the QLL or to the interface with air. Ice growth from supercooled water and aqueous solutions has been the subject of several studies. Nada and Furukawa[151-153] investigated ice growth from supercooled water via molecular simulations, and Vrbka and Jungwith[154] studied the growth of ice from supercooled aqueous solutions of NaCl, but these studies did not consider the presence of an interface with air. The effects of such an interface was taken into account in the work of Carignano and Szleifer,[155, 156] who performed molecular simulations of ice growth from pure water and from aqueous solutions of NaCl, in the presence of interfaces with air. Such an interface is required for ice to develop a QLL. The thickness of the QLL depends on the temperature and also is influenced by the presence of solutes.[157] Estimating the thickness of the QLL is hard due to the fact that the values obtained for thickness of the QLL are highly dependent on the experimental techniques used to measure it.[96, 101-108] In our simulation studies we also investigated the effect of benzene, naphthalene and phenanthrene on the thickness of the QLL, as well as monitored the orientation of the aromatic molecules that end up at the air/ice interface. This property is important due to the fact that reactions between PAHs and ROSs depend on the orientation of these molecules. We carried out our MD simulations at two different temperatures, 270 K and 260 K. In addition, we also performed several potential of mean force (PMF) calculations because of several reasons: (1) verify that our adopted force fields and parameters could reproduce experimental values of the free energy of hydration for benzene and phenanthrene, and (2) determine the PMF associated with moving a molecule of benzene or phenanthrene from the gas phase into the air/ice interface.

4.2. Simulation Details

All our MD simulations were conducted using the GROMACS software.[116] In analogy to our previous studies,[135, 136, 150] benzene, naphthalene and phenanthrene were modeled using the force fields and parameters from the work of Vácha *et al.*,[20, 145, 146] and water was modeled using the TIP5P water model.[112] However, the parameters from Vácha *et al.* were parameterized to reproduce the free energy of solvation of benzene, naphthalene and phenanthrene in combination with the SPC/E model for water.[115] In a previous study,[135] we determined from potential of mean force (PMF) calculations that the parameters from Vácha *et al.* for naphthalene, when used in combination with the TIP5P water model, can also reproduce the experimental value of its free energy of hydration. In order to reproduce the experimental free energy of hydration of benzene and phenanthrene, we followed previous work[20, 145, 149] and increased the atomic charges up to 10% of the original charges[20, 145, 146] when using the parameters of Vácha *et al.* in combination with the TIP5P water model (Supporting Information). We then tested these parameters by determining the PMF associated with moving one molecule of benzene or phenanthrene from the gas phase into a slab of liquid TIP5P water, and corroborated that the experimental free energies of hydration of these molecules are correctly reproduced (Figures 3 and S.1, Supporting Information). However, this increase in the atomic charges does affect the interactions between molecules of aromatics, which might be important in our simulations of ice growth from supercooled aqueous solutions of benzene, naphthalene or phenanthrene because the concentrations of these species considered here (see below) are larger than the naturally-occurring concentrations of these species in the atmosphere. Simulation results for the liquid densities

of pure benzene, naphthalene and phenanthrene at atmospheric pressures (not shown for brevity) using our modified models show deviations of less than 10% from reported experimental values. These results suggest that the interactions between aromatics, although not completely accurate, are still somewhat being captured by our models. Furthermore, our models can reproduce the experimental free energy of hydration of these aromatic molecules (see Figures 3 and S.1, Supporting Information), which is a physical characteristic thought to be of importance for this particular study. One possible way to overcome this issue is to consider larger system sizes (i.e., lower concentrations of aromatics), so that solute-solute interactions become less important. However, prohibitively large system sizes would be required in order to consider naturally-occurring concentrations of benzene, naphthalene and phenanthrene in atmospheric systems, as well as to obtain statistically-relevant results from the simulations. Afterwards, we performed similar calculations to determine the PMF associated with moving a molecule of benzene or phenanthrene from the gas phase into the air/ice interface. Details of all of these simulations (e.g., system sizes, methods) were exactly the same as those described thoroughly in our previous papers.[135, 150]

For our simulations of ice growth from supercooled aqueous solutions of benzene, naphthalene or phenanthrene, the simulated systems consist of a total of 1920 water molecules and 12 benzene, naphthalene or phenanthrene molecules. Following previous studies,[155, 156] the initial configurations were prepared by bringing together a block of hexagonal ice I_h (576 TIP5P molecules), and a slab of liquid water with 1344 molecules. Following our previous work,[135, 136, 150] the basal plane (0001 face) of the hexagonal ice is in contact with the liquid water. The slab of water/ice has x and y dimensions of

approximately 27 Å and 31.4 Å, and was placed in the center of an orthorhombic simulation box with the same *x* and *y* dimensions and elongated in the *z* direction (300 Å).

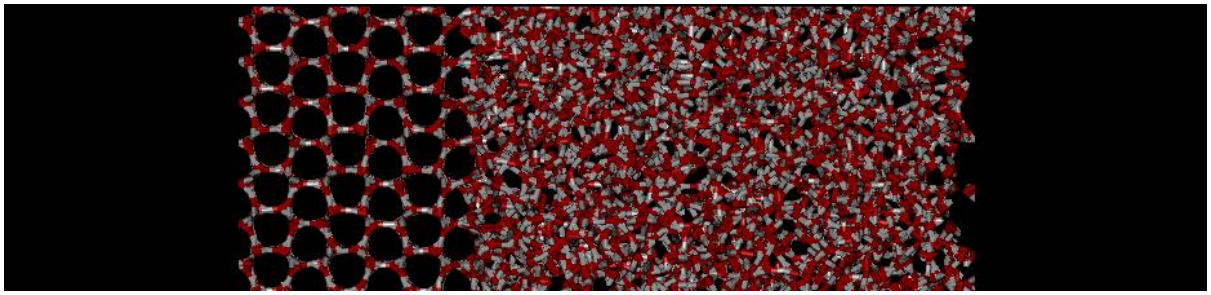

Figure 4.2. Illustration of the initial simulation setup.

This setup results in a heterogeneous ice/water system, where one of the sides of the ice block and one of the sides of the water slab are in contact with vacuum, mimicking one air/ice interface and one air/water interface (Figure 4.2). Afterwards, six molecules of benzene, naphthalene or phenanthrene were inserted at random positions within the slab of liquid water, and six additional molecules of benzene, naphthalene or phenanthrene were placed randomly at the air/ice interface at the left in Figure 4.2. The rationale behind the initial placement of these molecules is as follows. Water molecules in the liquid slab will gradually freeze during the simulation (i.e., ice growth will occur from left to right in Figure 4.2); in addition, water molecules at the initial air/ice interface (left in Figure 4.2) will melt (see Figure 4.5). This process will ultimately result in one large slab of ice with QLLs on both sides of it (i.e., two air/ice interfaces with two QLLs, see e.g., Figures 4.6 and 4.7). The six molecules of benzene, naphthalene or phenanthrene initially placed at the air/ice interface (left in Figure 4.2) will likely remain at the air/ice interface or within the QLL that will form at this interface. In contrast, the other six molecules of benzene, naphthalene or phenanthrene that were initially inserted in the slab of liquid water will either get incorporated into the ice structure, migrate to the QLL that will form at the air/ice interface on the right side of Figure

4.2, or move to that particular interface. Therefore, our initial placement of the 12 molecules of benzene, naphthalene or phenanthrene provides the opportunity for significant fractions of these molecules to be incorporated into the ice lattice or to lie at any of the two QLLs.

The initial configurations of each simulated system were first relaxed using the steepest descent energy minimization method. Afterwards, MD simulations were conducted in which the x and y dimensions of the simulation box were allowed to fluctuate with a coupling to a semi-isotropic Parrinello-Rahman barostat that keeps the z-dimension constant at 300 Å. Thermal coupling of all systems were done using Nose-Hoover thermostat following previous studies.[155, 156] Simulations were run at a pressure of 1 atm and at two temperatures, 270 K and 260 K. Periodic boundary conditions were applied in all three directions. A time step of 1 fs was used in all our MD simulations and data were collected every 10 ps. Bond lengths were constrained using the LINCS algorithm.[119] A cut-off distance of 0.9 nm was used for the Lennard-Jones interactions. The particle-mesh Ewald (PME) method[122] was used with a cutoff of 0.9 nm and a grid spacing of 0.12 nm in order to account for long-range Coulombic interactions. All our MD simulations were run for up to 150 ns, and at least three independent simulation runs starting from different initial configurations were performed for each system. We used the software VMD[126] for all our visualizations.

4.3. Results and Discussion

4.3.1. PMF of Benzene and Phenanthrene in Air/water and Air/ice Interfaces

As indicated above, we first determined the PMF associated with moving one molecule of benzene or phenanthrene from the gas phase into a slab of liquid water (Figure 4.3), with

the goal of testing that our adopted force fields for benzene and phenanthrene, when used in combination with the TIP5P water model, are capable of reproducing the experimental free energies of hydration. The air/water interface is arbitrarily depicted in Figure 4.3 as the point where the density of water reaches 500 kg/m^3.

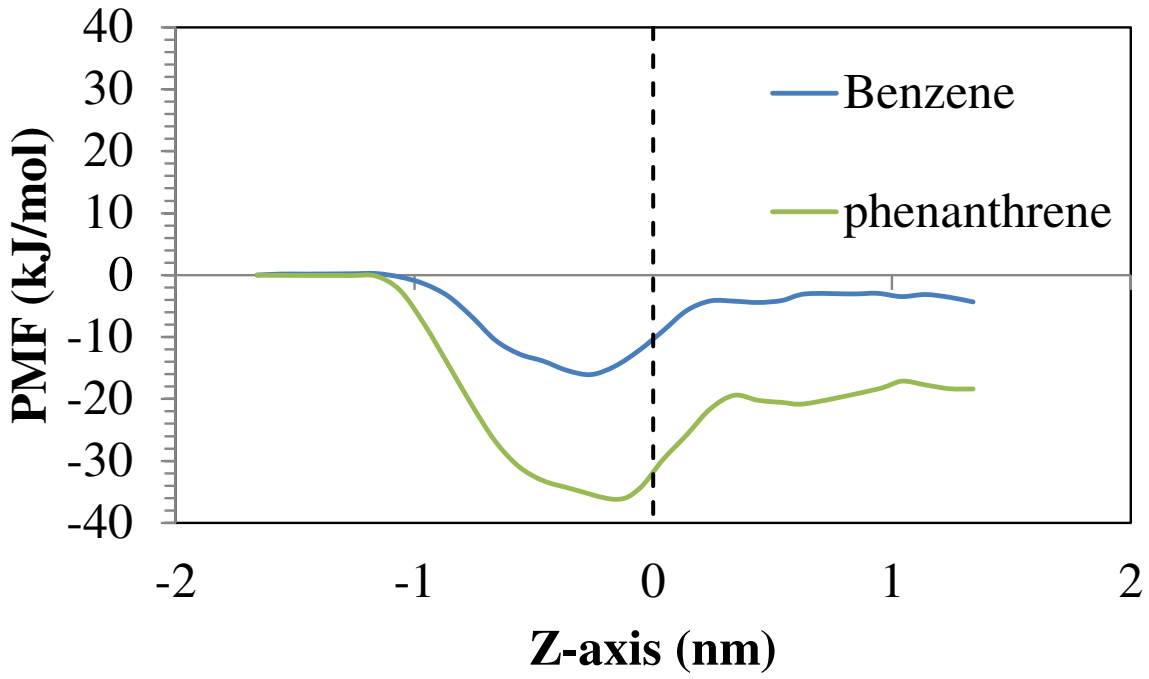

Figure 4.3. PMF of moving one benzene or phenanthrene molecule from the gas phase into the water molecules in air/water systems at 298 K. A value of zero in the *z*-axis represents the air/water interface (arbitrarily defined as the point where the density of water reaches 500 kg/m^3); positive values of *z*-axis represent the bulk water phase.

From Figure 4.3, the simulated hydration free energy obtained for benzene is about -3.1 kJ/mol, and for phenanthrene is about -18.0 kJ/mol. These results are similar to those obtained by Vácha *et al.*,[20] and by Wick *et al.*[149] in their simulation studies. These results are also consistent with reported experimental values of the free energies of hydration for these molecules: between -3.0 and -4.5 kJ/mol for benzene, and between -14.0 and -17.5 kJ/mol for phenanthrene, as determined from Henry's law constants.[20, 28] In Figure B.1 (APPENDIX B: SUPPORTING INFORMATION (CHAPTER 4)) we present PMF results

obtained for benzene using the original set of atomic charges for this molecule, and using the modified atomic charges used in this work. The original set of atomic charges for benzene, when used in combination with the TIP5P water model, give results for the free energy of hydration of benzene that deviate significantly from the experimental values (Figure B.1). The calculated free energy of hydration falls within the experimental values when the atomic charges are increased in 10% from the original charges. These results corroborate that the combination of force fields used in our study can reproduce experimental values of the free energy of hydration of benzene and phenanthrene in air/water systems. Furthermore, the free energy minima found at the air/water interface from our PMF calculations (around -16.0 kJ/mol for benzene, and -36.2 kJ/mol for phenanthrene) are similar to those reported in simulations by Vácha *et al.*[20, 28, 158] and Wick et al.[149]

In Figure 4.4 we present the PMF obtained by moving one benzene or one phenanthrene molecule from the gas phase into the bulk ice systems at 270 K. The air/ice interface is arbitrarily depicted in Figure 4.4 as the point where the density of water reaches 500 kg/m^3. The PMF profiles exhibit deep minima at the air/ice interface, suggesting that from the thermodynamic point of view both benzene and phenanthrene prefer to be adsorbed at the air/ice interface, rather than staying in the gas phase or being dissolved in the QLL. In addition, all PMF profiles show sharp increases as the molecule of benzene or phenanthrene is dragged close to the frozen water molecules.

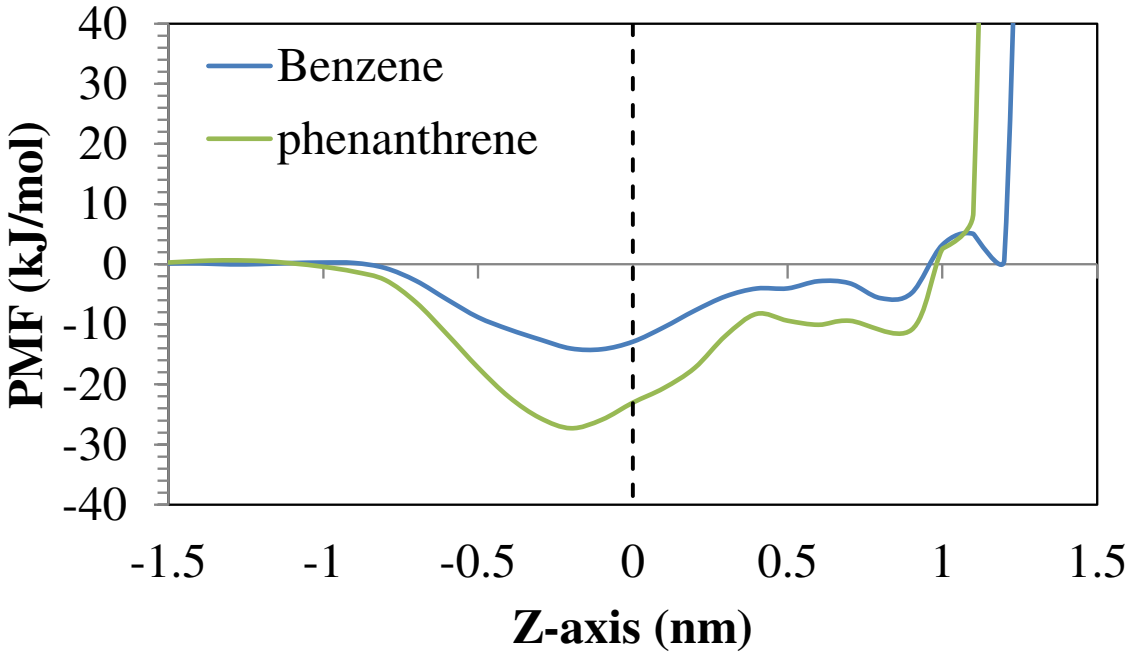

Figure 4.4. PMF of moving one benzene or phenanthrene molecule from the gas phase into the mobile water molecules in air/ice systems at 270 K. A value of zero in *z*-axis represents the air/ice interface (arbitrarily defined as the point where the density of water reaches 500 kg/m^3); positive values of *z*-axis represent the QLL and the bulk ice.

These results are consistent with those presented in our previous work[135, 150], which showed that naphthalene also prefers to be adsorbed at the air/ice interface. The PMF minima observed at the air/ice interface for benzene and phenanthrene are -14.2 kJ/mol and -27.3 kJ/mol. A PMF minimum value of -22.2 kJ/mol was computed in our previous work for naphthalene at the bare air/ice interface.[135] These results suggest that an increase in the number of aromatic rings in PAHs leads to deeper minima in the PMF at the air/ice interface, which is also consistent with the trends observed for PAHs at air/water interfaces.[20]

4.3.2. Ice Growth from Supercooled Aqueous Solutions of Benzene, Naphthalene or Phenanthrene

In Figure 4.5 we present the time evolution of the density profiles of the water molecules at 270 K, when no solutes are present. Variations in the density profile of the water molecules

were observed during the ice growth period (during the first 120 ns of our runs), but no significant variations in the density profiles were observed after 120 ns.

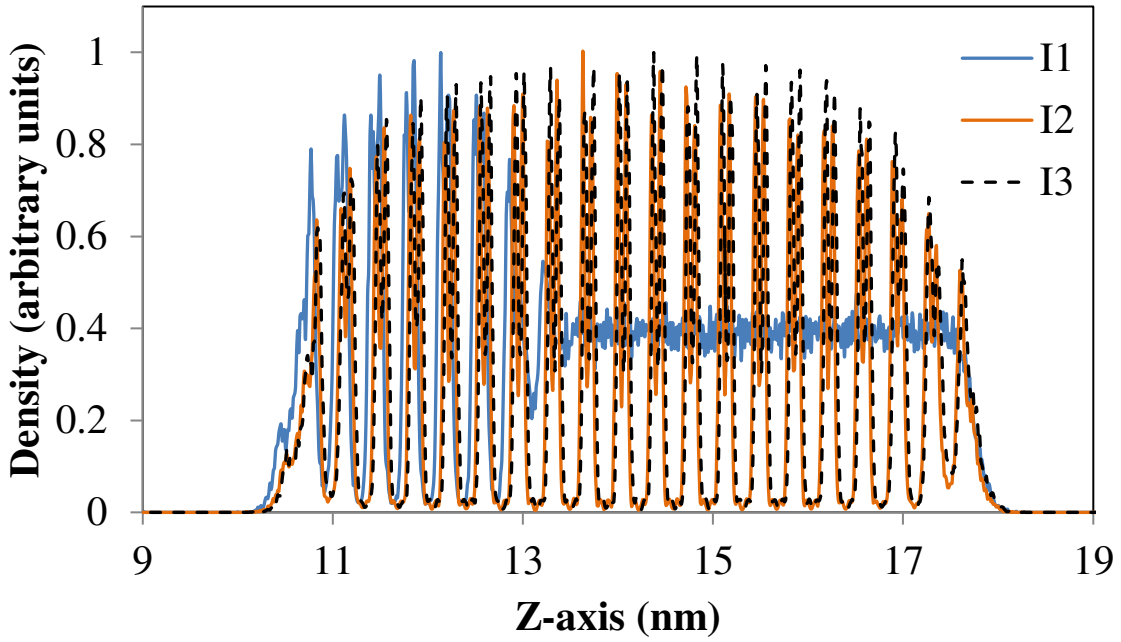

Figure 4.5. Average density profiles of water molecules in air/ice systems at 270 K, averaged over the following time periods: I1 = 0 to 1 ns; I2 = 120 to 121 ns; I3 = 129 to 130 ns. All values are normalized by dividing by the largest value of the local density of water.

These results suggest that part of the pure water slab freeze and part of the pure ice slab (at air/ice interface) melt during the first 120 ns of our simulations, as suggested by the large peaks and the deep local minima observed in the water density profiles shown in Figure 4.5. These results also suggest that the QLL in our systems eventually reach a stable thickness after 120 ns. Similar trends were observed for ice growth from supercooled aqueous solutions of benzene, naphthalene or phenanthrene at both 270 K and 260 K. In order to estimate the QLL thickness, we followed previous studies[159, 160] and calculated the root mean square fluctuations δ in the oxygen-oxygen distance between water molecules:

$$\delta = \frac{2}{n(n-1)} \sum_{i<j}^{n} \left[\frac{\sqrt{\langle r_{ij}^2 \rangle - \langle r_{ij} \rangle^2}}{\langle r_{ij} \rangle} \right] \quad (1)$$

Where n is the number of water molecules, r_{ij} is the distance between the oxygen atoms of molecules i and j, and the brackets $\langle\ \rangle$ represent time average. Following previous studies,[159, 160] $\delta \geq 0.1$ in the QLL (Lindemann criterion). Using this criterion, we determined that after the ice growth period, the QLLs present at both air/ice interfaces have a similar thickness of approximately 8.5 Å at 270 K, and about 7.5 Å at 260 K. These two QLLs were formed by two different paths; the first one formed by melting of ice at the interface (left side in Figure 4.2), and the second one formed by the growth of ice from the initially thicker slab of liquid water (right side in Figure 4.2). The uniformity in the thickness of both QLLs further suggests that the system has reached its equilibrium during the ice growth time period. The values reported above for the QLL thickness in contact with the basal plane of ice for the TIP5P water model with respect to its melting temperature (273.9 K[153]), are in good agreement with the QLL thickness reported for other water models with respect to their specific melting points.[117, 155, 160]

When solutes are added and ice grows from supercooled aqueous solutions of either benzene, naphthalene or phenanthrene, the thickness of the two QLLs grows to approximately 10.5 Å at 270 K, and to about 8.5 Å at 260 K. This observation suggests that the aromatic hydrocarbons dissolved in water tend to increase the thickness of the QLLs formed at the air/ice interfaces from ice growth. Differences in the number of aromatic rings (benzene, naphthalene or phenanthrene) do not seem to induce significant variations in the thickness of the QLLs at both temperatures. In Figures 4.6 we present the density profiles of benzene or phenanthrene and water molecules in air/ice systems at 270 K, after ice growth from supercooled aqueous solutions.

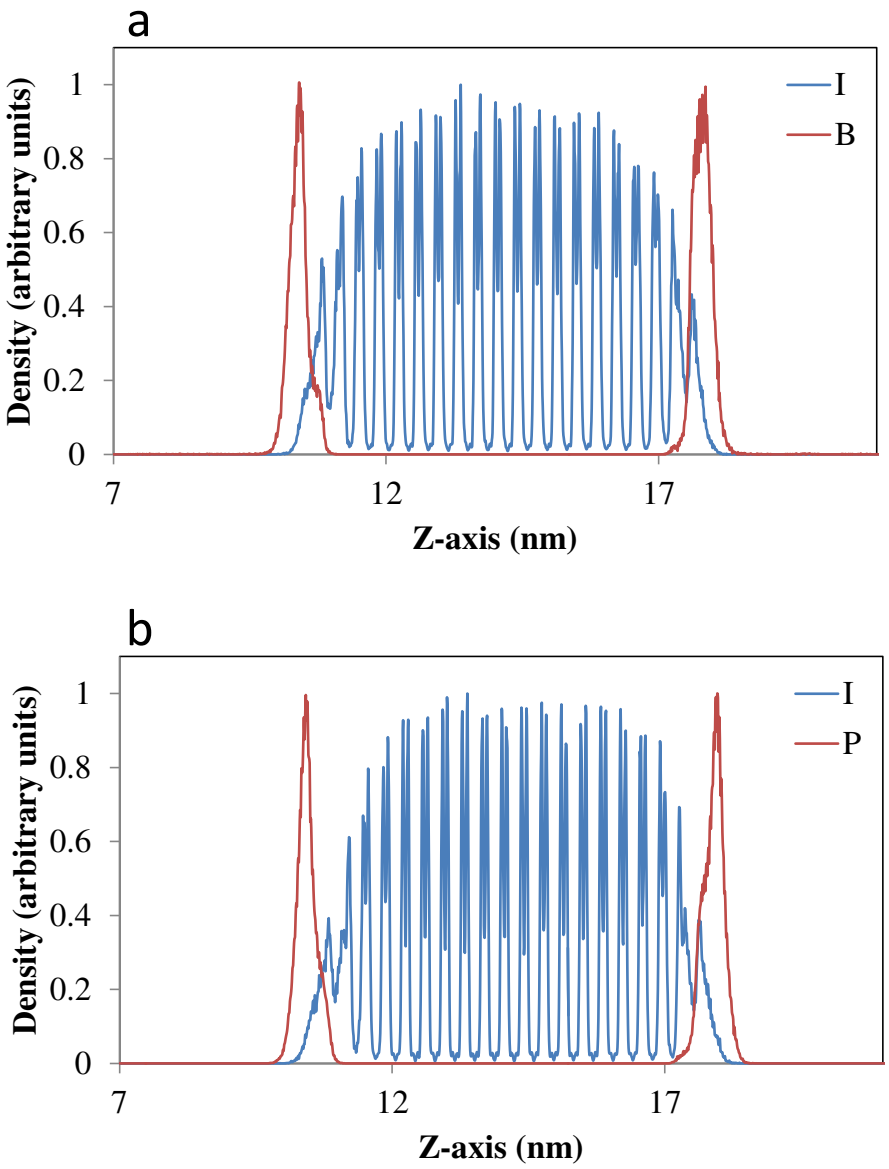

Figure 4.6. Density profiles of benzene or phenanthrene / ice systems after freezing at 270 K. Letters I, B and P represent water, benzene and phenanthrene molecules respectively. **(a)** System with 12 benzene molecules **(b)** System with 12 phenanthrene molecules. The density profile of each species is normalized by dividing by the maximum value of the local density of each species in the simulation box.

Side views of representative simulation snapshots of these systems are depicted in Figure 4.7.

These results indicate that the benzene and phenanthrene molecules that were initially placed at the original air/ice interface (left side in Figure 2) remain at this particular air/ice interface.

On the other hand, the benzene and phenanthrene molecules that were initially placed within

the original slab of liquid water (Figure 2) tend to migrate to the air/ice interface formed at the right side of Figure 4.7 during ice growth.

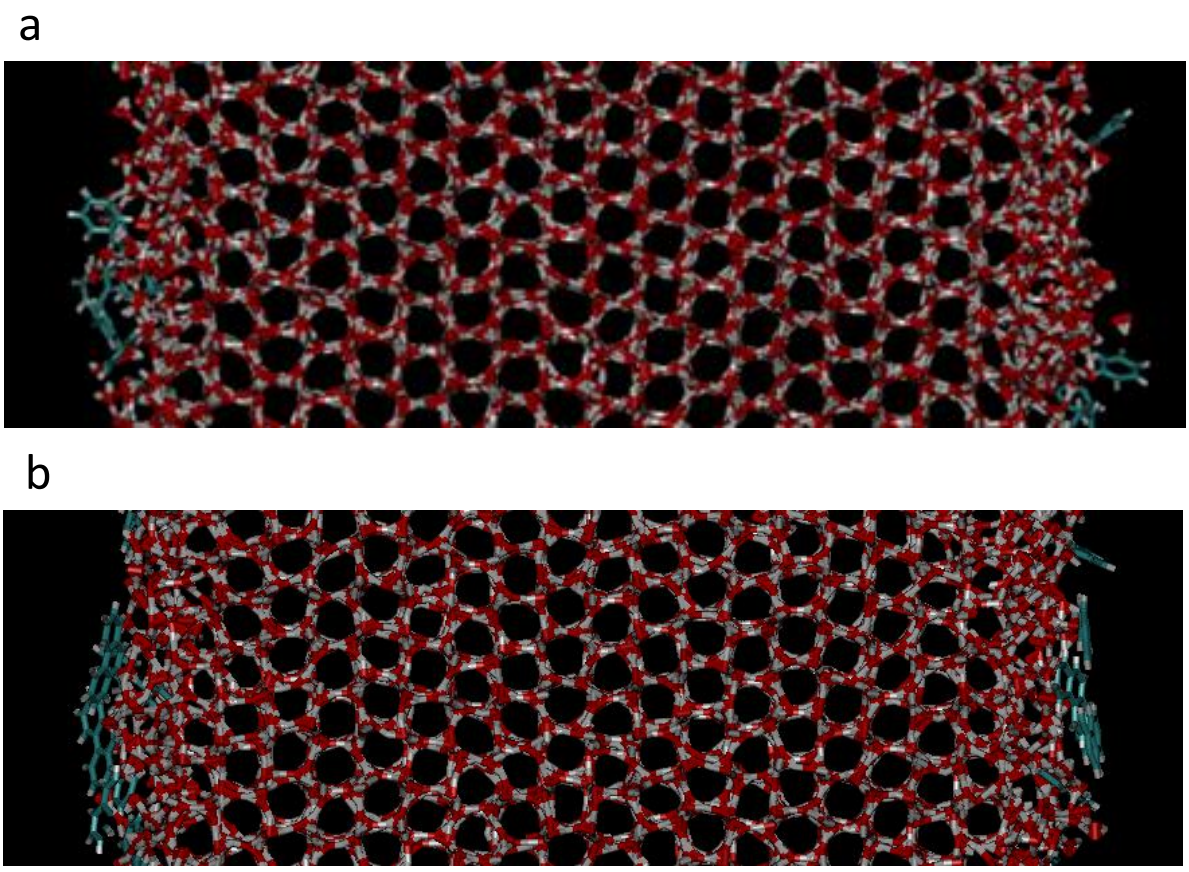

Figure 4.7. Side view of representative simulation snapshots of benzene or phenanthrene/ice systems after freezing at 270 K. **(a)** System with 12 benzene molecules. **(b)** System with 12 phenanthrene molecules. Benzene and phenanthrene = cyan and grey; water molecules = red and white.

These molecules did not remain inside the ice lattice that grew during any of the independent simulations performed for these systems at 270 K. Considerable overlap between the density profiles of benzene or phenanthrene and water in the QLLs is observed in Figure 4.6, indicating that benzene and phenanthrene molecules spend a considerable time inside the QLL. These results are consistent with those observed for ice growth from supercooled aqueous solutions of naphthalene at 270 K (results not shown for brevity).

In Figure 4.8 we present density profiles of benzene, naphthalene and water molecules in air/ice systems at 260 K after ice growth from supercooled aqueous solutions, and in Figure 4.9 we present representative snapshots of these systems.

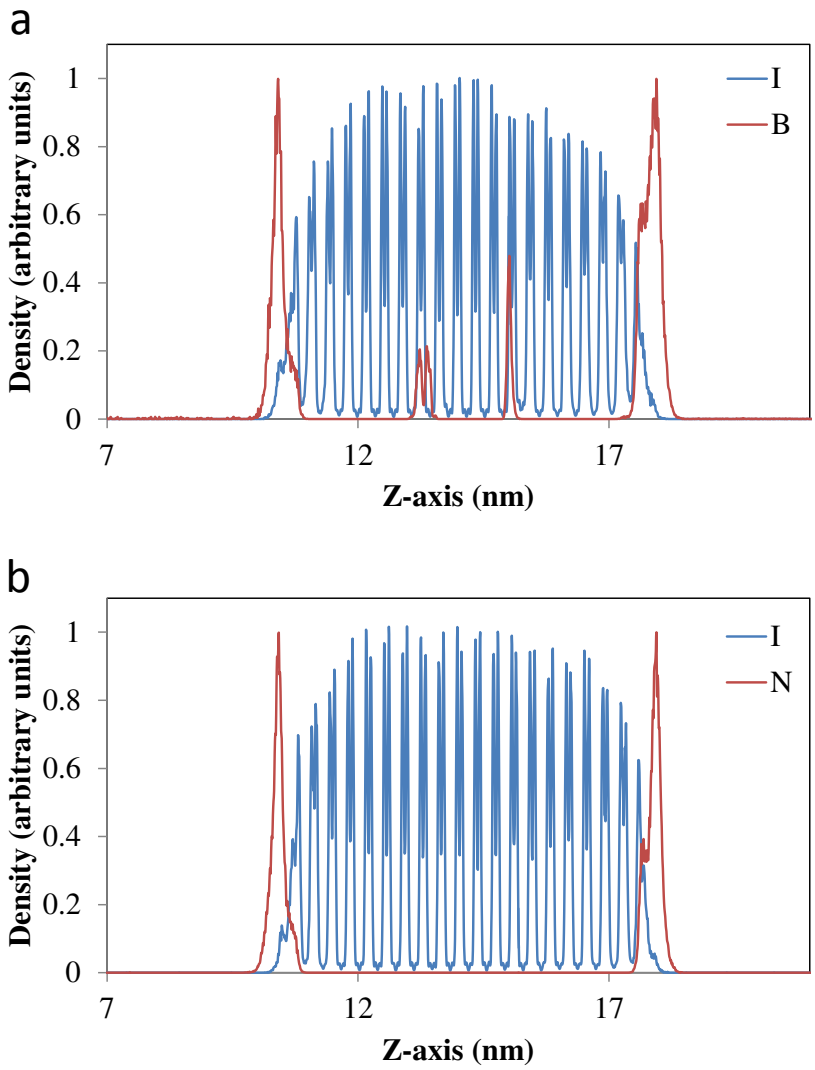

Figure 4.8. Density profiles of benzene or naphthalene / ice systems after freezing at 260 K. Letters I, B and N represent water,benzene and naphthalene molecules respectively. **(a)** System with 12 benzene molecules **(b)** System with 12 naphthalene molecules. The density profile of each species is normalized by dividing by the maximum value of the local density of each species in the simulation box.

For naphthalene systems at 260 K, the observations are similar to those described above for benzene and phenanthrene systems at 270K, i.e., aromatic molecules that were placed at the original air/ice interface (left side in Figure 4.2) remain there, and the naphthalene

molecules initially placed in slab of liquid water (Figure 4.2) migrate to the air/ice interface formed at the right side of Figure 4.9.

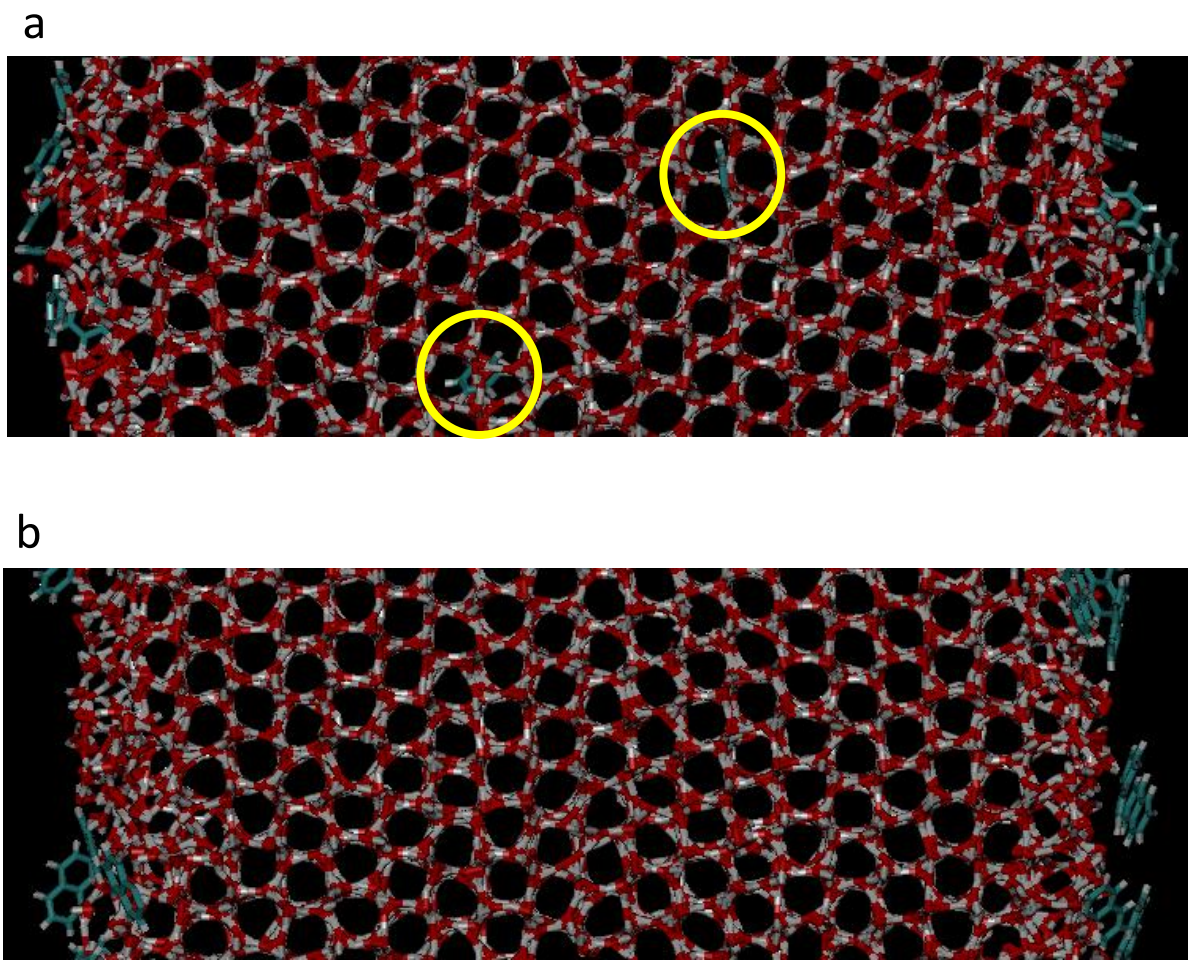

Figure 4.9. Side view of representative simulation snapshots of benzene or naphthalene / ice systems after freezing at 260 K. **(a)** System with 12 benzene molecules (benzene molecules incorporated into the ice lattice are circled in yellow). **(b)** System with 12 naphthalene molecules. Benzene and naphthalene = cyan and grey; water molecules = red and white.

Similar trends were observed after freezing of supercooled phenanthrene aqueous solutions at 260 K (results not shown for brevity). However, the results observed for supercooled aqueous solutions of benzene at 260 K exhibit a different trend. The benzene molecules initially placed at the original air/ice interface (left side in Figure 4.2) remain at the QLL formed there during the simulation run, in analogy to the results discussed above. In contrast, only some of the benzene molecules initially placed in the water slab migrate to the

air/ice interface and QLL formed on the right side of Figure 4.9 after ice growth; several of the benzene molecules get incorporated into the crystalline ice structure formed during the ice growth time period (Figures 4.7 and 4.8). These results were consistently observed in all of the independent simulation runs (started from different initial configurations) that were conducted for benzene systems at 260 K. Mean square displacement (MSD) results at 260 K for the benzene molecules that are inside the ice lattice or at the QLLs at the air/ice interfaces are shown in Figure 4.10.

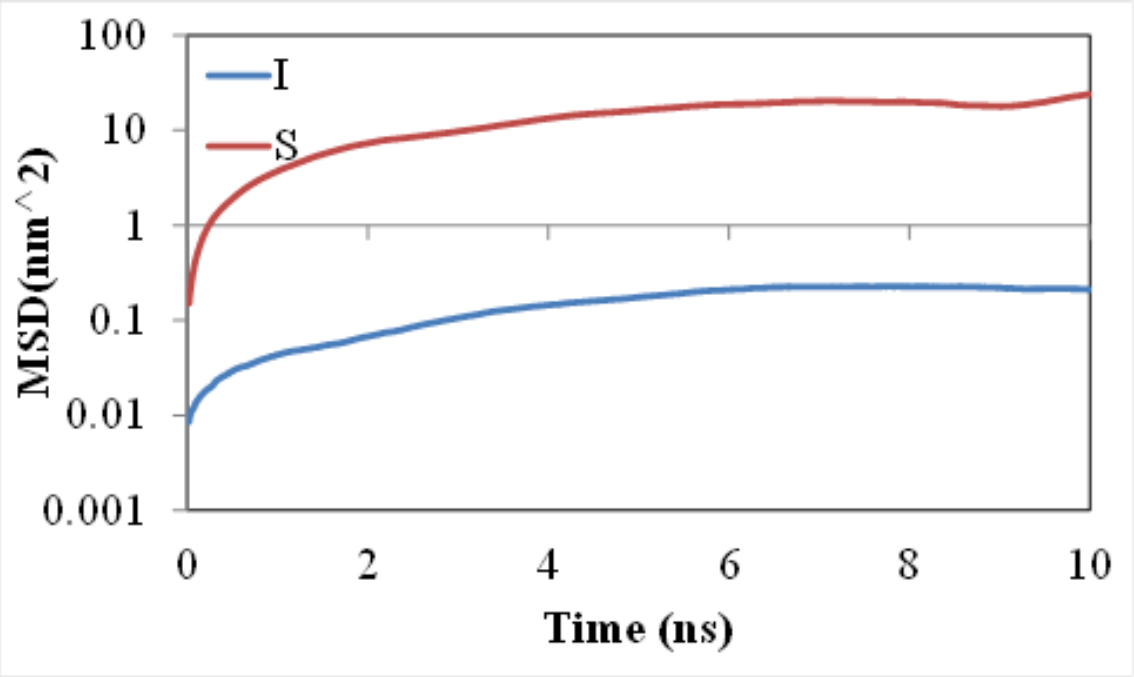

Figure 4.10. Mean square displacement (MSD) of benzene molecules after freezing at 260 K. Letters I and S represent benzene molecules trapped in the ice lattice and at the QLLs at the air/ice interfaces.

The dynamics of the benzene molecules inside the ice lattice are significantly slower than those of the benzene molecules at the air/ice interfaces, indicating that the former molecules are indeed trapped inside the lattice structure of ice. These results indicate that benzene molecules can be incorporated in the crystalline structure of ice as the freezing temperature is decreased to 260 K. In contrast, benzene molecules were not trapped in the ice structure at

270 K; furthermore, larger aromatic molecules such as naphthalene or phenanthrene are not incorporated into the crystalline structure of ice at any of these two temperatures. We further explored the structure of the water molecules in the ice lattice close to the trapped benzene molecules, by measuring oxygen-oxygen, oxygen-hydrogen and hydrogen-hydrogen radial distribution functions for water molecules within a 1×1×1 nm^3 cube enclosing a trapped benzene molecule. We then compared those results against those obtained for water molecules within a cube of similar size far away from the trapped benzene molecules. These results are shown in Figure B.2 (APPENDIX B: SUPPORTING INFORMATION (CHAPTER 4)). The structure of ice I_h as given by these $g(r)$ functions agree with the results obtained by Vega *et al.*[161] These results also show that the structure of ice near the trapped benzene molecules is only slightly distorted with respect to the ice structure far away from the trapped benzene species. In contrast, the incorporation of larger molecules such as naphthalene or phenanthrene into the ice crystals would significantly alter the structure of the ice lattice, which might be one of the reasons why these molecules were not trapped inside ice in our simulations. Intermolecular interactions between water and the guest molecules should also play a role in determining which molecules can become trapped inside the ice lattice and which cannot. The structure of the water molecules near and far away from the benzene molecules trapped in ice I_h could be further explored using the tetrahedral order parameter proposed by Errington and Debenedetti.[162] Such detailed investigations of the structure of ice, as well as freezing of supercooled aqueous solutions of ROSs, will be considered in upcoming studies from our group.

The orientation of benzene, naphthalene and phenanthrene molecules at the air/ice interfaces was investigated in the MD simulations after ice growth from supercooled aqueous solutions. In Figure 4.11 we present the distribution of the angle θ formed between a vector normal to the aromatic rings of the hydrocarbons and a vector normal to the air/ice interface (z-direction). A value of 1 for cos(θ) indicates that the aromatic ring is parallel to the ice surface, and a value of 0 for cos(θ) indicates that the aromatic ring is perpendicular to the ice surface.

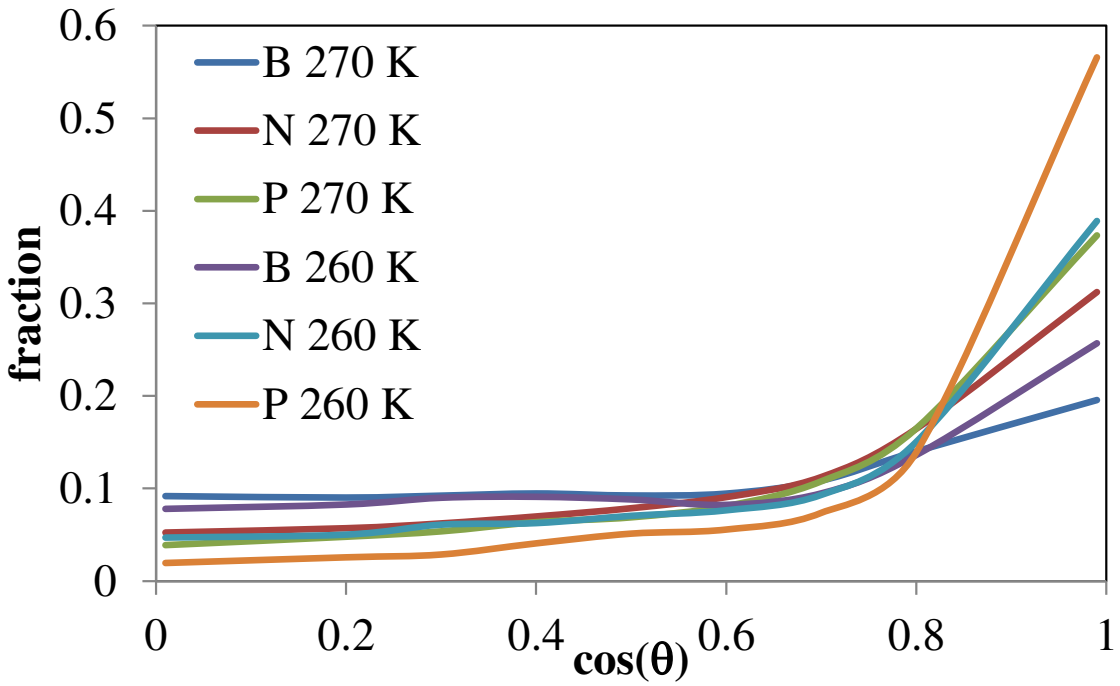

Figure 4.11. Average angle distributions of benzene,naphthalene and phenanthren molecules at 270 K and 260 K at air/ice interfaces. Letters I, B and N represent water,benzene and naphthalene molecules respectively.

It is observed that the molecules of benzene, naphthalene and phenanthrene prefer to lie flat at the air/ice interface. However, all the molecules retain a considerable ability to rotate around its molecular axis, as represented by the wide distribution of angles observed. Furthermore, the preference to orient parallel to the air/ice surface is enhanced as the number of aromatic rings increases; phenanthrene shows a larger preference to lie flat at the air/ice

interface as compared to naphthalene and benzene. This trend might result from an increase in the magnitude of the interactions between the aromatic hydrocarbons and the water molecules in the QLL, as the number of aromatic rings per molecule increases. Furthermore, the preference to orient parallel to the air/ice surface for each species increases with decreasing temperature. These results are consistent with those from our previous work,[135, 136] and also with those obtained by Vácha *et al.*[146] and Wick *et al.*[149] for aromatic hydrocarbons at air/water interfaces.

4.4. Concluding Remarks

MD simulations were performed to investigate the growth of ice from supercooled aqueous solutions of benzene, naphthalene or phenanthrene. The objectives of this study were to explore the fate of those aromatic molecules after the freezing process (i.e., whether these molecules become trapped inside the ice crystals, or if they are displaced to the QLL or to the interface with air), and to investigate properties such as the thickness of the QLL and the orientation of the aromatic molecules that end up at the air/ice interface. We first successfully verified that our combination of force fields (TIP5P[112] for water and the force field from Vácha *et al.*[20] for benzene and phenanthrene) could reproduce experimental values of the free energies of hydration of these aromatics. Afterwards, we performed PMF calculations for adsorption of gas-phase benzene and phenanthrene on air/ice systems, which indicate the presence of deep free energy minima for these species at the air/ice interface (-14.2 and -27.3 kJ/mol; a PMF minimum of -22.2 kJ/mol was computed in our previous work[135] for naphthalene at this interface). These results indicate that there is a thermodynamic incentive for these molecules to remain at the interface, and that the PMF minimum becomes deeper

with an increasing number of aromatic rings in the hydrocarbon. Ice growth from pure supercooled TIP5P water resulted in air/ice interfaces with QLLs that had thicknesses of approximately 8.5 Å at 270 K and about 7.5Å at 260 K. The presence of benzene, naphthalene or phenanthrene in the supercooled water leads to thicker QLLs formed after ice growth, approximately 10.5 Å thick at 270 K and about 8.5 Å thick at 260 K. During the ice growth process, naphthalene and phenanthrene molecules are displaced from the ice lattice, ending up at the air/ice interface at both 270 K and 260 K; no incorporation of naphthalene or phenanthrene into the ice lattice was observed throughout the freezing process in any of the independent simulation runs performed as part of this study. Similar trends were observed during freezing of supercooled aqueous solutions of benzene at 270 K. In contrast, a fraction of the benzene molecules become trapped inside the ice lattice during the freezing process at 260 K, with the rest of the benzene molecules being displaced to the air/ice interface. These results suggest that the size of the aromatic molecule in the supercooled aqueous solution is an important parameter in determining whether these molecules become trapped inside the ice crystals. All the aromatic hydrocarbons studied preferred to adopt a flat orientation at the air/ice interface. The preference to stay flat at the interface increased as the temperature decreases and also with the increasing number of aromatic rings for aromatic hydrocarbons.

In upcoming studies we will study freezing of supercooled aqueous solutions of ROSs, as well as consider the effect of other species in these systems (PAHs, surfactants). All these results are relevant to understand the multiple ways PAHs and ROSs can undergo photochemical reactions in atmospherically relevant air/water and air/ice interfaces, and ultimately to understanding the fate of PAHs and ROSs in the atmosphere.

CHAPTER 5 ICE GROWTH FROM SUPERCOOLED AQUEOUS SOLUTIONS OF REACTIVE OXYGEN SPECIES[**]

Contents of this chapter have already been published (T. P. Liyana-Arachchi, K. T. Valsaraj and F. R. Hung, Ice growth from supercooled aqueous solutions of reactive oxygen species. Theor. Chem. Acc, 2013, 132, 1309). In this chapter, we report molecular dynamics (MD) results of adsorption and ice growth from supercooled aqueous solutions of hydroxyl (OH), hydroperoxy (HO_2) or hydrogen peroxide (H_2O_2). The main objective of this study is to explore the fate of OH, HO_2 or H_2O_2 molecules after freezing of the supercooled aqueous solutions. The rest of this paper is structured as follows. Section 5.2 contains details about our computational models and methods. Results are presented and discussed in Section 5.3, and concluding remarks are included in Section 5.4.

5.1 Introduction

Ice growth from supercooled water is a process that occurs in natural environmental conditions, in scenarios such as freezing of lakes and formation of snow pellets. Prior to this freezing process, atmospheric gases can be adsorbed at air/water interfaces such as water droplets, aerosols, fog and mist. This process typically involves adsorption at the interface and dissolution in the bulk water [1, 20, 136, 142, 145, 163]. Both hydrophobic gases (nitrogen, oxygen and ozone) and hydrophilic species (hydroxyl radicals (·OH), hydroperoxy radicals ($\cdot HO_2$), hydrogen peroxide (H_2O_2), etc.) can be adsorbed at atmospheric air/water interfaces. From the thermodynamic point of view, the former gases do not show a favorability to dissolve in water [145], but the latter hydrophilic species are known to be solvated to a considerable degree in bulk water at environmentally relevant conditions [145].

[**] Reprinted with permission of Theor. Chem. Acc, 2013, 132, 1309

These aqueous solutions of hydroxyl, hydroperoxy and hydrogen peroxide can then undergo freezing in the environment. Understanding this process is important because other species, such as polycyclic aromatic hydrocarbons (PAHs) can also adsorb at atmospheric air/water interfaces and solvate in bulk water to a considerable degree [20, 135, 149, 164]. PAHs are ubiquitous atmospheric pollutants [14] that can react with reactive oxygen species (ROSs) (e.g., ozone, hydroperoxy, hydroxyl, hydrogen peroxide) on air/water and air/ice interfaces, to produce toxic products [165] that can contribute to the formation of secondary organic aerosols (SOAs) [1, 14, 16]. SOAs are a major fraction of particulate matter, which is known to have adverse effects on human health and the climate; however, the mechanisms of formation of SOAs are not well understood at present [48, 166, 167]. Therefore, understanding the processes that happen between solutes such as PAHs and ROSs at atmospheric air/water and air/ice interfaces, as well as during freezing of aqueous solutions containing these compounds, will contribute at shedding light at issues related to SOAs and particulate matter.

In principle, PAHs and ROSs can react in gas phase, at air/water and air/ice interfaces, inside bulk water or within the quasi-liquid layer (QLL) of water formed at air/ice interfaces, or inside ice. Heterogeneous reactions between PAHs and ROSs at air/ice interfaces can exhibit kinetics that is much faster than those of their homogeneous counterparts in bulk and gas phase [1, 12, 13, 164, 168, 169]. Previous studies indicate that freezing of aqueous solutions of a number of solutes causes ice and solute molecules to separate [45, 156, 170-173]. However, in our previous simulation study for freezing of supercooled aqueous solutions of aromatics [164], we observed that benzene could become trapped inside the ice

lattice if the freezing process takes place at 260 K; increasing the temperature to 270 K causes the benzene molecules in the supercooled aqueous solution to be displaced to the air/ice interfaces formed during the freezing process. Furthermore, larger aromatic molecules such as naphthalene and phenanthrene always migrated to the air/ice interface when their aqueous solutions froze at both 270 K and 260 K. Migration of these molecules to the air/ice interfaces results in increased local concentrations at these interfaces and/or at the QLLs formed there, which in turn could result in faster reaction rates involving solutes at the air/ice interface, as observed in previous experimental studies [174-177]. Therefore, determining the final location of solutes after their aqueous solutions undergo a freezing process (i.e., whether solutes are trapped in the ice lattice, or are displaced to atmospheric air/ice interfaces or their QLLs) is important to understand the reaction mechanisms between these solutes and to determine their fate in the atmosphere.

In direct relation to our previous work of ice growth from supercooled aqueous solutions of aromatic hydrocarbons (benzene, naphthalene and phenanthrene) [164], here we report molecular dynamics (MD) simulations of ice growth from supercooled aqueous solutions of ROSs, specifically hydroxyl or hydroperoxy radicals or hydrogen peroxide molecules. First we explored the effect of these ROSs on the thickness of the QLLs formed at the air/ice interfaces. This thickness is known to depend on the temperature and is also affected by the presence of solutes [157]; in our previous study [164], we determined that the presence of aromatics in the supercooled water undergoing freezing leads to increases in the thickness of the QLLs. Experimental measurements of the thickness of the QLL are not straightforward and depend highly on the techniques used [96, 101-108]. In our simulations we also explored

whether the ROSs become trapped inside the ice lattice, or if they are displaced to the QLL or to the interface with air after freezing of their supercooled solutions. We also studied the ice growth of supercooled aqueous solutions containing ROSs and benzene, and we coated the interfaces with air with molecules of 1-octanal, simply because atmospheric water and ice films typically contain surfactants such as humic and fulvic acid-like species [21, 23, 24, 26, 48, 137, 163]. Surface-active organic molecules (e.g., alcohols, acids, amines, carbonyls, etc.) are important contributors to the total organics found on atmospheric air/water interfaces in both urban and rural areas [48, 138-140]. These surfactant-like molecules can significantly alter the interfacial properties of ice surfaces (such as QLL thickness), as well as the reactivity between PAHs and ROSs at the air/ice interface. Previous studies determined that the presence of surfactant-like molecules or other impurities at the interface enhances the adsorption of aromatic hydrocarbons and ROSs at the air/water and air/ice interface [135, 149, 178, 179]. Here we also investigated the effect of 1-octanal on the thickness of the QLL and on the fate of benzene and the ROSs after freezing of their supercooled aqueous solutions. In addition, potential of mean force (PMF) calculations for ROSs at air/water and air/ice interfaces were performed with a two-fold objective: (1) test that our chosen force fields and parameters could reproduce experimental values of the free energy of hydration of the selected ROSs (see Models and methods, below), and (2) study the thermodynamics of adsorption of these ROSs on atmospheric air/ice interfaces.

5.2. Models and Methods

Following our previous studies [135, 136, 164, 178], our PMF calculations and MD simulations reported here were performed using the GROMACS software [116]. Water was

modeled using the TIP5P model [112]. Benzene was modeled using the force fields and parameters from our previous work [164], which are able to reproduce experimental values of the free energy of solvation when used in combination with the TIP5P water model. The OPLS all-atom force field [147] was used to model 1-octanal, as we did in one of our previous studies[150]. The hydroxyl and hydroperoxy radicals, and the molecules of hydrogen peroxide were modeled using the force fields and parameters from the work of Vácha and coworkers [20, 145, 146]. However, the parameters from Vácha *et al.* were adjusted to reproduce the free energy of solvation of these ROSs in combination with the SPC/E water model [115]. Therefore, and in order to check that the ROSs parameters considered here could reproduce the experimental free energies of hydration for these species when combined with the TIP5P water model, we determined the PMF associated with moving one hydroxyl radical, one hydroperoxy radical or one molecule of hydrogen peroxide from the gas phase into a slab of liquid TIP5P water, in analogy to previous studies [20, 135, 145, 149, 164]. These results (see §5.3.1) verified that the models used here are able to reproduce experimental values of the free energies of hydration of the ROSs considered in this study. Afterwards, we performed similar calculations to determine the PMF associated with moving a hydroxyl, a hydroperoxy radical, or a molecule of hydrogen peroxide from the gas phase into the air/ice interface. Specifics of these PMF calculations are exactly the same as those described in detail in our previous papers [135, 164, 178].

For our simulations of ice growth from supercooled aqueous solutions, we followed previous studies [155, 156, 164] and prepared our initial configurations by assembling a

block of hexagonal ice I_h (576 water molecules), and put its basal plane (0001 face) in contact with a slab of 1344 molecules of liquid water, as shown in Figure 5.1.

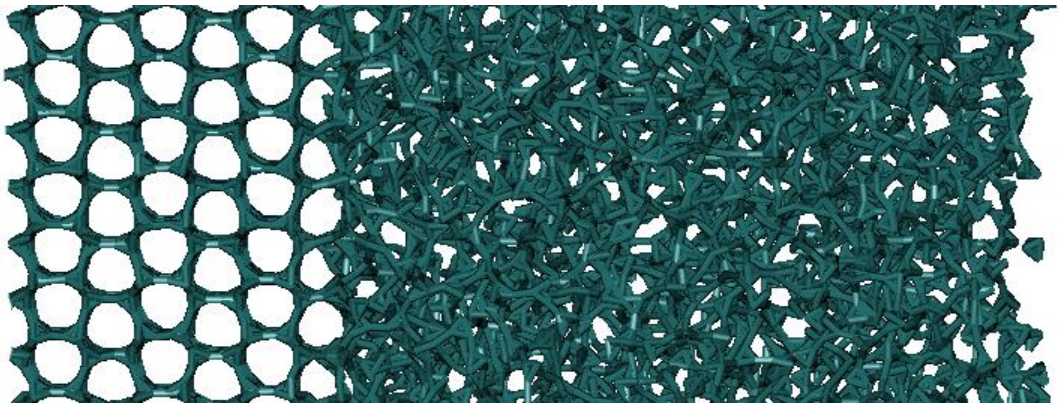

Figure 5.1. Illustration of the initial simulation system.

The ice/water slab was placed in the center of an orthorhombic simulation box with L_x = 27 Å, L_y = 31.4 Å (similar to the dimensions of the ice/water slab) and L_z = 300 Å (much larger than the z-dimension of the ice/water slab). This setup results in two vacuum regions (mimicking air), one in contact with ice (left side of Figure 5.1) and one in contact with water (right side, Figure 5.1). In our first series of simulations, six hydroxyl, hydroperoxy radicals, or six molecules of hydrogen peroxide were inserted at random positions within the slab of liquid water, and six additional hydroxyl, hydroperoxy radicals, or hydrogen peroxide molecules were placed randomly at the air/ice interface at the left in Figure 5.1. In our second series of simulations, the air/ice and air/water interfaces in Figure 5.1 were first coated each with 18 molecules of 1-octanal. Afterwards, six molecules of benzene and six hydroxyl radicals (or six molecules of hydrogen peroxide) were inserted at random positions within the slab of liquid water; six additional molecules of benzene and six additional hydroxyl radicals (or six molecules of hydrogen peroxide) were also placed randomly at the air/ice interface (left side of Figure 5.1). During the freezing process, water molecules in the liquid slab will gradually freeze and water molecules at the initial air/ice interface will melt, resulting in a

large slab of ice with two QLLs on both sides of it. The six radicals of hydroxyl, hydroperoxy, or the six molecules of hydrogen peroxide, and/or the six molecules of benzene initially placed at the air/ice interface will likely remain at this interface or within the QLL formed at this interface. The other six radicals/molecules of ROSs, and/or the other six benzene molecules that were initially inserted in the slab of liquid water, will either get incorporated into the ice lattice, or will migrate to the air/ice interface or the QLL formed after freezing at the right side of Figure 5.1. Each of the simulated systems was first relaxed using the steepest descent energy minimization method. Afterwards, MD simulations were conducted following the procedure described in previous studies [155, 156, 164]. The system was thermally coupled to a Nosé-Hoover thermostat, and a Parrinello-Rahman barostat set at 1 atm was coupled only on the *xy* plane (where the *z* direction is perpendicular to the air/ice interface), allowing the *x* and *y* dimensions of the simulation box to fluctuate while keeping its *z*-dimension constant at 300 Å. Two temperatures, 270 K and 260 K, were considered in our first set of simulations (without benzene and 1-octanal), whereas our second set of simulations (including benzene and 1-octanal) were run only at 260 K. Periodic boundary conditions were applied in all three directions. A time step of 1 fs was used in all our MD simulations and data were collected every 10 ps. Bond lengths were constrained using the LINCS algorithm [119]. A cut-off distance of 0.9 nm was used for the Lennard-Jones interactions. The particle-mesh Ewald (PME) method [122] was used with a cutoff of 0.9 nm and a grid spacing of 0.12 nm in order to account for long-range Coulombic interactions. MD simulations were run for up to 220 ns, and at least two independent simulation runs starting

from different initial configurations were performed for each system. We used the software VMD [126] for all our visualizations.

5.3. Results and Discussion

5.3.1. PMF of Hydroxyl, Hydroperoxy and Hydrogen peroxide in Air/water and Air/ice Interfaces

In Figure 5.2 we present the PMF associated with moving one radical of hydroxyl or hydroperoxy, or one molecule of hydrogen peroxide from the gas phase to the air/water interface and then into the bulk water phase. In Figure 5.2 the air/water interface is arbitrarily depicted as the point where the density of water reaches 500 kg/m^3.

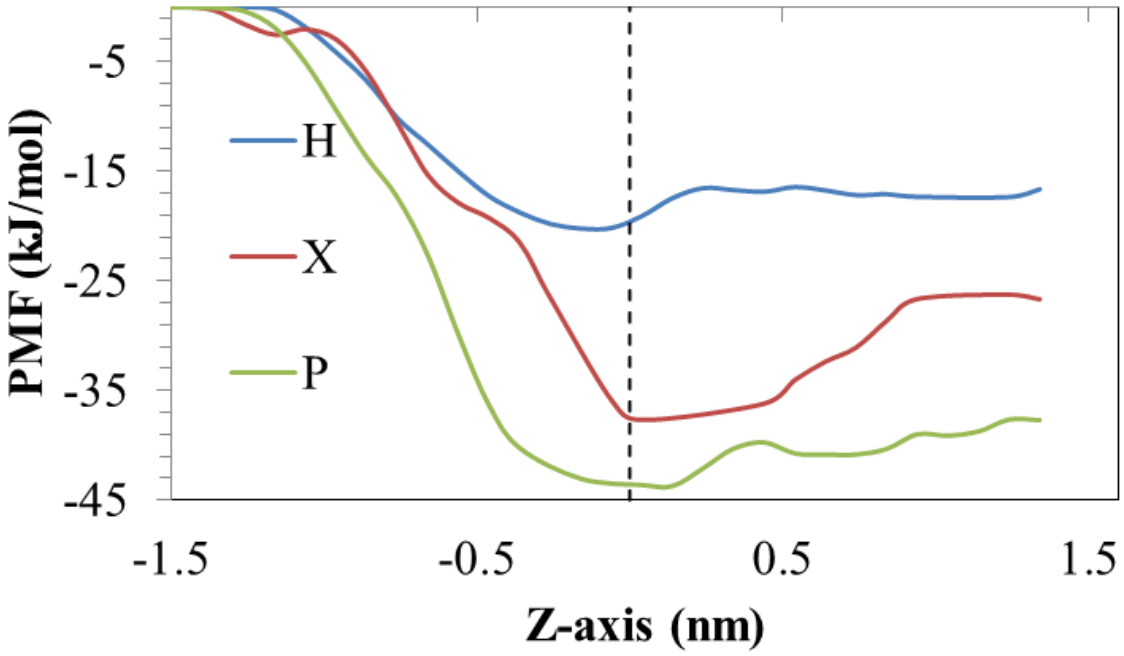

Figure 5.2. PMF of moving one hydroxyl or hydroperoxy radical, or one molecule of hydrogen peroxide from the gas phase into water in air/water systems at 298 K. Letters H, X and P represent the PMF for hydroxyl radical, hydroperoxy radical and hydrogen peroxide. A value of zero in the *z*-axis represents the air/water interface (arbitrarily defined as the point where the water density reaches 500 kg/m^3); positive values in the *z*-axis represent the bulk water phase.

As indicated above, the goal of our PMF calculations is to verify whether the experimental free energies of hydration of these ROSs can be reproduced satisfactorily with our chosen combination of models (see Models and methods). From Figure 5.2, the simulated free energy of hydration for the hydroxyl and hydroperoxy radicals, and for hydrogen peroxide, is about -16.5 kJ/mol, -26.0 kJ/mol and -37.0 kJ/mol, respectively. These results are similar to reported experimental values: between -15.9 and -16.7 kJ/mol for hydroxyl radical, -25.1 to -31.3 kJ/mol for hydroperoxy radical, and between -35.5 and -37.6 kJ/mol for hydrogen peroxide, as determined from Henry's law constants [145]. Our results are also consistent with the simulated hydration free energies obtained for the same ROSs but with SPC/E water by Vácha *et al.* [145]. These results show that the experimental free energy of hydration of the ROSs considered in this study can be reproduced satisfactorily with our chosen models for ROSs and water. The PMF profiles for the ROSs studied exhibit minima at the air/water interface, with values of -20.2 kJ/mol (hydroxyl radical), -37.6 kJ/mol (hydroperoxy radical) and -43.7 kJ/mol (hydrogen peroxide). These values are very similar to those reported by Vácha *et al.* [145], and suggest that these ROSs have a thermodynamic incentive to be adsorbed at the air/water interface.

In Figure 5.3 we present the PMF obtained by moving one hydroxyl or one hydroperoxy radical, or one hydrogen peroxide molecule from the gas phase into the air/ice systems at 270 K. In analogy to what we did for air/water systems, the air/ice interface is arbitrarily illustrated in Figure 5.3 as the point where the density of water reaches 500 kg/m^3. All PMF profiles show sharp increases as the ROSs are dragged close to the frozen water molecules. The PMF profile for the hydroxyl radical exhibits a minimum of -15.9 kJ/mol at the air/ice

interface. This minimum is deeper than the PMF value observed for hydroxyl radical within the QLL (around -10 kJ/mol). In contrast, the PMF profiles for hydroperoxy radical and hydrogen peroxide exhibit minima at the air/ice interface that are on the order of -33 kJ/mol and -36 kJ/mol respectively, but these values are very similar to those observed for these ROSs inside the QLL (Figure 5.3).

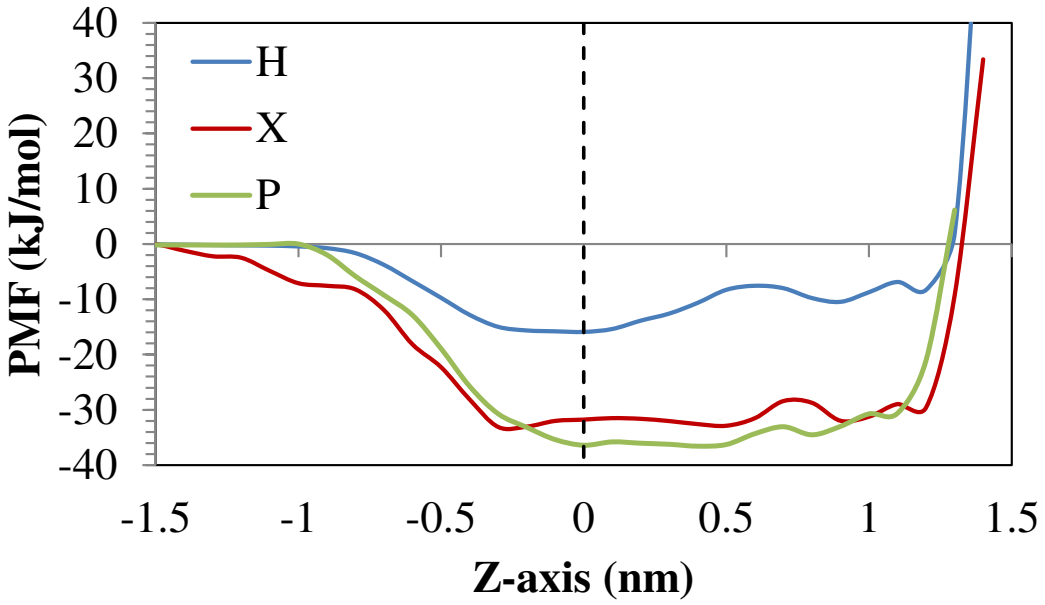

Figure 5.3. PMF of moving one hydroxyl or hydroperoxy radical, or one molecule of hydrogen peroxide from the gas phase into water in air/ice systems at 270 K. Letters H, X and P represent the PMF for hydroxyl radical, hydroperoxy radical and hydrogen peroxide. A value of zero in the *z*-axis represents the air/ice interface (arbitrarily defined as the point where the water density reaches 500 kg/m^3); positive values in the *z*-axis represent the QLL and the bulk ice.

These trends suggest that from the thermodynamic point of view, in air/ice systems a hydroperoxy radical and a molecule of hydrogen peroxide can be adsorbed at the air/ice interface or be dissolved in the QLL, rather than staying in the gas phase; in contrast, a hydroxyl radical has a thermodynamic incentive to remain at the air/ice interface. These trends shown in Figure 5.3 also contrast to those observed in Figure 5.2, where all ROSs considered prefer to remain at the air/water interface. The PMF curves for hyperoxy depicted

in Figures 5.2 and 5.3 exhibit small minima around 1.2 nm away from both water and ice surfaces. After reviewing movies of the simulation trajectories, we observed that a few water molecules leave the bulk system and bind to the hyperoxy molecule when it is about 1.2 nm away from the air/water and air/ice interfaces, which might be the reason for these small local minima in the PMF. The results shown in Figures 5.2 and 5.3 suggest that the air/ice interface represent a rather different environment for the ROSs studied here as compared to the air/water interface.

5.3.2. Ice Growth from Supercooled Aqueous Solutions of ROSs, and ROSs/benzene/1-octanal

As indicated in the Models and methods section and in our previous study [164], when the initial system shown in Figure 5.1 is allowed to evolve in time, water molecules in the liquid slab gradually freeze and water molecules at the air/ice interface at the left of Figure 5.1 melted, resulting in a large slab of ice with two equilibrated QLLs on both sides of it. During our simulations of ice growth, we monitored the time evolution of the density profiles of the water molecules in each of the systems studied, and after some time we observed negligible variations in these density profiles of water and in the thicknesses of both QLLs, which suggests that the systems have reached stable conditions. In addition, and because the two QLLs were formed by two different paths (one from freezing and the other from melting), the fact that both QLLs have similar thicknesses is a strong indication that the system has reached stable conditions. Following previous studies [159, 160, 164], the thickness of the QLLs was estimated by calculating the root mean square fluctuations δ in the oxygen-oxygen distance between water molecules for all the systems:

$$\delta = \frac{2}{n(n-1)} \sum_{i<j}^{n} \left[\frac{\sqrt{\langle r_{ij}^2 \rangle - \langle r_{ij} \rangle^2}}{\langle r_{ij} \rangle} \right] \quad (1)$$

where n is the number of water molecules in a given region, r_{ij} is the distance between the oxygen atoms of molecules i and j, and the brackets represent time average. Following the Lindemann criterion used in previous studies [159, 160, 164], a region where $\delta \geq 0.1$ is considered as the QLL region. For ice growth from supercooled aqueous solutions of hydroxyl or hydroperoxy radicals, or hydrogen peroxide, we determined the thickness of the two QLLs to be approximately 10.0 Å, 11.0 Å and 11.0 Å respectively at 270 K, and around 8.0 Å for all systems at 260 K. From our previous work [164], the QLL thickness obtained from ice growth from a water/ice system with no solutes was 8.5 Å at 270 K and 7.5 Å at 260 K. This comparison suggests that the presence of dissolved ROSs tend to increase the thickness of the QLLs formed at the air/ice interfaces from ice growth. We observed similar results in our previous work [164], where aromatic solutes (benzene, naphthalene and phenanthrene) dissolved in water also lead to an increase in the QLL thickness. These phenomena are related to colligative properties, where the presence of solutes cause changes in the chemical potential of the liquid phase, and lead to reductions in the freezing point and vapor pressure, and increases in the boiling point of solutions.

In Figure 5.4 we present the density profiles obtained for hydroxyl, hydroperoxy or hydrogen peroxide and water molecules in air/ice systems at 270 K, after ice growth from supercooled aqueous solutions; side views of representative simulation snapshots for hydroxyl and hydrogen peroxide systems are depicted in Figure 5.5 (snapshots of hydroperoxy systems are not shown for brevity).

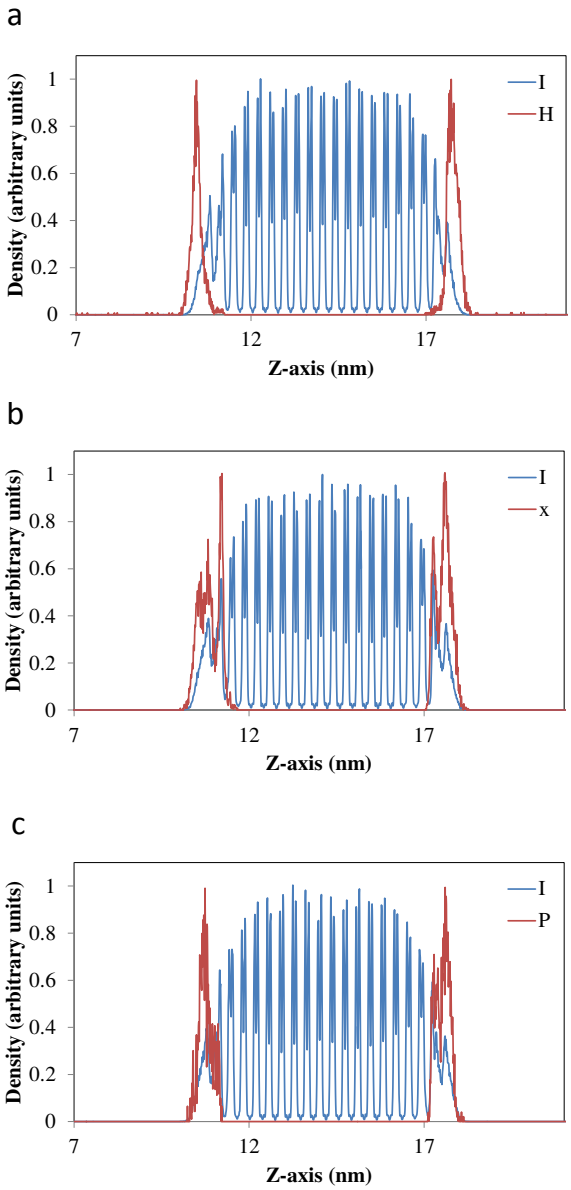

Figure 5.4. Density profiles of sub-cooled aqueous systems of hydroxyl and hydroperoxy radicals and hydrogen peroxide after freezing at 270 K. Letters I, H, X and P represent water, hydroxyl, hydroperoxy and hydrogen peroxide. **(a)** System with 12 hydroxyl radicals. **(b)** System with 12 hydroperoxy radicals. **(c)** System with 12 hydrogen peroxide molecules. The density profile of each species is normalized by dividing by the maximum value of the local density of each species in the simulation box.

These results suggest that at 270 K, none of the ROSs that were initially placed within the original slab of liquid water (Figure 5.1) get trapped inside the ice lattice as water freezes; rather, the ROSs are displaced to the air/ice interface formed at the right side of Figures 5.1 and 5.5, or to its QLL during the growth of ice. Likewise, the ROSs that was initially placed

at the original air/ice interface (left side in Figure 5.1) remains at this interface or inside its QLL.

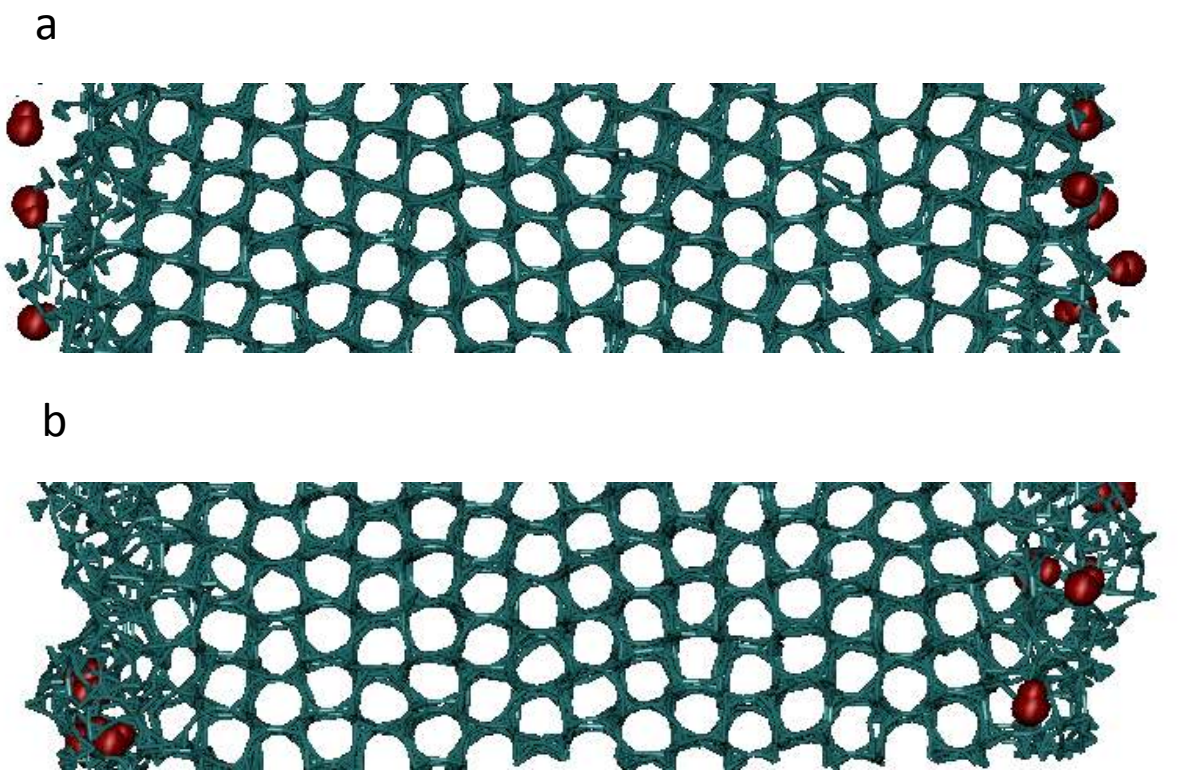

Figure 5.5. Side view of representative simulation snapshots obtained after freezing of supercooled aqueous solutions of hydroxyl or hydrogen peroxide at 270 K. **(a)** System with 12 hydroxyl radicals. **(b)** System with 12 hydrogen peroxide molecules. Hydroxyl and hydrogen peroxide = red; water molecules = cyan.

The results shown in Figures 5.4 and 5.5 indicate that the hydroxyl radicals tend to remain at the air/ice interfaces or slightly inside the QLLs. In contrast, hydroperoxy radical and hydrogen peroxide remain mostly inside the QLLs (Figures 5.4 and 5.5). Similar results were obtained in each of the independent simulation runs performed for these systems at 270 K. In our previous study [164] we also observed that PAHs tend to migrate to the air/ice interface or its QLL during freezing of supercooled aqueous solutions at 270 K.

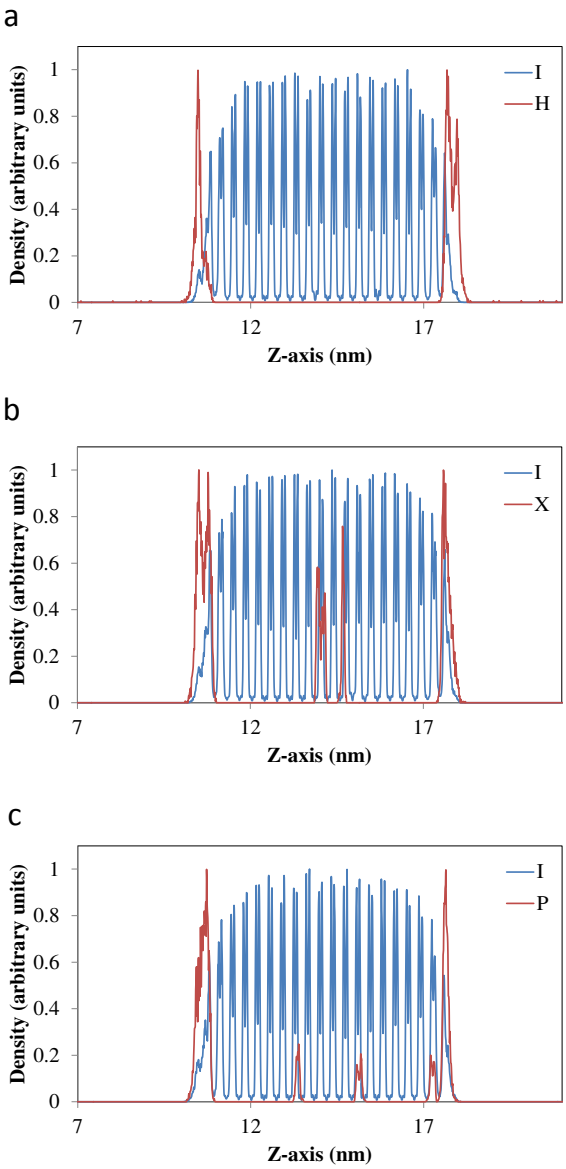

Figure 5.6. Density profiles of sub-cooled aqueous systems of hydroxyl, hydroperoxy or hydrogen peroxide after freezing at 260 K. Letters I, H, X and P represent water, hydroxyl radicals, hydroperoxy radicals and hydrogen peroxide molecules. **(a)** System with 12 hydroxyl radicals. **(b)** System with 12 hydroperoxy radicals. **(c)** System with 12 hydrogen peroxide molecules. The density profile of each species is normalized by dividing by the maximum value of the local density of each species in the simulation box.

These results are important because the migration of these PAHs and ROSs from bulk liquid water to the air/ice interface or its QLL during ice growth would result in higher local concentrations of these species at these interfaces, which in turn could cause larger reaction rates between PAHs and ROSs under relevant atmospheric conditions.

In Figure 5.6 we present density profiles of hydroxyl, hydroperoxy, hydrogen peroxide and water molecules in air/ice systems at 260 K after ice growth from supercooled aqueous solutions, and representative snapshots of hydroxyl radical and hydrogen peroxide systems are shown in Figure 5.7 (snapshots of hydroperoxy radical systems are not shown for brevity). For hydroxyl radical systems at 260 K, the observations are similar to those described above for the same system at 270 K, namely that these radicals tend to stay at the air/ice interface or inside the QLLs formed after the freezing process.

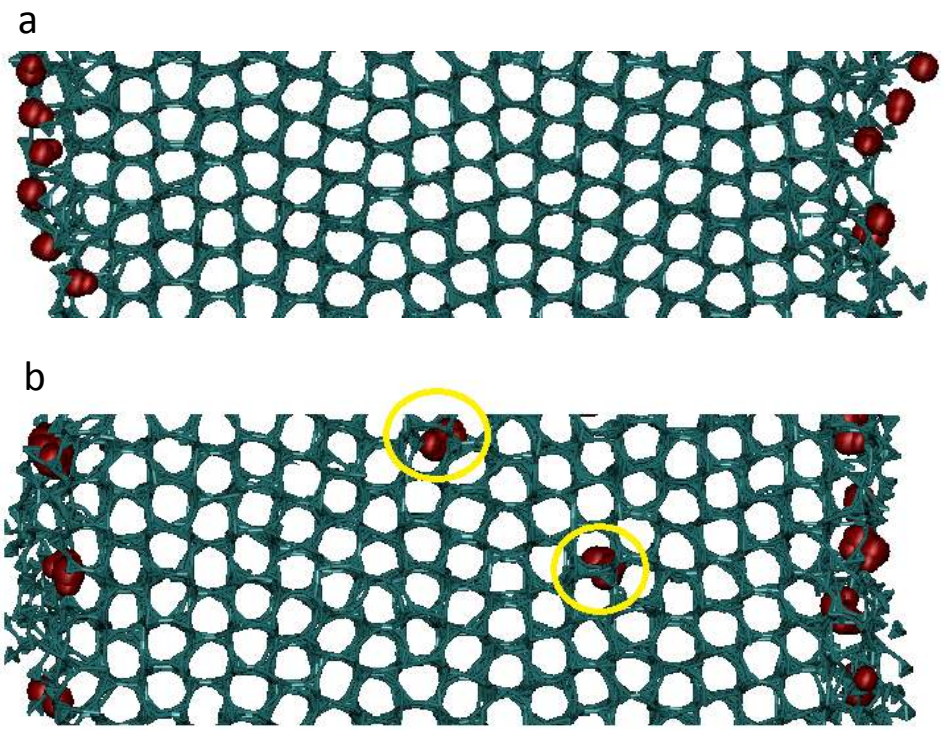

Figure 5.7. Side view of representative simulation snapshots obtained after freezing of supercooled aqueous solutions of hydroxyl or hydrogen peroxide at 260 K. **(a)** System with 12 hydroxyl radicals. **(b)** System with 12 hydrogen peroxide molecules. Hydroxyl and hydrogen peroxide = red; water molecules = cyan.

In contrast, several of the hydroperoxy radicals or hydrogen peroxide molecules initially placed in the water slab (Figure 5.1) become trapped inside the ice lattice as water freezes, while the rest of these ROSs migrate to the QLL near the air/ice interface formed on the right side of Figures 5.6 and 5.7. The hydroperoxy radicals or hydrogen peroxide

molecules initially placed at the air/ice interface on the left side of Figure 5.1 remain at this interface, mostly inside its QLL (Figures 5.6 and 5.7). These trends were observed in each of the independent simulation runs performed at 260 K. In analogy to hydroperoxy and hydrogen peroxide systems, in our previous study [164] we observed that benzene can be trapped inside the ice lattice during ice growth at 260 K, but not during the freezing process at 270 K. Likewise, naphthalene and phenanthrene could not be trapped inside the ice lattice at either 260 K or 270 K [164], in analogy to what we observed for hydroxyl radical systems here. These combined results suggest that the local concentrations of PAHs and ROSs at air/ice interfaces would also depend on the temperature, which in turn affects the reactivity of these species at these atmospheric interfaces. These results for hydroperoxy and hydrogen peroxide (Figures 5.6 and 5.7), as well as those for benzene [164] at 260 K, are based on the short-time dynamics of those systems, as our MD simulations covered over a few hundreds of nanoseconds. Experimental studies on similar systems are currently being performed by us and will likely lead to more insights about these systems.

Mean square displacement (MSD) results for hydroxyl and hydroperoxy radicals and hydrogen peroxide molecules after ice growth at 270 K are shown in Figure 5.8a. At this temperature, all ROSs are displaced to the air/ice interfaces or their QLLs (Figures 5.4 and 5.5). The dynamics of the hydroperoxy radicals and the hydrogen peroxide molecules at the air/ice interface are significantly slower than those of the hydroxyl radicals. This observation can be explained from Figures 5.3-5, where we discussed that hydroxyl radicals prefer to stay at the air/ice interface, whereas hydroperoxy and hydrogen peroxide tend to remain slightly deeper inside the QLL, which may slow down their dynamics.

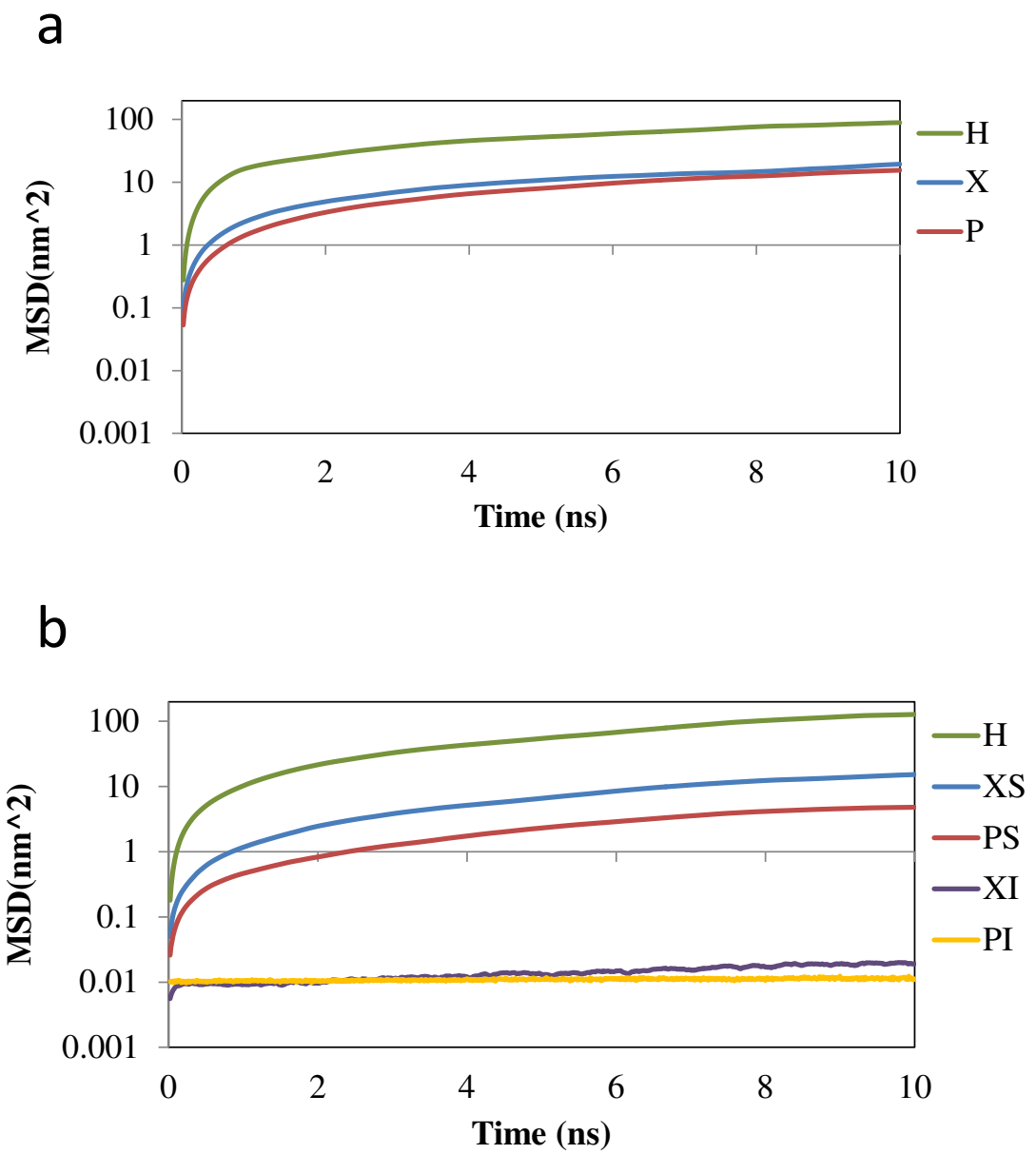

Figure 5.8. Mean square displacements of hydroxyl and hydroperoxy radicals and hydrogen peroxide molecules after freezing at **(a)** 270 K and **(b)** 260 K. In **(a)**, letters H, X and P represent hydroxyl, hydroperoxy and hydrogen peroxide. In **(b)**, letters H, XS and PS represent hydroxyl, hydroperoxy and hydrogen peroxide at the air/ice interfaces, and letters XI and PI represent hydroperoxy and hydrogen peroxide trapped inside the ice lattice.

Furthermore, hydroperoxy and hydrogen peroxide have a larger size and could form more hydrogen bonds with water molecules as compared to hydroxyl radicals. In Figure 5.8b we show MSD results for hydroxyl and hydroperoxy radicals, and hydrogen peroxide molecules after ice growth at 260 K; results are shown for the ROSs at the air/ice interface

and for those trapped inside the ice lattice. As expected, all MSDs decrease with temperature, and the MSDs of the hydroperoxy radicals and hydrogen peroxide molecules trapped in the ice lattice are much lower than those of the same species displaced to the air/ice interfaces or their QLLs. In analogy to the MSD results at 270 K, the dynamics of the hydroxyl radicals at the air/ice interface are faster than those of the hydroperoxy radicals and hydrogen peroxide molecules at the interfaces. The dynamics of hydroperoxy and hydrogen peroxide and hydroxyl shown in Figure 5.8 may also explain why the former ROSs can be trapped by the growing ice lattice at 260 K (Figures 5.6 and 5.7), but not at 270 K (Figures 5.4 and 5.5), whereas hydroxyl is displaced to the air/ice interfaces at these two temperatures.

In our second series of simulations, we considered freezing of supercooled aqueous solutions containing benzene and hydroxyl (or hydrogen peroxide); in addition, the two interfaces with air in our initial setup (Figure 5.1) were coated with a fixed number of 1-octanal molecules (see Models and methods). Simulations were run only at 1 atm and 260 K. The thickness of the QLLs obtained after freezing in these systems was determined using the criteria outlined in the previous section, and it was found to be approximately 6.5 Å at 260 K for both systems (benzene/hydroxyl/1-octanal, and benzene/hydrogen peroxide/1-octanal). This observation suggests that the presence of surfactant-like molecules such as 1-octanal at the air/ice interfaces tends to decrease the thickness of the QLLs formed after ice growth (δ = 8 Å for both hydroxyl or hydrogen peroxide, as discussed above; δ = 8.5 Å for benzene [164], all after freezing at 260 K). A decrease in QLL thickness, in this case due to the presence of surfactant-like molecules at the interface, is relevant because it would result in a larger local concentration of solutes such as aromatics and ROSs inside the QLL

after freezing of aqueous solutions, and could in turn affect the rate of reactions between these species at atmospheric air/ice interfaces.

In Figure 5.9 we depict density profiles of hydroxyl radical (or hydrogen peroxide), benzene, 1-octanal and water molecules, as obtained after freezing of these supercooled aqueous solutions at 260 K.

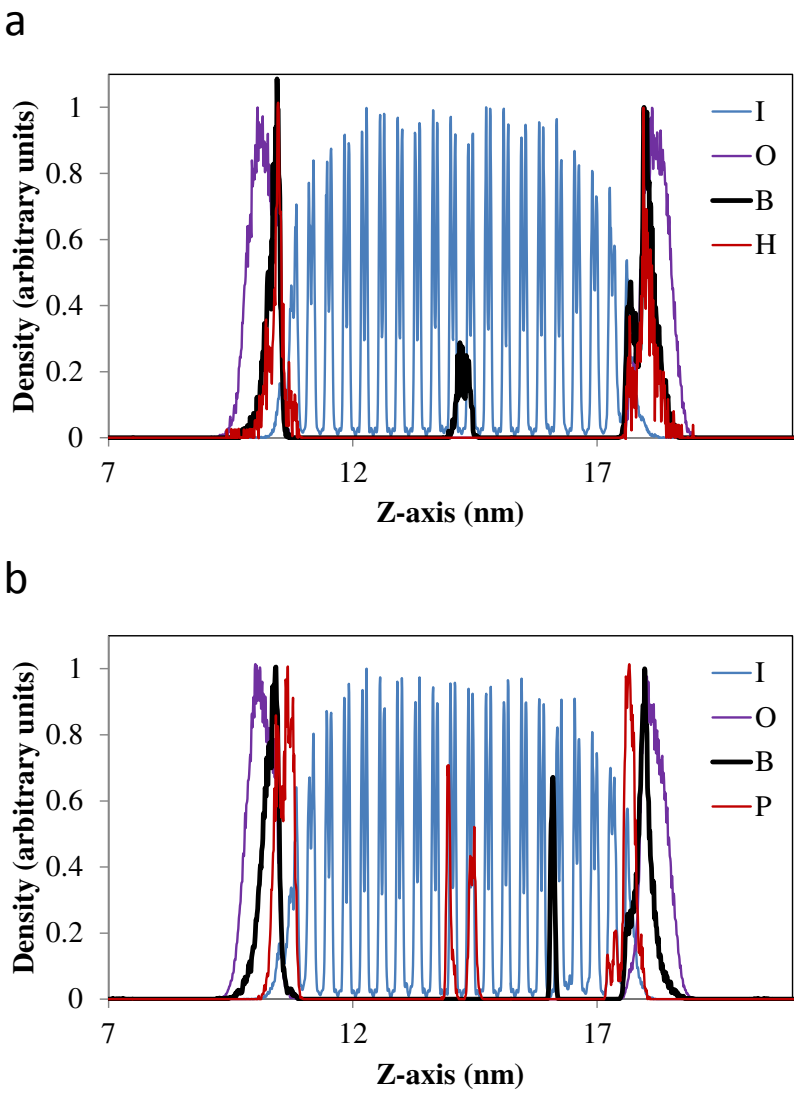

Figure 5.9. Density profiles of benzene, 1-octanal, water and **(a)** hydroxyl radical, or **(b)** hydrogen peroxide, after freezing of these sub-cooled aqueous solutions at 260 K. Letters I, O, B, H and P represent water, 1-octanal, benzene, hydroxyl or hydrogen peroxide. The density profile of each species is normalized by dividing by the maximum value of the local density of each species in the simulation box

Side views of representative simulation snapshots of these two systems are presented in Figure 5.10. These results indicate that benzene and hydrogen peroxide can be trapped inside the growing ice lattice, but hydroxyl radicals cannot, in analogy to the results discussed above (Figures 5.5-5.8, freezing of supercooled solutions of ROSs) and in our previous paper ([164], freezing of supercooled solutions of aromatics).

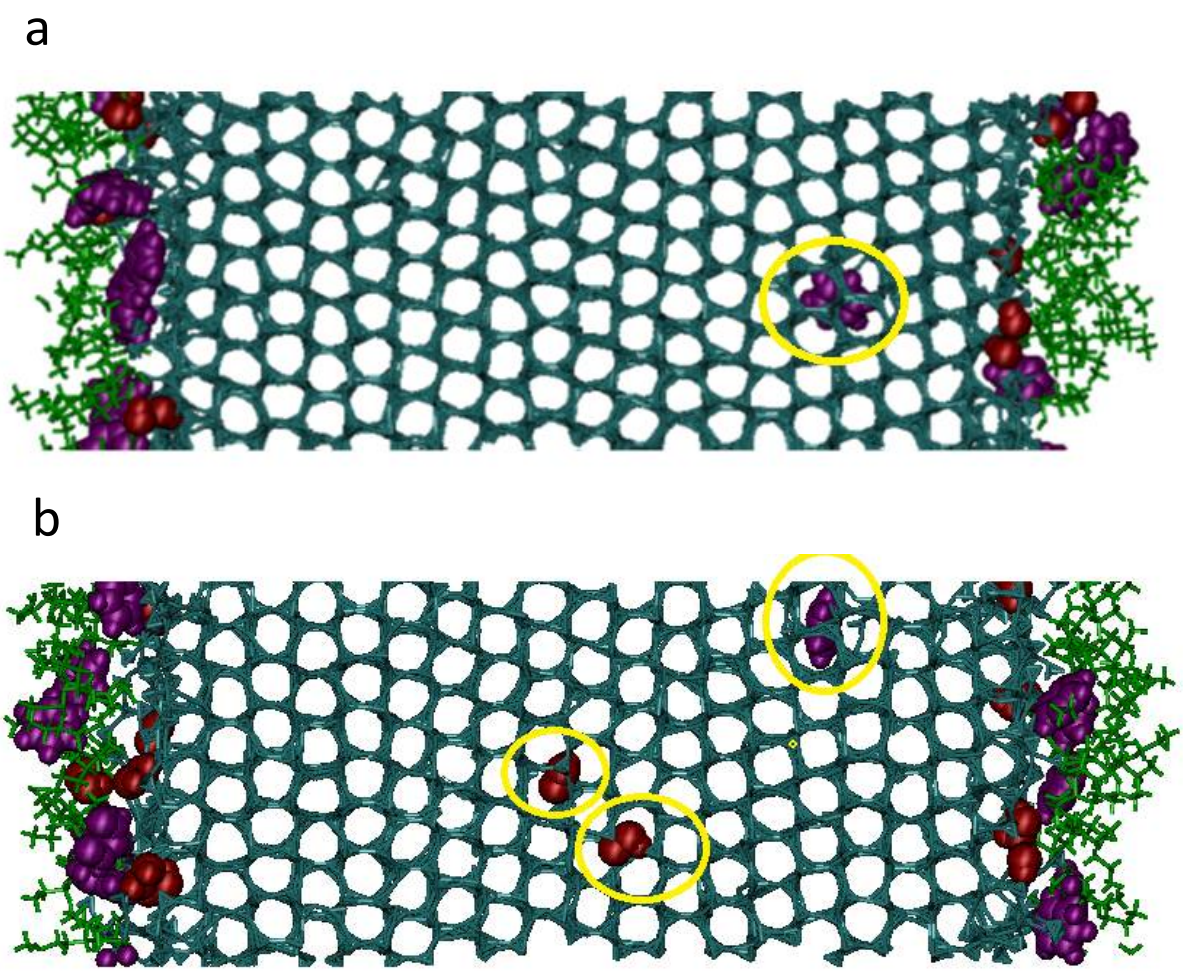

Figure 5.10. Side view of representative simulation snapshots of sub-cooled aqueous solutions containing benzene, 1-octanal, and hydroxyl radical or hydrogen peroxide after freezing at 260 K. **(a)** System with 12 hydroxyl radicals, 12 benzene and 36 1-octanal molecules. **(b)** System with 12 hydrogen peroxide, 12 benzene and 36 1-octanal molecules. Hydroxyl and hydrogen peroxide = red; water molecules = cyan; benzene molecules = purple; octanal molecules = green.

In other words, the presence of additional species such as 1-octanal and benzene does not allow hydroxyl radicals to become trapped inside the ice crystal during freezing, nor allows

hydrogen peroxide (or benzene) to escape the growing ice lattice. The hydroxyl radicals tend to remain inside the 1-octanal layer in the air/ice interfaces; in contrast, the hydrogen peroxide molecules tend to lie inside the QLL, slightly away from the layer of 1-octanal. These trends are similar to those observed for the same ROSs in systems where the interfaces are not coated with 1-octanal (see Figures 5.5-5.8 and their discussion above). Benzene molecules tend to remain inside the 1-octanal layer in both systems, which is similar to what we observed for adsorption of naphthalene on air/ice interfaces coated with 1-octanal [178]. The trends observed in this study are important to understand the reactivity between ROSs and aromatics at atmospheric air/ice interfaces. For example, a reduction in the QLL thickness and the migration of ROSs and aromatics to the air/ice interface and/or its QLL could result in enhanced reaction rates between these species because of their larger local concentrations at these interfaces. Mean square displacement (MSD) results at 260 K for hydroxyl radical, hydrogen peroxide and benzene molecules in air/ice systems coated with 1-octanal are shown in Figure 5.11. Again, the dynamics of the hydrogen peroxide and benzene molecules trapped inside the ice lattice are significantly slower than those observed for the molecules of the same species that are at the interfaces. In addition, the dynamics of hydroxyl, hydrogen peroxide and benzene at the air/ice interfaces coated with 1-octanal are significantly slower than those observed for the same species at bare air/ice interfaces (see Figure 8 above, and Figure 10 in [164]). These trends are consistent with those observed in our previous study [178], where the dynamics of naphthalene molecules were also hindered by the presence of surfactants at the air/ice interface.

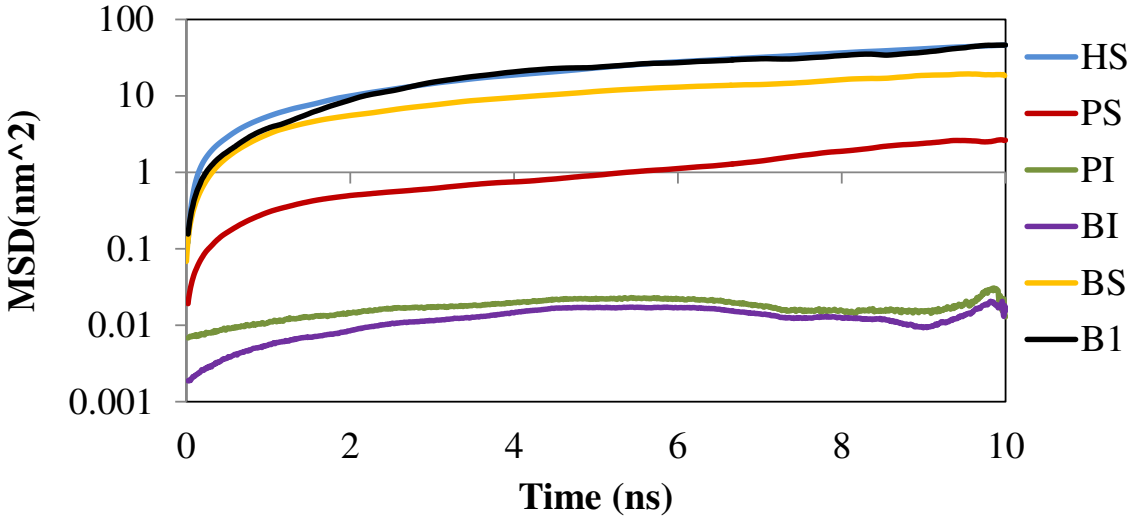

Figure 5.11. Mean square displacement of hydroxyl radical, hydrogen peroxide and benzene molecules after freezing at 260 K. Letters HS, PS, PI, BI, BS and B1 respresents hydroxyl at the surface, hydrogen peroxide at the surface, hydrogen peroxide inside ice, benzene inside ice, benzene at the surface, and benzene on bare air/ice interface, respectively.

We further explored the structure of water in the ice lattice near the hydroperoxy radicals and hydrogen peroxide and benzene molecules that were trapped in ice, by measuring the tetrahedral orientational order parameter q_i as defined by Errington and Debenedetti [162]:

$$q_i = \left[1 - \frac{3}{8}\sum_{j=1}^{3}\sum_{k=j+1}^{4}\left(\cos\theta_{i,j,k} + \frac{1}{3}\right)^2\right] \qquad (2)$$

The tetrahedral order parameter q_i of water molecule i is calculated by running sums over the oxygen atoms of the four nearest neighbors of molecule i. $\theta_{i,j,k}$ is the angle formed between the oxygens of molecules i, j and k, with the oxygen atom of molecule i placed as the angle vertex. q_i = 1 for an ideal ice crystal (i.e., a perfect tetrahedral network), and q_i = 0 for an ideal gas. Following methods described in previous studies [180, 181], we calculated the threshold order parameter q_t for TIP5P water model to be around 0.92. This threshold is defined in such a way that $q_i > q_t$ represents ice-like molecules, and $q_i < q_t$ represents liquid-like (disordered) molecules. Then q_i was measured for water molecules within a 1×1×1 nm^3 cube enclosing a hydroperoxy radical, benzene, or hydrogen peroxide molecule trapped

in the ice lattice. We then compared those results against those obtained for water molecules in the ice lattice far away from these trapped species. The distribution of q_i is shown in Figure 5.12.

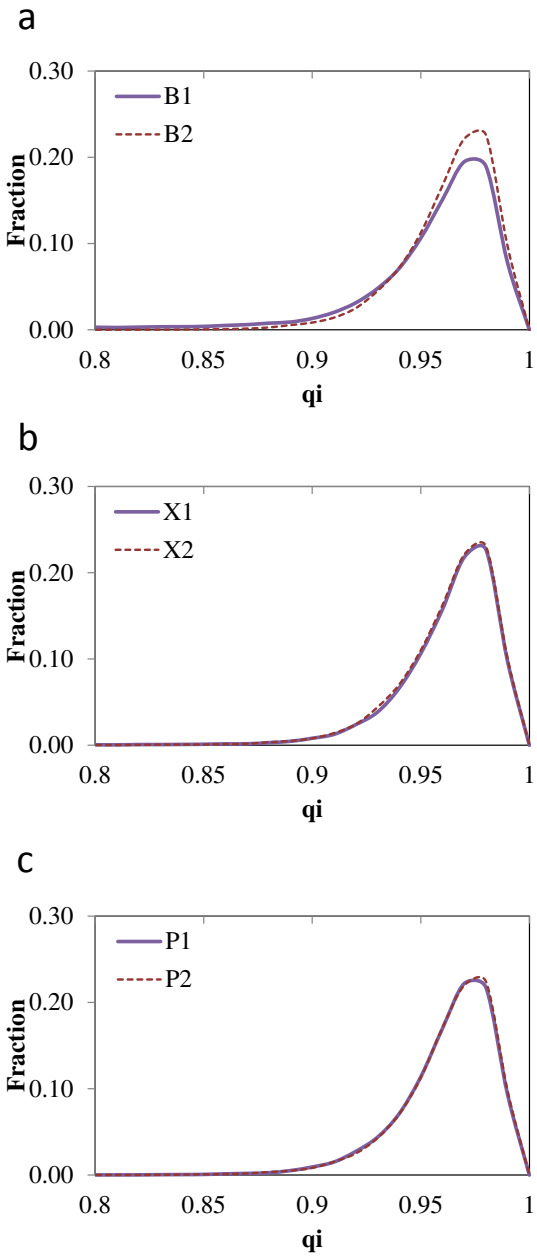

Figure 5.12. Tetrahedral order parameter q_i of water molecules near and far away from the hydroperoxy radicals, hydrogen peroxide or benzene molecules trapped inside the ice lattice. **(a)** Around benzene. **(b)** Around hydroperoxy. **(c)** Around hydrogen peroxide. In all cases, the blue continuous lines represent q_i of water molecules close to the ice-trapped aromatics or ROSs, and the red dashed lines represent q_i of water molecules far away from the trapped species.

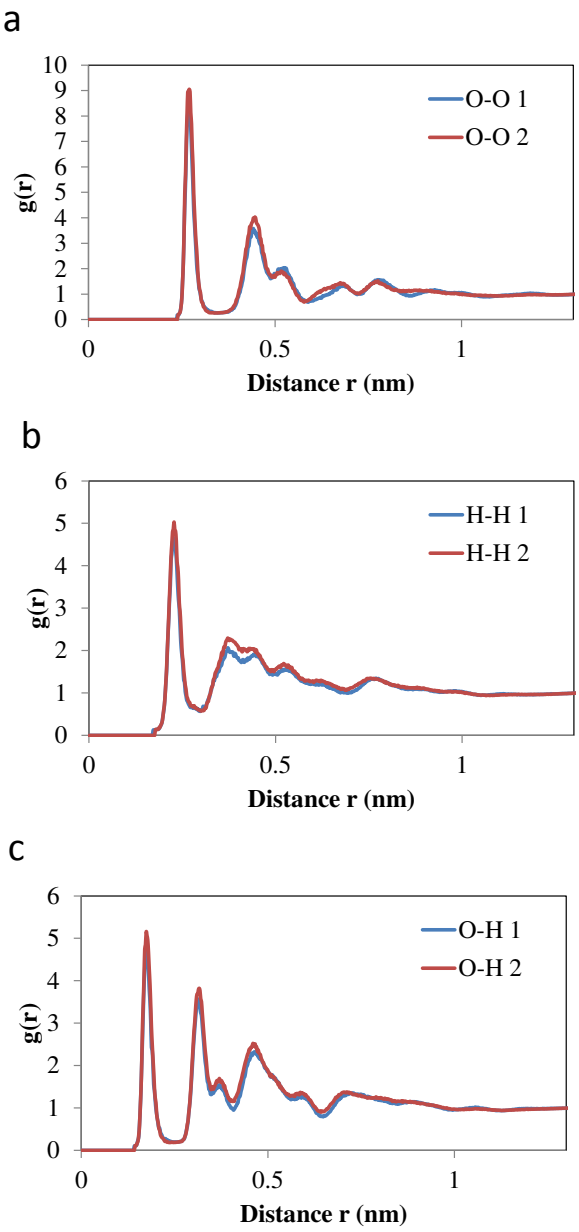

Figure 5.13. Radial distribution functions $g(r)$ of water molecules near and far away from the hydrogen peroxide molecules trapped inside the ice lattice. (a) oxygen-oxygen. (b) hydrogen-hydrogen. (c) oxygen-hydrogen. 1 represents the radial distribution function between water molecules close to the trapped hydrogen peroxide molecules, and 2 represents the water molecules far away from the trapped hydrogen peroxide molecules.

The average value of q_i for molecules far away from the trapped species was approximately 0.96 in all cases, whereas the average values of q_i close to trapped benzene, hydroperoxy or hydrogen peroxide were approximately 0.93, 0.96 and 0.96 respectively. Negligible variations in the distributions of q_i of water molecules near and far away species

trapped in the ice are observed; only slight differences are observed for water molecules near and far away from benzene trapped in the ice lattice. These results suggest that the structure of ice is minimally affected by the species trapped in the ice lattice. The structure of ice I_h as given by these values of q_i around and far away solutes agree with results obtained in previous studies, where q_i = 0.8-0.96 for crystalline ice for different water models [180, 182-184]. The structure of water in the ice lattice near and far away from the trapped species was further explored by computing oxygen-oxygen, oxygen-hydrogen and hydrogen-hydrogen radial distribution functions for water. These $g(r)$ functions are shown in Figure 5.13 only for water molecules close to and far away from hydrogen peroxide molecules trapped in the ice lattice; similar results were obtained for water close to and far away from trapped hydroperoxy and benzene [164]. These results further corroborate that the structure of ice near the trapped ROSs and aromatics is only slightly distorted when compared to that far away from the trapped species.

5.4. Concluding Remarks

MD simulations were performed to investigate the growth of ice from supercooled aqueous solutions containing (1) ROSs such as hydroxyl or hydroperoxy radicals, and hydrogen peroxide molecules, and (2) mixtures of the same ROSs with benzene molecules, and with molecules of 1-octanal present at the interfaces with air. We intended to explore the effects of these species on the thickness of the QLL formed at the air/ice interface, as well as to investigate the fate of the ROSs and aromatics after the freezing process, namely if these species become trapped by the growing ice lattice, or if they are displaced to the air/ice interface or to its QLL. Before running these simulations, we verified that our combination of

force fields (TIP5P [112] for water, and the parameters from Vácha *et al.* [145] for hydroxyl, hydroperoxy and hydrogen peroxide) could reproduce the experimental free energies of hydration of these ROSs, by performing PMF calculations for these ROSs on air/water interfaces. We then performed similar PMF calculations for the same ROSs at air/ice interfaces, finding that the PMF minima for hydroperoxy and hydrogen peroxide at the air/ice interface are very similar to the PMF values observed for these species inside the QLL. These trends contrast to what was observed for hydroxyl at air/ice interfaces, and for the ROSs at air/water interfaces, for which the PMF minima was deeper than the value of PMF observed inside the QLL (air/ice systems) or inside bulk water (air/water systems). Our MD simulations of ice growth from supercooled aqueous solutions indicate that the presence of ROSs or benzene in the water leads to the formation of QLLs in the air/ice interfaces that are thicker than those formed when pure supercooled water is frozen; in contrast, coating the interfaces with 1-octanal leads to the formation of thinner QLLs. ROSs were always displaced from the ice lattice into the air/ice interface after the freezing process at 270 K. At 260 K, hydroxyl was always displaced to the air/ice interface, but a significant fraction of hydroperoxy and hydrogen peroxide become trapped by the growing ice lattice during the freezing process at this temperature. These observations might be explained by the facts that (1) our PMF calculations indicate that hydroxyl radicals prefer to remain at the air/interface, whereas hydroperoxy and hydrogen peroxide prefer to lie inside the QLL; (2) the dynamics of hydroxyl in these systems are significantly faster than those observed for hydroperoxy and hydrogen peroxide; and (3) hydroperoxy and hydrogen peroxide have a larger size and could form more hydrogen bonds with water molecules as compared to hydroxyl radicals. The

structure of water as determined from the tetrahedral order parameter and radial distribution functions is not significantly altered by the presence of hydroperoxy, hydrogen peroxide or benzene trapped in the ice lattice. The presence of 1-octanal at the air/ice interfaces does not alter the trends described above, but tend to slow down the dynamics of ROSs and aromatics at the air/ice interface. Overall, these results are relevant to determining reactivity between aromatic hydrocarbons and ROSs in atmospheric air/ice interfaces, as well as to determining the faith of these species in the atmosphere.

CHAPTER 6 MOLECULAR SIMULATION OF GREEN LEAF VOLATILES AND ATMOSPHERIC OXIDANTS ON AIR/WATER INTERFACES[††]

Contents of this chapter have already been published (Thilanga P. Liyana-Arachchi, Christopher Stevens, Amie K. Hansel, Franz S. Ehrenhauser, Kalliat T. Valsaraj and Francisco R. Hung, Molecular simulations of green leaf volatiles and atmospheric oxidants on air/water interfaces, Phys. Chem. Chem. Phys. 2013, 15, 3583-3592). In this chapter, we report molecular dynamics (MD) results of the adsorption of gas-phase 2-methyl-3-buten-2-ol (MBO) on to air/water interfaces. The main objective of this study was to investigate the adsorption of gas-phase MBO on atmospheric air/water interfaces and investigate the interactions between MBO and OH radicals at the air/water interface. The rest of this chapter is structured as follows. Section 6.1 is the introduction. Section 6.2 contains computational and experimental methods. In Section 6.3 we present results and discussion and in Section 6.4 we summarize our main findings.

6.1. Introduction

MBO (Figure 1) is an unsaturated alcohol which is emitted in large quantities by some species of pine,[185-191] including some from high-altitude mountain sites and other remote areas,[192-195] where the concentrations of MBO can be 4-7 times those of isoprene; this fact strongly suggests that MBO and other GLVs can be a source of SOAs in the atmosphere. MBO emitted from plants can be oxidized by •OH, $•NO_3$ and O_3. MBO reactions with •OH dominate during day time, whereas reactions with $•NO_3$ take place mostly during the night;[196-198] MBO can account for a significant fraction (about 20%) of the •OH reactivity in areas such as the Sierra Nevada Mountains in California during the day.[195]

[††] Reprinted with permission of Phys. Chem. Chem. Phys. 2013, 15, 3583-3592

Oxidation and nitration reactions involving MBO yield products such as acetone, glycolaldehyde, 2-hydroxy-2-methylpropanal, formaldehyde, glyoxal and organic nitrates,[198-207] which are relevant to the formation of SOAs under atmospheric conditions.[208-212]

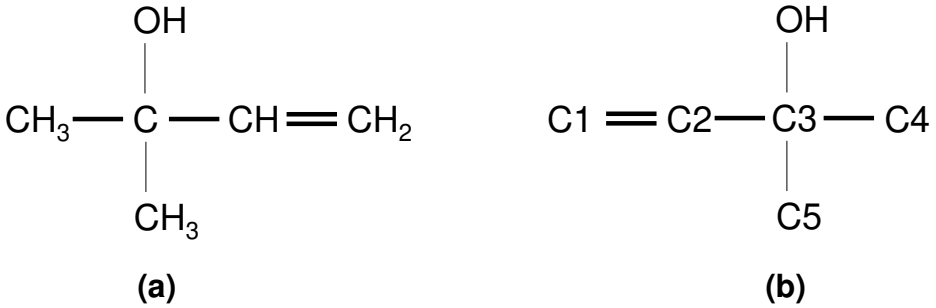

Figure 6.1. (a) 2-methyl-3-buten-2-ol (MBO). (b) Nomenclature of carbon atoms in MBO molecule as used in this study.

Molecular simulation studies, along with experiments, can lead to important insights on the processes taking place between GLVs and oxidants in atmospheric water drops, and ultimately contribute to a fundamental understanding of SOAs. To the best of our knowledge, GLVs have not been examined in molecular simulation studies in this context in the past. Here we investigate the adsorption of MBO and •OH at the air/water interface using molecular simulations. In order to ensure that our models can reproduce the physics relevant to this problem, we first computed the simulated free energy of hydration for MBO, and compared against previously reported experimental values (such a comparison was done for •OH using our chosen models in a previous study).[28] We also computed the simulated 1-octanol-water partition coefficient for MBO, and compared against our own experimental measurements of this property. Afterwards, we performed potential of mean force (PMF) calculations for MBO near atmospheric air/water interfaces, and then performed classical

molecular dynamics (MD) simulations to study several structural and dynamical properties of MBO and •OH that are relevant to their possible reactions in atmospheric water droplets.

6.2. Methods

6.2.1. Experimental Determination of the 1-octanol/water Partition Coefficient KOW for MBO

The experimental free energy of hydration of MBO, an important variable for the validation of our computational models, can be either determined from its Henry's constant in water[213] or from the 1-octanol/water partition coefficient. As only one value for the Henry's constant of MBO was reported,[214] we performed additional experimental measurements of the 1-octanol/water partition coefficient K_{OW} for MBO, closely following OECD guideline #107.[215] 2-methyl-3-buten-2-ol (>98%, Sigma-Aldrich, Milwaukee, WI, USA), water (Burdick and Jackson LC-MS grade, Honeywell, Muskegan, MI, USA) and 1-octanol (analytical grade, Sigma-Aldrich, Milwaukee, WI, USA) were used as received without further purification. For the determination of the 1-octanol/water-partition coefficient 10 mL, 13.33 mL and 6.67 mL of a 0.01 M solution of MBO in 1-octanol were mixed in 40 mL vials with 10 mL, 13.33 mL and 6.67 mL water-saturated 1-octanol and 20 mL, 13.33 mL and 26.66 mL 1-octanol-saturated water, respectively, yielding 1-octanol-water phase ratios of 1:1, 2:1 and 1:2. Each solution was tested in duplicate pairs with the same 1-octanol-water phase ratio. The vials were placed and shaken in a constant-temperature shaking water bath (25±1 °C) to allow for sufficient contact and equilibration. The concentration of MBO in each phase was measured via HPLC daily, until the difference of the K_{OW} between the individual

solutions was greater than the difference between the daily measurements, i.e. a constant K_{OW} was achieved.

For the HPLC analysis an Agilent 1100 HPLC-UV/DAD system was used consisting of the following components: a degasser (G1322A), a quaternary pump (G1311A), an autosampler (G1313A), a column compartment (G1316A) and a diode array detector (G1315A). 4 μL of each sample was injected onto a 2.1-mm×150-mm Ultra II^{TM} Aqueous C18 column (Restek Corp., Bellefonte, PA, USA) with 3-μm particle size, held at 25 °C. A water:acetonitrile gradient method with a 0.2 mL/min flow rate was used, starting with 100% water for the first five minutes, ramping linearly to 100% acetonitrile within 30 minutes, followed by a 30 minute isocratic hold at 100% acetonitrile, and a final ramp back to 100% water within 10 minutes, followed by a 100% water, 20-minute post time. The UV absorbance of 2-methyl-3-buten-2-ol was monitored with an averaged signal from 190 to 200 nm taking a data point every 2 s using the diode array detector with a slit of 4 nm. The concentration of 2-methyl-3-buten-2-ol was determined from the measured peak area via a calibration curve obtained through the analysis of standard solutions of known concentration (0.74 mg/L to 1589 mg/L).

6.2.2. Computational Models and Methods

6.2.2.1. Molecular Models and Validation: Free Energy of Hydration and 1-octanol/water Partition Coefficient for MBO

All our molecular simulations were conducted using the GROMACS software.[216] Water was modeled using the SPC/E model,[217] and the OPLS-AA force field[218] was adopted for MBO. •OH was modeled using the force field and parameters from Vácha *et al.*,[28] which can reproduce the free energy of hydration of •OH in SPC/E water.[28] In

order to validate our choice of models, we first determined the free energy of hydration and the 1-octanol/water partition coefficient for MBO, which are related according to the following relation:[219]

$$\log(K_{ow}) = \frac{\Delta G_{hydration} - \Delta G_{solvation}}{2.303\,RT} \quad (1)$$

Where $\Delta G_{hydration}$ is the free energy of a molecule of MBO solvated in water phase, and $\Delta G_{solvation}$ is the free energy of a molecule of MBO solvated in a water-saturated 1-octanol phase ("wet" octanol), which allows a more accurate determination of the free energies and partition coefficient for polar solutes.[220, 221] To calculate $\Delta G_{hydration}$, we considered simulation boxes of average dimensions of 40.48 Å × 40.48 Å × 40.48 Å (*x*, *y* and *z* respectively, which had a standard deviation of 0.007 Å, 0.007 and Å 0.007 Å on *x*, *y* and *z* dimensions respectively during the simulation time period) containing up to 2197 molecules of water. To calculate $\Delta G_{solvation}$, we used simulation boxes with average dimensions of 35.39 Å × 35.39 Å × 61.93 Å (*x*, *y* and *z* respectively, with a standard deviation of 0.008 Å, 0.008 Å and 0.014 Å on *x*, *y* and *z* dimensions respectively during the simulation time period) containing wet octanol (up to 96 molecules of water and 280 molecules of 1-octanol, which were modeled using the OPLS-AA force field).[218] The amounts of water and 1-octanol used in our wet octanol systems yield a water mole fraction of about 0.25, which is within the range of experimental values reported for water saturation in 1-octanol (water mole fraction between 0.21 and 0.29),[222] and is comparable to water mole fractions used in previous molecular simulation studies).[223] The water and wet octanol simulation boxes contained one molecule of MBO. Periodic boundary conditions were applied in all three directions. We then performed thermodynamic integration calculations following a procedure described in

previous studies.[224-226] We first model the molecule of MBO under vacuum conditions by 'switching off' all its interactions with the solvent molecules (water or wet octanol). Afterwards, we turn on the interactions between MBO and solvent gradually by coupling a parameter λ to the Hamiltonian $\mathcal{H}$, where λ varies between λ = 0 (initial state, MBO in vacuum) and λ = 1 (final state, MBO fully hydrated or solvated). The phase space between these initial and final states was divided into 21 intermediate states with equally-spaced values of λ, for which we conducted MD simulations in the *NPT* ensemble (P = 1 atm, T = 298 K) for a total of 2 ns, of which 1.5 ns were used to calculate averages. Pressure and temperature coupling was done using a Parrinello-Rahman barostat and the velocity-rescaling algorithm of Parrinello *et al.*[120] by numerically integrating $< \partial\mathcal{H} / \partial\lambda >$ over the 21 simulations we determine $\Delta G_{hydration}$ (MBO in water) and $\Delta G_{solvation}$ (MBO in wet octanol), and then use equation (1) to determine the simulated $\log(K_{OW})$ for MBO.

6.2.2.2. Potential of Mean Force (PMF) Calculations and Molecular Dynamics (MD) Simulations

For simulations in air/water interfaces, we considered an orthorhombic simulation box of dimensions up to 60 Å × 60 Å × 300 Å (x, y and z respectively) and we performed those simulations in the *NVT* ensemble. Periodic boundary conditions were applied in the x, y and z directions. We first placed a slab of up to 5805 SPC/E water molecules in the center of the simulation box, forming two interfaces with vacuum regions mimicking air. In our first series of simulations, we determined the potential of mean force (PMF) associated with moving one molecule of MBO from the gas phase into the water slab (air/water system), using the constraint force method.[124, 125, 227] Each of the simulations in our PMF calculations was run at 298 K for at least 27 ns, of which at least 20 ns were used to average the forces at each

value of z-distance considered. Afterwards, we performed unconstrained, classical MD simulations of MBO and •OH on air/water systems, which were equilibrated over at least 2 ns and with at least 25 ns for averaging. Up to four molecules of MBO and •OH radicals were considered in these simulations, which were run at 298 K and 280 K. Additional details of our PMF calculations and MD simulations are exactly the same as those used in our previous studies for polycyclic aromatic hydrocarbons on air/water and air/ice interfaces.[228-232] We used the software VMD[126] to generate all the simulation snapshots analyzed in this study.

6.3. Results and Discussion

6.3.1. Validation of Force Fields: Experimental vs. Simulation Results for Free Energy of Hydration and 1-octanol/water Partition Coefficient for MBO

Following the procedure described in §6.2.1, we determined the experimental value of the 1-octanol/water partition coefficient of MBO as $\log(K_{OW}) = 0.69 \pm 0.01$; and from the only reported experimental value[214] of the Henry's law constant for MBO in water, we determined its free energy of hydration to be about -19.5 kJ/mol. In order to ensure that our molecular models can reproduce the physics relevant to the systems considered here, we computed the simulated free energy of hydration and the 1-octanol-water partition coefficient for MBO following the methods described in §6.2.2. From these calculations, the simulated free energy of hydration was found to be -22.75 ± 0.79 kJ/mol, and the free energy of solvation of MBO in wet 1-octanol is equal to -27.30 ± 0.90 kJ/mol, yielding a simulated partition coefficient of $\log(K_{OW}) = 0.79 \pm 0.20$. Following previous work,[225] uncertainties in the free energies of hydration and solvation of MBO were computed from binning analysis,[233] and the error associated with $\log(K_{OW})$ was determined from these

uncertainties and equation (1). These values are in good agreement with the experimental values reported above. In particular, the difference found between the simulated and experimental values of $\log(K_{OW})$, as well as the magnitude of the error bar associated with the determination of this property ins simulations, are comparable to those found in recent simulation studies for n-alkanes and ionic liquids using a different technique.[219, 223] Likewise, the simulated free energy of hydration for our chosen •OH model in SPC/E water was equal to -17.8 kJ/mol, as determined by Vácha *et al.*[28] This value is reasonably close to the reported experimental free energy of hydration for •OH (between -15.9 and -16.7 kJ/mol); these experimental and simulation values also agree with the value we computed recently[232] for the free energy of hydration of our chosen •OH model in TIP5P water,[112] which was equal to -16.5 kJ/mol. All these comparisons between simulation and experimental results indicate that our choice of molecular models can reproduce physical properties that are relevant for these systems.

6.3.2. PMF of MBO in Air/water Systems

In Figure 6.2a we present the PMF obtained when one molecule of MBO is moved from the gas phase to the air/water interface, and then inside the bulk of the water slab. The PMF was arbitrarily set equal to zero when the MBO molecule is in the gas phase far away from the air/water interface. From Figure 6.2a, the simulated free energy of hydration of MBO is about -22.3 kJ/mol (when the molecule of MBO is inside the bulk of the water slab). This result is in good agreement with the experimental value (-19.5 kJ/mol), and with the thermodynamic integration result as described above (-22.7 kJ/mol), which further validates our choice of force fields.

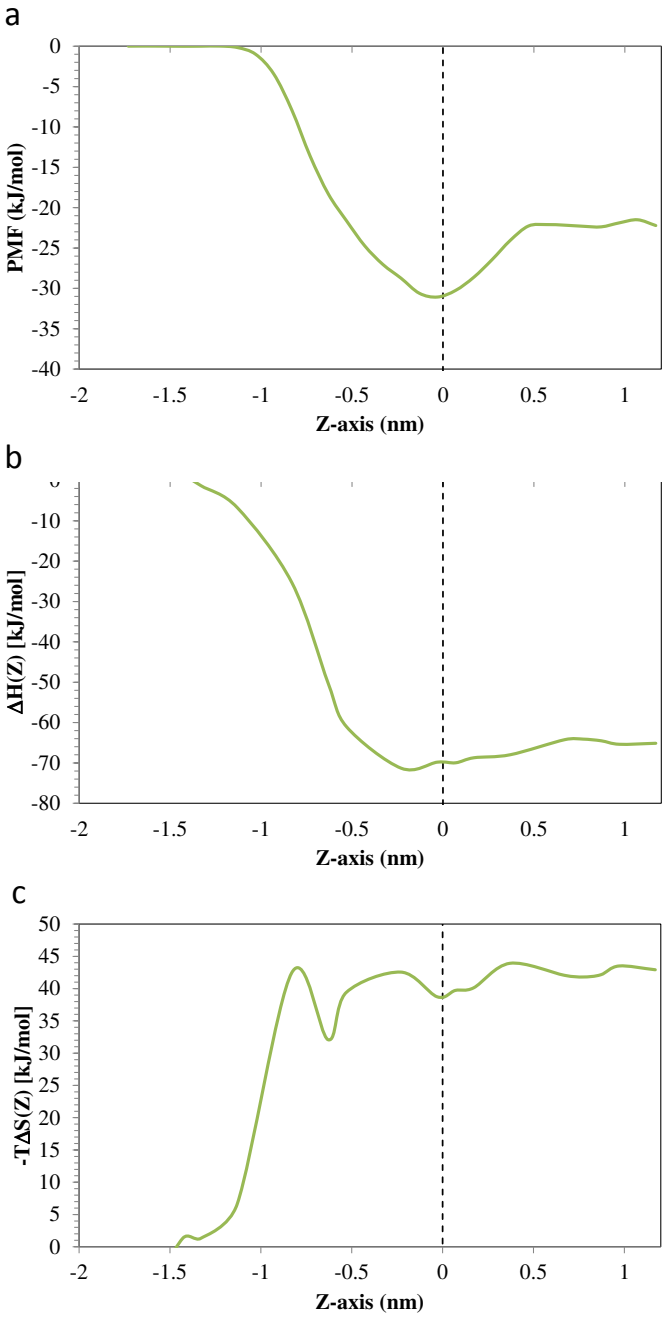

Figure 6.2. **(a)** PMF, **(b)** enthalpy and **(c)** entropy associated to moving an MBO molecule from gas phase into the water molecules in air/water systems at 298 K. The dashed line represents the location of the air/water interface; positive and negative values in the *z*-axis represent the water and gas phases.

The PMF profile of Figure 6.2a also exhibits a deep minimum for MBO at the air/water interface. This minimum is equal to -31.0 kJ/mol, which suggests that MBO has a thermodynamic incentive to be adsorbed at the air/water interface, as opposed to being

dissolved in the bulk water or remaining at the gas phase. This finding is congruent with our previous studies where we observed PMF minima for polycyclic aromatic hydrocarbons (benzene, naphthalene and phenanthrene) and reactive oxygen species (•OH, $•HO_2$ and H_2O_2) on air/water interfaces.[228, 231, 234-236]. Following recent studies by van der Spoel *et al*.,[225, 237] we decomposed the PMF into an enthalpic contribution and an entropic component, as shown in Figures 6.2b-c. The enthalpic component was determined as the average potential energy of the system in each of the PMF simulations, and the entropic component was calculated as the difference between the PMF and the enthalpic contribution at any given value of the *z* coordinate.[225, 237] From Figure 6.2b, the enthalpy contribution to the PMF also exhibits a minimum at the interface. This finding shows that the stability of MBO at the interface is mainly enthalpic in nature, in analogy to what was found for other organic molecules and several halide ions at the air/water interface.[76,88] For MBO, the entropic contribution (Figure 6.2c) just slightly enhance the depth of the PMF minimum. These trends can be rationalized following the same arguments as discussed by Hub *et al*.[225] for small alcohols at the air/water interface: (1) an MBO molecule in bulk water disrupts a number of water-water hydrogen bonds, but if this MBO molecule is at the air/water interface it disrupts less water-water hydrogen bonds; therefore, water 'pushes' the MBO solute from bulk to the air/water interface; (2) similarly, an MBO molecule that is in gas phase but reasonably close to the air/water interface is dragged into the interface, because the MBO-water interactions provide an energetic incentive for MBO to be at the interface rather than in the gas phase. The enthalpy and entropy change rapidly as the MBO approaches the water surface before it is much closer to the air/water interface. By reviewing

movies of the simulation trajectories, we observed that a few water molecules leave the bulk water system and interact with the MBO molecule when it is about 1.0 nm away from the interface, which in turn makes the MBO molecule to orient in such a way that its OH group points towards the air/water interface.

Likewise, from previous studies, •OH also has a PMF minimum at the air/water interface (between -20 kJ/mol[236] and -24 kJ/mol[28]), which indicates that •OH also has a thermodynamic preference to remain at the air/water interface. Those results suggest that chemical reactions between MBO and •OH are more likely to take place at the air/water interface, rather than inside the bulk of atmospheric water droplets or in gas phase. Therefore, we performed classical MD simulations to study several structural and dynamical properties of MBO and •OH that might be relevant to their possible reactions at the air/water interface.

6.3.3. Structural and Dynamical Properties of MBO and •OH at Air/water Interfaces

In Figure 6.3 we present density profiles of MBO, •OH and water molecules along the z-coordinate (perpendicular to the air/water interface) at 298 K. In these systems 2 molecules of MBO and 2 OH radicals are present at each air/water interface. Side and top views of representative simulation snapshots of these systems are depicted in Figure 6.4. In analogy to the PMF results shown in Figure 6.2, these density profiles indicate that both MBO and •OH prefer to stay at the air/water interfaces, although they also spend a significant fraction of time inside the bulk of the water slab. The density profiles of MBO and •OH exhibit significant overlap and peak at similar values of z. These results suggest again that chemical reactions between MBO and •OH are very likely to occur at the air/water interface. The

density profiles of these systems at 280 K exhibit similar trends and are not shown for brevity.

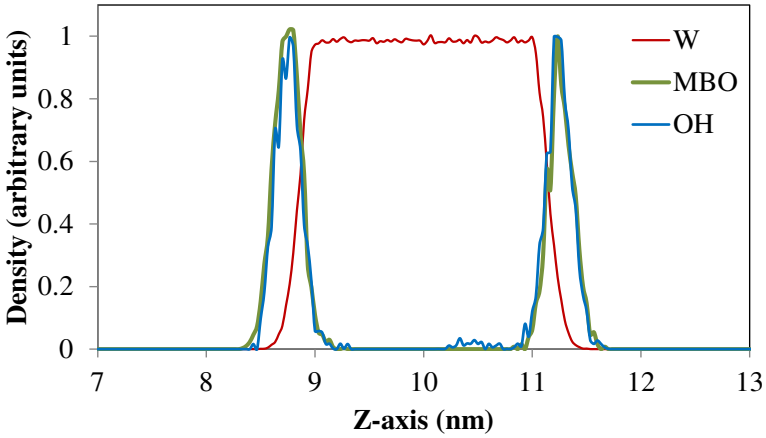

Figure 6.3. Density profiles of MBO, •OH and water at 298 K. The density profile of each species is normalized by dividing by the maximum value of their respective local density in the simulation box.

Reactions between MBO and •OH generate a number of possible first generation oxidation products such as acetone, formaldehyde, formic acid, glycolaldehyde, 2-hydroxy-2-methylpropanal, CO and CO_2, where •OH attacks the C1, C2 carbons in the double bond in MBO (Figure 1).[198]

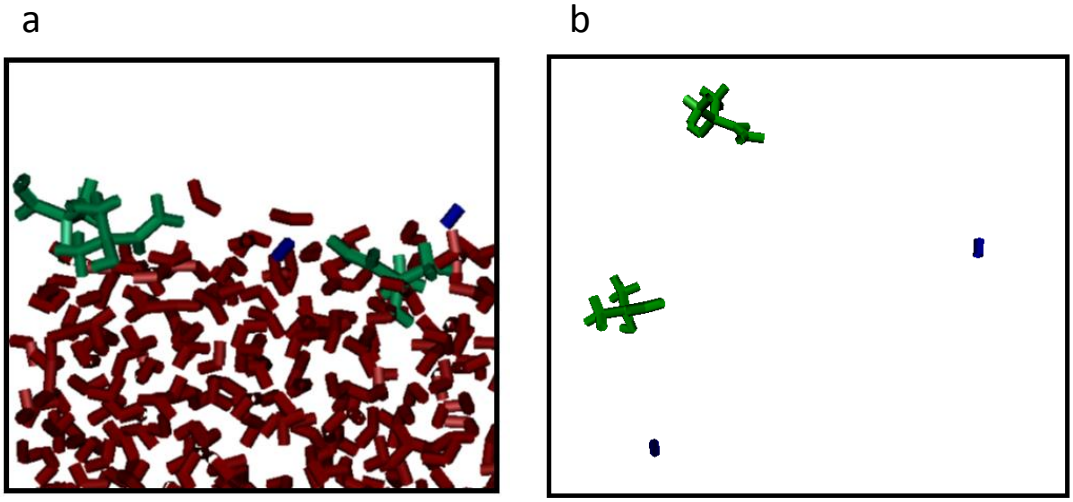

Figure 6.4. **(a)** Side and **(b)** top views of representative simulation snapshots of MBO and •OH at the air/water interface at 298 K. Systems contain two MBO molecules and two OH radicals per air/water interface. MBO = green, •OH = blue, water = red. In **(b)**, water molecules are not depicted for clarity.

The orientation of MBO molecules at the air/water interfaces is therefore relevant to their reactions with oxidizing species originating in the gas phase such as •OH. In Figure 6.5a we present the distribution of cos(θ), where θ is the angle formed between the vector joining the C1 and C3 carbon atoms in MBO (Figure 6.1b), and the vector normal to the air/water interface. A value of 0 for cos(θ) indicates that the MBO molecules remains parallel to the air/water interface, whereas a value of 1 indicates that the MBO molecule lies perpendicular to the interface.

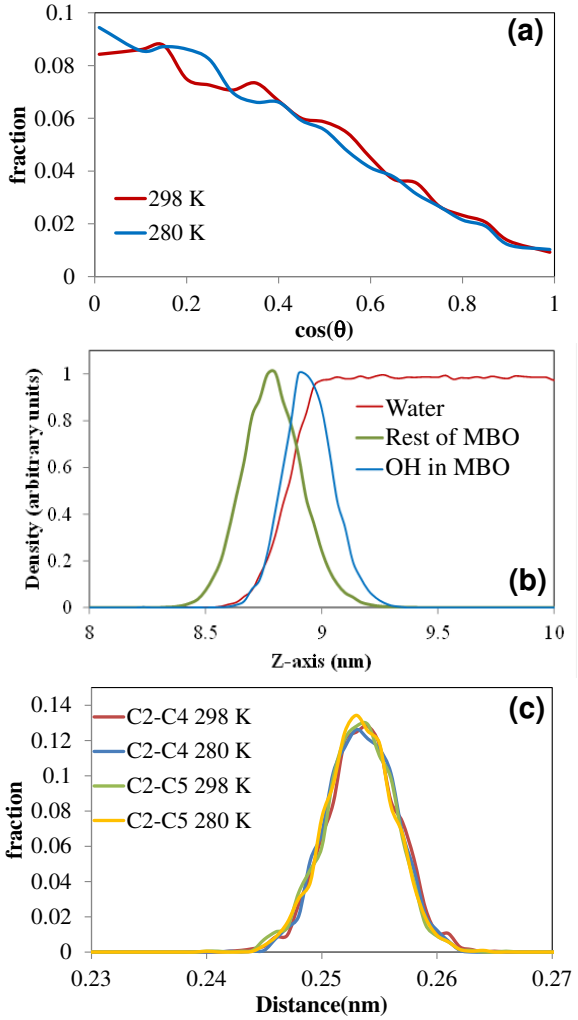

Figure 6.5. **(a)** Distributions of cos (θ), where θ is the angle formed between the vector joining the C1 and C3 carbon atoms in MBO (Figure 1b), and the vector normal to the air/water interface, at 298 K and 280 K. **(b)** Density profiles for OH, the rest of the MBO molecule, and water at 298 K. **(c)** Average distances between carbons C2-C4, C2-C5 (Figure 1b) in MBO at 298 K and 280 K at air/water interfaces.

These results suggest that MBO mostly prefers to lie parallel to the air/water interface, but retains a considerable ability to rotate around its molecular axis. No significant variations were observed in the angular distribution at the two temperatures examined (298 K and 280 K). As expected, MBO aligns with its OH group pointing to the water molecules at the interface, as shown in the density profiles presented in Figure 6.5b. The distribution of distances between the C2-C4 and C2-C5 carbon atoms in MBO (Figure 6.1b) was also monitored in our MD simulations and presented in Figure 5c for the two temperatures considered. This distance was monitored because the addition of •OH to the C2 carbon might be sterically hindered.[198] From Figure 6.5b, the C2-C4 and C2-C5 distribution of distances peak at ~2.53 Å, with no appreciable variations at the two temperatures considered here (298 K and 280 K).

The mean square displacement (MSD) of MBO molecules on air/water interfaces is presented in Figure 6.6 at both 298 K and 280 K. As expected, the MSDs at 298 K are larger than those observed at 280 K.

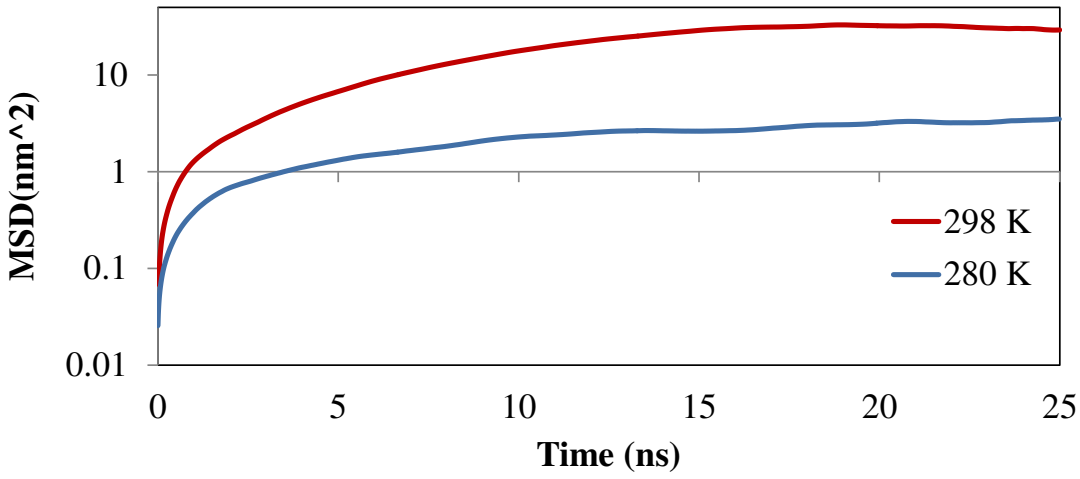

Figure 6.6. Mean square displacement (MSD) of MBO at 298 K and 280 K at the air/water interfaces.

The average diffusion coefficients of MBO molecules at the air/water interface were found to be 0.39 and 0.03 × 10^{-5} cm^2/s at 298 K and 280 K respectively. We also investigated the interaction between MBO and •OH radicals at the air/water interface by computing radial distribution functions g(r) between the oxygen of •OH and the carbons C1 and C2 in MBO at 298 K and 280 K. These results are shown in Figure 6.7; the first peak in the g(r) functions is observed around 0.45 nm, without significant variations at the two temperatures considered.

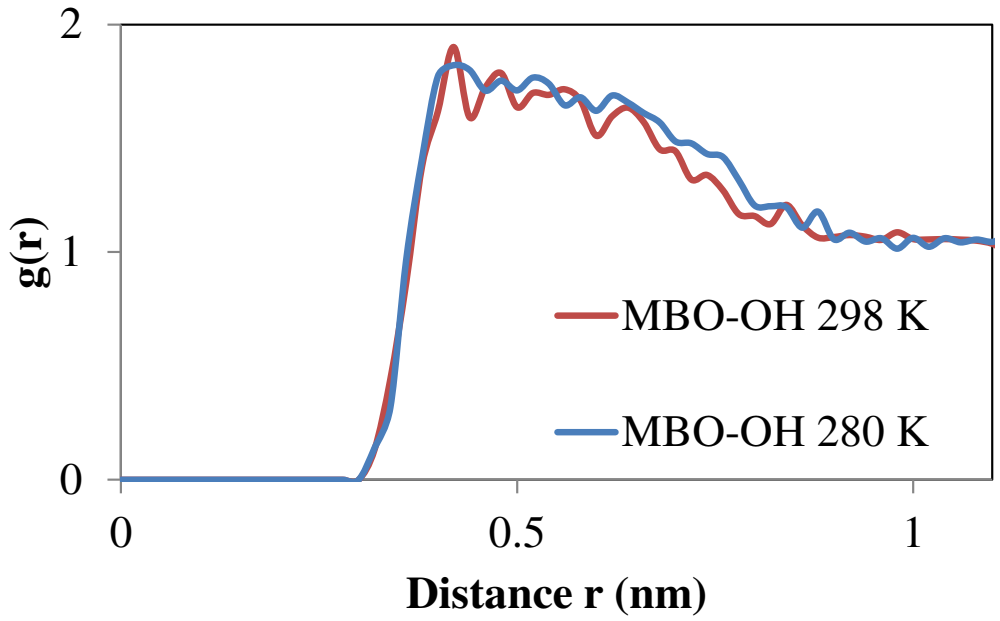

Figure 6.7. Radial distribution functions $g(r)$ between the oxygen atom of •OH and the carbon atoms C1 and C2 of MBO (Figure 1b) at 298 K and 280 K.

Finally, we monitored the number of contacts between the carbons C1 and C2 of MBO and the oxygen atoms of •OH. We arbitrarily considered that a contact happened when the O-C1 or O-C2 distance is less than 0.50 nm (previous studies[29, 234] used a distance equal to that at which the first local minimum in g(r) is observed; however, it was also argued that the results do not vary appreciably if a different distance is considered). These contacts could probably lead to chemical reactions between MBO and •OH, and we can assume that the reaction rate is proportional to the number of these contacts. From our simulations over a

total of 25 ns at the two temperatures considered (298 K and 280 K), we observed about 300 contacts between the two molecules of MBO and the two OH radicals at each interface (60 Å × 60 Å), which suggest that the number of contacts between these two species is significant and did not vary significantly in the range of temperatures considered here.

6.4. Concluding Remarks

MD simulations were performed to investigate the adsorption of MBO and OH radicals on atmospheric air/water interfaces. Our chosen combination of force fields for these systems were able to reproduce experimental measurements of the free energies of hydration for MBO and •OH, as well as the experimental 1-octanol/water partition coefficient for MBO. Potential of mean force (PMF) calculations show a deep free energy minimum for MBO at the air/water interface; similar findings were reported for •OH in previous studies,[28, 236] indicating, that from the thermodynamic point of view, these two species have a strong preference to remain at the air/water interface, as opposed to the bulk water or vapor phase. By decomposing the PMF into enthalpic and entropic contributions, we determined that the stability of MBO at the interface is mainly driven by enthalpy. Having MBO at the air/water interface leads to an optimal situation where, on the one hand, not so many water-water hydrogen bonds are disrupted (as opposed to the case where MBO is inside bulk water), and on the other hand, water-MBO interactions are still important (as opposed to the case where MBO is in the gas phase). These results suggest that chemical reactions between MBO and •OH are more likely to take place at the air/water interface, rather than inside of atmospheric water droplets or in the gas phase. We also monitored several variables relevant to the possible reactions of MBO and •OH at the air/water interface. In particular, the density

profiles of these two species overlap significantly at the interface, with MBO aligning parallel to the interface with their OH group into the water side of the interface. We found a significant number of contacts between MBO and •OH in our simulations, which could lead to reactions between these two species.

One particular issue in this area is the lack of experimental data for other green leaf volatiles (GLVs) and their first-generation products from their oxidation reactions. We are currently generating experimental data for these compounds, as well as investigating the possible reactions of GLVs in fog in the field and in the lab. We are also performing modeling studies for other GLVs, as well as their first-generation oxidation products.

CHAPTER 7 MOLECULAR MODELING OF THE GREEN LEAF VOLATILE METHYL SALICYLATE ON ATMOSPHERIC AIR/WATER INTERFACE

In this chapter, we report molecular dynamics (MD) results of the adsorption of gas-phase Methyl salicylate (MeSA) on to air/water interfaces. The main objective of this study was to investigate the adsorption of gas-phase MeSA on atmospheric air/water interfaces and investigate the air/water interfacial properties with respect to varying MeSA concentrations at the air/water interface. The rest of this chapter is structured as follows. Section 7.1 is the introduction. Section 7.2 contains computational and experimental methods. In Section 7.3 we present results and discussion and in Section 7.4 we summarize our main findings.

7.1. Introduction

In our previous work,[238] we have shown that MBO and oxygenated radicals such as •OH exhibit a strong thermodynamic preference to remain at the air/water interface, suggesting that chemical reactions between these species are more likely to take place at this interface, rather than in the bulk of the water droplets or in the gas phase. In that study we also determined experimentally the 1-octanol/water partition coefficient for MBO, which was then used to develop an accurate molecular model for MBO; we also pointed out at the lack of experimental data available for MBO and other GLVs, which hampers experimental and modeling efforts in this area. In the present study we focus on another GLV, methyl salicylate (MeSA), which is a semi-volatile organic compound which is emitted by plants such as tea.[239-242] MeSA is also produced by tobacco plants when infected with the tobacco mosaic virus,[243] and when exposed to high concentrations of ozone.[244] Although MeSA

is a semi volatile organic compound (its vapor pressure at 298 K is about 0.2 Torr),[245] it could be adsorbed on the surface of atmospheric water droplets, in analogy to what we observed with MBO in our previous study.[238]

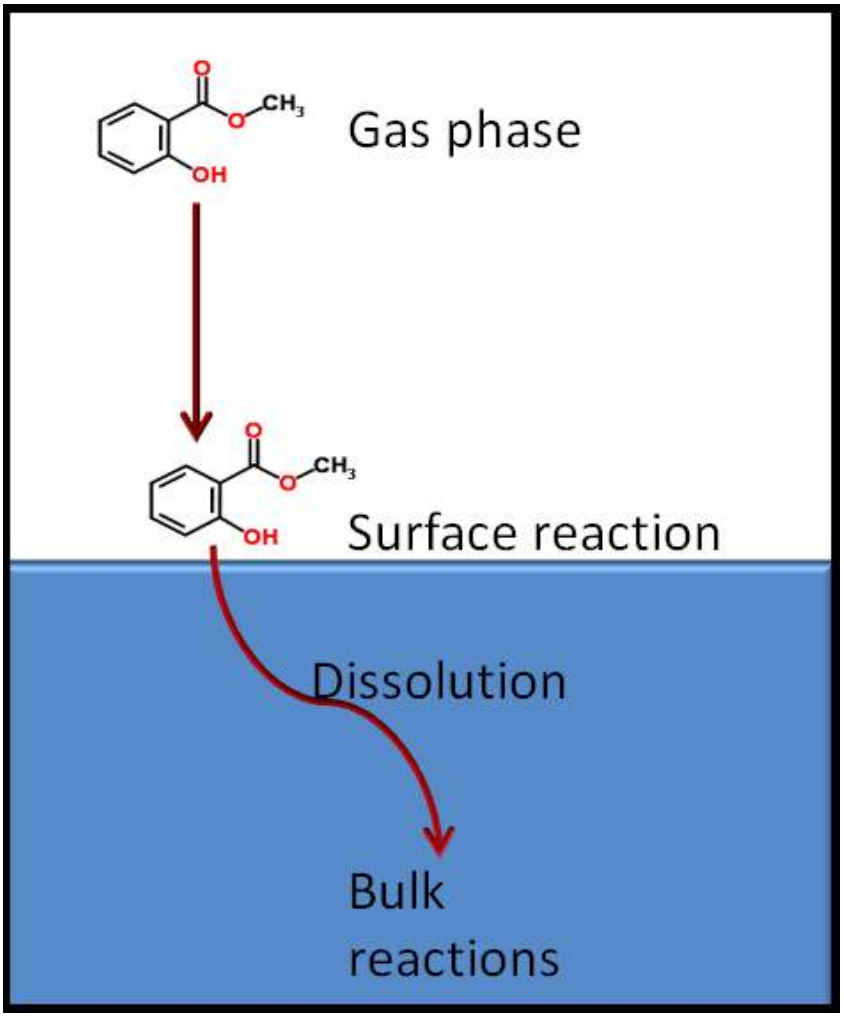

Figure 7.1. Adsorption and dissolution of methyl salicylate (MeSA) at air/water interfaces

It is important to elucidate where the reactions of GLVs with atmospheric oxidants are more likely to take place (i.e., in gas phase, at the air/water interface, or in the bulk of water droplets, Figure 7.1), as the kinetics of reactions involving atmospheric oxidants and other organic species in these environments may be significantly different,[1,16,40] which in turn may impact the formation of SOAs in the atmosphere. Combined molecular simulation/experimental studies can lead to fundamental discoveries on the processes taking

place between MeSA and atmospheric oxidants in atmospheric water droplets. To the best of our knowledge, MeSA has not been examined in this context in the past. Here we report a molecular modeling study of the properties of MeSA on atmospheric air/water interfaces. In order to confirm that our choice of molecular models can reproduce the physical behavior relevant to this problem, we first determined experimentally the 1-octanol-water partition coefficient of MeSA using thermodynamic integration (TI) calculations, and ensured that we could reproduce this value in our molecular simulations. Afterwards, we performed potential of mean force (PMF) calculations in order to investigate the thermodynamics of MeSA at the air/water interface, and studied the structural and dynamical properties of MeSA and water molecules in these systems using classical molecular dynamics (MD) simulations.

7.2. Methods

7.2.1. Practical Determination of the Octanol-water Partition Coefficient

The octanol-water partition coefficient of methyl salicylate was determined via shake-flask method following closely OECD guideline #107[215] and is further detailed in our previous work.[246] Methyl salicylate (>99%, Sigma-Aldrich, Milwaukee, WI, USA), water (Burdick and Jackson LC-MS grade, Honeywell, Muskegan, MI, USA) and 1-octanol (analytical grade, Sigma-Aldrich, Milwaukee, WI, USA) were used as received without further purification.

7.2.2. Computational Models and Methods

All our molecular simulations were conducted using the GROMACS software,[216] and all the simulation snapshots in this study were generated using the VMD software.[126] In analogy to our previous simulations of MBO on air/water interfaces,[238] we used the SPC/E

model[217] for water, and the OPLS-AA force field[218] for MeSA and 1-octanol. In order to ensure our choice of models can reproduce the physics that are relevant to this problem, we followed a strategy similar to the one used in our previous paper,[238] and determined the free energy of hydration ($\Delta G_{hydration}$) of MeSA in a water phase, and the free energy of solvation of MeSA in wet 1-octanol (a water-saturated 1-octanol phase which allows accurate determination of the free energy and partition coefficient of polar solutes.[220, 221]). We performed thermodynamic integration (TI) calculations[224-226, 238] to calculate $\Delta G_{hydration}$ and $\Delta G_{solvation}$, and used those to calculate the simulated 1-octanol/water partition coefficient for MeSA:[219]

$$\log(K_{ow}) = \frac{\Delta G_{hydration} - \Delta G_{solvation}}{2.303\,RT} \quad (1)$$

These thermodynamic integration calculations were performed at P = 1 atm and T = 298 K. Specifics of these calculations are exactly the same as those described in our previous paper.[238] As shown later in §7.3.1, the use of the OPLS-AA force field for MeSA resulted in a simulated value of $\log(K_{OW})$ that was significantly different from value measured in our experiments. As a result, we followed previous studies[20, 28, 149, 231] and increased the atomic charges in up to 10% of the original values taken from OPLS-AA; these new parameters led to a better agreement between the simulated and experimental 1-octanol/water partition coefficients for MeSA. Afterwards, we conducted simulations of MeSA in air/water interfaces at 298 K, for which we set up an orthorhombic simulation box of dimensions up to L_x = 40 Å, L_y = 40 Å and L_z = 240 Å, where we created two air/water interfaces by placing a water slab composed of up to 2197 SPC/E water molecules in the center of the simulation box. We first determined the potential of mean force (PMF) associated with moving one

molecule of MeSA from the gas phase into the water slab; specifics of these PMF calculations are exactly the same as those described in detail in our previous paper.[238] We also performed classical MD simulations with varying concentrations of MeSA (up to 32 molecules of MeSA per air/water interface). Additional details of our MD simulations are exactly the same as those used in our previous studies for MBO at air/water interfaces,[238] and polycyclic aromatic hydrocarbons (PAHs) on air/water and air/ice interfaces.[228-231, 247]

7.3. Results and Discussion

7.3.1. Experimental and Simulated 1-octanol/water Partition Coefficient of MeSA

We determined the experimental value of the 1-octanol/water partition coefficient of MeSA as $\log(K_{OW}) = 2.36 \pm 0.03$. This value is in very good agreement with the value of 2.55 available in the literature[248] at 25 ± 1 °C. In our previous study for MBO,[238] we found one experimental value for its Henry's law constant, from which we could determine the free energy of hydration for MBO; in contrast, we could not find reported experimental values of the Henry's law constant or the free energy of hydration for MeSA. Therefore, and in order to assess if our chosen molecular models could reproduce the physical interactions of interest in this problem, we performed a first series of TI calculations simulations where we computed the simulated 1-octanol/water partition coefficient for MeSA using parameters from the OPLS-AA force field. From these first series of TI calculations, the simulated free energies of hydration (MeSA in water) and solvation (MeSA in wet 1-octanol) were found to be -21.25 kJ/mol and -43.44 kJ/mol, yielding a simulated partition coefficient of $\log(K_{OW}) = 3.87 \pm 0.41$. This initial simulated value is significantly higher compared to the experimental value

[$\log(K_{OW})$ = 2.36 ± 0.03]. As a result, we followed previous work [20, 28, 149, 231] and increased the atomic charges of MeSA in up to 10% of the original charges taken from the OPLS-AA force field. Using this new set of atomic charges, we repeated our TI calculations obtaining values of -29.81 kJ/mol and -44.41 kJ/mol for the free energies of hydration and solvation of MeSA. From those values, the new simulated partition coefficient is $\log(K_{OW})$ = 2.55 ± 0.39, which is in better agreement with the experimental value [$\log(K_{OW})$ = 2.36 ± 0.03]. The magnitude of the error in our simulations, although relatively large, is comparable to that obtained in our previous work for MBO,[238] and to the estimated errors for n-alkanes and ionic liquids using a different technique.[219, 223] The satisfactory comparison between simulated and experimental results of the 1-octanol/water partition coefficient of MeSA indicates that our chosen molecular models can reproduce physical properties that are thought to be of relevance for these systems.

7.3.2. PMF of MeSA in Air/water Systems

We determined the PMF associated with moving one MeSA molecule between the gas phase and the bulk of the water slab through the air/water interface (Figure 7.2a). In these calculations, we arbitrarily assumed that the PMF of a MeSA molecule in the gas phase and far away from the air/water interface is equal to zero. From these PMF calculations, the simulated free energy of hydration for MeSA inside the bulk water phase was found to be -20.70 kJ/mol (Figure 7.2a; this is the difference between the PMF values observed in the gas and the bulk water phase). This value is different from the one determined from our TI calculations (-29.81 kJ/mol). Differences in the free energies of hydration estimated from TI and from PMF calculations seem to be molecule-specific; Hub *et al*.[225] reported significant

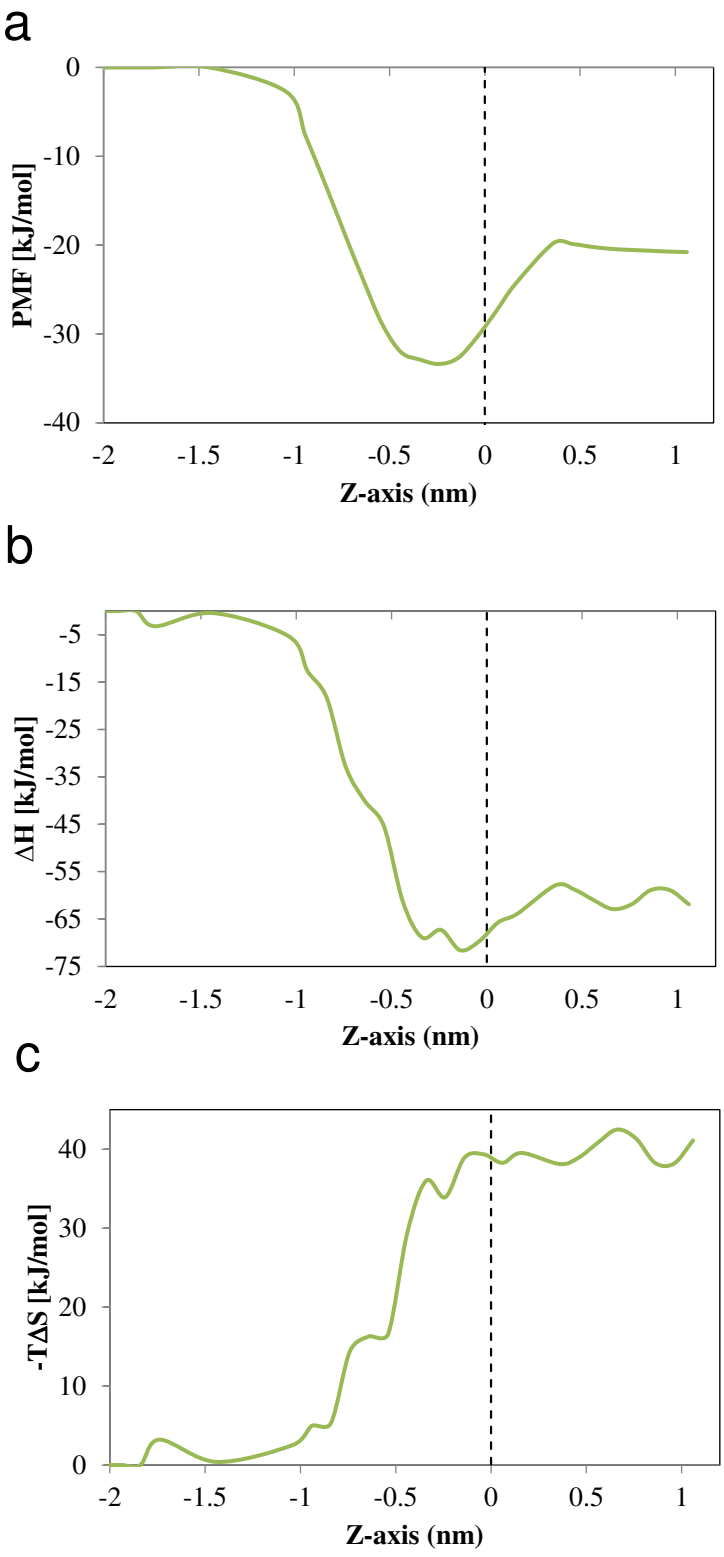

Figure 7.2. **(a)** Total potential of mean force (PMF), and enthalpic **(b)** and entropic **(c)** contributions to the PMF associated to moving a MeSA molecule between the gas phase and the bulk water phase in air/water systems at 298 K. The dashed line represents the location of the air/water interface (arbitrarily defined as the point where the water density reaches 500 kg/m^3). Positive and negative values in the *z*-axis represent the water and gas phases.

differences for a number of organic molecules, but in contrast, the hydration free energies of MBO as estimated from TI and from PMF calculations were in excellent agreement.[238]

As discussed by Caleman *et al*.[237] for ions at the air/water interface, these differences in calculated free energies of hydration might be due to the fact that, in PMF calculations using the constraint force method, solutes in the gas phase but very close to the interface can induce water molecules to jump into the solute. These water jumps, which are not present in our TI calculations (i.e., there is no air/water interface in these TI calculations), can cause slow convergence in the mean force measured in the PMF calculations and can lead to an underestimation of the free energy of hydration. In their study of ions at air/water interfaces, Caleman *et al*.[237] decided to add a correction in their PMF curves to ensure that the hydration free energies match the values determined from their TI calculations; in contrast, the same group did not add any corrections to their PMF curves in a later study of organic molecules at the air/water interface.[225] The PMF curves shown in Figure 7.2 do not include any correction to ensure that the free energy of hydration match the value estimated from our TI calculations.

At the air/water interface, the PMF profile for MeSA (Figure 7.2a) exhibits a deep free energy minimum equal to -33.4 kJ/mol, which strongly indicates that this molecule has a thermodynamic preference to remain adsorbed at the air/water interface. This minimum in free energy could be even deeper, reaching about -42 kJ/mol, due to the fact that we did not add a correction to ensure that the free energy of hydration match the value estimated from our TI calculations. For MBO, another GLV, we found that the simulated free energy of hydration and the PMF minimum at the air/water interface were equal to -22.3 kJ/mol and

-31.0 kJ/mol.[238] The relative magnitudes of these free energies for MeSA and MBO can be explained as MeSA is more hydrophilic than MBO (see Figure 1 here and in ref.[238]). The findings reported here are also consistent with the results shown in our previous studies of PAHs and ROSs, which also exhibited free energy minima on air/water and air/ice interfaces.[228-231, 247]

Inspired by the recent work of van der Spoel *et al*.,[225, 237] and in analogy to our previous study,[238] we split the PMF of MeSA into its enthalpic and entropic components as a function of the z-position of the MeSA molecule. These calculations were done in an attempt to better understand the adsorption process of MeSA on the air/water interface. The enthalpic and entropic contributions to the PMF were determined according to the procedure explained in detail before,[225, 237, 238] and are shown in Figs. 7.2b and 7.2c. The enthalpic component exhibits a deep minimum at the interface (Fig. 2b), which indicates that the thermodynamic stability of MeSA at the interface is mainly driven by its energy interactions with the water molecules. Entropy seems to provide a slight enhancement to the depth of the PMF minimum at the air/water interface (Fig. 7.2c). The entropic contribution is very low when MeSA is in the gas phase, and increases when it approaches the air/water interface; this observation is mainly due to the fact that MeSA molecules near the interface tend to adopt an orientation where its oxygenated groups point towards the water molecules, whereas its aromatic group tends to lie farther away from water (see Figs. 7.6 and 7.7).

Following again the work of van der Spoel *et al*.,[225, 237] we further decomposed the enthalpic contribution to the PMF (Fig. 7.2b) into water–water and water–MeSA interaction energies as a function of the z-coordinate of the MeSA molecule. These contributions are

presented in Figures 7.3a and 7.3b. These results show that when the MeSA molecule moves from the gas phase into the air/water interface, the water-water interactions become more positive (Fig. 7.3a); a very sharp increase in the water-water energy is observed when the MeSA molecule moves from the interface into the bulk water phase.

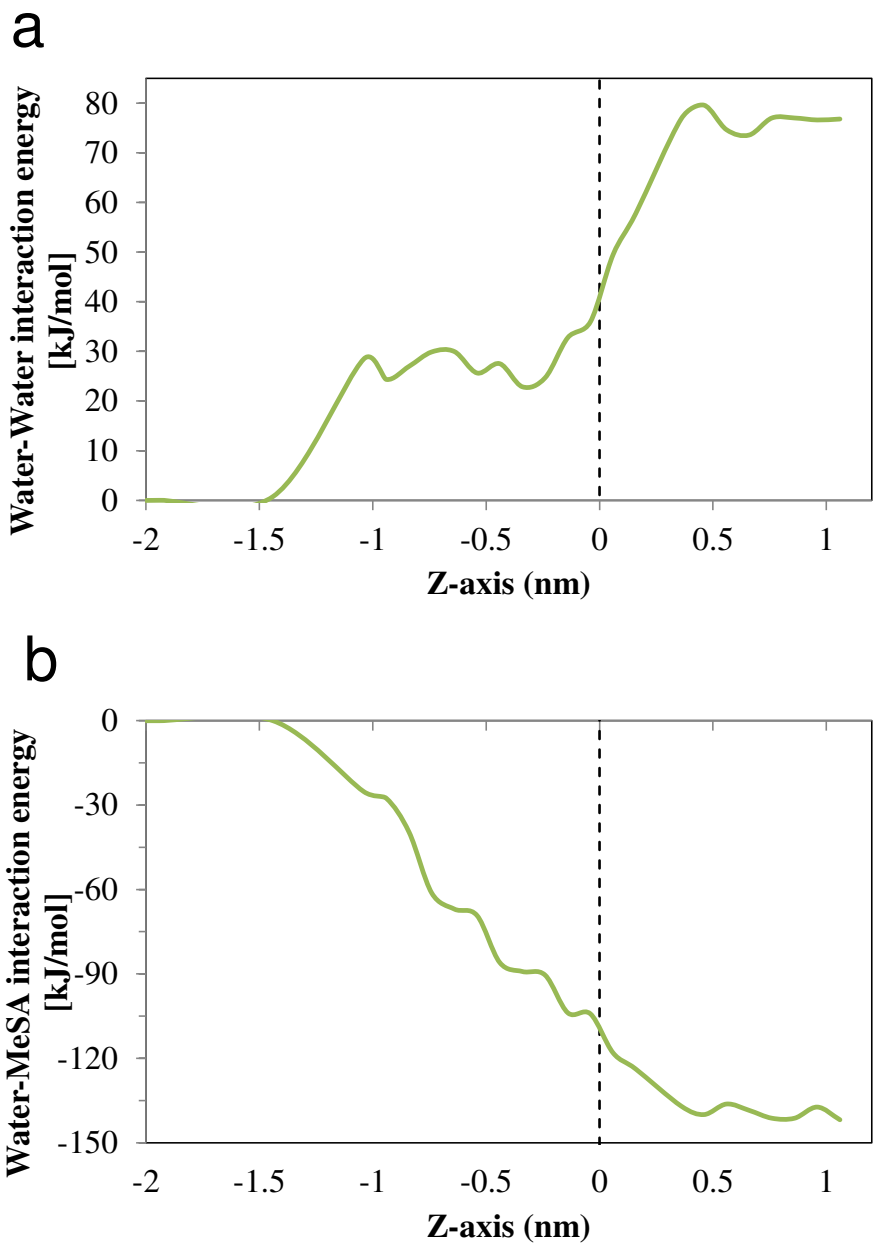

Figure 7.3. Decomposition of the enthalpic contribution to the PMF (Fig. 2b) into **(a)** water–water, and **(b)** water–MeSA interaction energies at 298 K

This finding reflects the fact that, when the MeSA molecule is inside the bulk water phase, it disrupts a larger number of water-water hydrogen bonds as compared to when MeSA is at the interface. From Fig. 3b, it can be observed that the water-MeSA interactions become more favorable (more negative) when the MeSA molecule migrates from the gas phase into the air/water interface and then into the bulk water phase. In contrast to what was observed in Fig. 7.3a, no sharp decreases are observed in the water-MeSA energy interactions. These favorable water-MeSA interactions arise because MeSA can form hydrogen bonds with water, and its aromatic group also provides additional energetic interactions with water. Therefore, a molecule of MeSA that is in the gas phase but in the proximity of the air/water interface is 'dragged' into the interface, due to the thermodynamic incentive provided by the water-MeSA interactions. These energy interactions continue to become more negative as the MeSA molecule moves towards the bulk water phase, but are outweighed by the sharp increase in the water-water energy; therefore, water tends to 'push' the MeSA molecule from the bulk water phase into the air/water interface. As a result, the air/water interface provides a favorable environment where the MeSA molecule has important energy interactions with the water molecules and does not disrupt too many water-water hydrogen bonds. These observations are similar to those discussed in the work of Hub *et al.*[225] for small alcohols at the air/water interface, and similar to what we discussed for MBO in air/water systems.[238]

Previous results for ROSs[28, 231] indicate that these atmospheric oxidants also have a thermodynamic preference to remain at the air/water interface. These observations, when combined with results from this study, strongly suggest that the reactions between MeSA and

other ROSs in the atmosphere are very likely to take place at the air/water interface, as opposed to inside the bulk of atmospheric water droplets or in the gas phase.

7. 3.3. MD Simulations: Structural and Dynamical Properties at Air/water Interfaces

In Figure 7.4 we present density profiles of MeSA and water molecules as a function of the *z*-coordinate (perpendicular to the air/water interface) at 298 K, for low and high concentrations of MeSA at the air/water interface (2 and 32 MeSA molecules on each air/water interface).

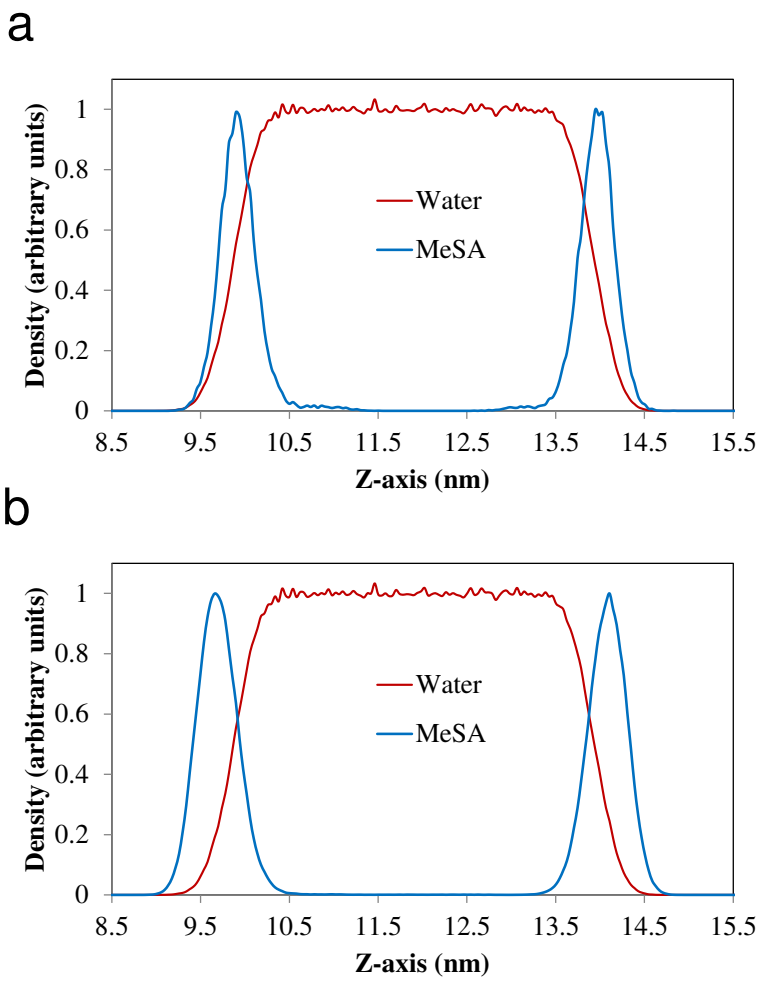

Figure 7.4. Density profiles of MeSA and water obtained from classical molecular dynamics simulations at 298 K. The systems contain **(a)** 2 MeSA molecules, and **(b)** 32 MeSA molecules per air/water interface. The density profile of each species is normalized by dividing by the maximum value of their respective local density in the simulation box.

Side views of snapshots from these classical MD simulations are depicted in Figure 7.5. In analogy to the results shown in Figs. 7.2 and 7.3, the density profiles and snapshots from Figs. 7.4 and 7.5 indicate that the MeSA molecules mainly prefer to stay at the air/water interfaces, although some of these molecules spent a minor fraction of the simulation time inside the bulk water phase. No significant variations in the density profiles are observed for the range of concentrations of MeSA considered here.

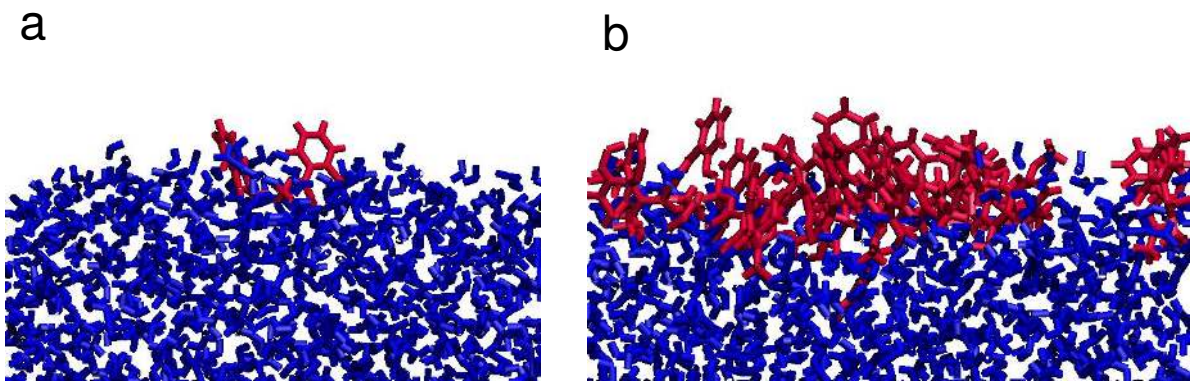

Figure 7.5. Side views of representative snapshots from MD simulations of MeSA at the air/water interface at 298 K. Systems contain **(a)** 2 MeSA molecules, and **(b)** 32 MeSA molecules per air/water interface. MeSA = red, water = blue.

The results shown in Figs.7.2-5 strongly suggest that the reactions between MeSA and atmospheric oxidants are most likely to occur at the air/water interface, and therefore the orientation of MeSA molecules at this interface is a property that is relevant in this context. In Figure7.6 we decomposed the density profiles of MeSA into the contributions from the aromatic ring (hydrophobic group) and the oxygenated groups of the molecule including the methyl group (hydrophilic group, see also Fig. 7.1). As expected, the density profile of the hydrophilic group remains closer to the water side of the interface, whereas the hydrophobic group is farther from water, indicating that MeSA aligns with its oxygenated groups pointing to the water molecules at the interface. These results are similar for the range of concentrations of MeSA considered here. In Figure 7.7 we present top views of simulation

snapshots of air/water systems, and in Figure 7.8 we show the radial distribution functions $g(r)$ computed between MeSA molecules, for varying concentrations of MeSA at the air/water

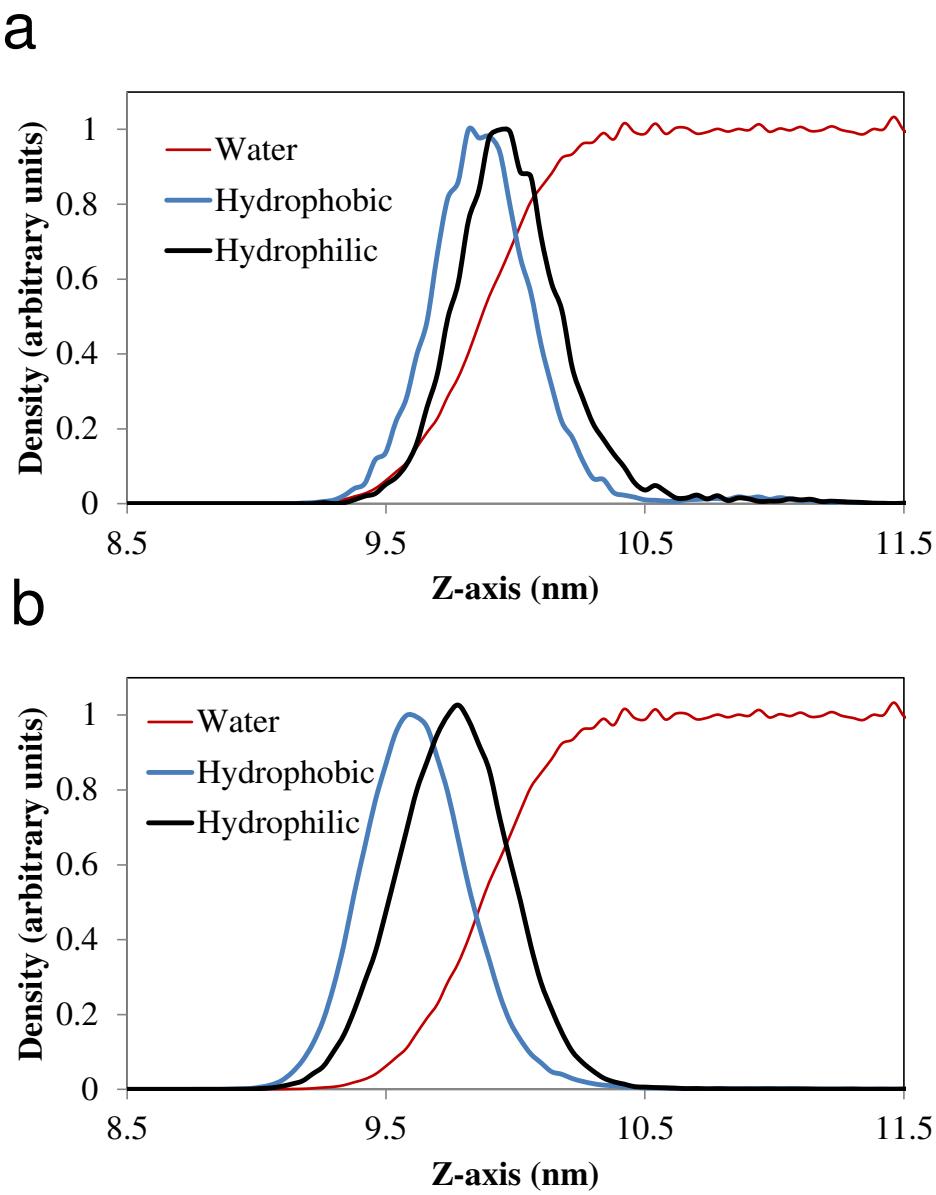

Figure 7.6. Density profiles for aromatic ring (hydrophobic group), the rest of the MeSA molecule containing the oxygenated and methyl groups (hydrophilic group), and water at 298 K. Systems contain **(a)** 2 MeSA molecules, and **(b)** 32 MeSA molecules per air/water interface. The density profile of each species is normalized by dividing by the maximum value of their respective local density in the simulation box.

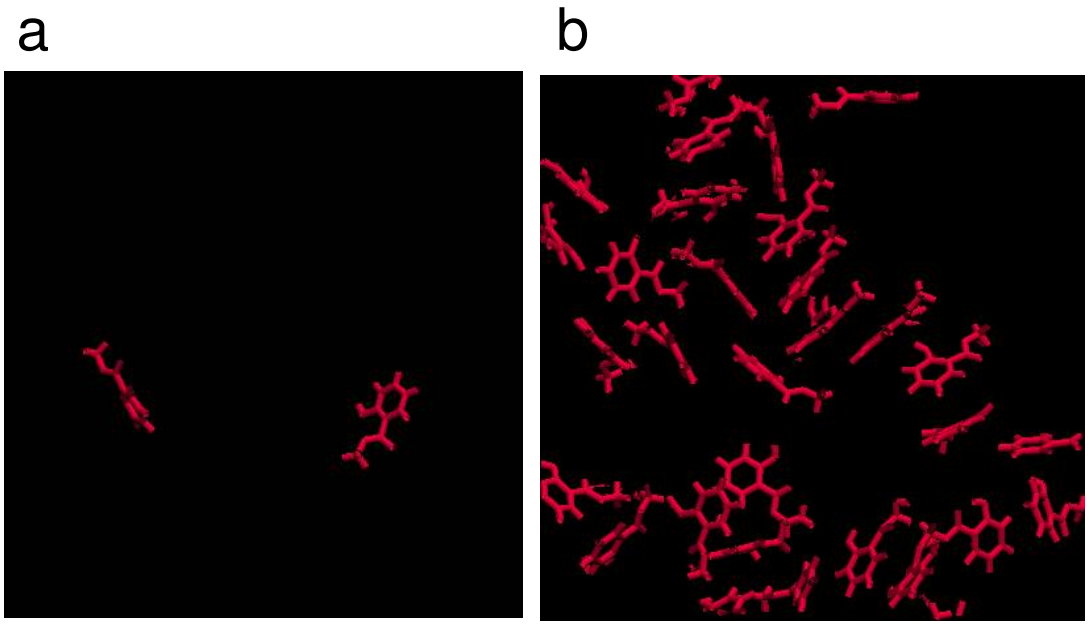

Figure 7.7. Top views of representative simulation snapshots of systems of MeSA on air/water interfaces at 298 K. Systems contain **(a)** 2 MeSA molecules, and **(b)** 32 MeSA molecules per air/water interface. Only MeSA molecules are depicted for clarity.

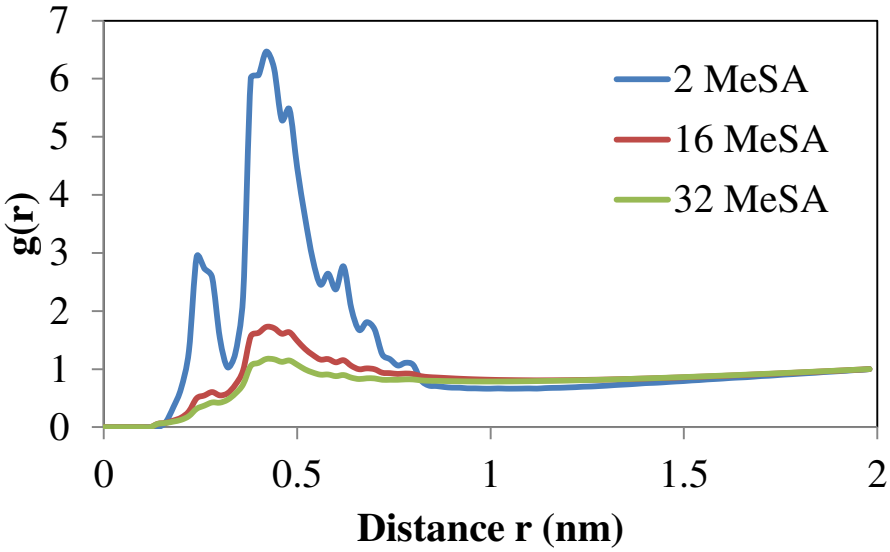

Figure 7.8. Radial distribution functions $g(r)$ between MeSA molecules at the air/water interface

interface. When only 2 MeSA molecules are present at each air/water interface, the $g(r)$ function shows two major peaks at r = 0.24 nm and at r = 0.42 nm.

The height of each of these peaks diminishes as the concentration of MeSA increases at the interface. The mean square displacements (MSD) of MeSA and water molecules are shown in Figures 7.9a and 7.9b for varying concentrations of MeSA at the interface at 298 K.

The dynamics of MeSA and water molecules at high concentrations of MeSA are significantly slower, mainly due to crowding effects (see Fig. 7.7).

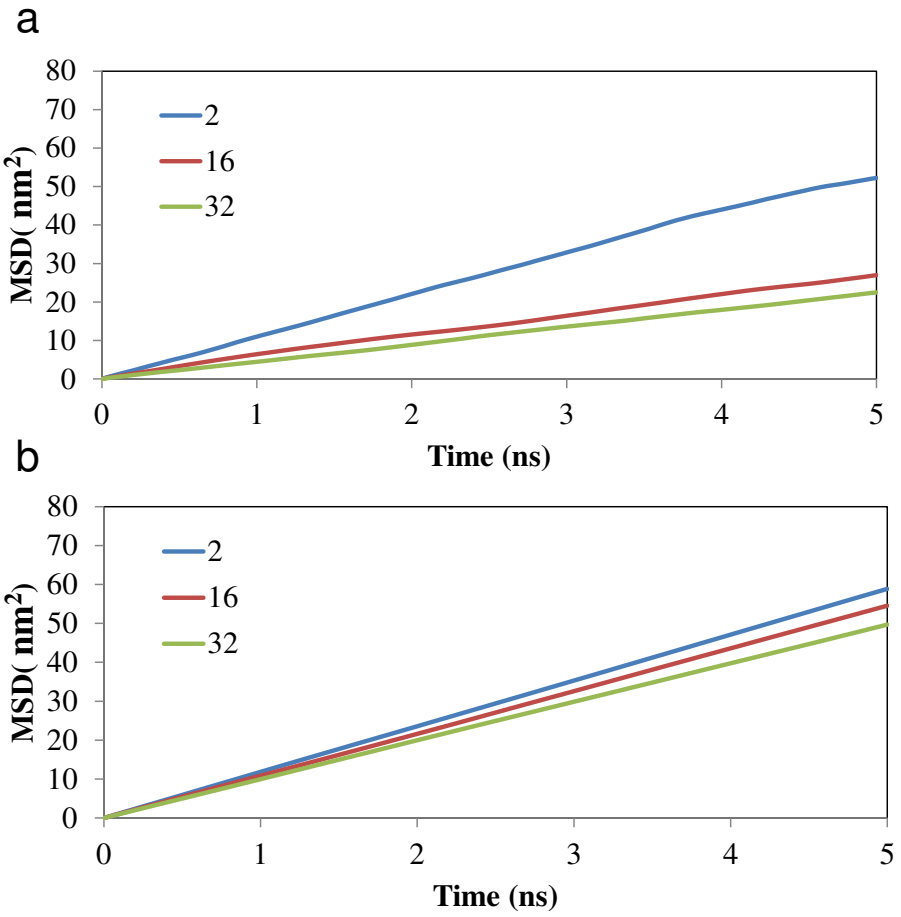

Figure 7.9. Mean square displacement (MSD) of **(a)** MeSA, and **(b)** water molecules at 298 K at the air/water interfaces. Systems contain 2, 16 and 32 molecules of MeSA per air/water interface.

To further investigate the air/water interfacial properties, the interfacial tensions (γ) of bare and MeSA coated air/water interfaces was calculated from the pressure tensors using the following equation:[216]

$$\gamma = \frac{L_z}{2}\left(\frac{p_{xx} + p_{yy}}{2} - p_{zz}\right) \qquad (2)$$

Where L_z is the box length in the z direction, and the diagonal components of the pressure tensor are represented by p_{xx}, p_{yy} and p_{zz}. The surface tension in the absence of MeSA molecule was found here to be 55.07 mN/m, which is within the range of values previously

reported for SPC/E water.[249-253] In Figure 7.10 we present the variation of the surface tension in our systems at the interface, for varying number of MeSA molecules; these results show that the interfacial surface tension decreases as the number of MeSA molecules at the air/water interface increases.

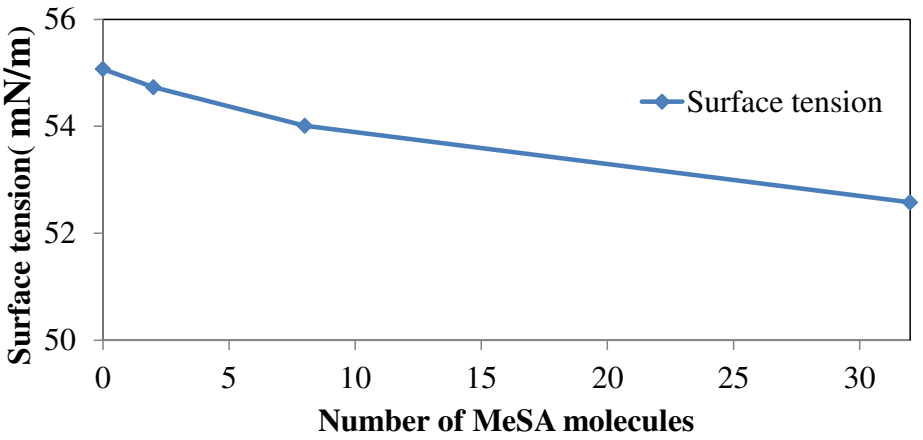

Figure 7.10. Interfacial surface tension with respect to varying number of MeSA molecules at the air/water interface. Line is a guide to the eye.

7.4. Concluding Remarks

We investigated the adsorption of the green leaf volatile (GLV) methyl salicylate (MeSA) on atmospheric air/water interfaces at 298 K using several molecular modeling techniques. In order to assess our molecular models, we first performed thermodynamic integration (TI) calculations to compute the simulated 1-octanol/water partition coefficient for MeSA, which was found to be in very good agreement with reported experimental values and our own experimental measurements. Potential of mean force (PMF) calculations show a deep free energy minimum for MeSA at the air/water interface, which can be explained by the energetic interactions between water and MeSA molecules. The interface provides a favorable environment where the MeSA molecules have important energy interactions with the water molecules at the air/water interface, and do not disrupt too many water-water hydrogen bonds

as compared to the case where MeSA molecules are within the bulk water phase. These PMF results, as well as molecular dynamics (MD) simulation results, indicate that MeSA has a strong thermodynamic preference to remain at the air/water interface, and thus chemical reactions with atmospheric oxidants are more likely to take place at the interface, rather than within atmospheric water droplets or in the gas phase. At the interface, the oxygenated groups in MeSA tend to point towards the water side of the interface, with the aromatic group of MeSA lying farther away from water. Increases in the concentrations of MeSA lead to reductions in the height of the peaks in the MeSA-MeSA $g(r)$ functions, a slowing down of the dynamics of both MeSA and water at the interface, and a reduction in the interfacial surface tension.

CHAPTER 8 OIL ALKANES AND SURFACTANTS IN ATMOSPHERIC AIR/SALT WATER INTERFACES: A MOLECULAR SIMULATION STUDY

In this chapter, we report molecular dynamics (MD) results of the long chain alkanes (Pentadecane and Icosane) and sodium dodecyl sulfate (SDS) at air/salt water interfaces. The main objective of this study is to explore the air/salt water interfacial properties under the influence of long chain alkanes and sodium dodecyl sulfate (SDS) molecules. The rest of this article is structured as follows. Section 8.2 contains details of our computational models and methods. The main results and discussion from this study are presented in section 8.3, and concluding remarks are included in section 8.4.

8.1. Introduction

Previous simulations on adsorption of polycyclic aromatic hydrocarbons (PAHs) and reactive oxygen species on the interfaces of air with pure water or ice (i.e., no salts dissolved) have established the presence of deep free energy minima for adsorption of these species at these interfaces.[20, 135, 136, 149, 158, 247, 254-256] Other experimental and simulation studies have focused on the interfacial properties of aqueous salt solutions with or without surfactants (i.e., no organic molecules adsorbed).[257-267] Several experimental and simulation studies have focused on the properties of air/water interfaces (i.e., no salts dissolved) when alkanes with less than 12 carbon atoms are adsorbed at the interface;[268-277] the structural properties of water at the interface and the interfacial width is known to be significantly influenced by the presence of hydrocarbons and surfactants at air/water interfaces.[77-80] Nevertheless, to the best of our knowledge, no studies have focused on the properties of alkanes with more than 15 carbon atoms when they are adsorbed

on air/salt water interfaces, when dispersants are present. In this work we report classical molecular dynamics (MD) simulations and potential of mean force (PMF) calculations to study the properties of the linear alkanes pentadecane (C15) and icosane (C20) on atmospheric air/salt water interfaces. We focused on these particular n-alkanes because they are representative of IVOCs and SVOCs in Louisiana sweet crude oil, and because they have been found in analysis of oil mousse samples from the DWH oil spill. We then compared these interfacial properties against those obtained for similar systems where the air/salt water interfaces are coated with surfactants. However, and due to the complexity of the species present in the Corexit dispersant used in the oil spill,[278-283] as a first approach to this problem we decided to coat the air/salt water interfaces in our simulated systems with a standard anionic surfactant, sodium dodecyl sulfate (SDS). We also investigated how the structural properties of the alkane and SDS molecules change with variations in their concentrations. These simulations were performed in combination with experimental studies from K. T. Valsaraj's group (to be reported in an upcoming publication), aiming at fundamentally understanding the interfacial properties of these systems. Such a fundamental understanding is crucial to test our working hypothesis, that processes such as aerosolization via bursting bubbles and white caps are likely mechanisms for the ejection of oil spill matter (i.e., heavier IVOCs and SVOCs) into the atmosphere.

8.2. Simulation Details

Classical MD simulations were performed to study the properties of C15, C20 and SDS at air/salt water interfaces at 298 K, where for simplicity salt water was modeled as a NaCl/water solution. For simplicity, and because our main focus is on the properties of the

n-alkanes and SDS, we have modeled water using the non-polarizable SPC/E model,[115] and for NaCl we used the non-polarizable parameters from the work of Vácha *et al.*[283] These NaCl parameters were initially developed using a polarizable water model; however, the study of Auffinger *et al.*[284] showed that this NaCl model is also consistent with the SPC/E water model. In future studies we intend to evaluate similar systems using polarizable force fields for water and the salts, which might be needed to capture specific ion effects at the interfaces.[257-261] We used the OPLS-all atom force field[147] to model the n-alkanes C15 and C20, and parameters for the SDS molecules were taken from the work of Polat *et al.*,[285] which in turn is based on the OPLS-all atom force field.[147] We used the GROMACS software[116] to perform all our MD simulations in the NVT ensemble (constant number of molecules, volume and temperature). In our simulations we considered orthorhombic simulation boxes of dimensions 60 Å × 60 Å × 300 Å (*x*, *y* and *z* respectively) and periodic boundary conditions were applied in all three directions. We placed 5805 SPC/E water molecules and 63 NaCl ion pairs in the middle of the simulation box, creating a salt water slab with two air/salt water interfaces. This results in a salt water slab with salinity comparable to that of sea water.

In the present study we performed both potential of mean force (PMF) calculations and conventional MD simulations. In the former series of calculations, we determined the free energy profile associated with moving one molecule of C15 or C20 between the liquid and gas phases, across air/salt water interfaces that are either bare or SDS-coated. All PMF calculations were run for a total of up to 2 ns, from which up to 1.5 ns were used for accumulating averages. PMF simulations were run at 298 K on both bare and SDS-coated

air/salt water systems. Our MD simulations also included bare and SDS coated-air/salt water systems, which were equilibrated for up to 5 ns and at least 5 ns were used for accumulating averages. In these MD simulations we considered varying concentrations of n-alkanes and SDS molecules; up to 32 molecules of C15, C20 and SDS per air/salt water interface were considered. Remaining simulation details are exactly the same as those used in our previous publications.[135, 150, 164, 238, 247]

8.3. Results and Discussion

8.3.1. PMF of C15 and C20 on Dare and SDS Coated-air/salt Water Systems

In Figure 8.1 and 8.2 we show the PMF associated by moving one molecule of the n-alkanes C15 and C20 between the bulk salt water and the gas phases, across air/salt water interfaces that are bare (Fig. 8.1) or coated with 32 molecules of SDS (Fig. 8.2) at 298 K. We arbitrarily assumed that the PMF of a C15 or C20 molecule in the gas phase is equal to zero. In all cases, the PMF profiles exhibit deep minima at the air/salt water interface, and a sharp increase as the molecule of C15 or C20 is in the bulk of the salt water phase. These observations suggest that, from the thermodynamic point of view, both C15 and C20 prefer to be at the air/salt water interface (bare of SDS-coated), as compared to being in the salt water phase or in the gas phase. This is consistent with previous studies, where organic species such as PAHs[20, 135, 149, 256] and green leaf volatiles[238] also showed a preference to stay at the air/water interface; in turn, the n-alkanes C15 and C20 are relatively large hydrophobic molecules with limited solubility in salt water and relatively low volatility. The minima in the PMF for C15 and C20 at the bare air/salt water interface are about -13.3 kJ/mol and -15.0

kJ/mol respectively, and about -26.4 kJ/mol and -34.9 kJ/mol at SDS-coated air/salt water interfaces.

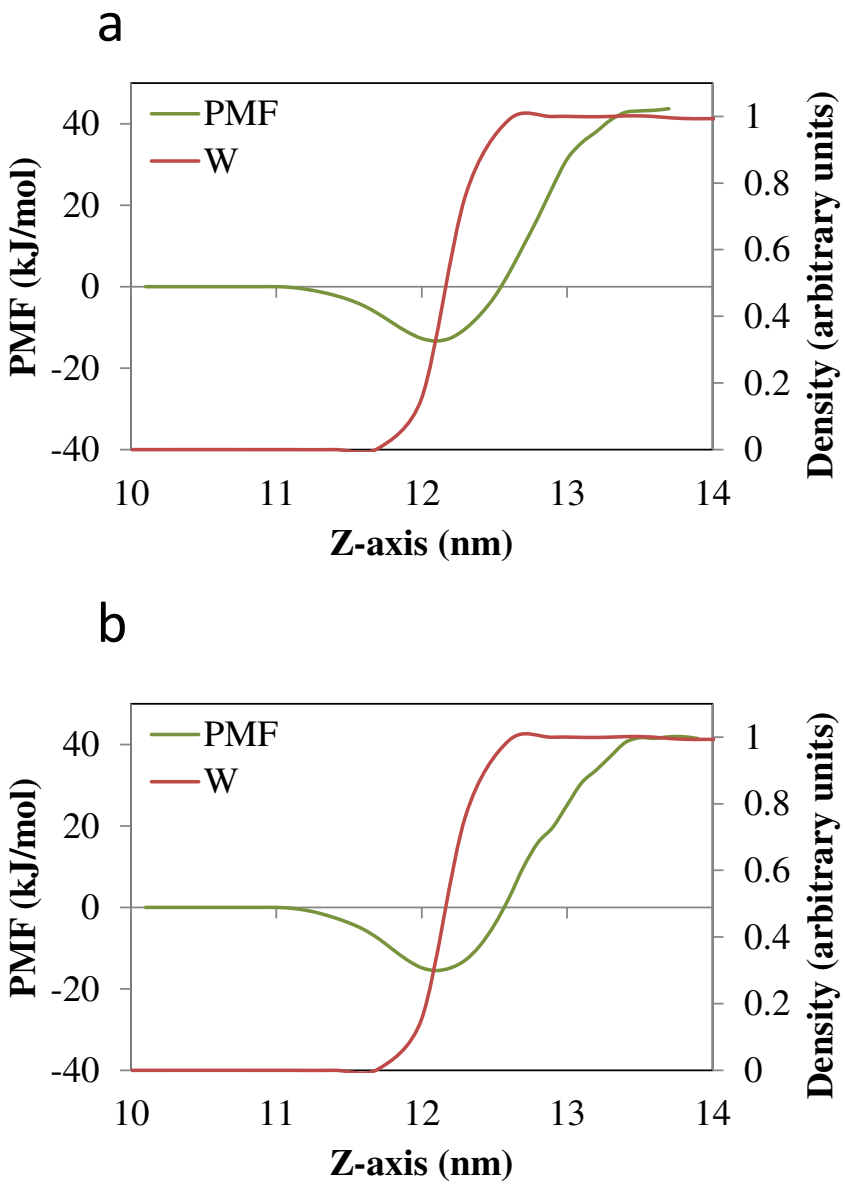

Figure 8.1. PMF (green lines) associated with moving one molecule of n-alkane between the bulk of the salt water phase and the gas phase, across a bare air/salt water interface at 298 K. **(a)** PMF of pentadecane (C15); **(b)** PMF of icosane (C20). The red lines represent the density profiles of water (W). These density profiles are normalized with respect to the maximum value of the local density of water found in the simulation box.

These results suggest that, from the thermodynamic point of view, n-alkanes have a stronger tendency to remain at the air/salt water interface as their chain length increases and as the SDS concentration at the interface increases. These observations are consistent with the

previous simulation studies of Wick *et al.*[149] and Vácha *et al.*,[20] where larger PAHs showed a stronger preference to remain at the air/water interface. In SDS-coated air/salt water interfaces (Fig. 8.2), the minima in the PMF is observed at a value of the *z*-coordinate that is within the SDS layer, indicating that the n-alkanes C15 and C20 prefer to stay dissolved inside the SDS layer and close to the air side of the interface.

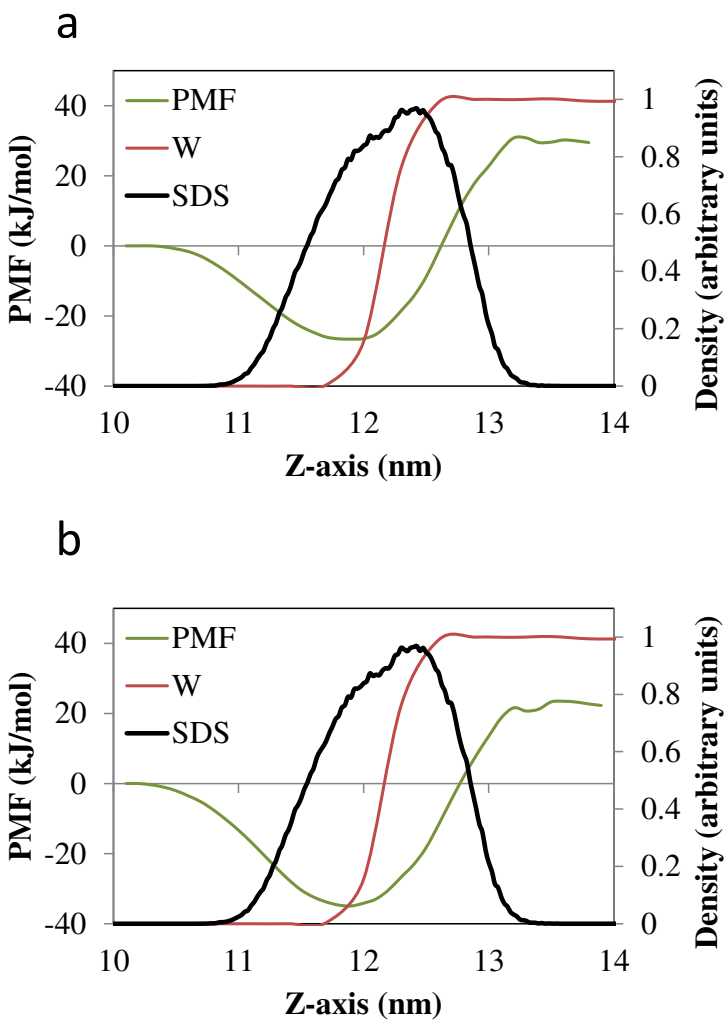

Figure 8.2. PMF (green lines) associated with moving one molecule of n-alkane between the bulk of the salt water phase and the gas phase, across an SDS-coated air/salt water interface at 298 K. **(a)** PMF of pentadecane (C15); **(b)** PMF of icosane (C20). The red and black lines represent the density profiles of water (W) and SDS. These density profiles are normalized with respect to the maximum value of the local density of water or SDS found in the simulation box.

The results described above are especially relevant to our working hypothesis stated in the Introduction: the fact that C15 and C20 have a strong thermodynamic preference to remain at the air/salt water interfaces, especially if these interfaces are coated with surfactants, makes these oil hydrocarbons and dispersants more likely to be ejected to the atmosphere by sea surface processes such as breaking waves and bubble bursting.

8.3.2. Structural Properties of C15, C20 and SDS at the Air/salt Water Interface

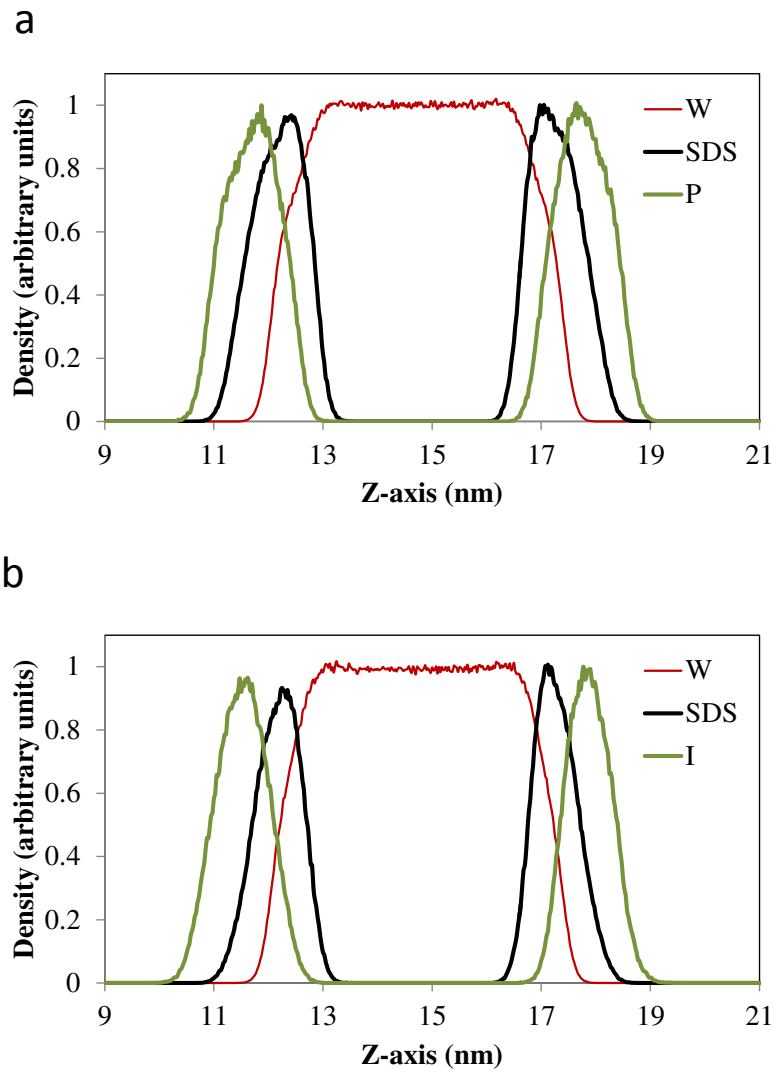

Figure 8.3. Density profiles of pentadecane (C15), icosane (C20) and SDS molecules in air/salt water systems at 298 K. All systems contain 16 molecules of C15 or C20, and 32 SDS molecules per air/salt water interface. The nomenclature W, P and I represent density profiles of water, pentadecane and icosane respectively. The density profile of each species is

normalized by dividing by the maximum value of the local density of each species in the simulation box.

In Figure 8.3 we present density profiles of C15, C20, SDS and water molecules in air/salt water systems at 298 K, as obtained from MD simulations. Up to 16 molecules of C15 or C20, and 32 molecules of SDS are present at each air/salt water interface. Side views of representative simulation snapshots of these systems are presented in Figure 8.4.

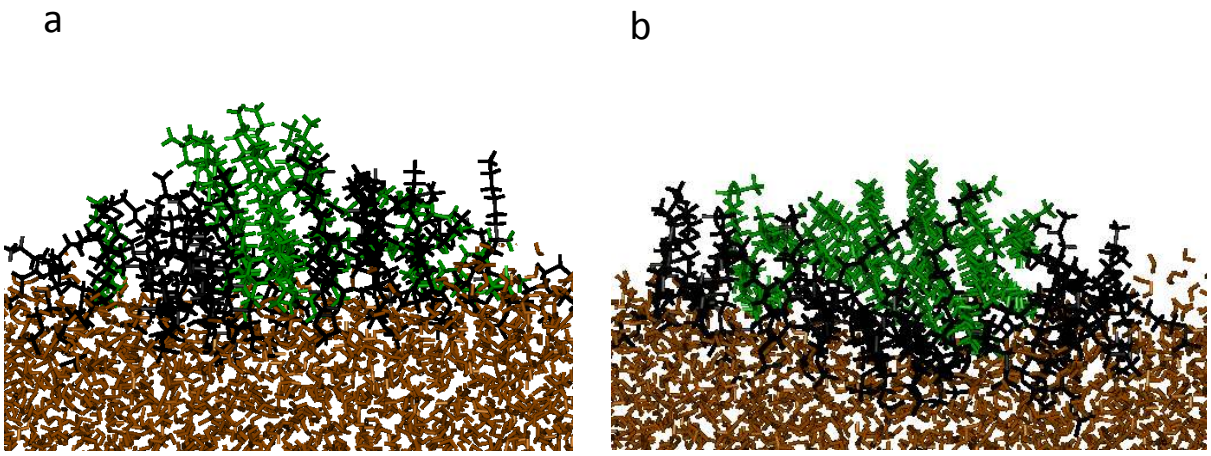

Figure 8.4. Side view of representative simulation snapshots of pentadecane (C15) and icosane (C20) on SDS-coated air/salt water interfaces at 298 K. **(a)** System with 16 molecules of C15 and 32 molecules of SDS per air/salt water interface. **(b)** System with 16 molecules of C20 and 32 molecules of SDS per air/salt water interface. C15 and C20 = green; SDS = black; water = orange (NaCl not shown for clarity).

The density profiles and the snapshots indicate again that both C15 and C20 prefer to stay at the SDS-coated air/salt water interfaces. When we compare the z coordinates of the peaks in the density profiles of C15 or C20 and SDS (Fig. 8.3), we observe that the peaks for SDS molecules are closer to the water molecules in the salt water. The peaks for C15 and C20 are closer to the air side of the interface, however significant overlap in the density profiles of C15 or C20 and SDS is observed in Fig. 3, in agreement with the PMF results shown in Fig. 8.2. Visual inspections of simulation snapshots of our systems (Fig. 8.4) also indicate that the n-alkanes C15 and C20 tend to penetrate into the SDS films at the air/salt water interface. Similar trends were observed for the different concentrations of C15, C20 and SDS

considered here (up to 32 molecules of C15, C20 and SDS per air/salt water interface); these results are not shown for brevity.

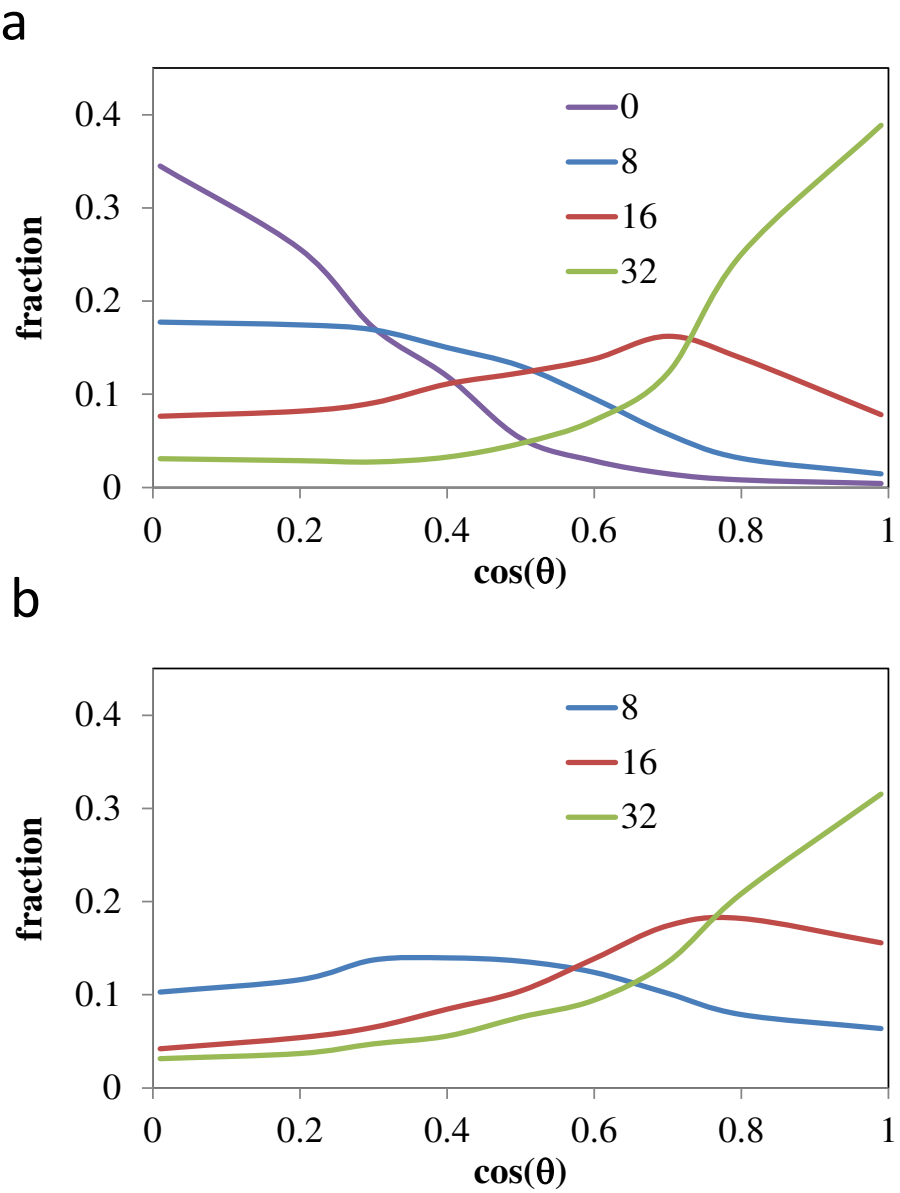

Figure 8.5. Average angle distributions of **(a)** pentadecane (C15), and **(b)** SDS molecules at the air/salt water interface at 298 K, at several concentrations of SDS (8, 16 and 32 SDS molecules per air/salt water interface). All systems contain 16 molecules of C15 in each air/salt water interface.

The orientation of the molecules of C15, C20 and SDS at the air/salt water interface was monitored in our MD simulations. In Figure 8.5 we show the distribution of the angle θ formed between the vector normal to the interface (z-direction) and (1) the vector joining the

carbon atoms at both ends of the C15 molecule, or (2) the vector joining both ends of the carbon chain of the SDS molecule.

In Figure 8.5, a value of $\cos(\theta) = 1$ indicates that the carbon chain of C15 and SDS remains perpendicular with respect to the interface, and a value of $\cos(\theta) = 0$ indicates that these carbon chains lie flat at the air/salt water interface. These orientations were investigated with respect to varying concentrations of SDS at the air/salt water interface. From Figure 8.5a, it can be observed that the molecules of C15 prefer to lie flat when the air/salt water interface is bare. In contrast, when this interface is coated with SDS, the pentadecane chains prefer to adopt a tilted orientation, and become more perpendicular as the SDS concentration increases at the air/salt water interface. From Figure 8.5b, it can also be observed that the angle distribution of the SDS molecules is rather broad at low concentrations, but as concentration increases the SDS molecules tend to adopt a perpendicular orientation with respect to the interface. The trends observed for systems containing C20 molecules are consistent with the results shown in Fig. 8.5 for C15, and are not shown for clarity.

To further investigate the structural properties of pentadecane and icosane at bare and SDS-coated air/salt water interfaces, we computed the C15−C15 and C20−C20 radial distribution functions $g(r)$ for varying concentrations of SDS at the air/salt water interface. Our results for C15 (Figure 8.6a) indicate that increasing concentrations of SDS at the air/salt water interfaces leads to reductions in the height of the peaks of $g(r)$. In contrast, for C20 the height of the peaks of $g(r)$ does not vary significantly when the concentration of SDS increases. Varying concentrations of SDS does not lead to new peaks in the $g(r)$ functions shown in Figure 8.6. These results can be explained with the help of the simulation snapshots

shown in Figure 8.7, which suggest that both C15 and C20 form dense aggregates at the bare air/salt water interfaces. Increasing concentrations of SDS are able to partially disperse the aggregates of C15 (Fig. 8.7b), but cannot break down the C20 aggregates (Fig. 8.7d). The mixtures of molecules in the Corexit dispersant used in the oil spill[51-56] are larger and more complex than SDS, and thus have a better performance in dispersing oil components. We are currently modeling systems containing oil hydrocarbons and representative molecules from Corexit; these results will be reported in an upcoming publication.

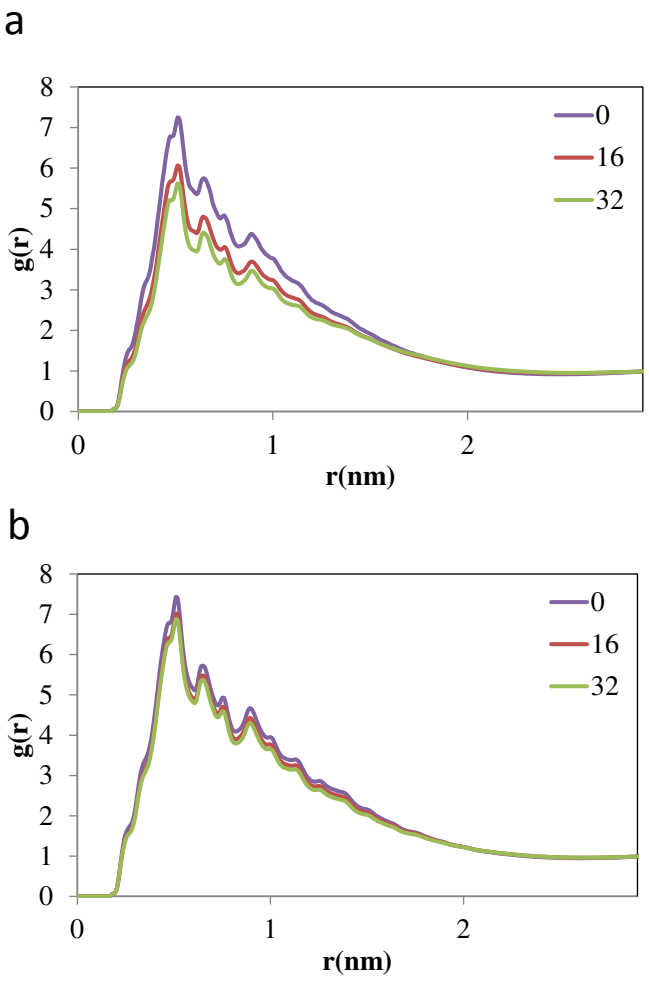

Figure 8.6. Radial distribution functions $g(r)$ of Pentadecane−Pentadecane and Icosane−Icosane molecules at both bare and SDS coated-air/salt water interfaces at 298 K. **(a)** Radial distribution functions $g(r)$ Pentadecane−Pentadecane molecules. **(b)** Radial distribution functions $g(r)$ of Icosane−Icosane molecules. In each figures 0, 16 and 32 represents 0, 16 and 32 SDS molecules at air/salt water interface respectively.

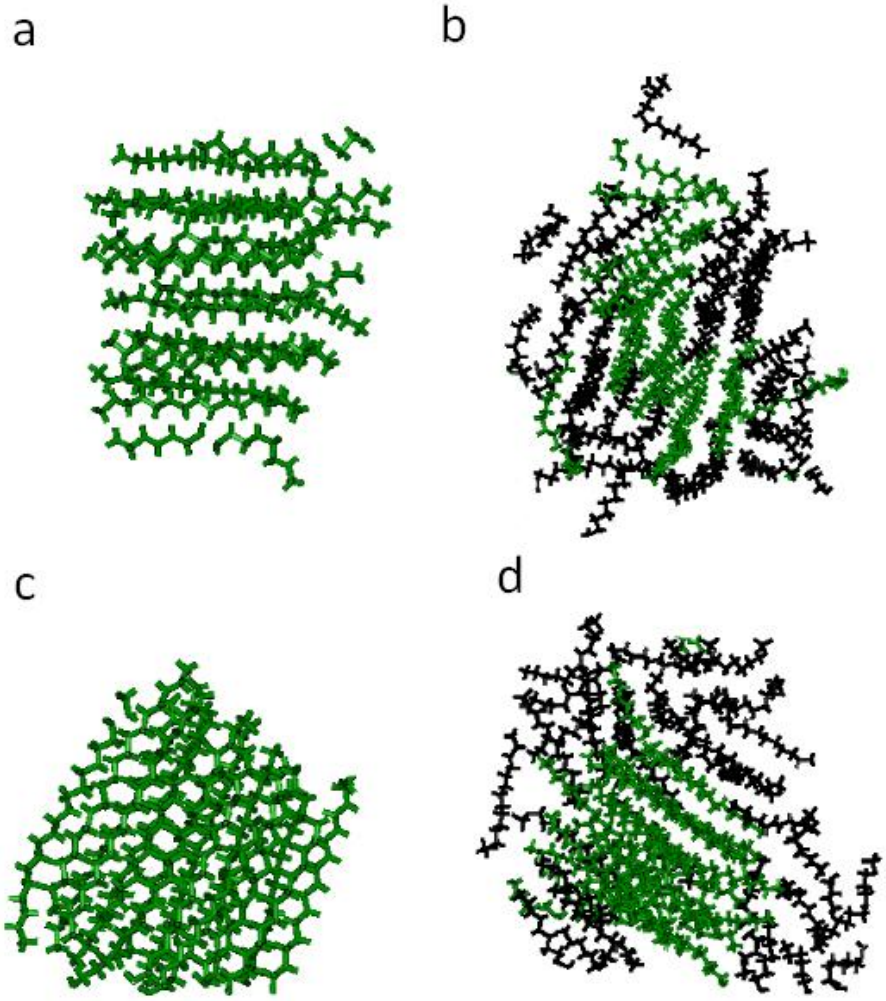

Figure 8.7. Top views of representative simulation snapshots of systems of Pentadecane and Icosane on bare and SDS coated-air/salt water interfaces at 298 K. **(a)** System with 16 molecules of Pentadecane on bare air/salt water. **(b)** System with 16 molecules of Pentadecane on SDS (32 molecules) coated-air/salt water. **(c)** System with 16 molecules of Icosane on bare air/salt water. **(d)** System with 16 molecules of Icosane on SDS (32 molecules) coated-air/salt water. . Pentadecane and Icosane = green; SDS molecules = black.

8.4. Concluding Remarks

Potential of mean force (PMF) calculations and molecular dynamics (MD) simulations were performed to investigate the properties of the oil hydrocarbons pentadecane (C15) and icosane (C20), as well as a standard anionic surfactant, sodium dodecyl sulfate (SDS) at air/salt water interfaces. This work was motivated by the 2010 Deepwater Horizon (DWH) oil spill, and we specifically focus on intermediate- and semi-volatile organic compounds

(IVOCs and SVOCs, namely hydrocarbons with 14 to 31 carbon atoms). A significant fraction of IVOCs and SVOCs released during the DWH oil spill reached the sea surface despite the large amounts of Corexit dispersant used, which in turn could have also reached the sea surface. The working hypothesis of this study, which is part of a series of studies from our group, is that a significant fraction of these IVOCs, SVOCs and the dispersants that reached the sea surface did not evaporate but remained there, and phenomena such as white caps (breaking waves) and bubble bursting on the sea surface eject these compounds into the atmosphere. Negligible data has been gathered so far on wave- and bubble-generated aerosolization of oil near the DWH accident site. Our results show that, from the thermodynamic point of view, the n-alkanes C15 and C20 have a strong preference to remain at the air/salt water interface, as indicated by the presence of deep free energy minima at these interfaces. The free energy minimum becomes deeper as the chain length of the n-alkanes increases, and as the concentration of SDS at the interface increases. The fact that C15 and C20 have a strong thermodynamic preference to remain at the air/salt water interfaces, especially if these interfaces are coated with surfactants, makes these oil hydrocarbons and dispersants more likely to be ejected to the atmosphere by sea surface processes such as breaking waves and bubble bursting.

Both pentadecane and icosane tend to adopt a flat orientation and form aggregates at the bare air/salt water interface. When this interface is coated with SDS, the molecules of C15 and C20 tend to adopt a titled angle with respect to the vector normal to the interface, and become more perpendicular as the concentration of SDS increases. Increasing concentrations of SDS are able to partially disperse the aggregates of C15, but cannot break down the C20

aggregates formed at the air/salt water interface. The mixtures of molecules in the Corexit dispersant used in the oil spill[51-56] are larger and more complex than SDS, and thus have a better performance in dispersing oil components. In this initial study in this area we decided to study a standard surfactant such as SDS, mainly due to the complexity of the molecules present in Corexit.[51-56] In an upcoming publication we will present simulation results of systems containing oil hydrocarbons and representative molecules from Corexit. We have also studied the ejection rates of oil hydrocarbons and Corexit dispersant in experiments using a bubble column reactor, where we have simulated bubble-bursting processes at the sea surface. These experimental results agree with the simulation trends presented here, namely that more oil hydrocarbons are ejected when Corexit is present in the system. These results will be featured in several upcoming publications. Our combined simulation and experimental results suggest that aerosolization via bursting bubbles and breaking waves at the sea surface is a likely transport mechanism for the ejection of oil spill organics into the atmosphere.

CHAPTER 9 CONCLUSIONS ONGOING AND FUTURE WORK

9.1 Conclusions

In chapters 2-5, we focused on the properties of PAHs and ROSs on atmospheric air/ice interfaces. In chapter 2, the adsorption of gas-phase phenanthrene, naphthalene and ozone on atmospheric air/ice interfaces was investigated using classical molecular dynamics (MD) simulations and potential of mean force (PMF) calculations. Phenanthrene, naphthalene and ozone exhibit a strong preference to be adsorbed at the air/ice interface, rather than being dissolved into the bulk of the quasi-liquid layer (QLL) or incorporated into the ice crystals. It is also observed that a decrease in temperature causes surface adsorption to become more significant than bulk phase partitioning for naphthalene and phenanthrene molecules. When the air/ice interface is coated with increasing concentrations of naphthalene molecules, the QLL becomes thinner and surface adsorption of ozone is enhanced. Furthermore, ozone tends to adsorb on top of the naphthalene film, although significant penetration of ozone into this film is also observed. Both phenanthrene and naphthalene molecules tend to adopt a flat orientation on the air/ice interface, less variation in the orientation was observed for lower concentrations of naphthalene, whereas variations in the ozone concentration do not affect the orientation of naphthalene molecules. However, as the concentration of ozone increases, most of the naphthalene molecules still prefer to stay close to the mobile water molecules in the QLL, but a significant fraction of the naphthalene molecules spends a considerable amount of time inside the thicker layer of ozone. We also monitored the number of contacts between naphthalene and ozone at the air/ice interface upon variations in the concentrations of these two species. These contacts were assumed to be proportional to the reaction rate between

these two species. When the number of ozone molecules was held constant, the number of contacts showed a linear relationship to the number of naphthalene molecules. However, when the naphthalene concentration was held constant, for all systems we observed a linear relationship at low ozone concentrations and a plateau at high ozone concentrations.

The adsorption of gas-phase naphthalene and ozone molecules onto air/ice interfaces coated with different surfactant species (1-octanol, 1-hexadecanol or 1-octanal) was also investigated using classical MD simulations in chapter 3. Naphthalene and ozone exhibit a strong preference to be adsorbed at the surfactant-coated air/ice interfaces, as opposed to either being dissolved into the bulk of the quasi-liquid layer (QLL) or being incorporated into the ice crystals. The QLL becomes thinner when the air/ice interface is coated with surfactant molecules. The adsorption of both naphthalene and ozone onto surfactant-coated air/ice interfaces is enhanced when compared to bare air/ice interface. Both naphthalene and ozone tend to stay dissolved in the surfactant layer and close to the QLL, rather than adsorbing on top of the surfactant molecules and close to the air region of our systems. Surfactants prefer to orient at a tilted angle with respect to the air/ice interface; the angular distribution and the most preferred angle vary depending on the hydrophilic end group, the length of the hydrophobic tail, and the surfactant concentration at the air/ice interface. Naphthalene prefers to have a flat orientation on the surfactant coated air/ice interface, except at high concentrations of 1-hexadecanol at the air/ice interface; the angular distribution of naphthalene depends on the specific surfactant and its concentration at the air/ice interface. The dynamics of naphthalene molecules at the surfactant-coated air/ice interface slow down as compared to those observed at bare air/ice interfaces. The presence of surfactants does not

seem to affect the self-association of naphthalene molecules at the air/ice interface, at least for the specific surfactants and the range of concentrations considered in this study.

Classical MD simulations were performed in chapter 4 to investigate the growth of ice from supercooled aqueous solutions of benzene, naphthalene or phenanthrene. The main objective of this study is to explore the fate of those aromatic molecules after freezing of the supercooled aqueous solutions, i.e., if these molecules become trapped inside the ice lattice, or if they are displaced to the QLL or to the interface with air. Ice growth from supercooled aqueous solutions of benzene, naphthalene or phenanthrene result in the formation of quasi-liquid layers (QLLs) at the air/ice interface that are thicker than those observed when pure supercooled water freezes. Naphthalene and phenanthrene molecules in the supercooled aqueous solutions are displaced to the air/ice interface during the freezing process at both 270 K and 260 K; no incorporation of these aromatics into the ice lattice is observed throughout the freezing process. Similar trends were observed during freezing of supercooled aqueous solutions of benzene at 270 K. In contrast, a fraction of the benzene molecules become trapped inside the ice lattice during the freezing process at 260 K, with the rest of the benzene molecules being displaced to the air/ice interface. These results suggest that the size of the aromatic molecule in the supercooled aqueous solution is an important parameter in determining whether these molecules become trapped inside the ice crystals. Finally, we also report potential of mean force (PMF) calculations aimed at studying the adsorption of gas-phase benzene and phenanthrene on atmospheric air/ice interfaces. Our PMF calculations indicate the presence of deep free energy minima for both benzene and phenanthrene at the air/ice interface, with these molecules adopting a flat orientation at the air/ice interface.

In chapter 5, classical MD simulations and potential of mean force (PMF) calculations were performed to study (1) the adsorption of several reactive oxygen species (ROSs, namely •OH, •HO2 and H2O2) on atmospheric air/ice interfaces, and (2) the growth of ice from supercooled aqueous solutions of these ROSs. Free energy minima were observed for these ROSs at the air/ice interfaces. The presence of ROSs in supercooled water during the freezing process leads to the formation of quasi-liquid layers (QLLs) that were thicker than those formed from freezing of pure supercooled water. The ROSs in the supercooled water were always displaced to the air/ice interface during the freezing process at 270 K, but if the freezing process is carried out at 260 K, a significant fraction of hydroperoxy and hydrogen peroxide become trapped by the growing ice lattice. We also studied freezing of supercooled aqueous solutions containing ROSs and benzene, with 1-octanal at the interfaces with air. The structure of ice is not significantly altered by hydroperoxy, hydrogen peroxide or benzene being trapped in the ice lattice. The presence of 1-octanal at the interfaces does not alter the trends described above; however, thinner QLLs are formed after the freezing process, and 1-octanal tends to slow down the dynamics of ROSs and aromatics at the air/ice interface.

In chapters 6 and 7, we focused on green leaf volatiles (GLVs), which are oxygenated hydrocarbons that are emitted by plants, especially under stress conditions such as mechanical damage and local weather changes. GLVs can react with photochemically-generated oxidants (e.g., OH radicals) in atmospheric water drops, and contribute to the formation of secondary organic aerosols (SOAs). In chapter 6, we investigated the adsorption of a gas phase GLV, 2-methyl-3-buten-2-ol (MBO) and OH radicals on atmospheric air/water interfaces using classical molecular dynamics (MD)

simulations and potential of mean force (PMF) calculations. Our models can reproduce experimental values of the free energy of hydration of MBO and •OH, as well as 1-octanol/water partition coefficients of MBO determined experimentally in this study. Both MBO and •OH have a strong thermodynamic incentive to remain at the air/water interface, with their density profiles overlapping significantly at the interface. These results suggest that chemical reactions between MBO and •OH are more likely to take place at the interface, rather than inside the bulk of water droplets or in the vapor phase. We found a significant number of contacts between MBO and •OH in our simulations, which could lead to reactions between these two species.

In chapter 7, we studied the GLV methyl salicylate (MeSA), which is emitted by plants under stress conditions in the environment. We investigated the adsorption of gas phase MeSA on atmospheric air/water interfaces under atmospheric conditions. Our model for MeSA is able to reproduce the 1-octanol/water partition coefficients of MeSA determined experimentally in this study, and is also able to give accurate estimates of the free energy of hydration and interfacial partition of MeSA at the air/water interface. MeSA has a strong preference to be adsorbed at the air/water interface, as opposed to either being dissolved into bulk water phase or staying in the gas phase. MeSA prefers to orient such that the hydrophilic end of MeSA is pointing towards the water at the air/water interface, and its hydrophobic ring is away from the air/water interface. The dynamics of MeSA and water molecules at the air/water interface slow down as the concentration of MeSA at the air/water interface increases. The presence of MeSA molecules at the air/water interface decreases the surface

tension at the air/water interface. No aggregation of MeSA was observed at the air/water interface.

In chapter 8, we performed MD simulations of long chain alkanes (pentadecane, C15) and icosane, C20) on bare and sodium dodecyl sulfate (SDS)-coated air/salt water interfaces. Potential of mean force (PMF) calculations and molecular dynamics (MD) simulations were performed to investigate the properties of the oil hydrocarbons pentadecane (C15) and icosane (C20), as well as a standard anionic surfactant, sodium dodecyl sulfate (SDS) at air/salt water interfaces. This work was motivated by the 2010 Deepwater Horizon (DWH) oil spill, where a significant fraction of intermediate- and semi-volatile organic compounds (IVOCs and SVOCs, namely hydrocarbons with 14 to 31 carbon atoms) released during the DWH oil spill reached the sea surface, together with a fraction of the Corexit oil dispersant used. This work, which is the first of a series of studies from our group, aims at testing the hypothesis that a significant fraction of the IVOCs, SVOCs and the dispersants that reached the sea surface did not evaporate but remained there, and phenomena such as white caps (breaking waves) and bubble bursting on the sea surface would eject these compounds into the atmosphere. Our simulation results show that, from the thermodynamic point of view, the n-alkanes C15 and C20 have a strong preference to remain at the air/salt water interface, as indicated by the presence of deep free energy minima at these interfaces. The free energy minimum becomes deeper as the chain length of the n-alkanes increases, and as the concentration of SDS at the interface increases. The fact that C15 and C20 have a strong thermodynamic preference to remain at the air/salt water interfaces, especially if these interfaces are coated with surfactants, makes these oil hydrocarbons and dispersants more

likely to be ejected to the atmosphere by sea surface processes such as breaking waves and bubble bursting. Both pentadecane and icosane tend to adopt a flat orientation and form aggregates at the bare air/salt water interface. When this interface is coated with SDS, the molecules of C15 and C20 tend to adopt a titled angle with respect to the vector normal to the interface, and become more perpendicular as the concentration of SDS increases. Increasing concentrations of SDS are able to partially disperse the aggregates of C15, but cannot break down the C20 aggregates formed at the air/salt water interface.

9.2. Ongoing and Future Work

9.2.1 Oxygenated PAHs (OPAHs) and Nitrated PAHs (NPAHs) at Air/water and Air/ice Interfaces

PAHs compounds can undergo photo chemically induced oxidation and nitration reactions and produce oxygenated PAHs (OPAHs) and nitrated PAHs (NPAHs), e.g. Figure 9.1. These compounds are more toxic than PAHs (up to 105 times larger carcinogenic and mutagenic activities).

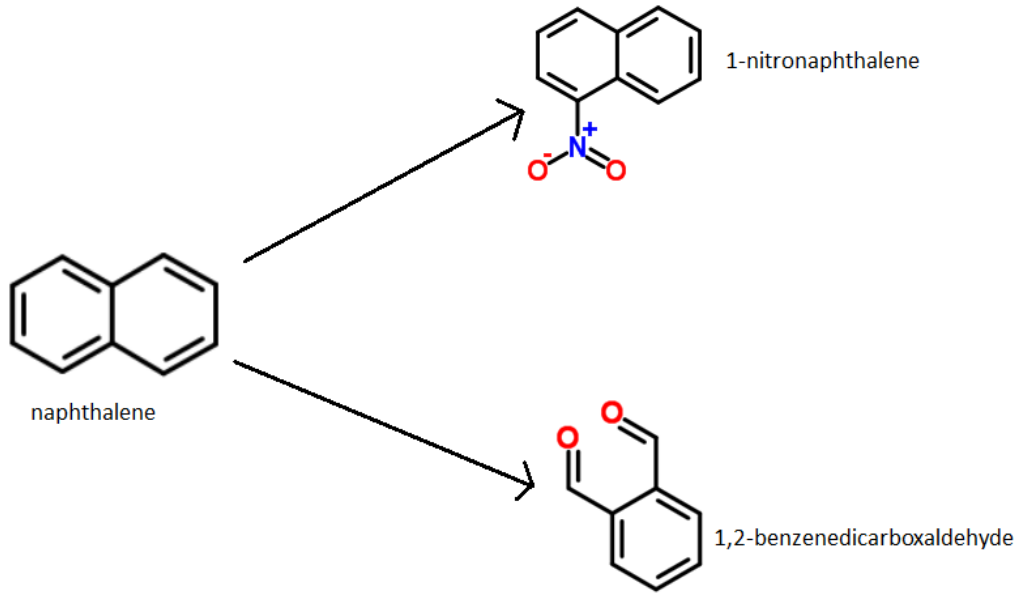

Figure 9.1. Examples of NPAHs and OPAHs from naphthalene

Understanding the faith of these OPAHs and NPAHs at air/water and air/ice interfaces, as well as their dissolution in bulk water, crystalline ice and in the QLL is important to understand the fate and transport of these organic pollutants in the environment.

9.2.2 Adsorption of Other Green Leaf Volatiles (GLVs) at Air/water Interface

Other compounds in this class include cis-3-hexen-1-ol (HxO) and cis-3-hexenylacetate, (HxAc) as presented by figure 9.2. Furthermore, these compounds are chemically active and participate in controlling the oxidative capacity of the troposphere.

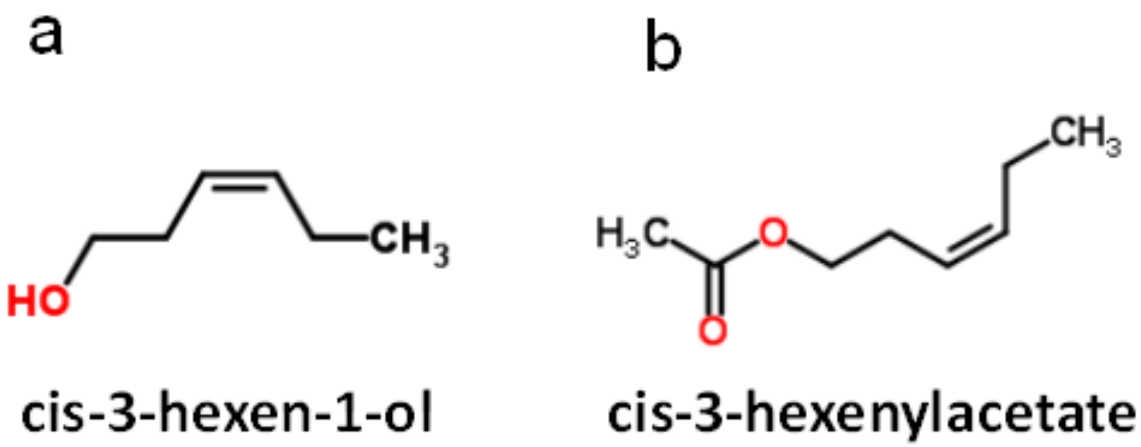

Figure 9.2. First generation GLVs

As discussed earlier in chapter 1, GLVs have been shown to be SOA precursors in the atmosphere. These GLVs also react with gas-phase oxidants to produce first generation oxidation products such as 3-hydroxypropanal (3HPA) from HxO and HxAC. So it is important to understand the properties of these GLVs at air/water interfaces in order to understand the fate of these species in the environment and how they contribute to formation of SOAs in the atmosphere.

9.2.3 Dispersants at Air/salt Water Interfaces

In this dissertation we investigated the influence of n-alkanes and SDS molecules on the air/salt water interfacial properties. We would extend this study of air/salt water interface by using model compounds from Corexit 9500/9527 used in the 2010 Deep-water Horizon (DWH) accident such as Polyoxyethylene(20)sorbitan monooleate (Tween) and Polyoxyethylene(20)sorbitan trioleate (Span) as presented by figure 9.3.

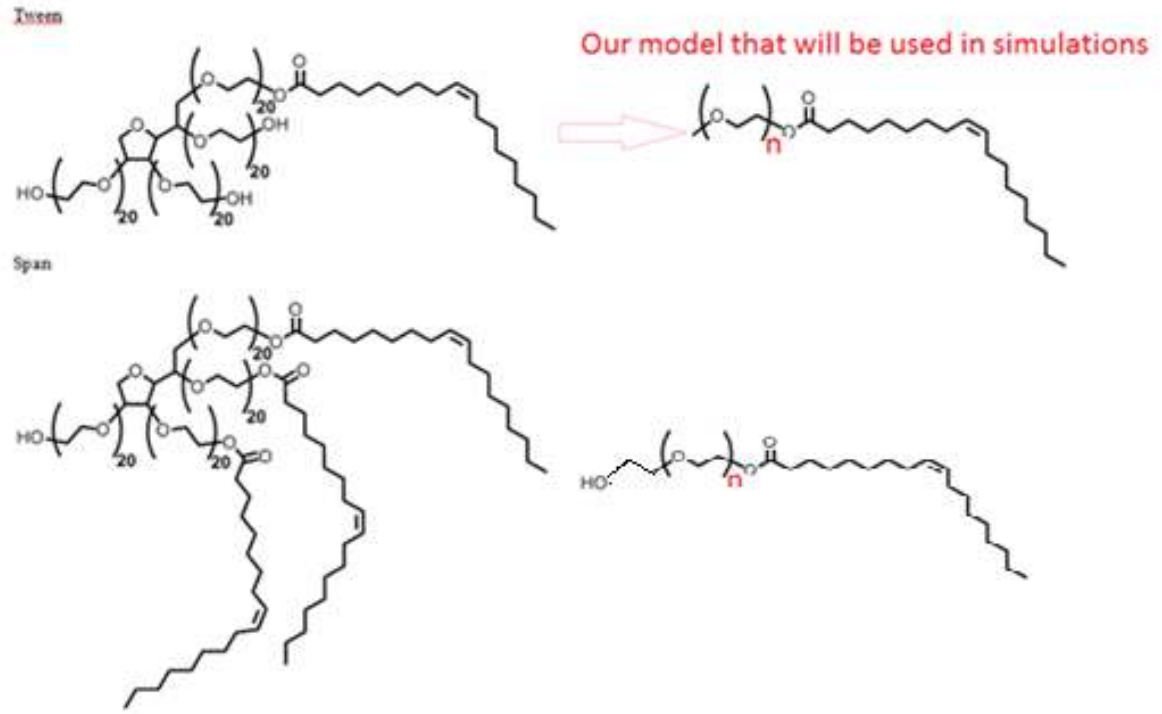

Figure 9.3. Polyoxyethylene(20)sorbitanmonooleate(Tween) and Polyoxyethylene(20)sorbitan trioleate (Span).

REFERENCES

1. Donaldson, D.J., Valsaraj, K. T., *Adsorption and Reaction of Trace Gas-Phase Organic Compounds on Atmospheric Water Film Surfaces: A Critical Review.* Environ. Sci. Technol., 2010. **44**(3): p. 865-873.

2. Dominé, F. and P.B. Shepson, *Air-Snow Interactions and Atmospheric Chemistry.* Science, 2002. **297**(5586): p. 1506-1510.

3. Kanakidou, M., et al., *Organic aerosol and global climate modelling: a review.* Atmospheric Chemistry and Physics, 2005. **5**: p. 1053-1123.

4. George, I.J. and J.P.D. Abbatt, *Heterogeneous oxidation of atmospheric aerosol particles by gas-phase radicals.* Nature Chemistry, 2010. **2**(9): p. 713-722.

5. Monks, P.S., et al., *Atmospheric composition change - global and regional air quality.* Atmospheric Environment, 2009. **43**(33): p. 5268-5350.

6. Hallquist, M., et al., *The formation, properties and impact of secondary organic aerosol: current and emerging issues.* Atmospheric Chemistry and Physics, 2009. **9**(14): p. 5155-5236.

7. Donahue, N.M., A.L. Robinson, and S.N. Pandis, *Atmospheric organic particulate matter: From smoke to secondary organic aerosol.* Atmospheric Environment, 2009. **43**(1): p. 94-106.

8. Andreae, M.O. and D. Rosenfeld, *Aerosol-cloud-precipitation interactions. Part 1. The nature and sources of cloud-active aerosols.* Earth-Science Reviews, 2008. **89**(1-2): p. 13-41.

9. Kroll, J.H. and J.H. Seinfeld, *Chemistry of secondary organic aerosol: Formation and evolution of low-volatility organics in the atmosphere.* Atmospheric Environment, 2008. **42**(16): p. 3593-3624.

10. Poschl, U., *Atmospheric aerosols: Composition, transformation, climate and health effects.* Angewandte Chemie-International Edition, 2005. **44**(46): p. 7520-7540.

11. Munger, J.W., et al., *Fogwater chemistry in an urban atmosphere.* J. Geophys. Res. - Oc. Atm., 1983. **88**(NC9): p. 5109-5121.

12. Raja, S., et al., *Monitoring of fogwater chemistry in the gulf coast urban industrial corridor: Baton Rouge (Louisiana).* Environmental Monitoring and Assessment, 2005. **110**(1-3): p. 99-120.

13. Kahan, T.F., N.O.A. Kwamena, and D.J. Donaldson, *Heterogeneous ozonation kinetics of polycyclic aromatic hydrocarbons on organic films.* Atmospheric Environment, 2006. **40**(19): p. 3448-3459.

14. Finlayson-Pitts, B., Pitts, J. N., *Chemistry of the upper and lower atmosphere*. 2000, New York: Academic Press.

15. *http://www.epa.gov/waterscience/methods/pollutants.htm*. Available from: http://www.epa.gov/waterscience/methods/pollutants.htm.

16. Xu, J.H. and F.S.C. Lee, *Quantification of nitrated polynuclear aromatic hydrocarbons in atmospheric particulate matter.* Analytica Chimica Acta, 2000. **416**(1): p. 111-115.

17. Poschl, U., et al., *Interaction of ozone and water vapor with spark discharge soot aerosol particles coated with benzo a pyrene: O-3 and H2O adsorption, benzo a pyrene degradation, and atmospheric implications.* Journal of Physical Chemistry A, 2001. **105**(16): p. 4029-4041.

18. Poschl, U., *Formation and decomposition of hazardous chemical components contained in atmospheric aerosol particles.* Journal of Aerosol Medicine-Deposition Clearance and Effects in the Lung, 2002. **15**(2): p. 203-212.

19. Valsaraj, K.T., *Trace gas adsorption thermodynamics at the air-water interface: Implications in atmospheric chemistry.* Pure and Applied Chemistry, 2009. **81**(10): p. 1889-1901.

20. Vacha, R., Jungwirth, P., Chen, J., Valsaraj, K. T., *Adsorption of Polycyclic Aromatic Hydrocarbons at the Air-water Interface: Molecular Dynamics Simulations and Experimental Atmospheric Observations.* Physical Chemistry Chemical Physics, 2006. **8**: p. 4461-4467.

21. Ellison, G.B., A.F. Tuck, and V. Vaida, *Atmospheric processing of organic aerosols.* Journal of Geophysical Research-Atmospheres, 1999. **104**(D9): p. 11633-11641.

22. Cappiello, A., De Simoni, E., Fiorucci, C., Mangani, F., Palma, P., Trufelli, H., Decesari, S., Facchini, M. C., Fuzzi, S., *Molecular Characterization of the Water-soluble Organic Compounds in Fogwater by ESIMS/MS.* Environ. Sci. Technol., 2003. **37**: p. 1229-1240.

23. Zhang, Q. and C. Anastasio, *Conversion of fogwater and aerosol organic nitrogen to ammonium, nitrate, and NOx during exposure to simulated sunlight and ozone.* Environmental Science & Technology, 2003. **37**(16): p. 3522-3530.

24. Latif, M.T. and P. Brimblecombe, *Surfactants in atmospheric aerosols.* Environmental Science & Technology, 2004. **38**(24): p. 6501-6506.

25. Chen, J., Ehrenhauser, F. S., Valsaraj, K. T., Wornat, M. J., *Uptake and UV-photooxidation of Gas-phase PAHs on the Surface of Atmospheric Water Films. 1. Naphthalene.* . Journal of Physical Chemistry A, 2006. **110**: p. 9161-9168.

26. Donaldson, D.J. and V. Vaida, *The influence of organic films at the air-aqueous boundary on atmospheric processes.* Chemical Reviews, 2006. **106**(4): p. 1445-1461.

27. Kwamena, N.O.A., et al., *Role of the aerosol substrate in the heterogeneous ozonation reactions of surface-bound PAHs.* Journal of Physical Chemistry A, 2007. **111**(43): p. 11050-11058.

28. Vacha, R., et al., *Adsorption of atmospherically relevant gases at the air/water interface: Free energy profiles of aqueous solvation of N-2, O-2, O-3, OH, H2O, HO2, and H2O2.* Journal of Physical Chemistry A, 2004. **108**(52): p. 11573-11579.

29. Vacha, R., et al., *Adsorption of aromatic hydrocarbons and ozone at environmental aqueous surfaces.* Journal of Physical Chemistry A, 2008. **112**(22): p. 4942-4950.

30. Vieceli, J., et al., *Molecular dynamics simulations of atmospheric oxidants at the air-water interface: Solvation and accommodation of OH and O-3.* Journal of Physical Chemistry B, 2005. **109**(33): p. 15876-15892.

31. Vieceli, J., O.L. Ma, and D.J. Tobias, *Uptake and collision dynamics of gas phase ozone at unsaturated organic interfaces.* Journal of Physical Chemistry A, 2004. **108**(27): p. 5806-5814.

32. Jungwirth, P. and D.J. Tobias, *Specific ion effects at the air/water interface.* Chemical Reviews, 2006. **106**(4): p. 1259-1281.

33. Wick, C.D., B. Chen, and K.T. Valsaraj, *Computational Investigation of the Influence of Surfactants on the Air-Water Interfacial Behavior of Polycylic Aromatic Hydrocarbons.* Journal of Physical Chemistry C, 2010. **114**(34): p. 14520-14527.

34. Ram, K. and C. Anastasio, *Photochemistry of phenanthrene, pyrene, and fluoranthene in ice and snow.* Atmospheric Environment, 2009. **43**(14): p. 2252-2259.

35. Domine, F., Cincinelli, A., Bonnaud, E., Martellini, T., Picaud, S., *Adsorption of Phenanthrene on Natural Snow.* Environ. Sci. Technol., 2007. **41**: p. 6033-6038.

36. Kahan, T.F. and D.J. Donaldson, *Photolysis of polycyclic aromatic hydrocarbons on water and ice surfaces.* Journal of Physical Chemistry A, 2007. **111**(7): p. 1277-1285.

37. Kahan, T.F. and D.J. Donaldson, *Heterogeneous ozonation kinetics of phenanthrene at the air-ice interface.* Environmental Research Letters, 2008. **3**(4): p. 045006.

38. Ardura, D., T.F. Kahan, and D.J. Donaldson, *Self-Association of Naphthalene at the Air-Ice Interface.* Journal of Physical Chemistry A, 2009. **113**(26): p. 7353-7359.

39. Kahan, T.F., Reid, J. P., and Donaldson, D. J., *Spectroscopic Probes of the Quasi-Liquid Layer on Ice.* Journal of Physical Chemistry A, 2007. **111**: p. 11006-11012.

40. Kahan, T.F., R. Zhao, and D.J. Donaldson, *Hydroxyl radical reactivity at the air-ice interface.* Atmospheric Chemistry and Physics, 2010. **10**(2): p. 843-854.

41. Kahan, T.F., et al., *Anthracene Photolysis in Aqueous Solution and Ice: Photon Flux Dependence and Comparison of Kinetics in Bulk Ice and at the Air-Ice Interface.* Environmental Science & Technology, 2010. **44**(4): p. 1302-1306.

42. Kahan, T.F. and D.J. Donaldson, *Benzene Photolysis on Ice: Implications for the Fate of Organic Contaminants in the Winter.* Environmental Science & Technology, 2010. **44**(10): p. 3819-3824.

43. Chen, J., Ehrenhauser, F., Liyana-Arachchi, T. P., Hung, F. R., Wornat, M. J., and Valsaraj, K. T., *Adsorption of gas-phase phenanthrene on atmospheric water and ice films.* Polycyclic Aromatic Compounds, 2011: p. accepted.

44. Rosenberg, R., *Why is ice slippery?* Physics Today, 2005. **58**(12): p. 50-55.

45. Grannas, A.M., et al., *An overview of snow photochemistry: evidence, mechanisms and impacts.* Atmospheric Chemistry and Physics, 2007. **7**(16): p. 4329-4373.

46. Herckes, P., et al., *Organic compounds in radiation fogs in Davis (California).* Atmos. Res., 2002. **64**(1–4): p. 99-108.

47. Alves, C.A., *Characterisation of solvent extractable organic constituents in atmospheric particulate matter: an overview.* An. Acad. Bras. Cienc., 2008. **80(1)** p. 21-82.

48. Raja, S., et al., *Fog chemistry in the Texas-Louisiana Gulf Coast corridor.* Atmospheric Environment, 2008. **42**(9): p. 2048-2061.

49. Chen, J., Ehrenhauser, F. S., Valsaraj, K. T., Wornat, M. J., *Uptake and UV-photooxidation of Gas-phase PAHs on the Surface of Atmospheric Water Films. 1. Naphthalene.* J. Chem. Phys. A, 2006. **110**: p. 9161-9168.

50. Chen, J. and K.T. Valsaraj, *Uptake and UV-Photooxidation of Gas-Phase Polyaromatic Hydrocarbons on the Surface of Atmospheric Water Films. 2. Effects of Dissolved Surfactants on Naphthalene Photooxidation.* Journal of Physical Chemistry A, 2007. **111**(20): p. 4289-4296.

51. Saxena, P. and L.M. Hildemann., *Water-soluble organics in atmospheric particles: A critical review of the literature and application of thermodynamics to identify candidate compounds.* J. Atmos. Chem., 1996. **24(1)**: p. 57-109.

52. Daly, G.L. and F. Wania, *Organic contaminants in mountains.* Environ. Sci. Technol., 2005. **39**(2): p. 385-398.

53. Steiner, A. and A.L. Goldstein, *Biogenic VOCs, in VOCs in the Environment, R. Koppelman, Editor Blackwell Publishers: Ames, Iowa.* 2007: p. 82-128.

54. Birdwell, J.E. and K.T. Valsaraj, *Characterization of dissolved organic matter in fogwater by excitation-emission matrix fluorescence spectroscopy.* Atmospheric Environment, 2010. **44(27)**: p. 3246-3253.

55. Guenther, A., et al., *A global model of natural volatile organic compound emissions.* J. Geophys. Res., 1995. **100**(D5): p. 8873-8892.

56. Atkinson, R. and J. Arey, *Atmospheric chemistry of biogenic organic compounds.* Accounts Chem. Res., 1998. **31(9)**: p. 574-583.

57. Ortega, J. and D. Helmig, *Approaches for quantifying reactive and low-volatility biogenic organic compound emissions by vegetation enclosure techniques – Part A.* Chemosphere, 2008. **72**: p. 343–364.

58. Claeys, M., Graham, B., Vas, G., Wang, W., Vermeylen, R., Pashynska, V., Cafmeyer, J., Guyon, P., Andreae, M. O., Artaxo, P., and Maenhaut, W, *Formation of secondary organic aerosols through photooxidation of isoprene.* Science, 2004. **303**: p. 1173–1176.

59. Henze, D.K. and J.H. Seinfeld, *Global secondary organic aerosol from isoprene oxidation.* Geophys. Res. Lett., 2006. **33**(9): p. L09812.

60. Larsen, B.R., Di Bella, D., Glasius, M., Winterhalter, R., Jensen, N. R., and Hjorth, J, *Gasphase OH oxidation of monoterpenes: Gaseous and particulate products.* J. Atmos. Chem., 2001. **38**: p. 231–276.

61. Goldstein, A.H. and I.E. Galbally, *Known and unexplored organic constituents in the earth's atmosphere.* Environ. Sci. Technol, 2007. **41**: p. 1514–1521.

62. Penuelas, J. and J. Llusia, *Seasonal patterns of non-terpenoid C6-C10 VOC emission from seven Mediterranean woody species* Chemosphere, 2001. **45**: p. 237-244.

63. Arey, J., et al., *Hydrocarbon emissions from natural vegetation in California's South Coast Air Basin.* Atmospheric Environment, 1995. **29**(21): p. 2977-2988.

64. König, G., et al., *Relative contribution of oxygenated hydrocarbons to the total biogenic VOC emissions of selected mid-European agricultural and natural plant species.* Atmospheric Environment, 1995. **29**(8): p. 861-874.

65. Olofsson, M., et al., *Flux of organic compounds from grass measured by relaxed eddy accumulation technique.* J. Environ. Monitor., 2003. **5(6)**: p. 963-970.

66. Brock, C.A., et al., *Formation and growth of organic aerosols downwind of the Deepwater Horizon oil spill.* Geophys. Res. Lett., 2011. **38**(17): p. L17805.

67. Crone, T.J. and M. Tolstoy, *Magnitude of the 2010 Gulf of Mexico Oil Leak.* Science, 2010. **330**(6004): p. 634.

68. de Gouw, J.A., et al., *Organic Aerosol Formation Downwind from the Deepwater Horizon Oil Spill.* Science, 2011. **331**(6022): p. 1295-1299.

69. Ryerson, T.B., et al., *Atmospheric emissions from the Deepwater Horizon spill constrain air-water partitioning, hydrocarbon fate, and leak rate.* Geophys. Res. Lett., 2011. **38**(7): p. L07803.

70. Coe, H., *Aerosol Chemistry and the Deepwater Horizon Spill.* Science, 2011. **331**(6022): p. 1273-1274.

71. De Gouw, J. and J.L. Jimenez, *Organic Aerosols in the Earth's Atmosphere.* Environmental Science & Technology, 2009. **43**(20): p. 7614-7618.

72. Brunekreef, B. and S.T. Holgate, *Air pollution and health.* The Lancet, 2002. **360**(9341): p. 1233-1242.

73. Volkamer, R., et al., *Secondary organic aerosol formation from anthropogenic air pollution: Rapid and higher than expected.* Geophys. Res. Lett., 2006. **33**(17): p. L17811.

74. Heald, C.L., et al., *A large organic aerosol source in the free troposphere missing from current models.* Geophys. Res. Lett., 2005. **32**(18): p. L18809.

75. Jimenez, J.L., et al., *Evolution of Organic Aerosols in the Atmosphere.* Science, 2009. **326**(5959): p. 1525-1529.

76. Spracklen, D.V.A., S. R.; Sciare, J.; Carslaw, K. S.; Pio, C, *Globally significant oceanic source of organic carbon aerosol.* Geophysical Research Letters, 2008. **35 (12), 5**.

77. Freiser, H., *Metal complexation at the liquid-liquid interface.* Chemical Reviews, 1988. **88**(4): p. 611-616.

78. Conboy, J., J. Daschbach, and G. Richmond, *Studies of Alkane/Water Interfaces by Total Internal Reflection Second Harmonic Generation.* The Journal of Physical Chemistry, 1994. **98**(39): p. 9688-9692.

79. Walker, D.S., et al., *Evidence for a Diffuse Interfacial Region at the Dichloroethane/Water Interface.* The Journal of Physical Chemistry B, 2004. **108**(7): p. 2111-2114.

80. Walker, D.S., F.G. Moore, and G.L. Richmond, *Vibrational Sum Frequency Spectroscopy and Molecular Dynamics Simulation of the Carbon Tetrachloride−Water and 1,2-Dichloroethane−Water Interfaces.* The Journal of Physical Chemistry C, 2007. **111**(16): p. 6103-6112.

81. Hautala, E.L., et al., *Deposition of motor-vehicle emissions and winter maintenance along roadside assessed by snow analyses.* Environmental Pollution, 1995. **87**(1): p. 45-49.

82. Herbert, B.M.J., S. Villa, and C. Halsall, *Chemical interactions with snow: Understanding the behavior and fate of semi-volatile organic compounds in snow.* Ecotoxicology and Environmental Safety, 2006. **63**(1): p. 3-16.

83. Reinosdotter, K., M. Viklander, and P.A. Malmqvist, *Polycyclic aromatic hydrocarbons and metals in snow along a highway.* Water Science and Technology, 2006. **54**(6-7): p. 195-203.

84. Schrimpff, E., W. Thomas, and R. Herrmann, *Regional patterns of contaminants (pah, pesticides and trace-metals) in snow of northeast bavaria and their relationship to human influence and orographic effects.* Water Air and Soil Pollution, 1979. **11**(4): p. 481-497.

85. Sharma, M. and E.A. McBean, *PAH deposition to snow surface - Chemical analysis and interpretation of results.* Environmental Science and Pollution Research, 2001. **8**(1): p. 11-18.

86. Viskari, E.L., et al., *Airborne pollutants along a roadside: Assessment using snow analyses and moss bags.* Environmental Pollution, 1997. **97**(1-2): p. 153-160.

87. Carrera, G., et al., *Persistent organic pollutants in snow from European high mountain areas.* Atmospheric Environment, 2001. **35**(2): p. 245-254.

88. Cincinelli, A., et al., *Enrichment of organic pollutants in the sea surface microlayer (SML) at Terra Nova Bay, Antarctica: influence of SML on superfacial snow composition.* Journal of Environmental Monitoring, 2005. **7**(12): p. 1305-1312.

89. Daly, G.L. and F. Wania, *Organic contaminants in mountains.* Environmental Science & Technology, 2005. **39**(2): p. 385-398.

90. Melnikov, S., et al., *Snow and ice concentrations of selected persistent pollutants in the Ob-Yenisey River watershed.* Science of the Total Environment, 2003. **306**(1-3): p. 27-37.

91. Slater, J.F., et al., *Distinguishing the relative contribution of fossil fuel and biomass combustion aerosols deposited at Summit, Greenland through isotopic and molecular characterization of insoluble carbon.* Atmospheric Environment, 2002. **36**(28): p. 4463-4477.

92. Wang, X.P., et al., *The historical residue trends of DDT, hexachlorocyclohexanes and polycyclic aromatic hydrocarbons in an ice core from Mt. Everest, central Himalayas, China.* Atmospheric Environment, 2008. **42**(27): p. 6699-6709.

93. Wang, X.P., et al., *The recent deposition of persistent organic pollutants and mercury to the Dasuopu glacier, Mt. Xixiabangma, central Himalayas.* Science of the Total Environment, 2008. **394**(1): p. 134-143.

94. Welch, H.E., et al., *Brown snow - a long-range transport event in the canadian arctic.* Environmental Science & Technology, 1991. **25**(2): p. 280-286.

95. Roth, C.M., Goss, K.-U., Schwarzenbach, R. P., *Sorption of Diverse Organic Vapors to Snow.* Environ. Sci. Technol., 2004. **38**(15): p. 4078-4084.

96. Elbaum, M., S.G. Lipson, and J.G. Dash, *Optical study of surface melting on ice.* Journal of Crystal Growth, 1993. **129**(3-4): p. 491-505.

97. Hendrik, B. and et al., *The premelting of ice studied with photoelectron spectroscopy.* Journal of Physics: Condensed Matter, 2002. **14**(8): p. L227.

98. Golecki, I. and C. Jaccard, *Intrinsic surface disorder in ice near the melting point.* Journal of Physics C: Solid State Physics, 1978. **11**(20): p. 4229.

99. Nason, D. and N.H. Fletcher, *Photoemission from ice and water surfaces: Quasiliquid layer effect.* The Journal of Chemical Physics, 1975. **62**(11): p. 4444-4449.

100. Dosch, H., A. Lied, and J.H. Bilgram, *Disruption of the hydrogen-bonding network at the surface of Ih ice near surface premelting.* Surface Science, 1996. **366**(1): p. 43-50.

101. Beaglehole, D. and D. Nason, *Transition layer on the surface on ice.* Surface Science, 1980. **96**(1-3): p. 357-363.

102. Jellinek, H.H.G., *Liquid-Like (Transition) Layer on Ice.* J. Colloid Interface Sci., 1967. **25**: p. 192-205.

103. Doppenschmidt, A. and H.J. Butt, *Measuring the thickness of the liquid-like layer on ice surfaces with atomic force microscopy.* Langmuir, 2000. **16**(16): p. 6709-6714.

104. Li, Y. and G.A. Somorjai, *Surface Premelting of Ice.* The Journal of Physical Chemistry C, 2007. **111**(27): p. 9631-9637.

105. Engemann, S., et al., *Interfacial Melting of Ice in Contact with SiO_{2}.* Physical Review Letters, 2004. **92**(20): p. 205701.

106. Golecki, I. and C. Jaccard, *The surface of ice near 0°C studied by 100 keV proton channeling.* Physics Letters A, 1977. **63**(3): p. 374-376.

107. Lied, A., H. Dosch, and J.H. Bilgram, *Surface melting of ice I_{h} single crystals revealed by glancing angle x-ray scattering.* Physical Review Letters, 1994. **72**(22): p. 3554.

108. Sadtchenko, V. and G.E. Ewing, *Interfacial melting of thin ice films: An infrared study.* The Journal of Chemical Physics, 2002. **116**(11): p. 4686-4697.

109. Lei, Y.D., Wania, F., *Is Rain or Snow a More Efficient Scavenger of Organic Chemicals?* Atmospheric Environment, 2004. **38**: p. 3557-3571.

110. Wania, F., Hoff, J. T., Jia, C. Q., Mackay, D., *The Effects of Snow and Ice on the Environmental Behaviour of Hydrophobic Organic Chemicals.* Environmental Pollution, 1998. **102**: p. 25-41.

111. Hoff, J.T., Wania, F., Mackay, D., Gillham, R., *Sorption of Nonpolar Organic Vapors by Ice and Snow.* Environ. Sci. Technol., 1995. **29**: p. 1982-1989.

112. Mahoney, M.W. and W.L. Jorgensen, *A five-site model for liquid water and the reproduction of the density anomaly by rigid, nonpolarizable potential functions.* Journal of Chemical Physics, 2000. **112**(20): p. 8910-8922.

113. Chen, J., Ehrenhauser, F., Liyana-Arachchi, T. P., Hung, F. R., Wornat, M. J., and Valsaraj, K. T. , *Adsorption of gas-phase phenanthrene on atmospheric water and ice*

films. Polycyclic Aromatic Compounds, 2010: p. submitted.

114. Vega, C., E. Sanz, and J.L.F. Abascal, *The melting temperature of the most common models of water.* Journal of Chemical Physics, 2005. **122**(11): p. 114507.

115. Berendsen, H.J.C., J.R. Grigera, and T.P. Straatsma, *The missing term in effective pair potentials.* The Journal of Physical Chemistry, 1987. **91**(24): p. 6269-6271.

116. Hess, B., et al., *GROMACS 4: Algorithms for Highly Efficient, Load-Balanced, and Scalable Molecular Simulation.* Journal of Chemical Theory and Computation, 2008. **4**(3): p. 435-447.

117. Conde, M.M., C. Vega, and A. Patrykiejew, *The thickness of a liquid layer on the free surface of ice as obtained from computer simulation.* Journal of Chemical Physics, 2008. **129**(1): p. 014702.

118. *http://www.lsbu.ac.uk/water/ice1h.html*. Available from: http://www.lsbu.ac.uk/water/ice1h.html.

119. Hess, B., et al., *LINCS: A linear constraint solver for molecular simulations.* Journal of Computational Chemistry, 1997. **18**(12): p. 1463-1472.

120. Bussi, G., D. Donadio, and M. Parrinello, *Canonical sampling through velocity rescaling.* Journal of Chemical Physics, 2007. **126**: p. 014101.

121. Bussi, G., T. Zykova-Timan, and M. Parrinello, *Isothermal-isobaric molecular dynamics using stochastic velocity rescaling.* Journal of Chemical Physics, 2009. **130**: p. 074101.

122. Darden, T., D. York, and L. Pedersen, *Particle mesh ewald - an n.log(n) method for Ewald sums in large systems.* Journal of Chemical Physics, 1993. **98**(12): p. 10089-10092.

123. Dang, L.X., *Computational Study of Ion Binding to the Liquid Interface of Water†.* The Journal of Physical Chemistry B, 2002. **106**(40): p. 10388-10394.

124. Trzesniak, D., A.P.E. Kunz, and W.F. van Gunsteren, *A comparison of methods to compute the potential of mean force.* Chemphyschem, 2007. **8**(1): p. 162-169.

125. Miller, C.A., N.L. Abbott, and J.J. de Pablo, *Surface Activity of Amphiphilic Helical beta-Peptides from Molecular Dynamics Simulation.* Langmuir, 2009. **25**(5): p. 2811-2823.

126. Humphrey, W., A. Dalke, and K. Schulten, *VMD: Visual molecular dynamics.* Journal

of Molecular Graphics, 1996. **14**(1): p. 33-&.

127. Czech, C., et al., *Adsorption sites, adsorption enthalpies and potential removal of terpenoids by atmospheric ice.* Atmospheric Environment, 2011. **45**: p. 687-693.

128. Adamson, A.W., *Physical Chemistry of Surfaces*. 5th ed. 1990, New York: Wiley.

129. Raja, S. and K.T. Valsaraj, *Heterogeneous oxidation by ozone of naphthalene adsorbed at the air-water interface of micron-size water droplets.* Journal of the Air & Waste Management Association, 2005. **55**(9): p. 1345-1355.

130. Donaldson, D.J., et al., *Uptake and reaction of atmospheric organic vapours on organic films.* Faraday Discussions, 2005. **130**: p. 227-239.

131. Ammann, M., U. Poschl, and Y. Rudich, *Effects of reversible adsorption and Langmuir-Hinshelwood surface reactions on gas uptake by atmospheric particles.* Physical Chemistry Chemical Physics, 2003. **5**(2): p. 351-356.

132. Hoff, J.T., Wania, F., Mackay, D., Gillham, R., *Sorption of Nonpolar Organic Vapors by Ice and Snow.* Environmental Science & Technology, 1995. **29**: p. 1982-1989.

133. Donaldson, D.J., Valsaraj, K. T., *Adsorption and Reaction of Trace Gas-Phase Organic Compounds on Atmospheric Water Film Surfaces: A Critical Review.* Environmental Science & Technology, 2010. **44**(3): p. 865-873.

134. Shiraiwa, M., et al., *The role of long-lived reactive oxygen intermediates in the reaction of ozone with aerosol particles.* Nature Chemistry, 2011. **3**(4): p. 291-295.

135. Liyana-Arachchi, T.P., K.T. Valsaraj, and F.R. Hung, *A Molecular Simulation Study of the Adsorption of Naphthalene and Ozone on Atmospheric Air/Ice Interfaces.* The Journal of Physical Chemistry A, 2011. **115**: p. 9226-9236.

136. Chen, J., Ehrenhauser, F., Liyana-Arachchi, T. P., Hung, F. R., Wornat, M. J., and Valsaraj, K. T., *Adsorption of gas-phase phenanthrene on atmospheric water and ice films.* Polycyclic Aromatic Compounds, 2011. **31**: p. 201-226.

137. Cappiello, A., De Simoni, E., Fiorucci, C., Mangani, F., Palma, P., Trufelli, H., Decesari, S., Facchini, M. C., Fuzzi, S., *Molecular Characterization of the Water-soluble Organic Compounds in Fogwater by ESIMS/MS.* Environmental Science & Technology, 2003. **37**: p. 1229-1240.

138. Diamond, M.L., et al., *Evidence for Organic Film on an Impervious Urban Surface: Characterization and Potential Teratogenic Effects.* Environmental Science & Technology, 2000. **34**(14): p. 2900-2908.

139. Gingrich, S.E., et al., *Atmospherically Derived Organic Surface Films along an Urban-Rural Gradient.* Environmental Science & Technology, 2001. **35**(20): p. 4031-4037.

140. Lam, B., et al., *Chemical composition of surface films on glass windows and implications for atmospheric chemistry.* Atmospheric Environment, 2005. **39**(35): p. 6578-6586.

141. Crahan, K.K., et al., *Speciation of Organic Aerosols in the Tropical Mid-Pacific and Their Relationship to Light Scattering.* Journal of the Atmospheric Sciences, 2004. **61**(21): p. 2544-2558.

142. Chen, J. and K.T. Valsaraj, *Uptake and UV-Photooxidation of Gas-Phase Polyaromatic Hydrocarbons on the Surface of Atmospheric Water Films. 2. Effects of Dissolved Surfactants on Naphthalene Photooxidation.* The Journal of Physical Chemistry A, 2007. **111**(20): p. 4289-4296.

143. Mmereki, B.T., et al., *Kinetics and products of the reaction of gas-phase ozone with anthracene adsorbed at the air-aqueous interface.* Atmospheric Environment, 2004. **38**(36): p. 6091-6103.

144. Hullar, T. and C. Anastasio, *Yields of hydrogen peroxide from the reaction of hydroxyl radical with organic compounds in solution and ice.* Atmospheric Chemistry and Physics, 2011. **11**(14): p. 7209-7222.

145. Vacha, R., et al., *Adsorption of atmospherically relevant gases at the air/water interface: Free energy profiles of aqueous solvation of N-2, O-2, O-3, OH, H2O, HO2, and H2O2.* The Journal of Physical Chemistry A, 2004. **108**(52): p. 11573-11579.

146. Vacha, R., et al., *Adsorption of aromatic hydrocarbons and ozone at environmental aqueous surfaces.* The Journal of Physical Chemistry A, 2008. **112**(22): p. 4942-4950.

147. Jorgensen, W.L., D.S. Maxwell, and J. Tirado-Rives, *Development and Testing of the OPLS All-Atom Force Field on Conformational Energetics and Properties of Organic Liquids.* Journal of the American Chemical Society, 1996. **118**(45): p. 11225-11236.

148. Ardura, D., T.F. Kahan, and D.J. Donaldson, *Self-Association of Naphthalene at the Air-Ice Interface.* The Journal of Physical Chemistry A, 2009. **113**(26): p. 7353-7359.

149. Wick, C.D., B. Chen, and K.T. Valsaraj, *Computational Investigation of the Influence of Surfactants on the Air−Water Interfacial Behavior of Polycylic Aromatic Hydrocarbons.* The Journal of Physical Chemistry C, 2010. **114**(34): p. 14520-14527.

150. Liyana-Arachchi, T.P., K.T. Valsaraj, and F.R. Hung, *Adsorption of naphthalene and*

ozone on atmospheric air/ice interfaces coated with surfactants: A molecular simulation study", J. Phys. Chem. A 2012, 116, 2519-2528.

151. Nada, H., J.P. van der Eerden, and Y. Furukawa, *A clear observation of crystal growth of ice from water in a molecular dynamics simulation with a six-site potential model of H2O.* Journal of Crystal Growth, 2004. **266**(1–3): p. 297-302.

152. Nada, H. and Y. Furukawa, *Anisotropic growth kinetics of ice crystals from water studied by molecular dynamics simulation.* Journal of Crystal Growth, 1996. **169**(3): p. 587-597.

153. Nada, H. and Y. Furukawa, *Anisotropy in growth kinetics at interfaces between proton-disordered hexagonal ice and water: A molecular dynamics study using the six-site model of H2O.* Journal of Crystal Growth, 2005. **283**(1–2): p. 242-256.

154. Vrbka, L. and P. Jungwirth, *Brine Rejection from Freezing Salt Solutions: A Molecular Dynamics Study.* Physical Review Letters, 2005. **95**(14): p. 148501.

155. Carignano, M.A., P.B. Shepson, and I. Szleifer *, *Molecular dynamics simulations of ice growth from supercooled water.* Molecular Physics, 2005. **103**(21-23): p. 2957-2967.

156. Carignano, M.A., P.B. Shepson, and I. Szleifer, *Ions at the ice/vapor interface.* Chemical Physics Letters, 2007. **436**(1–3): p. 99-103.

157. Wettlaufer, J.S., *Impurity Effects in the Premelting of Ice.* Physical Review Letters, 1999. **82**(12): p. 2516.

158. Vácha, R., et al., *Adsorption of Atmospherically Relevant Gases at the Air/Water Interface: Free Energy Profiles of Aqueous Solvation of N2, O2, O3, OH, H2O, HO2, and H2O2.* The Journal of Physical Chemistry A, 2004. **108**(52): p. 11573-11579.

159. Kaelberer, J.B. and R.D. Etters, *Phase transitions in small clusters of atoms.* The Journal of Chemical Physics, 1977. **66**(7): p. 3233-3239.

160. Nada, H. and Y. Furukawa, *Anisotropy in structural phase transitions at ice surfaces: a molecular dynamics study.* Applied Surface Science, 1997. **121–122**(0): p. 445-447.

161. Vega, C., et al., *Radial distribution functions and densities for the SPC/E, TIP4P and TIP5P models for liquid water and ices I, I, II, III, IV, V, VI, VII, VIII, IX, XI and XII.* Physical Chemistry Chemical Physics, 2005. **7**(7): p. 1450-1456.

162. Errington, J.R. and P.G. Debenedetti, *Relationship between structural order and the anomalies of liquid water.* Nature, 2001. **409**(6818): p. 318-321.

163. Chen, J., Ehrenhauser, F. S., Valsaraj, K. T., Wornat, M. J., *Uptake and UV-photooxidation of Gas-phase PAHs on the Surface of Atmospheric Water Films. 1. Naphthalene.* . The Journal of Physical Chemistry A, 2006. **110**: p. 9161-9168.

164. Liyana-Arachchi, T.P., K.T. Valsaraj, and F.R. Hung, *Ice Growth from Supercooled Aqueous Solutions of Benzene, Naphthalene, and Phenanthrene.* The Journal of Physical Chemistry A, 2012. **116**(33): p. 8539-8546.

165. Vione, D., et al., *Photochemical reactions in the tropospheric aqueous phase and on particulate matter.* Chemical Society Reviews, 2006. **35**(5): p. 441-453.

166. Goldstein, A.H. and I.E. Galbally, *Known and Unexplored Organic Constituents in the Earth's Atmosphere.* Environmental Science & Technology, 2007. **41**(5): p. 1514-1521.

167. Herckes, P., et al., *Organic compounds in radiation fogs in Davis (California).* Atmospheric Research, 2002. **64**(1–4): p. 99-108.

168. Abbatt, J.P.D., *Interactions of Atmospheric Trace Gases with Ice Surfaces: Adsorption and Reaction.* Chemical Reviews, 2003. **103**(12): p. 4783-4800.

169. Kurková, R., et al., *Chemistry of Small Organic Molecules on Snow Grains: The Applicability of Artificial Snow for Environmental Studies.* Environmental Science & Technology, 2011. **45**(8): p. 3430-3436.

170. Heger, D., J. Jirkovsky, and P. Klan, *Aggregation of Methylene Blue in Frozen Aqueous Solutions Studied by Absorption Spectroscopy.* The Journal of Physical Chemistry A, 2005. **109**(30): p. 6702-6709.

171. Heger, D. and P. Klán, *Interactions of organic molecules at grain boundaries in ice: A solvatochromic analysis.* Journal of Photochemistry and Photobiology A: Chemistry, 2007. **187**(2–3): p. 275-284.

172. Heger, D., J. Klánová, and P. Klán, *Enhanced Protonation of Cresol Red in Acidic Aqueous Solutions Caused by Freezing.* The Journal of Physical Chemistry B, 2006. **110**(3): p. 1277-1287.

173. Wren, S.N. and D.J. Donaldson, *Exclusion of Nitrate to the Air–Ice Interface During Freezing.* The Journal of Physical Chemistry Letters, 2011. **2**(16): p. 1967-1971.

174. Grannas, A.M., A.R. Bausch, and K.M. Mahanna, *Enhanced Aqueous Photochemical Reaction Rates after Freezing.* The Journal of Physical Chemistry A, 2007. **111**(43): p. 11043-11049.

175. O'Driscoll, P., et al., *Release of Nitric Oxide and Iodine to the Atmosphere from the Freezing of Sea-Salt Aerosol Components.* The Journal of Physical Chemistry A, 2008. **112**(8): p. 1677-1682.

176. Wren, S.N., et al., *Spectroscopic studies of the heterogeneous reaction between O3(g) and halides at the surface of frozen salt solutions.* J. Geophys. Res., 2010. **115**(D16): p. D16309.

177. Takenaka, N., et al., *Acceleration Mechanism of Chemical Reaction by Freezing: The Reaction of Nitrous Acid with Dissolved Oxygen.* The Journal of Physical Chemistry, 1996. **100**(32): p. 13874-13884.

178. Liyana-Arachchi, T.P., K.T. Valsaraj, and F.R. Hung, *Adsorption of naphthalene and ozone on atmospheric air/ice interfaces coated with surfactants: A molecular simulation study.* The Journal of Physical Chemistry A, 2012. **116**: p. 2519-2528.

179. Ray, D., et al., *Determination of the Specific Surface Area of Snow Using Ozonation of 1,1-Diphenylethylene.* Environmental Science & Technology, 2011. **45**(23): p. 10061-10067.

180. Gladich, I. and M. Roeselova, *Comparison of selected polarizable and nonpolarizable water models in molecular dynamics simulations of ice Ih.* Physical Chemistry Chemical Physics, 2012. **14**(32): p. 11371-11385.

181. Conde, M.M., C. Vega, and A. Patrykiejew, *The thickness of a liquid layer on the free surface of ice as obtained from computer simulation.* The Journal of Chemical Physics, 2008. **129**(1): p. 014702.

182. Muchová, E., et al., *The Ice−Vapor Interface and the Melting Point of Ice Ih for the Polarizable POL3 Water Model.* The Journal of Physical Chemistry A, 2011. **115**(23): p. 5973-5982.

183. González, B.S., et al., *Nuclear Quantum Effects in Water Clusters: The Role of the Molecular Flexibility.* The Journal of Physical Chemistry B, 2010. **114**(7): p. 2484-2492.

184. Fernandez, R.G., J.L.F. Abascal, and C. Vega, *The melting point of ice I[sub h] for common water models calculated from direct coexistence of the solid-liquid interface.* The Journal of Chemical Physics, 2006. **124**(14): p. 144506-11.

185. Birgersson, G. and G. Bergström, *Volatiles released from individual spruce bark beetle entrance holes.* J. Chem. Ecol., 1989. **15**: p. 2465-2483.

186. Lanne, B.S., et al., *Biosynthesis of 2-methyl-3-buten-2-ol, a pheromone component of*

Ips typographus (Coleoptera: Scolytidae). Insect Biochem., 1989. **19**: p. 163-167.

187. Harley, P., et al., *Emission of 2-methyl-3-buten-2-ol by pines: A potentially large natural source of reactive carbon in the atmosphere.* J. Geophys. Res, 1998. **103 (D19)**: p. 25479–25486.

188. Baker, B., et al., *Canopy fluxes of 2-methyl-3-buten-2-ol over a ponderosa pine forest by relaxed eddy accumulation: Field data and model comparison.* J. Geophys. Res, 1999. **104 (D21)**: p. 26107–26114.

189. Schade, G.W., et al., *Canopy and leaf level 2-methyl-3-buten-2-ol fluxes from a ponderosa pine plantation.* Atmospheric Environment, 2000. **34**: p. 3535– 3544.

190. Schade, G.W. and A.H. Goldstein., *Fluxes of oxygenated volatile organic compounds from a ponderosa pine plantation.* J. Geophys. Res, 2001. **106(D3)**: p. 3111– 3124.

191. Tarvainen, V., *Temperature and light dependence of the VOC emissions of Scots pine.* Atmos. Chem. Phys, 2005. **5**: p. 989–998.

192. Zimmerman, P., et al., *Field deployment of a GC-MS system for determination of biogenic hydrocarbons in vegetation enclosures and ambient air (abstract).* Eos Transactions AGU, 1991. **72**: p. 88.

193. Ciccioli, P., Cecinato, A., Brancaleoni, E., Bracchetti, A. and Frattoni, M, *Polar volatile organic compounds (VOC) of natural origin as precursors of ozone.* Environmental Monitoring and Assessment, 1994. **31**: p. 211-217.

194. Goldan, P.D., Kuster, W. C. and Fehsenfeld, F. C, *The observation of a C5 alcohol emission in a North American pine forest.* Geophysical Research Letters, 1993. **20**: p. 1039-1042.

195. Lamanna, M.S. and A.H. Goldstein, *In situ measurements of C2–C10 volatile organic compounds above a Sierra Nevada ponderosa pine plantation* J. Geophys. Res., 1999. **104(D7)**: p. 247–262.

196. Rudich, Y., et al., *Reaction of Methylbutenol with the OH Radical: Mechanism and Atmospheric Implications.* J. Phys. Chem., 1995. **99**(32): p. 12188-12194.

197. Hallquist, M., et al., *Rates of reaction between the nitrate radical and some unsaturated alcohols.* Int. J. Chem. Kinet., 1996. **28**(6): p. 467-474.

198. Fantechi, G., et al., *Mechanistic studies of the atmospheric oxidation of methyl butenol by OH radicals, ozone and NO3 radicals.* Atmospheric Environment, 1998. **32**(20): p. 3547-3556.

199. Ferronato, C., J.J. Orlando, and G.S. Tyndall, *Rate and mechanism of the reactions of OH and Cl with 2-methyl-3-buten-2-ol* J.Geophys. Res., 1998. **103**: p. 25579–25586.

200. Alvarado, A., et al., *Products and mechanisms of the gas-phase reactions of OH radicals and O3 with 2-methyl-3-buten-2-ol.* Atmospheric Environment, 1999. **33**: p. 2893–2905.

201. Reisen, F.A., S. M.; Atkinson, R.; Arey, J, *Hydroxyaldehyde products from hydroxyl radical reactions of Z-3-hexen-1-ol and 2-methyl-3-buten-2-ol quantified by SPME and APIMS.* Environ. Sci. Technol, 2003. **37**: p. 4664–4671.

202. Carrasco, N., et al., *Simulation chamber studies of the atmospheric oxidation of 2-methyl-3-buten-2-ol: Reaction with hydroxyl radicals and ozone under a variety of conditions.* . J. Atmos. Chem., 2007. **56**: p. 33–55.

203. Niki, H., et al., *Fourier transform infrared study of the kinetics of mechanisms for the Cl-atom- and HO-radical-initiated oxidation of glycolaldehyde.* J. Phys. Chem., 1987. **91**: p. 2174–2178.

204. Bacher, C., G.S. Tyndall, and J.J. Orlando, *The atmospheric chemistry of glycolaldehyde.* J. Atmos. Chem., 2001. **39**: p. 171–189.

205. Magneron, I.M., A.; Le Bras, G.; Moortgat, G. K.; Horowitz, A.; Wirtz, K, *Photolysis and OH-initiated oxidation of glycolaldehyde under atmospheric conditions.* J. Phys. Chem, 2005. **109**: p. 4552–4561.

206. Butkovskaya, N.I., et al., *Mechanism of the OH-initiated oxidation of glycolaldehyde over the temperature range 233-296 K.* Journal of Physical Chemistry A, 2006. **110**: p. 13492–13499.

207. Jacob, D.J., et al., *Atmospheric budget of acetone.* J. Geophys. Res., 2002. **107(D10)**: p. 4100.

208. Liggio, J., S.-M. Li, and R. McLaren, *Reactive uptake of glyoxal by particulate matter.* J. Geophys. Res., 2005. **110**: p. D10304.

209. Kroll, J.H., et al., *Chamber studies of secondary organic aerosol growth by reactive uptake of simple carbonyl compounds.* J. Geophys. Res., 2005. **110**: p. D23207.

210. Volkamer, R., et al., *A missing sink for gas-phase glyoxal in Mexico City: Formation of secondary organic aerosol.* Geophys. Res. Lett., 2007. **34**: p. L19807.

211. Carlton, A.G., et al., *Atmospheric oxalic acid and SOA production from glyoxal: Results of aqueous photooxidation experiments.* Atmospheric Environment, 2007. **41**:

p. 7588–7602.

212. Noda, J. and E. Ljungström, *Aerosol formation in connection with NO3 oxidation of unsaturated alcohols.* Atmospheric Environment, 2002. **36**.

213. Sander, R., *Modeling atmospheric chemistry: Interactions between gas-phase species and liquid cloud/aerosol particles.* Surveys in Geophysics, 1999. **20**(1): p. 1-31.

214. Sander, R. *Compilation of Henry's Law Constants for Inorganic and Organic Species of Potential Importance in Environmental Chemistry, version 3.* http://www.rolf-sander.net/henry/.

215. OECD, *OECD GUIDELINE FOR THE TESTING OF CHEMICALS # 107 Partition Coefficient (n-octanol/water): Shake Flask Method*. 1995, OECD. p. 4.

216. Hess, B., et al., *GROMACS 4: Algorithms for Highly Efficient, Load-Balanced, and Scalable Molecular Simulation.* J. Chem. Theory Comput., 2008. **4**(3): p. 435-447.

217. Berendsen, H.J.C., J.R. Grigera, and T.P. Straatsma, *The missing term in effective pair potentials.* J. Phys. Chem., 1987. **91**(24): p. 6269-6271.

218. Jorgensen, W.L., D.S. Maxwell, and J. Tirado-Rives, *Development and Testing of the OPLS All-Atom Force Field on Conformational Energetics and Properties of Organic Liquids.* J. Am. Chem. Soc., 1996. **118**(45): p. 11225-11236.

219. Kamath, G., et al., *Computational prediction of ionic liquid 1-octanol/water partition coefficients.* Physical Chemistry Chemical Physics, 2012. **14**(13): p. 4339-4342.

220. Chen, B. and J.I. Siepmann, *Partitioning of alkane and alcohol solutes between water and (Dry or wet) 1-Octanol.* J. Am. Chem. Soc., 2000. **122**(27): p. 6464-6467.

221. Chen, B. and J.I. Siepmann, *Microscopic structure and solvation in dry and wet octanol.* Journal of Physical Chemistry B, 2006. **110**(8): p. 3555-3563.

222. Sangster, J., *Octanol-Water Partition Coefficients;Fundamentals and Physical Chemistry.* John Wiley & Sons, U.K., 1997.

223. Bhatnagar, N., et al., *Direct calculation of 1-octanol-water partition coefficients from adaptive biasing force molecular dynamics simulations.* Journal of Chemical Physics, 2012. **137**(1): p. 014502.

224. Shirts, M.R., et al., *Extremely precise free energy calculations of amino acid side chain analogs: Comparison of common molecular mechanics force fields for proteins.* Journal of Chemical Physics, 2003. **119**(11): p. 5740-5761.

225. Hub, J.S., C. Caleman, and D. van der Spoel, *Organic molecules on the surface of water droplets - an energetic perspective.* Physical Chemistry Chemical Physics, 2012. **14**(27): p. 9537-9545.

226. Bennett, C.H., *Efficient estimation of free energy differences from Monte Carlo data.* J. Comput. Phys., 1976. **22**(2): p. 245-268.

227. Dang, L.X., *Computational Study of Ion Binding to the Liquid Interface of Water†.* Journal of Physical Chemistry B, 2002. **106**(40): p. 10388-10394.

228. Chen, J., Ehrenhauser, F., Liyana-Arachchi, T. P., Hung, F. R., Wornat, M. J., and Valsaraj, K. T., *Adsorption of gas-phase phenanthrene on atmospheric water and ice films.* Polycycl. Aromat. Comp., 2011. **31**: p. 201-226.

229. Liyana-Arachchi, T.P., K.T. Valsaraj, and F.R. Hung, *A Molecular Simulation Study of the Adsorption of Naphthalene and Ozone on Atmospheric Air/Ice Interfaces.* Journal of Physical Chemistry A, 2011. **115**: p. 9226-9236.

230. Liyana-Arachchi, T.P., K.T. Valsaraj, and F.R. Hung, *Adsorption of Naphthalene and Ozone on Atmospheric Air/Ice Interfaces Coated with Surfactants: A Molecular Simulation Study.* Journal of Physical Chemistry A, 2012. **116**(10): p. 2519-2528.

231. Liyana-Arachchi, T.P., K.T. Valsaraj, and F.R. Hung, *Ice Growth from Supercooled Aqueous Solutions of Benzene, Naphthalene, and Phenanthrene.* J. Phys.Chem. A, 2012. **116**(33): p. 8539-8546.

232. Liyana-Arachchi, T.P., K.T. Valsaraj, and F.R. Hung, *Ice growth from supercooled aqueous solutions of reactive oxygen species.* Theor. Chem. Acc., 2012. **submitted**.

233. Hess, B., *Determining the shear viscosity of model liquids from molecular dynamics simulations.* The Journal of Chemical Physics, 2002. **116**(1): p. 209-217.

234. Liyana-Arachchi, T.P., K.T. Valsaraj, and F.R. Hung, *A Molecular Simulation Study of the Adsorption of Naphthalene and Ozone on Atmospheric Air/Ice Interfaces.* J. Phys. Chem. A, 2011. **115**: p. 9226-9236.

235. Liyana-Arachchi, T.P., K.T. Valsaraj, and F.R. Hung, *Adsorption of Naphthalene and Ozone on Atmospheric Air/Ice Interfaces Coated with Surfactants: A Molecular Simulation Study.* J. Phys. Chem. A, 2012. **116**(10): p. 2519-2528.

236. Liyana-Arachchi, T.P., K.T. Valsaraj, and F.R. Hung, *Ice growth from supercooled aqueous solutions of reactive oxygen species.* Theor. Chem. Acc., 2012. **accepted**.

237. Caleman, C., et al., *Atomistic simulation of ion solvation in water explains surface*

preference of halides. Proceedings of the National Academy of Sciences of the United States of America, 2011. **108**(17): p. 6838-6842.

238. Liyana-Arachchi, T.P., et al., *Molecular simulations of green leaf volatiles and atmospheric oxidants on air/water interfaces.* Physical Chemistry Chemical Physics, 2013. **15**(10): p. 3583-3592.

239. Wayne, R.P., *Chemistry of Atmospheres.* Oxford University Press, Oxford, 2000(3rd edition).

240. Gulati, A., S.D. Ravindranath, and A.K. Gupta, *Variation in chemical composition and quality of tea (Camellia sinensis) with increasing blister blight (Exobasidium vexans) severity.* Mycological research, 1999. **103**(11): p. 1380-1384.

241. Kumazawa, K., Masuda, H., Nishimura, O., Kato, T., , *Identification of potent aroma components in brewed black-teas.* Journal of the Japanese Society for Food Science and Technology—Nippon Shokuhin Kagaku Kaishi, 1998. **45**: p. 728–734.

242. Nishikitani, M., et al., *(Z)-3-Hexenyl and trans-Linalool 3,7-oxide β-Primeverosides Isolated as Aroma Precursors from Leaves of a Green Tea Cultivar.* Bioscience, Biotechnology, and Biochemistry, 1999. **63**(9): p. 1631-1633.

243. Shulaev, V., P. Silverman, and I. Raskin, *Airborne signalling by methyl salicylate in plant pathogen resistance.* Nature, 1997. **385**(6618): p. 718-721.

244. Heiden, A.C., et al., *EMISSION OF VOLATILE ORGANIC COMPOUNDS FROM OZONE-EXPOSED PLANTS.* Ecological Applications, 1999. **9**(4): p. 1160-1167.

245. Canosa-Mas, C.E., et al., *The atmospheric chemistry of methyl salicylate—reactions with atomic chlorine and with ozone.* Atmospheric Environment, 2002. **36**(13): p. 2201-2205.

246. Thilanga P. Liyana-Arachchi, C.S., Amie K. Hansel, Franz S. Ehrenhauser, Kalliat T. Valsaraj and Francisco R. Hung, , *Molecular simulations of green leaf volatiles and atmospheric oxidants on air/water interfaces,* . Phys. Chem. Chem. Phys, 2013. **accepted**.

247. Liyana-Arachchi, T.P., K.T. Valsaraj, and F.R. Hung, *Ice growth from supercooled aqueous solutions of reactive oxygen species.* Theoretical Chemistry Accounts, 2013. **132**(1).

248. Sangster, J., *LOGKOW Databank. A databank of evaluated octanol-water partition coefficients (Log P) on microcomputer diskette.* . 1994, Sangster Research Laboratories. Montreal, Quebec, Canada:.

249. Chen, F. and P.E. Smith, *Simulated surface tensions of common water models.* The Journal of Chemical Physics, 2007. **126**(22): p. 221101-3.

250. Yuet, P.K. and D. Blankschtein, *Molecular Dynamics Simulation Study of Water Surfaces: Comparison of Flexible Water Models.* The Journal of Physical Chemistry B, 2010. **114**(43): p. 13786-13795.

251. Vega, C. and E. de Miguel, *Surface tension of the most popular models of water by using the test-area simulation method.* The Journal of Chemical Physics, 2007. **126**(15): p. 154707-10.

252. Ismail, A.E., G.S. Grest, and M.J. Stevens, *Capillary waves at the liquid-vapor interface and the surface tension of water.* The Journal of Chemical Physics, 2006. **125**(1): p. 014702-10.

253. Wemhoff, A.P. and V.P. Carey, *Surface Tension Prediction Using Characteristics of the Density Profile Through the Interfacial Region.* International Journal of Thermophysics, 2006. **27**(2): p. 413-436.

254. Vácha, R., et al., *Adsorption of Aromatic Hydrocarbons and Ozone at Environmental Aqueous Surfaces.* The Journal of Physical Chemistry A, 2008. **112**(22): p. 4942-4950.

255. Liyana-Arachchi, T.P., K.T. Valsaraj, and F.R. Hung, *Adsorption of Naphthalene and Ozone on Atmospheric Air/Ice Interfaces Coated with Surfactants: A Molecular Simulation Study.* The Journal of Physical Chemistry A, 2012. **116**(10): p. 2519-2528.

256. Liyana-Arachchi, T.P., K.T. Valsaraj, and F.R. Hung, *Ice Growth from Supercooled Aqueous Solutions of Benzene, Naphthalene, and Phenanthrene.* The Journal of Physical Chemistry A, 2012.

257. Tobias, D.J. and J.C. Hemminger, *Getting Specific About Specific Ion Effects.* Science, 2008. **319**(5867): p. 1197-1198.

258. Jungwirth, P.T., D. J, *Specific ion effects at the air/water interface.* Chemical Reviews, 2006. **106 (4), 1259-1281**.

259. Finlayson-Pitts, B.J., *Reactions at surfaces in the atmosphere: integration of experiments and theory as necessary (but not necessarily sufficient) for predicting the physical chemistry of aerosols.* Physical Chemistry Chemical Physics, 2009. **11 (36), 7760-7779**.

260. Krisch, M.J.D.A., R.; Brown, M. A.; Tobias, D. J.; Hemminger, J. C.; Ammann, M.; Starr, D. E.; Bluhm, H., , *The effect of an organic surfactant on the liquid-vapor*

interface of an electrolyte solution. Journal of Physical Chemistry C, 2007. **111 (36), 13497-13509**.

261. Callahan, K.M.C.-I., N. N.; Xu, M.; Roeselova, M.; Allen, H. C.; Tobias, D.J, *Effect of Magnesium Cation on the Interfacial Properties of Aqueous Salt Solutions.* Journal of Physical Chemistry A, 2010. **114 (32), 8359-8368**.

262. Jungwirth, P. and D.J. Tobias, *Ions at the Air/Water Interface.* The Journal of Physical Chemistry B, 2002. **106**(25): p. 6361-6373.

263. Sokhan, V.P. and T. D. J, *The free surface of water: molecular orientation, surface potential and nonlinear susceptibility.* Molecular Physics, 1997. **92**(4): p. 625-640.

264. Wilson, M.A., A. Pohorille, and L.R. Pratt, *Surface potential of the water liquid--vapor interface.* The Journal of Chemical Physics, 1988. **88**(5): p. 3281-3285.

265. Wang, H., E. Borguet, and K.B. Eisenthal, *Polarity of Liquid Interfaces by Second Harmonic Generation Spectroscopy.* The Journal of Physical Chemistry A, 1997. **101**(4): p. 713-718.

266. Richmond, G.L., *Molecular Bonding and Interactions at Aqueous Surfaces as Probed by Vibrational Sum Frequency Spectroscopy.* Chemical Reviews, 2002. **102**(8): p. 2693-2724.

267. Du, Q., et al., *Vibrational spectroscopy of water at the vapor/water interface.* Physical Review Letters, 1993. **70**(15): p. 2313-2316.

268. Scatena, L.F. and G.L. Richmond, *Orientation, Hydrogen Bonding, and Penetration of Water at the Organic/Water Interface.* The Journal of Physical Chemistry B, 2001. **105**(45): p. 11240-11250.

269. Brown, M.G., et al., *Vibrational Sum-Frequency Spectroscopy of Alkane/Water Interfaces: Experiment and Theoretical Simulation.* The Journal of Physical Chemistry B, 2002. **107**(1): p. 237-244.

270. Brooks, S.A.P.C.L. and Iii, *Revisiting the hexane-water interface via molecular dynamics simulations using nonadditive alkane-water potentials.* The Journal of Chemical Physics, 2006. **124**(20): p. 204706-14.

271. Michael, D. and I. Benjamin, *Solute Orientational Dynamics and Surface Roughness of Water/Hydrocarbon Interfaces.* The Journal of Physical Chemistry, 1995. **99**(5): p. 1530-1536.

272. Bresme, F., et al., *Intrinsic Structure of Hydrophobic Surfaces: The Oil-Water*

Interface. Physical Review Letters, 2008. **101**(5): p. 056102.

273. Nicolas, J.P. and N.R. de Souza, *Molecular dynamics study of the n-hexane--water interface: Towards a better understanding of the liquid--liquid interfacial broadening.* The Journal of Chemical Physics, 2004. **120**(5): p. 2464-2469.

274. Chang, T.-M. and L.X. Dang, *Recent Advances in Molecular Simulations of Ion Solvation at Liquid Interfaces.* Chemical Reviews, 2005. **106**(4): p. 1305-1322.

275. Miqueu, C., et al., *Simultaneous Application of the Gradient Theory and Monte Carlo Molecular Simulation for the Investigation of Methane/Water Interfacial Properties.* The Journal of Physical Chemistry B, 2011. **115**(31): p. 9618-9625.

276. Biscay, F., A. Ghoufi, and P. Malfreyt, *Adsorption of n-alkane vapours at the water surface.* Physical Chemistry Chemical Physics, 2011. **13**(23): p. 11308-11316.

277. Wick, C.D., et al., *Computational Investigation of the n-Alkane/Water Interface with Many-Body Potentials: The Effect of Chain Length and Ion Distributions.* The Journal of Physical Chemistry C, 2011. **116**(1): p. 783-790.

278. http://www.nalco.com/news-and-events/4297.htm. 02/19/2013].

279. *Patent number WO9834722*.

280. *Patent number WO0143860*.

281. *Patent number WO9413397*.

282. *Patent number EP0860203*.

283. Vácha, R., et al., *Effects of Alkali Cations and Halide Anions on the DOPC Lipid Membrane†.* The Journal of Physical Chemistry A, 2009. **113**(26): p. 7235-7243.

284. Auffinger, P., T.E. Cheatham, and A.C. Vaiana, *Spontaneous formation of KCl aggregates in biomolecular simulations: A force field issue?* Journal of Chemical Theory and Computation, 2007. **3**(5): p. 1851-1859.

285. Polat, B.E., et al., *Experimental and Molecular Dynamics Investigation into the Amphiphilic Nature of Sulforhodamine B.* The Journal of Physical Chemistry B, 2011. **115**(6): p. 1394-1402.

APPENDIX A: PERMISSION LETTERS

A.1 Permission for Chapter 2

PERMISSION/LICENSE IS GRANTED FOR YOUR ORDER AT NO CHARGE

This type of permission/license, instead of the standard Terms & Conditions, is sent to you because no fee is being charged for your order. Please note the following:

- Permission is granted for your request in both print and electronic formats, and translations.
- If figures and/or tables were requested, they may be adapted or used in part.
- Please print this page for your records and send a copy of it to your publisher/graduate school.
- Appropriate credit for the requested material should be given as follows: "Reprinted (adapted) with permission from (COMPLETE REFERENCE CITATION). Copyright (YEAR) American Chemical Society." Insert appropriate information in place of the capitalized words.
- One-time permission is granted only for the use specified in your request. No additional uses are granted (such as derivative works or other editions). For any other uses, please submit a new request.

A.2 Permission for Chapter 3

PERMISSION/LICENSE IS GRANTED FOR YOUR ORDER AT NO CHARGE

This type of permission/license, instead of the standard Terms & Conditions, is sent to you because no fee is being charged for your order. Please note the following:

- Permission is granted for your request in both print and electronic formats, and translations.
- If figures and/or tables were requested, they may be adapted or used in part.
- Please print this page for your records and send a copy of it to your publisher/graduate school.
- Appropriate credit for the requested material should be given as follows: "Reprinted (adapted) with permission from (COMPLETE REFERENCE CITATION). Copyright (YEAR) American Chemical Society." Insert appropriate information in place of the capitalized words.
- One-time permission is granted only for the use specified in your request. No additional uses are granted (such as derivative works or other editions). For any other uses, please submit a new request.

A.3 Permission for Chapter 4

Copyright Clearance Center RightsLink®

Home | Create Account | Help

ACS Publications High quality. High impact.

Title: Ice Growth from Supercooled Aqueous Solutions of Benzene, Naphthalene, and Phenanthrene

Author: Thilanga P. Liyana-Arachchi, Kalliat T. Valsaraj, and Francisco R. Hung

Publication: The Journal of Physical Chemistry A

Publisher: American Chemical Society

Date: Aug 1, 2012

Copyright © 2012, American Chemical Society

User ID

Password

Enable Auto Login

LOGIN

Forgot Password/User ID?

If you're a copyright.com user, you can login to RightsLink using your copyright.com credentials. Already **a RightsLink user** or want to learn more?

PERMISSION/LICENSE IS GRANTED FOR YOUR ORDER AT NO CHARGE

This type of permission/license, instead of the standard Terms & Conditions, is sent to you because no fee is being charged for your order. Please note the following:

- Permission is granted for your request in both print and electronic formats, and translations.
- If figures and/or tables were requested, they may be adapted or used in part.
- Please print this page for your records and send a copy of it to your publisher/graduate school.
- Appropriate credit for the requested material should be given as follows: "Reprinted (adapted) with permission from (COMPLETE REFERENCE CITATION). Copyright (YEAR) American Chemical Society." Insert appropriate information in place of the capitalized words.
- One-time permission is granted only for the use specified in your request. No additional uses are granted (such as derivative works or other editions). For any other uses, please submit a new request.

A.4 Permission for Chapter 5

SPRINGER LICENSE
TERMS AND CONDITIONS

Dec 11, 2012

This is a License Agreement between thilanga p liyana arachchi ("You") and Springer ("Springer") provided by Copyright Clearance Center ("CCC"). The license consists of your order details, the terms and conditions provided by Springer, and the payment terms and conditions.

All payments must be made in full to CCC. For payment instructions, please see information listed at the bottom of this form.

License Number	3046191015258
License date	Dec 11, 2012
Licensed content publisher	Springer
Licensed content publication	Theoretical Chemistry Accounts
Licensed content title	Ice growth from supercooled aqueous solutions of reactive oxygen species
Licensed content author	Thilanga P. Liyana-Arachchi
Licensed content date	Jan 1, 2012
Volume number	132
Issue number	1
Type of Use	Thesis/Dissertation
Portion	Full text
Number of copies	1
Author of this Springer article	Yes and you are the sole author of the new work
Order reference number	
Title of your thesis / dissertation	Molecular Dynamics of Interfacial Phenomena at Air/ice, Air/water and Air/salt Water Interfaces
Expected completion date	Mar 2013
Estimated size(pages)	190
Total	0.00 USD
Terms and Conditions	

Jurisdiction
All disputes that may arise in connection with this present License, or the breach thereof, shall be settled exclusively by arbitration, to be held in The Netherlands, in accordance with Dutch law, and to be conducted under the Rules of the 'Netherlands Arbitrage Instituut' (Netherlands Institute of Arbitration).***OR:***

All disputes that may arise in connection with this present License, or the breach thereof, shall be settled exclusively by arbitration, to be held in the Federal Republic of Germany, in accordance with German law.

Other terms and conditions:

v1.3

If you would like to pay for this license now, please remit this license along with your payment made payable to "COPYRIGHT CLEARANCE CENTER" otherwise you will be invoiced within 48 hours of the license date. Payment should be in the form of a check or money order referencing your account number and this invoice number RLNK500915651.
Once you receive your invoice for this order, you may pay your invoice by credit card. Please follow instructions provided at that time.

Make Payment To:
Copyright Clearance Center
Dept 001
P.O. Box 843006
Boston, MA 02284-3006

For suggestions or comments regarding this order, contact RightsLink Customer Support: customercare@copyright.com or +1-877-622-5543 (toll free in the US) or +1-978-646-2777.

Gratis licenses (referencing $0 in the Total field) are free. Please retain this printable license for your reference. No payment is required.

A.5 Permission for Chapter 6

Copyright Clearance Center RightsLink®

Home | Account Info | Help

Title: Molecular simulations of green leaf volatiles and atmospheric oxidants on air/water interfaces

Author: Thilanga P. Liyana-Arachchi,Christopher Stevens,Amie K. Hansel,Franz S. Ehrenhauser,Kalliat T. Valsaraj,Francisco R. Hung

Publication: Physical Chemistry Chemical Physics

Publisher: Royal Society of Chemistry

Date: Jan 11, 2013

Copyright © 2013, Royal Society of Chemistry

Logged in as:
thilanga liyana arachchi
Account #:
3000603027

LOGOUT

This reuse request is free of charge. Please review guidelines related to author permissions here:
http://www.rsc.org/AboutUs/Copyright/Permissionrequests.asp

BACK | CLOSE WINDOW

APPENDIX B: SUPPORTING INFORMATION (CHAPTER 4)

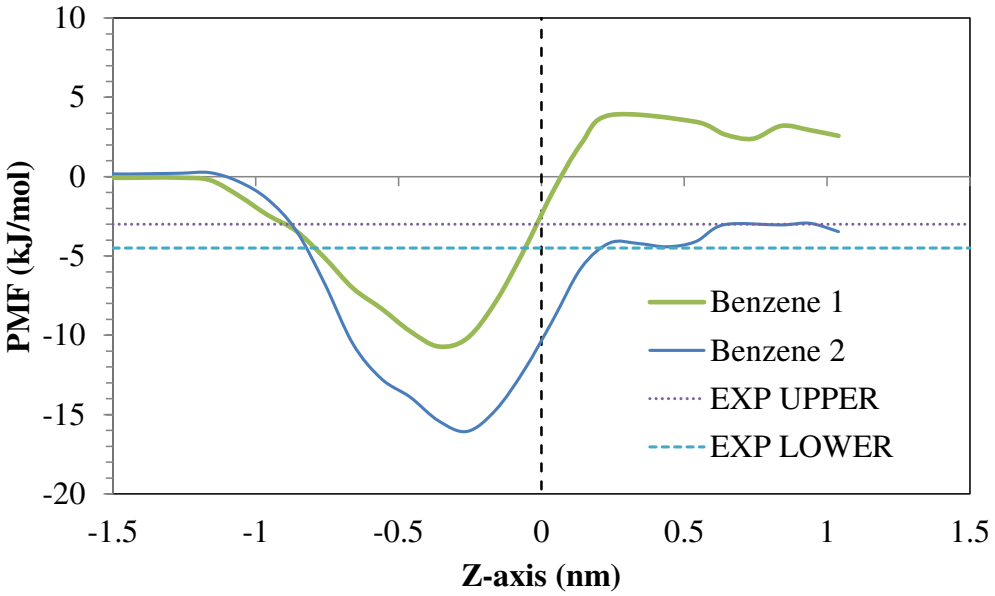

Figure B.1. PMF of moving one benzene molecule from the gas phase into the water molecules in air/water systems at 298 K. A value of zero in the *z*-axis represents the air/water interface (arbitrarily defined as the point where the density of water reaches 500 kg/m^3); positive values of *z*-axis represent the bulk water phase. Benzene 1 represent the PMF with the original set of atomic charges (refs. 17 and 35 in our paper), and Benzene 2 represents the PMF with the 10% increased charges for atoms in benzene molecule. EXP UPPER and EXP LOWER represent the upper and lower experimental values obtained for free energy of hydration for benzene respectively (from refs. 17 and 41 in our paper)

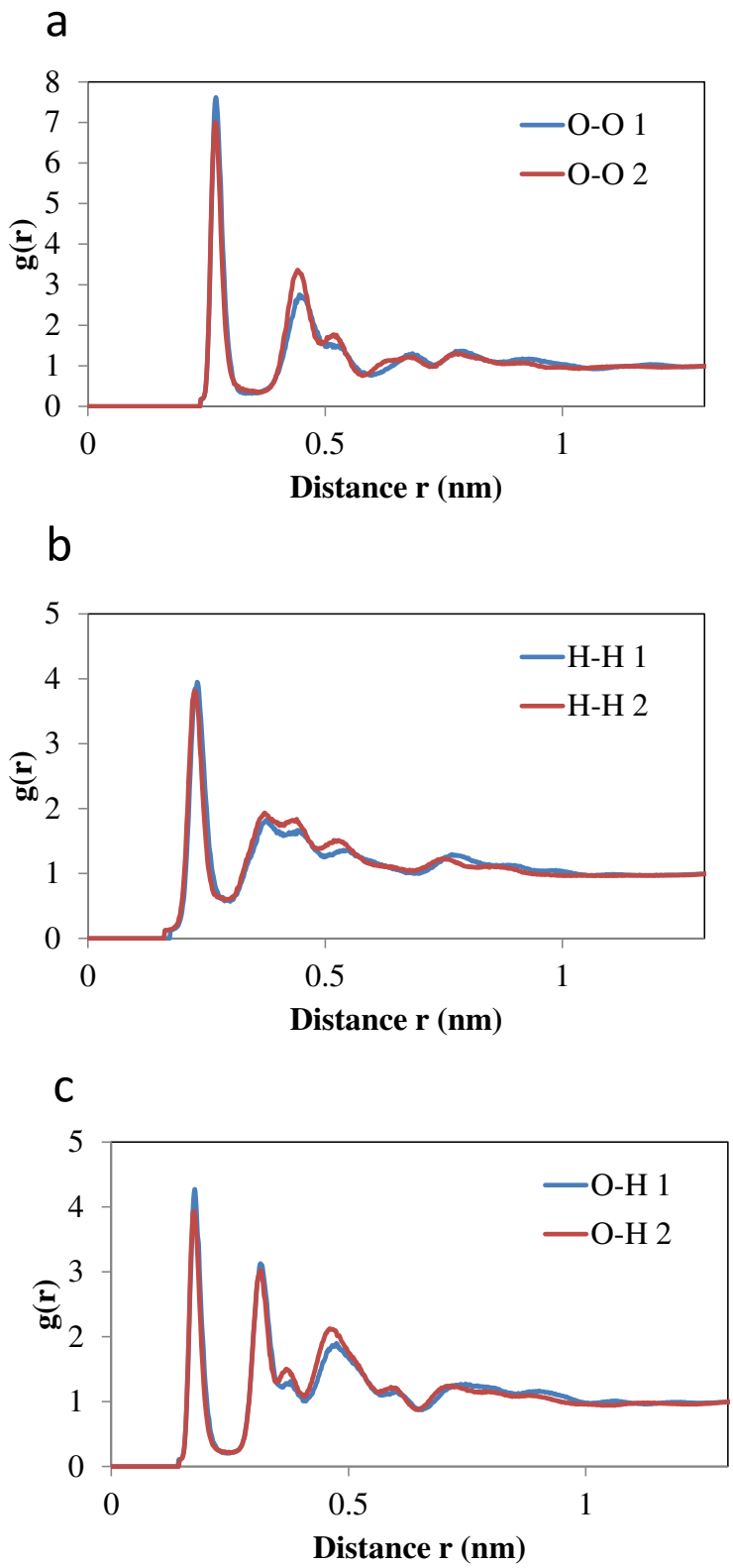

Figure B.2. Radial distribution functions $g(r)$ of water molecules near and far away the benzene molecules trapped inside the ice lattice. (a) oxygen-oxygen. (b) hydrogen-hydrogen. (c) oxygen-hydrogen. 1 represents the radial distribution function between water molecules close to the trapped benzene molecules, and 2 represents the water molecules far away from the trapped benzene molecules.

APPENDIX C: SUPPORTING INFORMATION (CHAPTER 7)

Table S1. Atomic charges in methyl salicylate (MeSA). See figure S1 for nomenclature of atoms in a molecule of MeSA. Representative Gromacs files (input, topology and coordinate) are available upon request.

Name	Original charges	New charges
C1	0.160	0.176
H2	0.030	0.033
H3	0.030	0.033
H4	0.030	0.033
O5	-0.330	-0.363
C6	0.625	0.688
O7	-0.430	-0.473
C8	-0.115	-0.127
C9	-0.115	-0.127
H10	0.115	0.127
C11	-0.115	-0.127
H12	0.115	0.127
C13	-0.115	-0.127
H14	0.115	0.127
C15	-0.115	-0.127
H16	0.115	0.127
C17	0.150	0.165
O18	-0.585	-0.644
H19	0.435	0.479

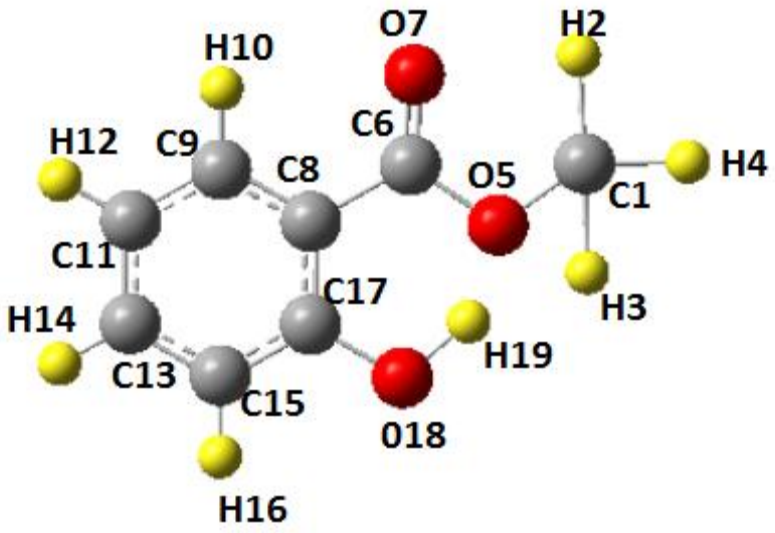

Figure S1. Nomenclature of atoms in a MeSA molecule

APPENDIX D: PUBLICATIONS AND CONFERENCE PRESENTATIONS

- T. P. Liyana-Arachchi, Christopher Stevens, Amie K. Hansel, Franz S. Ehrenhauser, K. T. Valsaraj and F. R. Hung, "Molecular simulations of adsorption and interfacial properties of methyl salicylate on air/water interfaces" (Submitted, 2013).
- T. P. Liyana-Arachchi, Shivkumar Bale, K. T. Valsaraj and F. R. Hung, "MD Simulations of n-Alkanes and Surfactants at Air/salt Water Interfaces" (Submitted, 2013).
- T. P. Liyana-Arachchi, Christopher Stevens, Amie K. Hansel, Franz S. Ehrenhauser, K. T. Valsaraj and F. R. Hung, "Molecular simulations of green leaf volatiles and atmospheric oxidants on air/water interfaces" *Phys. Chem. Chem. Phys.* 2013, *15*, 3583-3592 .
- T. P. Liyana-Arachchi, K. T. Valsaraj and F. R. Hung, "Ice growth from supercooled aqueous solutions of reactive oxygen species", *Theor. Chem. Acc.* 2013, *132*, 1309.
- T. P. Liyana-Arachchi, K. T. Valsaraj and F. R. Hung, "Ice Growth from Supercooled Aqueous Solutions of Benzene, Naphthalene and Phenanthrene", *J. Phys. Chem. A* 2012, *116*, 8539-8546.
- T. P. Liyana-Arachchi, K. T. Valsaraj and F. R. Hung, "Adsorption of naphthalene and ozone on atmospheric air/ice interfaces coated with surfactants: A molecular simulation study", *J. Phys. Chem. A* 2012, *116*, 2519-2528.
- T. P. Liyana-Arachchi, K. T. Valsaraj and F. R. Hung, "A molecular simulation study of the adsorption of naphthalene and ozone on atmospheric air/ice interfaces", *J. Phys. Chem. A* 2011*, 115,* 9226-9236.

- J. Chen, F. Ehrenhauser, T. P. Liyana-Arachchi, F. R. Hung, M. J. Wornat and K. T. Valsaraj, “Adsorption of gas-phase phenanthrene on atmospheric water and ice films”, *Polycycl. Aromat. Comp.* 2011*, 31,* 201-226.
- Thilanga P. Liyana-Arachchi, Kalliat T Valsaraj and Francisco R. Hung, “Molecular dynamics simulations of oil hydrocarbons and surfactants at atmospheric air/salt water interfaces”, ACS 2013 National Meeting, New Orleans, LA..
- Thilanga P. Liyana-Arachchi, Kalliat T Valsaraj and Francisco R. Hung, “Adsorption of Green Leaf Volatiles (GLVs) on Atmospheric Air/water Interfaces; Molecular Dynamic (MD) Study”, ACS 2013 National Meeting, New Orleans, LA..
- Thilanga P. Liyana-Arachchi, Kalliat T Valsaraj and Francisco R. Hung, “Molecular dynamics simulations of oil hydrocarbons and surfactants at atmospheric air/salt water interfaces”, Gulf of Mexico Oil Spill and Science Conference 2013, New Orleans, LA.
- Thilanga P. Liyana-Arachchi, Kalliat T Valsaraj and Francisco R. Hung, “A molecular simulation study of the adsorption of aromatic hydrocarbons and reactive oxygen species on atmospheric ice films”, AIChE 2012 Annual Meeting, Pittsburgh, PA.
- Thilanga P. Liyana-Arachchi, Kalliat T Valsaraj and Francisco R. Hung, “Ice growth from benzene, naphthalene and phenanthrene/super-cooled water solutions”, AIChE 2012 Annual Meeting, Pittsburgh, PA.
- Thilanga P. Liyana-Arachchi, Kalliat T Valsaraj and Francisco R. Hung, “Adsorption of Polycyclic Aromatic Hydrocarbons and Ozone on Atmospheric Air/Ice Interfaces”, FOMMS 2012, Mt. Hood, Oregon.

- Thilanga P. Liyana-Arachchi, Kalliat T Valsaraj and Francisco R. Hung, “Adsorption of atmospherically relevant gases on bare and surfactant coated ice films”, HPC User Symposium 2012, Baton Rouge, LA.
- Thilanga P. Liyana-Arachchi, Kalliat T Valsaraj and Francisco R. Hung, “Adsorption of polycyclic aromatic hydrocarbons and ozone on atmospheric air/ice interfaces: A molecular simulation study”, ACS 2012 National Meeting, San Diego, California.
- Thilanga P. Liyana-Arachchi, Kalliat T Valsaraj and Francisco R. Hung, “A molecular simulation study of the adsorption of polycyclic aromatic hydrocarbons and ozone on atmospheric ice films”, Mardi Gras Conference 2012, Baton Rouge, LA.
- Thilanga P. Liyana-Arachchi, Kalliat T Valsaraj and Francisco R. Hung, “A molecular simulation study of the adsorption of polycyclic aromatic hydrocarbons and ozone on atmospheric ice films”, AIChE 2011 Annual Meeting, Minneapolis, MN.
- Franz S. Ehrenhauser, Aubrey A. Heath, Thilanga P. Liyana-Arachchi, Mary J. Wornat, Francisco R. Hung, Pierre R. Herckes, Kalliat T. Valsaraj, “Chemistry at the interface – Chemical Transformation at the Air-Water Interface”, ACS 2013 National Meeting, New Orleans, LA.
- Thilanga P. Liyana-Arachchi, Kalliat T Valsaraj and Francisco R. Hung, “Molecular dynamics simulations of oil hydrocarbons and surfactants at atmospheric air/salt water interfaces”, ACS 2012 Southwest Regional Meeting, Baton Rouge, LA.
- T. P. Liyana-Arachchi, K. T. Valsaraj and Francisco R. Hung, “Green Leaf Volatiles (GLVs) on Atmospheric Air/water Interfaces; Molecular Dynamic (MD) Study”, AIChE

2012 Annual Meeting, Pittsburgh, PA (In Honor of Keith Gubbins' 75th Birthday II: Adsorption & Interfacial Properties).

VITA

Thilanga Prabhash Liyana-Arachchi was born in Colombo, Sri-Lanka. He completed his high school from St. Peter's College in 2003. He graduated with a bachelor's degree in Chemical Engineering from Louisiana State University in 2008. He entered the Ph.D. program in Chemical Engineering at Louisiana State University in Spring 2009 and joined Prof. Francisco R. Hung's research group, where he carried out the work presented here. After defending his dissertation, Thilanga will join Prof. J. Ilja Siepmann's research group at the University of Minnesota, to work as a postdoctoral research associate.